PROFESSIONAL REPORT 120

SHORT NOTES ON ALASKA GEOLOGY 2003

State of Alaska
Department of Natural Resources

DIVISION OF GEOLOGICAL & GEOPHYSICAL SURVEYS

Rodney A. Combellick
Acting Director
2003

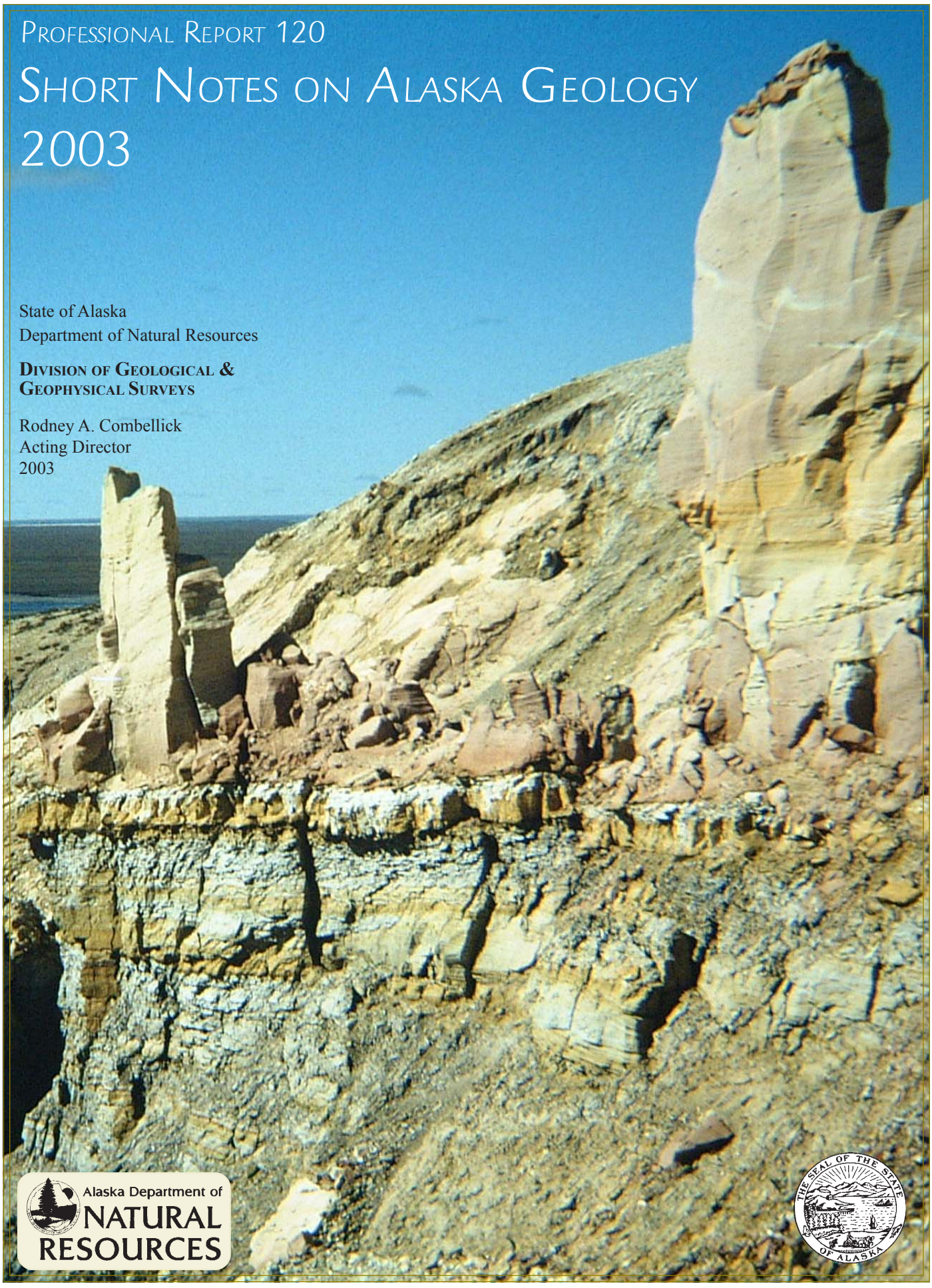

Alaska Department of NATURAL RESOURCES

THE SEAL OF THE STATE OF ALASKA

SHORT NOTES ON ALASKA GEOLOGY 2003

Edited by Karen H. Clautice and Paula K. Davis

Division of Geological & Geophysical Surveys
Professional Report 120
Recent research on Alaska geology
Fairbanks, Alaska
2003

Front cover photo: *Badlands topography in poorly consolidated sandstone of the Eocene Sagavanirktok Formation at Franklin Bluffs on Alaska's North Slope south of Prudhoe Bay. (Photo by Gil Mull)*

STATE OF ALASKA
Frank H. Murkowski, *Governor*

DEPARTMENT OF
NATURAL RESOURCES
Tom Irwin, *Commissioner*

DIVISION OF GEOLOGICAL &
GEOPHYSICAL SURVEYS
Rodney A. Combellick, *Acting Director*

Division of Geological & Geophysical Surveys publications may be inspected at the following locations. Address mail orders to the Fairbanks office.

Alaska Division of Geological &
Geophysical Surveys
Attn: Geologic Communications Section
794 University Avenue, Suite 200
Fairbanks, Alaska 99709-3645
http://wwwdggs.dnr.state.ak.us
dggspubs@dnr.state.ak.us

Department of Natural Resources
Public Information Center
550 W 7th Ave., Suite 1250
Anchorage, Alaska 99501-3557

This publication, released by the Division of Geological & Geophysical Surveys (DGGS), was produced and printed in Anchorage, Alaska, by A.T. Publishing & Printing Company, at a cost of $17 per copy. Authority to print this and other publications comes from Alaska Statute 41.08.020, which charges DGGS "to determine the potential of Alaskan land for production of metals, minerals, fuels, and geothermal resources; the location and supplies of groundwater and construction materials; the potential geologic hazards to buildings, roads, bridges, and other installations and structures; and . . . conduct such other surveys and investigations as will advance knowledge of the geology of Alaska."

FOREWORD

In keeping with the tradition of previous issues of *Short Notes on Alaska Geology*, this issue offers articles on a range of geologic topics in Alaska as diverse as the authors who prepared them. By my brief read, the articles cover the fields of geochemistry, geochronology, mineralogy, petrology, petrography, structural geology, stratigraphy, sedimentology, and paleontology. The authors represent the Alaska Division of Geological & Geophysical Surveys (DGGS), University of Alaska Fairbanks, U.S. Geological Survey, and numerous other universities and private companies in the U.S., Canada, Ireland, and even Czech Republic. We greatly appreciate their efforts in this significant contribution toward advancing the knowledge of Alaska's geology.

Assembling and publishing a high-quality collection of peer-reviewed articles such as this require significant dedication of time and effort over a period of at least a year and a half. For this issue of *Short Notes*, Karen Clautice served as technical editor and Paula Davis as publications specialist, in addition to their regular work commitments. Even in this age of sophisticated publication software, layout of a professional publication is a significant effort, here performed expertly by Joni Robinson. To the authors, editors, and publications staff we owe a large debt of gratitude.

Lastly, DGGS publications like *Short Notes on Alaska Geology* would not exist without the continued interest of you, our readers, in new information about the geology of this state for your own purposes in understanding, developing, and preserving its resources. We value your comments on this and other DGGS publications, nearly all of which are available through the DGGS Web site.

Rodney A Combellick

Rodney A. Combellick
Acting Director

CONTENTS

POTASSIC MAGMATISM ON ST. LAWRENCE ISLAND, ALASKA, AND CAPE DEZHNEV, NORTHEAST RUSSIA: EVIDENCE FOR EARLY CRETACEOUS SUBDUCTION IN THE BERING STRAIT REGION

Jeffrey M. Amato,[1] Elizabeth L. Miller,[2] Andrew T. Calvert,[3] Jaime Toro,[4] and James E. Wright[5]

ABSTRACT

Field mapping, geochemical investigations, and geochronology of Cretaceous igneous rocks on St. Lawrence Island were initiated to elucidate the geologic relationships between Russia and Alaska. These data suggest that the Cretaceous magmatic history of St. Lawrence Island can be divided into an early phase of potassic plutonism around 113 Ma and a subsequent phase of larger-volume subalkaline magmatism between 110 and 100 Ma (and possibly younger). A nepheline syenite on St. Lawrence Island is part of a roughly east–west belt of similar potassic/ultrapotassic plutons that stretches from the western Yukon–Koyukuk basin to Cape Dezhnev, Russia. $^{40}Ar/^{39}Ar$ biotite dates of 113 ± 1 Ma (St. Lawrence) and 110 ± 1 Ma (Dezhnev) indicate that these two plutons are coeval with the other plutons in the belt. The subalkaline Sevuokuk pluton ranges from granodiorite to granite. A $^{40}Ar/^{39}Ar$ biotite date from the northern part of the pluton is 110 ± 0.5 Ma, and a biotite from the southern part is 100 ± 0.6 Ma. Neodymium isotope data (ε_{Nd}) from the Sevuokuk pluton range from -0.75 to -3.09, and initial $^{87}Sr/^{86}Sr$ ranges from 0.7060 to 0.7076. The Iwoonut pluton is a monzodiorite that is alkaline but less potassic than the syenites. It has ε_{Nd} of -0.35 and initial $^{87}Sr/^{86}Sr$ of 0.7063, and a biotite from this pluton yields an age of 102 ± 0.5 Ma. The subalkaline plutonic and volcanic rocks are comagmatic. Plutonic rocks on St. Lawrence Island are unfoliated, but volcanic rocks dip dominantly to the southwest up to 70 degrees, with some units dipping more shallowly southeast or northwest. A subduction-related origin is proposed for both phases of magmatism on St. Lawrence Island. The potassic plutons may represent small degrees of partial melting of subcontinental lithosphere during the early phases of a north-directed subduction system. Younger subalkaline magmatism may represent higher degrees of partial melt of the same source region in the same tectonic setting. Deformation associated with this magmatism in the Bering Strait region occurred in an extensional regime possibly linked to slab-rollback within the subduction zone.

INTRODUCTION

St. Lawrence Island is the largest island on the Bering Shelf between Russia and Alaska and was the subject of reconnaissance investigations by the U.S.Geological Survey in the late 1960s and early 1970s (Patton and Csejtey, 1971; Csejtey and Patton, 1974). St. Lawrence Island is about 160 km long and contains exposures of Paleozoic sedimentary rocks, Permian(?) to Triassic gabbroic rocks, Cretaceous plutonic and volcanic rocks, and Quaternary basalt flows. This paper reports structural, geochemical, and geochronologic data from Cretaceous volcanic and plutonic rocks on St. Lawrence Island, as well as geochemical and geochronologic data from a syenite pluton at Cape Dezhnev on the Chukotka Peninsula of Russia. These geochemical data are used with field-based structural observations collected at a more regional scale to determine: (a) the petrogenesis of potassic magmatism in the Bering Strait region, (b) the relationship between the potassic plutons to major tectonic boundaries, (c) the relationship between younger subalkalic magmatism to the Okhotsk–Chukotsk volcanic belt in Russia, and (d) the tectonic setting of mid-Cretaceous magmatism in the Bering Strait region.

REGIONAL GEOLOGIC SETTING

Cretaceous igneous rocks in the Bering Strait region (fig. 1) form part of a circum-Pacific magmatic and orogenic belt extending from the Andes through the North American Cordillera to the Russian Far East and southward along the Asian margin. In the Russian Far East, most Cretaceous volcanic and related granitic rocks are part of a continuous ≈3,000-km-long belt known as the Okhotsk–Chukotsk volcanic belt (OCVB). Magmatism in the OCVB is interpreted as the product

[1]Department of Geological Sciences, New Mexico State University, Las Cruces, New Mexico, 88003
Email for Jeffrey M. Amato: amato@nmsu.edu
[2]Department of Geological and Environmental Sciences, Stanford University, Stanford, California, 94035
[3]U.S. Geological Survey, Menlo Park, California, 94025
[4]Department of Geology and Geography, West Virginia University, Morgantown, West Virginia, 26506
[5]Department of Geology, University of Georgia, Athens, Georgia, 30602

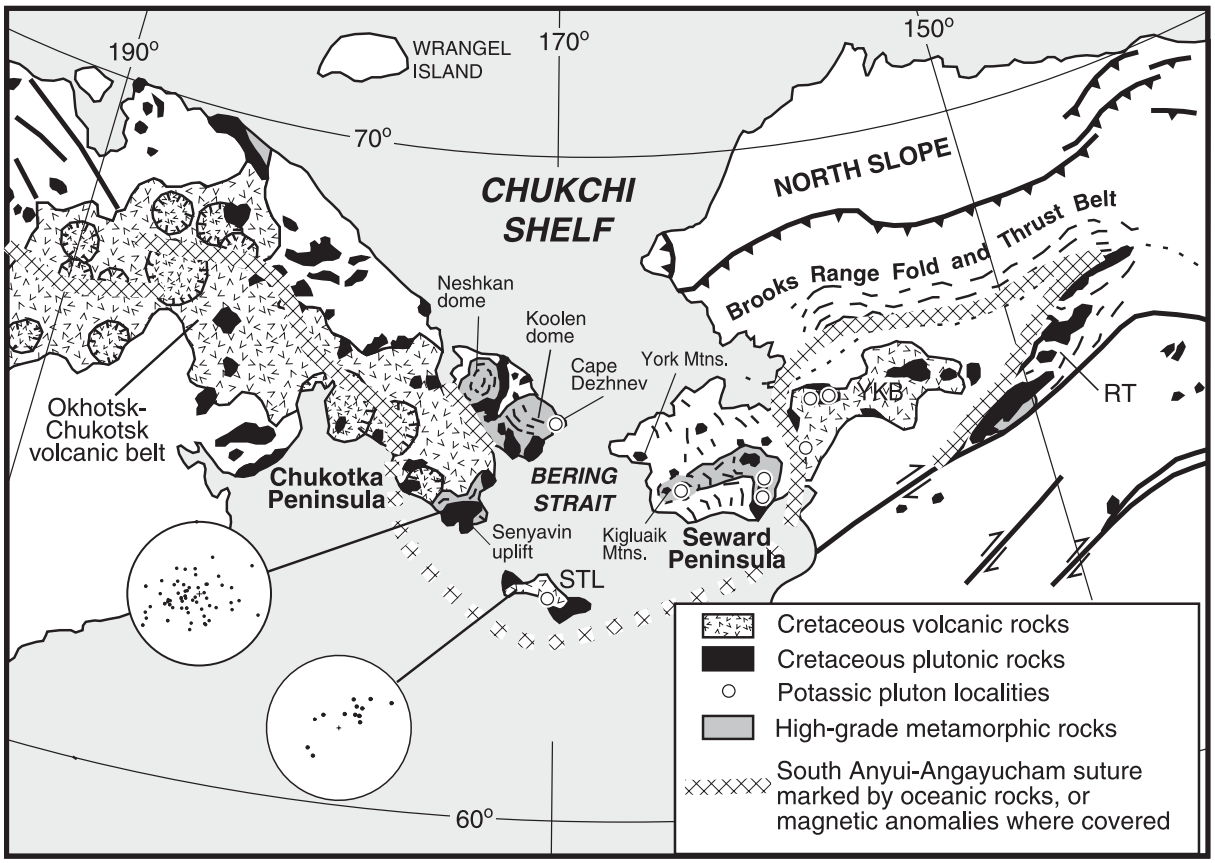

Figure 1. *Regional map showing the distribution of Cretaceous igneous and metamorphic rocks in the Bering Strait region. Also shown are the major physiographic elements of northern Alaska. The Angayucham terrane is a tectonically modified belt of Devonian through Jurassic oceanic rocks tectonically emplaced over the Arctic Alaska terrane, which includes most of Alaska north of this boundary, as well as Seward Peninsula and equivalent rocks on the eastern Chukotka Peninsula. Potassic pluton localities east of the Seward Peninsula represent several small plutons. Sample 94DV-1 is from Cape Dezhnev. Also shown are stereonet plots of poles to bedding of Cretaceous volcanic rocks in the Senyavin uplift (data from Calvert, 1999) and on St. Lawrence Island (this study). STL = St. Lawrence Island; YKB = Yukon–Koyukuk basin; RT = Ruby terrane. Modified from BSGFP (1997).*

of subduction of oceanic crust beneath the Pacific margin of northeastern Russia (for example, Zonenshain and others, 1990). In Alaska, Cretaceous magmatic rocks form a broader and more diffuse belt that narrows to the southeast (Plafker and Berg, 1994).

In northern Alaska, this belt includes the Cretaceous plutons of Seward Peninsula and the Yukon–Koyukuk Basin (Miller, 1994). Some of the older plutons (115–100 Ma) in this belt have distinctive ultrapotassic compositions. They make up a small percentage of this belt but are found throughout the Bering Strait region (fig. 1; Miller, 1972; Amato, 1996; Amato and Wright, 1998). Some of these potassic plutons have trace-element abundance patterns typical of magmas generated within continental (Andean type) subduction settings (Amato and Wright, 1997). Slightly younger plutons (100–80 Ma) in this belt are not ultrapotassic but some, like the Kigluaik pluton on Seward Peninsula, have higher K_2O concentrations than typical mafic plutonic rocks and may have resulted from small degrees of partial melting of lithospheric mantle that was metasomatized during Early to Late Cretaceous subduction (Amato and Wright, 1997).

Cretaceous gneiss complexes lie within the confines of the Cretaceous magmatic belt. Examples include those in the Ruby terrane (Roeske and others, 1995), the Kigluaik, Bendeleben, and Darby Mountains of Seward Peninsula (Miller and others, 1992; Amato and others, 1994), and the Koolen, Neshkan, and Senyavin complexes of the Chukotka Peninsula (Shuldiner and Nedomolkin, 1976; Natal'in, 1979; Calvert, 1999). The metamorphic culminations expose sillimanite-grade and, more rarely, granulite-grade metamorphic rocks of the middle crust that are often juxtaposed with supracrustal

rocks. On the Seward Peninsula, high-grade paragneisses that experienced peak metamorphism in the Cretaceous are flanked by lower grade greenschist and locally blueschist-facies metamorphic rocks that preserve an older metamorphic history (Forbes and others, 1984; Patrick and Evans, 1989; Miller and others, 1992; Hannula and McWilliams, 1995). The lower grade rocks are in turn in normal-fault contact with weakly metamorphosed, fossiliferous Paleozoic carbonates in the York Mountains (Sainsbury, 1969). In Russia, high-grade gneisses are flanked by variably deformed but little metamorphosed Paleozoic and Mesozoic metasedimentary rocks and thick sections of Cretaceous volcanic and sedimentary rocks of the Okhotsk–Chukotsk volcanic belt (fig. 1).

In both northern Alaska and Russia, plutonism postdates the Early Cretaceous closure of the Angayucham–South Anyui suture (fig. 1) that separates rocks of North American continental affinity to the north from rocks of island arc or oceanic affinity to the south (Moore and others, 1994; Patton and Box, 1989; Patton and others, 1994; Plafker and Berg, 1994). The rocks north of the suture compose the Arctic Alaska–Chukotka terrane. Miller and Hudson (1991) argued that closure of the suture and arc–continent collision was followed by extension, and therefore the Cretaceous plutons of northern Alaska were generated within an extensional tectonic setting. Rubin and others (1995) suggested that regional relations support continuous subduction beneath the Alaskan sector of the belt in Cretaceous time and that the width of the belt in the Bering Strait region could be a consequence of regional extension during magmatism. Amato and Wright (1997, 1998) used geochemical arguments to suggest that the tectonic setting for the Kigluaik pluton and similar plutons within the Late Cretaceous magmatic belt was likely a north-dipping continental subduction zone undergoing extension during south-directed trench rollback.

GEOLOGY OF ST. LAWRENCE ISLAND

The Cretaceous plutonic rocks on St. Lawrence Island (fig. 2) intrude Precambrian(?) to Paleozoic(?) calc–silicate hornfels that is undated, and Paleozoic carbonate rocks (Patton and Csejtey, 1980). Middle to Late Devonian dolomite and dolomitic limestone is correlative with units in the western and central Brooks Range (Patton and Csejtey, 1980; Till and Dumoulin, 1994). Late Mississippian limestone has been correlated with Lisburne Group carbonates in northern Alaska (Lane and Ressmeyer, 1985). Permian or Triassic gabbro and diabase are associated with deformed graywacke and shale of probable Permian or Triassic age and shale, limestone, and chert of Middle and Late Triassic age (Patton and Csejtey, 1980). These late Paleozoic to early

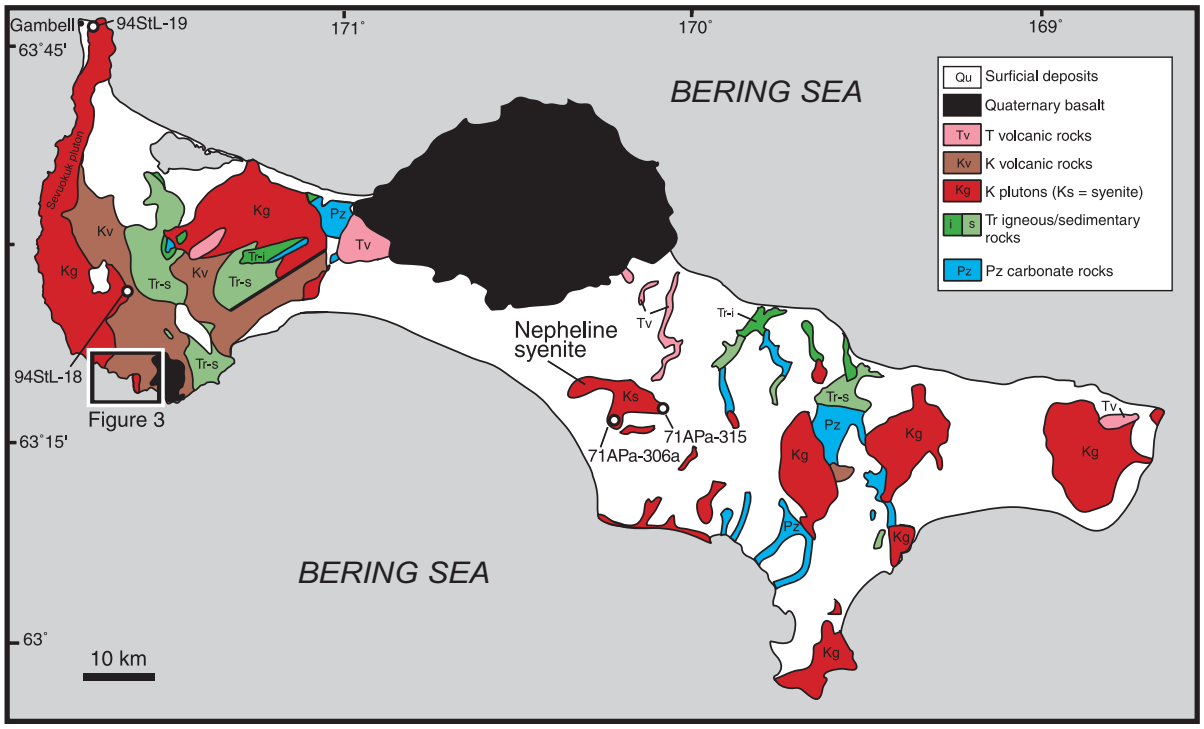

Figure 2. *Simplified geologic map of St. Lawrence Island. Cretaceous plutonic rocks appear to postdate Cretaceous volcanic rocks in the southwestern part of the island. Sample localities for the two samples of nepheline syenite and for two samples from the Sevuokuk pluton are also shown. After Patton and Csejtey (1980).*

Mesozoic rocks have been correlated with the oceanic rocks of the Angayucham terrane (for example, Jones and others, 1987; Plafker and Berg, 1994). These correlations indicate that St. Lawrence Island lies near the southern boundary of the Arctic Alaska–Chukotka terrane. Mid-Cretaceous plutons (figs. 2, 3) and Cretaceous through Tertiary volcanic rocks are also present.

CRETACEOUS PLUTONS

Mid-Cretaceous plutonic rocks on St. Lawrence Island include nepheline syenite, monzodiorite, diorite, granodiorite, and granite. The nepheline syenite (Patton and Csejtey, 1980) consists mainly of a 44-km^2 area of rubble exposure in the central part of the island (fig. 2). Major phases are K-feldspar grains up to 4 cm long, nepheline, biotite, and melanite garnet with minor andesine and hornblende, and accessory minerals include zircon, fluorite, magnetite, titanite, apatite, allanite, and calcite (Csejtey and Patton, 1974). SiO_2 is 53 percent, K_2O is 10 percent, and Na_2O is 8 percent (fig. 4; table 1). The nepheline syenite pluton is similar to many of the Bering Strait potassic plutons in that it is

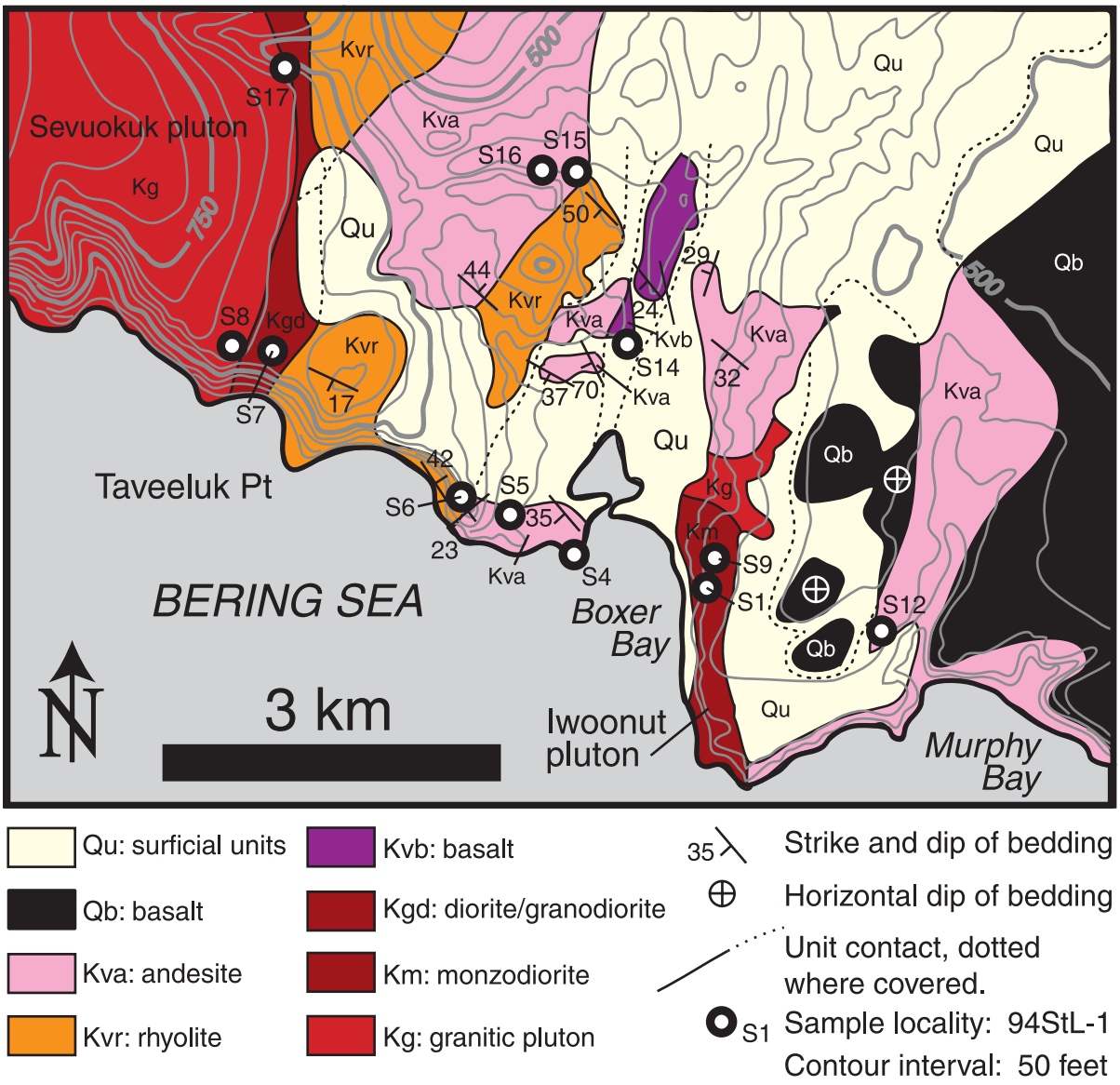

Figure 3. *Geologic map of the Boxer Bay area. Most contacts between volcanic units are obscured by float but are probably fault contacts. Quaternary basalt lies unconformably over Kva in the eastern part of the map area. Sample localities referred to in the text and tables are also shown. Map is based on 1994 reconnaissance field mapping by Amato and Miller on 1:20,000-scale aerial photographs, transfered onto the USGS 1:250,000-scale base map of St. Lawrence Island.*

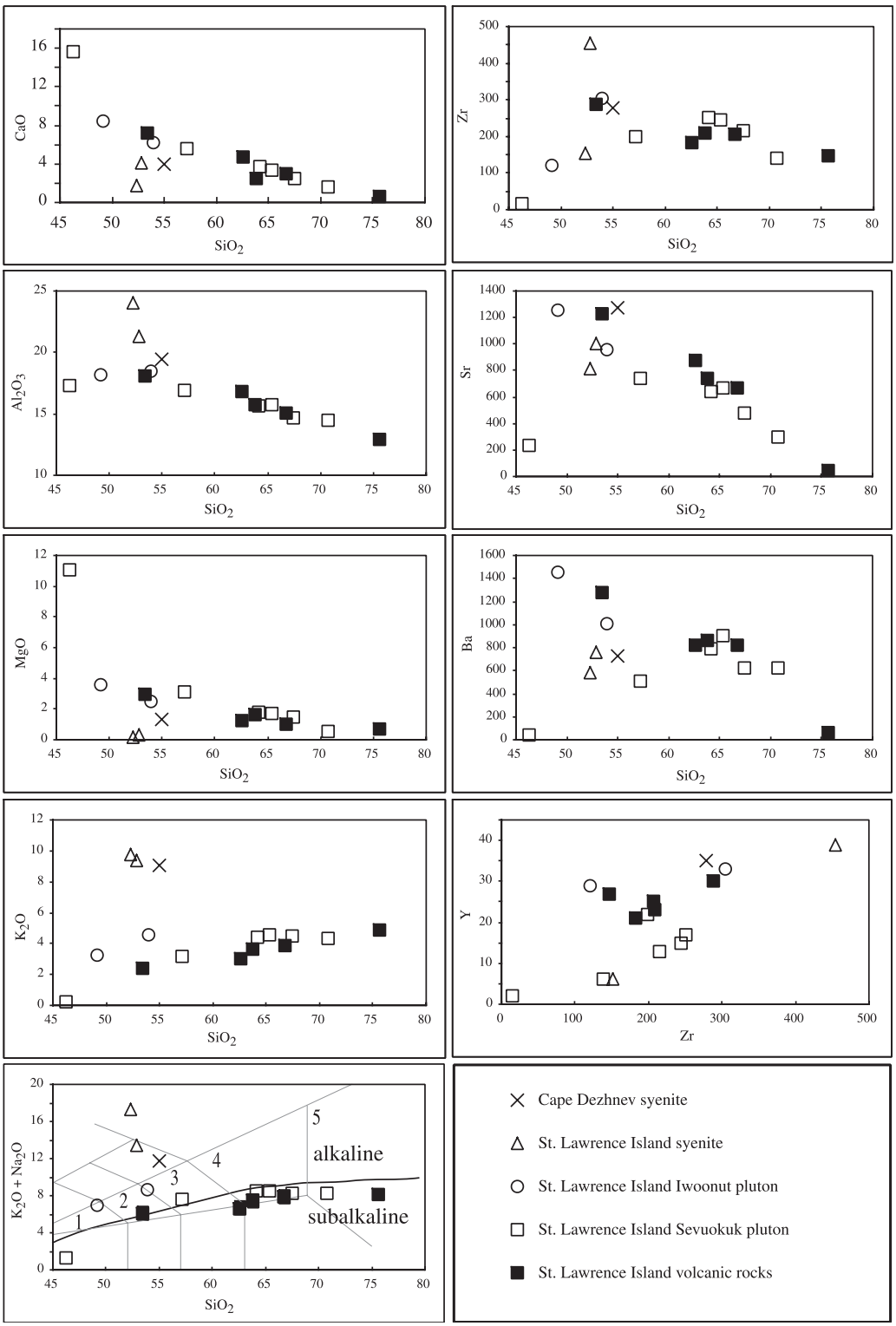

Figure 4. *Major and trace-element chemical variation diagrams for selected St. Lawrence Island igneous rocks. Also shown are data from the Cape Dezhnev syenite (see fig. 1 for locality). The syenites from St. Lawrence Island are geochemically similar to the syenite from Cape Dezhnev, but generally distinct from the other plutonic rocks from St. Lawrence Island. The Iwoonut pluton shows elevated K_2O values relative to the subalkalic St. Lawrence Island igneous rocks, but otherwise appears to vary colinearly with those samples. Fields in the $K_2O + Na_2O$ vs SiO_2 plot are: (1) trachybasalt, (2) basaltic trachyandesite, (3) trachyandesite, (4) trachydacite, (5) rhyolite; these and the subalkalic/alkalic division after Le Bas and others (1986).*

Table 1. *Whole-rock geochemistry from plutonic rocks*

Location[a]	St. Lawrence Island										Dezhnev
Unit[b]	Ks	Ks	Km	Km	Kd	Kg	Kg	Kg	Kg	Kg	Ks
Sample	71APa-306b	71APa-315[c]	94STL-9	94StL-1	94StL-7	94STL-8c	94StL-17	94StL-8a	94StL-18	94StL-19	94DV-1[c]
SiO_2	52.30	52.81	49.16	53.92	46.29	57.17	64.13	65.34	67.47	70.76	55.09
TiO_2	0.20	0.30	1.76	1.32	0.21	0.91	0.59	0.58	0.51	0.23	0.65
Al_2O_3	23.99	21.24	18.19	18.52	17.29	16.89	15.67	15.73	14.67	14.51	19.45
Fe_2O_3[d]	1.27	1.82	9.71	7.29	5.78	7.09	4.27	4.08	3.34	1.73	5.43
MnO	0.08	0.16	0.15	0.13	0.12	0.12	0.08	0.07	0.03	0.06	0.11
MgO	0.14	0.34	3.62	2.48	11.03	3.09	1.83	1.74	1.48	0.52	1.33
CaO	1.73	4.14	8.49	6.16	15.59	5.53	3.74	3.40	2.54	1.60	3.94
Na_2O	7.59	4.05	3.77	4.07	1.02	4.50	4.15	3.94	3.79	3.89	2.76
K_2O	9.73	9.36	3.25	4.55	0.23	3.15	4.39	4.57	4.48	4.36	9.04
P_2O_5	bd	bd	1.05	0.74	bd	0.31	0.18	0.18	0.13	bd	0.30
LOI[e]	2.03	3.50	0.56	0.79	1.60	0.56	0.89	0.66	0.91	1.63	1.00
Total	**99.08**	**97.78**	**99.70**	**99.98**	**99.16**	**99.32**	**99.92**	**100.28**	**99.36**	**99.34**	**99.12**
V	bd	35	206	120	115	151	74	69	63	bd	71
Cr	bd	bd	bd	bd	252	bd	bd	bd	bd	bd	bd
Ni	bd	bd	bd	bd	56	bd	bd	bd	bd	bd	bd
Cu	bd	bd	60	40	101	39	17	13	bd	bd	9
Zn	65	68	104	88	76	91	63	68	29	35	83
Rb	465	463	60	150	8	145	172	163	164	188	394
Sr	810	999	1251	953	231	739	643	667	482	298	1274
Y	bd	39	29	33	bd	22	17	15	13	bd	35
Zr	152	455	120	304	bd	199	251	245	215	139	278
Nb	20	21	bd	18	bd	17	20	17	18	22	20
Ba	579	756	1451	1011	bd	508	789	905	626	623	729

[a]See figures 2 and 3 for sample localities and unit designations. Whole-rock compositions were determined by X-ray fluorescence spectroscopy at New Mexico State University by using a Rigaku ZSX wavelength-dispersive spectrograph equipped with an end-window Rh target X-ray tube. Oxides are reported as weight percent, trace elements are in parts per million. Blank spaces indicate no analysis. bd = below detection limit.

[b]All rocks are assumed to be Cretaceous. Ks is syenite, Km is monzodiorite (Iwoonut pluton), Kd and Kg are diorite and granite–granodiorite, respectively, from the Sevuokuk pluton.

[c]Major element analyses for these samples represent the average of four analyses of the same sample.

[d]All Fe was calculated as Fe_2O_3

[e]LOI (loss on ignition) determined by weight loss after heating at 1,000°C for 20 minutes.

extremely enriched in the light rare-earth elements and has overall high rare-earth-element abundances (fig. 5; table 2).

The Iwoonut pluton (Patton and Csejtey, 1980) is an olivine-bearing monzodiorite (fig. 3). Overall grain size is variable, and there are compositional variations reflected in the two whole-rock analyses (fig. 4; table 1). Major phases include plagioclase, K-feldspar, augite, olivine, and interstitial biotite. Pyroxene and olivine are euhedral to subhedral. Biotite is intergrown with Fe–Ti oxides. Plagioclase grains are euhedral laths that range from 5 to 15 mm long, and K-feldspar is interstitial. SiO_2 ranges from 49 to 55 percent, and total alkalis range from 7 to 9 percent in these two samples. The Iwoonut pluton has linear trends in major elements such as CaO, Al_2O_3, and MgO vs SiO_2. Trace elements such as zirconium (Zr), strontium (Sr), and barium (Ba) also vary linearly against SiO_2 content.

The trace-element compositions of the St. Lawrence syenite and monzodiorite are similar to the Cape Dezhnev syenite (Perchuk, 1965) on the Chukotka Peninsula of Russia (fig. 1). The three alkaline intrusions all have 'troughs' on the chondrite-normalized diagram in elements such as niobium (Nb), tantalum (Ta), and titanium (Ti) (fig. 6). The monzodiorite has lower concentrations of large ion lithophile elements (LILE) such as rubidium (Rb), thorium (Th), and potassium (K), and lower concentrations of light rare-earth elements such as lanthanum (La) and cerium (Ce) relative to the Dezhnev syenite.

In addition to these two alkaline plutons, sub-alkaline granitic rocks are exposed throughout St. Lawrence Island (fig. 2). The Sevuokuk pluton appears to be a composite pluton of hornblende diorite, biotite granodiorite, and biotite granite. Major accessory minerals include biotite and augite. SiO_2 ranges from 46 percent to 73 percent. A horn-blende diorite (94StL-7) was collected from near the eastern margin of the Sevuokuk pluton where it appears to intrude adjacent rhyolite flows. Another sample taken from near the eastern contact of the pluton (94StL-8c) is more mafic than those from the interior and is granodioritic in composition.

We analyzed three plutonic rocks from western St. Lawrence Island to compare their strontium (Sr) and neodymium (Nd) isotope compositions to those from Cretaceous plutonic rocks on Seward Peninsula. The three samples are from the Sevuokuk pluton, both near Boxer Bay and near Gambell, and the Iwoonut pluton. Initial $^{87}Sr/^{86}Sr$ and ε_{Nd} values were calculated at the estimated ages (see

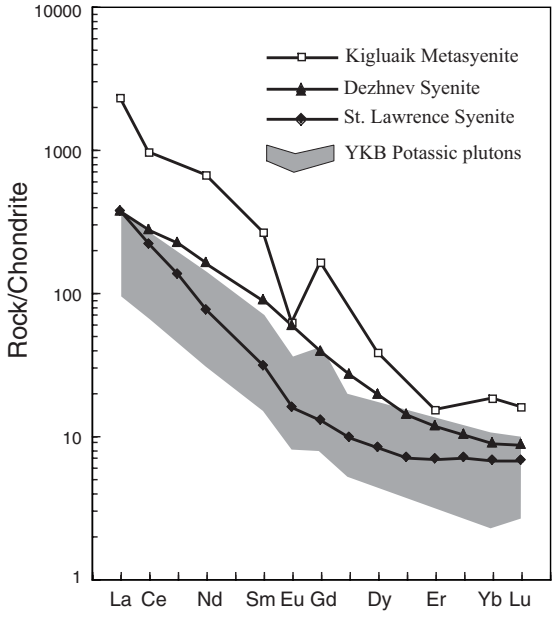

Figure 5. *Chondrite-normalized rare-earth-element plot for Bering Strait potassic rocks. Yukon–Koyukuk basin (YKB) potassic pluton data from Miller (1989). See table 2 for data. Normalization factors are from Evensen et al. (1979).*

Table 2. *Whole-rock trace-element geochemistry from selected potassic rocks*

Location	St. Lawrence Island		Dezhnev	Kigluaik Mtns.
Unit	Km	Ks	Ks	Metasyenite
Sample	94StL-1	71APa306b	94DV-1	91G-2a
Rb	151.9	457.4	393.6	
Sr	933.9	815.8	1234.6	
Y	33.5	19.4	33.8	
Nb	25.5	16.6	28.3	
Cs	5.5	16.8	37.0	
Ba	1055.8	507.6	703.9	
La	52.9	137.6	137.2	832.6
Ce	103.6	210.9	265.2	910.8
Pr	11.9	18.4	30.4	
Nd	46.2	53.7	114.9	464.3
Sm	9.4	7.2	20.7	60.2
Eu	2.4	1.4	5.1	5.4
Gd	7.1	3.9	12.0	49.1
Tb	1.1	0.6	1.6	
Dy	6.4	3.2	7.4	14.4
Ho	1.2	0.6	1.2	
Er	3.4	1.7	2.9	3.8
Tm	0.5	0.3	0.4	
Yb	3.1	1.7	2.2	4.5
Lu	0.5	0.3	0.3	0.6
Hf	6.6	2.6	7.2	
Ta	1.8	0.7	1.8	
Pb	20.2	79.3	115.9	
Th	8.7	90.3	28.7	
U	3.2	13.9	9.4	

Trace-element concentrations were determined by instrumental neutron activation analysis. Blanks indicate element was not analyzed.

geochronology section below) for all three samples (table 3). The two Sevuokuk pluton samples (94StL-19 and 94StL-8a) have ε_{Nd} of -3.09 near Gambell, and -0.75 near Boxer Bay, and initial $^{87}Sr/^{86}Sr$ of 0.7076 and 0.7060, respectively. This range of isotope ratios (and ages) suggests that this pluton is actually a composite pluton, with more mafic compositions and more primitive Nd isotope values in the south. The Iwoonut pluton (94StL-1) has ε_{Nd} of -0.35 and initial $^{87}Sr/^{86}Sr$ of 0.7063. The granite and the monzodiorite samples therefore both have ε_{Nd} near bulk earth. This is similar to the isotope composition of the mafic root of the Kigluaik pluton on Seward Peninsula (fig. 7).

CRETACEOUS VOLCANIC ROCKS

Mid-Cretaceous volcanic rocks are exposed throughout western St. Lawrence Island. Rock types include trachy-basalt, abundant trachy-andesite, trachydacite, and rhyolite (figs. 3, 4). These rocks are found as flows, tuffs, and volcaniclastic rocks. The Cretaceous volcanic rocks are intruded by the Sevuokuk pluton and display hornfels contact metamorphism (Patton and Csejtey, 1971). Felsic dikes were observed cutting the volcanic rocks, particularly at coastal exposures west of Boxer Bay.

Many of the samples collected in the Boxer Bay area are porphyries. The trachydacite has phenocrysts of plagioclase, altered amphibole, and resorbed quartz. The trachyandesite is similar but has fewer resorbed quartz phenocrysts. The five analyzed samples had silica contents ranging from 53.4 percent to 75.6 percent (fig. 4; table 4). Total alkalies range from 6 percent to 8 percent, placing these rocks in the trachytic series. CaO, MgO, Al_2O_3, Sr, and Ba all decrease linearly with silica.

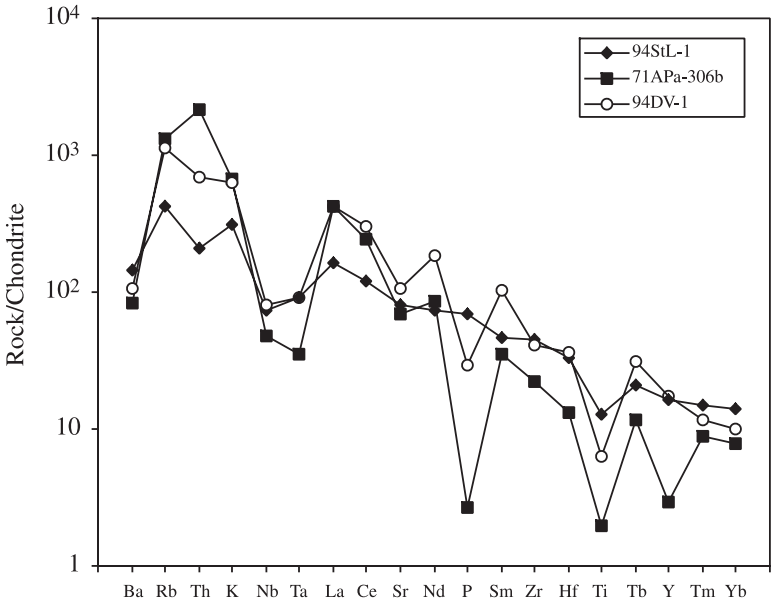

Figure 6. *Chondrite-normalized trace element 'spider' plot of the St. Lawrence Island monzodiorite (Iwoonut pluton) and nepheline syenite, as well as the syenite of Cape Dezhnev, Russia. Troughs at Nb, Ta, and Ti are typical of arc-related igneous rocks. Normalization factors from Thompson (1982).*

Table 3. *Isotope data from selected plutonic rocks on St. Lawrence Island*

Sample	Concentration			Atomic Ratio	Measured Ratio[b]	Initial Ratio[c]	Concentration ppm		Atomic Ratio	Measured Ratio	$\varepsilon_{Nd}(T)$[d]
	SiO_2 wt. %	Rb ppm	Sr ppm	$^{87}Rb/^{86}Sr$	$^{87}Sr/^{86}Sr$	$^{87}Sr/^{86}Sr$	Sm	Nd	$^{147}Sm/^{144}Nd$	$^{143}Nd/^{144}Nd$	
94StL-1	53.3	153	923	0.48	0.707023 ± 07	0.70633	8.72	47.95	0.1099	0.512562 ± 06	-0.35
94StL-8a	66.1	161	645	0.72	0.707020 ± 08	0.70599	4.72	27.38	0.1042	0.512539 ± 06	-0.75
94StL-19	73.0	191	292	1.89	0.710560 ± 08	0.70760	2.43	15.43	0.0951	0.512407 ± 06	-3.09

[a]Values used for chondritic uniform reservoir (CHUR) are $^{143}Nd/^{144}Nd = 0.512638$, $^{147}Sm/^{144}Nd = 0.1967$. Decay constants are Sm, 6.54E-12 yr^{-1}; Rb, 1.42E-11 yr^{-1}. Sm and Nd concentrations were determined by isotope dilution by addition of a mixed ^{149}Sm-^{150}Nd spike prior to sample dissolution. Rb and Sr concentrations determined by XRF (at NMSU). Repeated analysis (>80) of SRM-987 yielded $^{87}Sr/^{86}Sr = 0.710247 \pm 10$. Repeated analysis (>20) of BCR-1 yielded $^{143}Nd/^{144}Nd = 0.512633 \pm 10$.

[b]Ratios are corrected for mass fractionation by normalizing to $^{86}Sr/^{88}Sr = 0.1194$.

[c]All errors in measured isotopic ratios are at the 95% confidence limit. Corrected for mass fractionation by normalizing to $^{146}Nd/^{144}Nd = 0.72190$. Initial ratios were calculated at 102 Ma (94StL-1), 100 Ma (94StL-8a), and 110 Ma (94StL-19).

[d]$\varepsilon_{Nd}(T) = \{[^{143}Nd/^{144}Nd(T)sample/^{143}Nd/^{144}Nd(T)_{CHUR}] - 1\} \times 10{,}000$, at ages listed above.

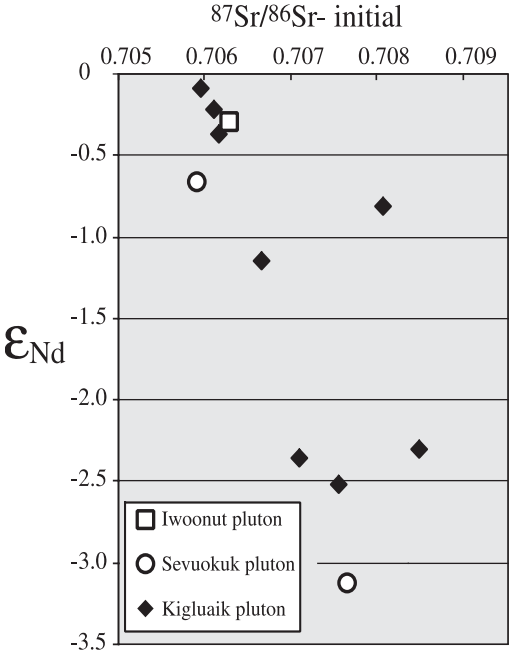

Figure 7. *Sr and Nd isotope data from the Sevuokuk and Iwoonut plutons, initial isotope ratios calculated at 108 Ma. Also plotted are data for the Kigluaik pluton, calculated at 90 Ma (Amato and Wright, 1997). Both samples from St. Lawrence Island that plot at ε_{Nd} near 0 are from the Boxer Bay area.*

Table 4. *Whole-rock geochemistry from volcanic rocks*

Location	**St. Lawrence Island**					**St. Lawrence**	**OCVB**
Unit	**Kva**	**Kva**	**Kva**	**Kva**	**Kvr**	**average**	**average**
Sample	**94StL-15**	**94StL-4**	**94StL-16**	**94StL-5**	**94StL-6**	**andesite**	**rock**
SiO_2	53.40	62.56	63.77	66.72	74.77	66.10	65.29
TiO_2	1.13	0.72	0.66	0.56	0.12	0.66	0.69
Al_2O_3	18.11	16.83	15.76	15.06	12.37	16.32	15.68
Fe_2O_3[b]	6.76	4.58	4.34	3.52	1.46	4.26	5.95
MnO	0.12	0.14	0.06	0.06	0.05	0.09	0.06
MgO	2.96	1.27	1.65	1.03	0.71	1.35	2.20
CaO	7.17	4.68	2.50	2.94	0.56	3.46	4.03
Na_2O	3.62	3.63	3.83	4.01	3.24	3.93	3.23
K_2O	2.42	3.01	3.65	3.90	4.83	3.62	2.87
P_2O_5	0.38	0.22	0.20	0.16	0	0.20	
LOI[c]	4.23	2.71	3.39	1.91	0.85		
Total	**100.29**	**100.35**	**99.81**	**99.89**	**98.98**	**100.0**	**100.0**
V	134	88	94	52	14		
Cr	23	bd	bd	bd	10		
Ni	bd	bd	bd	bd	11		
Cu	15	7	7	5	9		
Zn	80	89	71	87	38		
Rb	57	71	110	110	216		
Sr	1,224	876	744	664	48		
Y	30	21	23	25	24		
Zr	288	183	208	207	149		
Nb	13	12	13	11	22		
Ba	1,281	825	863	817	78		

[a]See figures 2 and 3 for sample localities and unit designations. St. Lawrence average andesite is the average anhydrous composition of samples 94-StL-4, -16, and –5. OCVB average rock is the average composition of the Okhotsk-Chukotk volcanic belt (Ustiev, 1965, reported in Kosygin and Parfenov, 1981). See table 1 for analytical details.
[b]All Fe was calculated as Fe_2O_3.
[c]LOI (loss on ignition) determined by weight loss after heating at 1,000°C for 20 minutes.

The volcanic rocks were mapped in the vicinity of Boxer Bay and display variable dips suggesting tilting along fault blocks (fig. 3). No folds were observed and each outcrop of layered volcanic rocks displayed consistent attitudes. Most of the beds strike northwest and dip ≈25–45 degrees southwest, with a few that dip southeast, west, and northeast (figs. 1, 3). If the tilting is related to faults, the faults should strike northwest as well. However, no faults were directly observed in the field.

GEOCHRONOLOGY

PUBLISHED AGES

Previously published K–Ar data for the calc–alkaline Cretaceous plutons on St. Lawrence Island include biotite dates ranging from 108 ± 3 Ma to 93.5 ± 3 Ma (Patton and Csejtey, 1980). For one pluton, a hornblende date is analytically indistinguishable from a biotite date (Patton and Csejtey, 1980), suggesting shallow emplacement and rapid cooling. Thus, the K–Ar dates probably approximate the age of intrusion, though no U–Pb ages have been determined for any of the plutons to confirm this. The plutons are thought to be generally younger than the volcanic rocks, but may overlap in age with the oldest volcanic rocks. In the area north of Taveeluk Point (fig. 3), the diorite pluton probably cuts the volcanic cover. Although Patton and Csejtey (1980) reported that the monzodiorite north of Iwoonut Point cuts the adjacent andesite, we found instead that andesite appears to be cut by a granite intrusion (fig. 3). Previously published K–Ar ages for Cretaceous–Tertiary volcanic rocks on St. Lawrence Island are 90.9 ± 3 Ma, 64.4 ± 2 Ma, 62.1 ± 2 Ma, and 39.3 ± 1 Ma (Patton and Csejtey, 1980).

NEW DATA

We present four new $^{40}Ar/^{39}Ar$ biotite ages from St. Lawrence Island, and one from Cape Dezhnev in Russia. The nepheline syenite from St. Lawrence Island has a biotite spectrum that is generally flat, although it does not fit the commonly accepted definition of a plateau (McDougall and Harrison, 1988) because steps in the central part are slightly older than adjacent ones (fig. 8; table 5). The pseudo-plateau age of this sample is 113 ± 1 Ma. This is a reliable age since it is within error of the total fusion age and the isochron age, albeit the fit of the isochronal line to the data is not ideal. The nepheline syenite unit is important because it provides another link between Alaska and Russia: potassic rocks of similar age are exposed on the Seward Peninsula, St. Lawrence

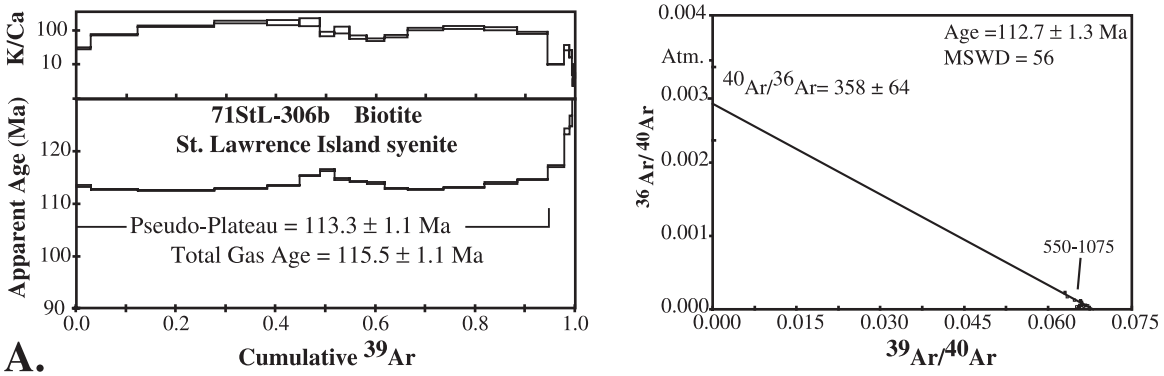

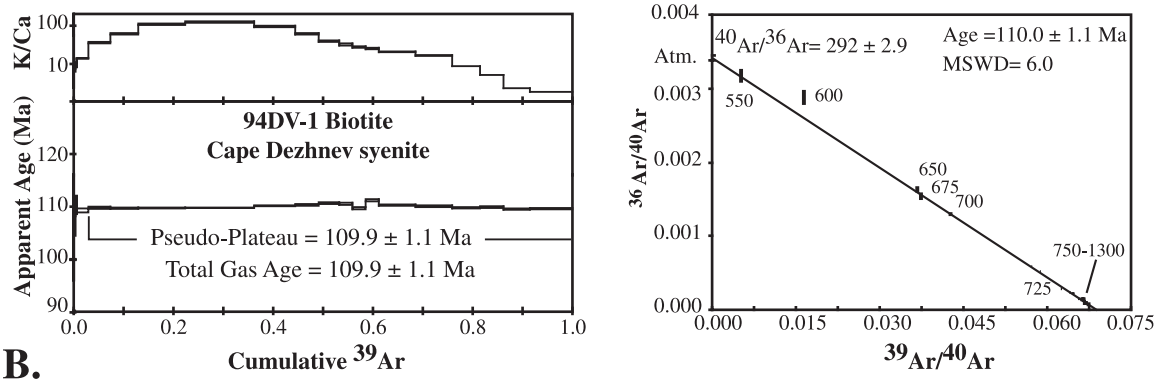

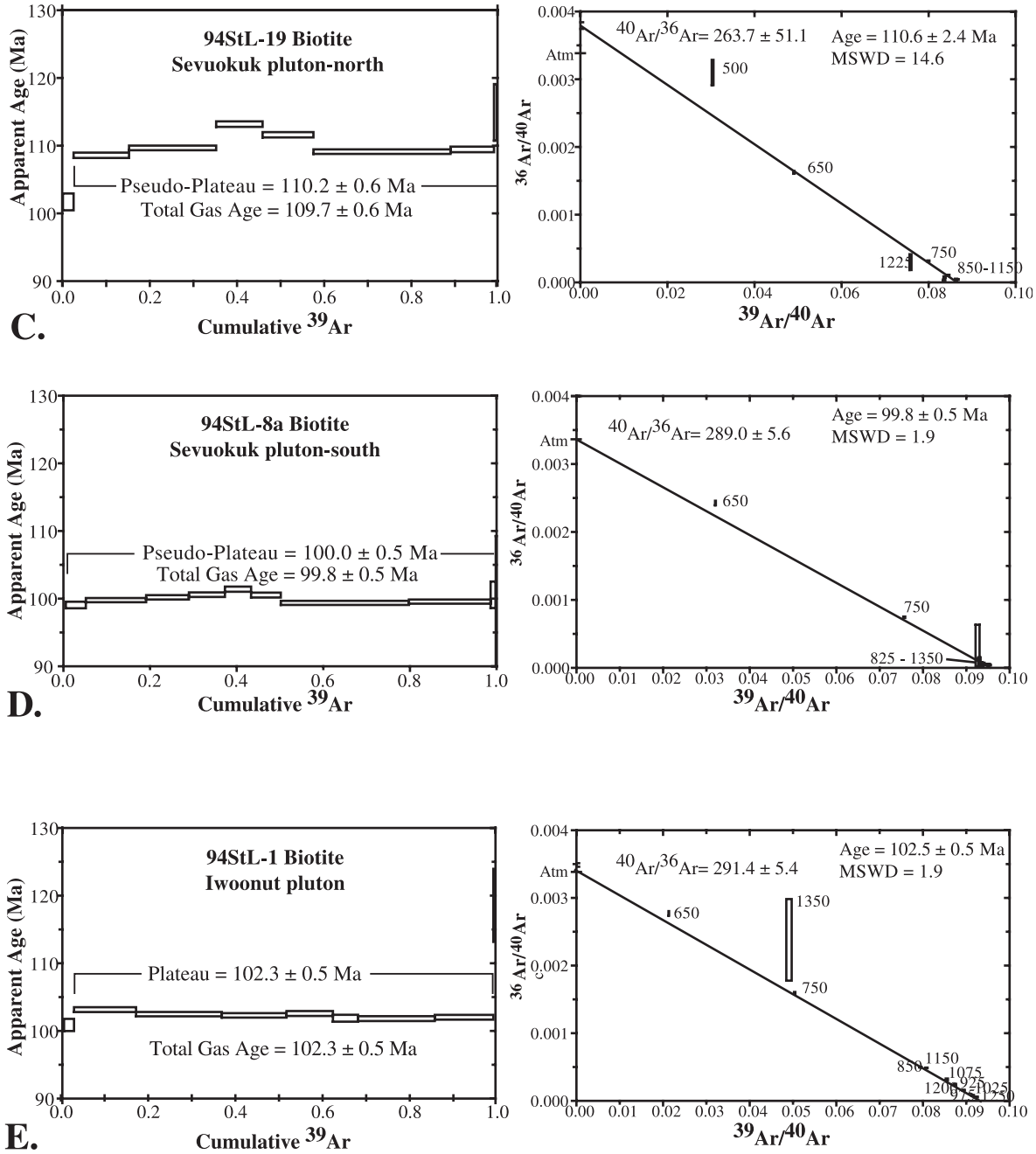

Figure 8. *$^{40}Ar/^{39}Ar$ age spectra, apparent K/Ca ratios, and inverse isochron plots of biotite samples from alkalic rocks from the Bering Strait region. See figures 1 and 2 for sample localities. "Pseudo-Plateau" refers to the Weighted Mean Plateau Age calculated using the portion of the spectrum marked. Some of these spectra do not fit the commonly accepted definition of a plateau (McDougall and Harrison, 1988) because they have a central hump. "MSWD" stands for Mean Square Weighted Deviation, a measure of the of fit of the isochron (Wendt and Carl, 1991). In A, B, and E, MSWD is larger than expected for well-behaved data. (A) syenite of Cape Dezhnev of easternmost Chukotka Peninsula; (B) nepheline syenite of Saint Lawrence Island; (C) granite from the northern end of the Sevuokuk pluton; (D) granodiorite from the southern end of the Sevuokuk pluton; (E) monzodiorite from St. Lawrence Island.*

Table 5. *Argon data for sample 71APa-306b*

T (°C)	40(mol)	40/39	37/39	36/39	K/Ca	Σ^{39}Ar	^{40}Ar*	Age (Ma)
550	5.2e14	15.0087	0.0167	0.0037	29	0.030	0.933	113.4 ± 1.1
600	1.6e13	14.9073	0.0066	0.0017	74	0.124	0.968	112.6 ± 1.1
650	2.6e13	14.8796	0.0037	0.0018	133	0.277	0.966	112.4 ± 1.1
675	1.8e13	14.9484	0.0028	0.0014	178	0.382	0.973	112.9 ± 1.1
700	l.le13	15.0236	0.0028	0.0008	174	0.447	0.985	113.5 ± 1.1
725	7.0e14	15.2729	0.0027	0.0007	182	0.488	0.988	115.3 ± 1.1
750	4.9e14	15.4244	0.0062	0.0005	79	0.517	0.990	116.4 ± 1.1
775	5.1e14	15.1903	0.0047	0.0008	105	0.547	0.984	114.7 ± 1.1
800	5.8e14	15.1221	0.0077	0.0008	63	0.581	0.984	114.2 ± 1.1
825	6.1e14	15.0746	0.0092	0.0007	53	0.618	0.987	113.8 ± 1.1
850	7.7e14	14.9357	0.0072	0.0009	68	0.664	0.982	112.8 ± 1.1
875	1.2e13	14.9062	0.0045	0.0007	110	0.736	0.986	112.6 ± 1.1
900	1.4e13	14.9650	0.0040	0.0012	123	0.817	0.978	113.0 ± 1.1
925	l.le13	15.0800	0.0044	0.0020	113	0.884	0.962	113.9 ± 1.1
950	l.le13	15.1713	0.0058	0.0028	85	0.945	0.949	114.5 ± 1.1
1000	5.8e14	15.5192	0.0501	0.0024	9.8	0.978	0.957	117.1 ± 1.1
1025	2.1e14	16.4242	0.0158	0.0024	31	0.988	0.958	123.7 ± 1.3
1050	9.9e15	16.7013	0.0234	0.0022	21	0.994	0.963	125.7 ± 1.6
1075	3.0e15	20.8910	0.0661	0.0091	7.4	0.995	0.886	155.9 ± 4.5
1100	2.2e15	29.9104	0.1690	0.0115	2.9	0.996	1.000	219.3 ± 6.9
1300	3.3e14	66.4827	0.1053	0.0024	4.7	1.000	0.989	455.6 ± 4.2

Sample locality: 63° 16.2'N, 170° 13.0' W
Total fusion age = 115.46 ± 1.11 Ma (including J)
Weighted mean plateau age = 113.33 ± 1.09 Ma (including J)
Inverse isochron age = 112.68 ± 1.28 Ma (MSWD = 56.04; ^{40}Ar/^{36}Ar = 357.6 ± 63.7)
Steps used: 550, 600, 650, 675, 700, 725, 750, 775, 800, 825, 850, 875, 900, 925, 950, (115/21 or 94% Σ^{39}Ar)
40(mol) = moles corrected for blank and reactor-produced ^{40}Ar
Σ^{39}Ar is cumulative
^{40}Ar* = radiogenic fraction
J = 0.0043210
Steps Used refers to the heating steps used to calculate the plateau age. These spectra do not fit the usual definition of a plateau since the central steps are not within error of each other (McDougall and Harrison, 1988).

The following is a summary of key laboratory procedures: Two sets of biotite separates were analyzed in different labs with similar protocols. Group 1 samples included 71StL-306b and 94DV-1 and were analyzed by Toro in the laboratory of M. McWilliams at Stanford University. Group 2 samples included 94STL-1, 8A and 19 and were analyzed by Calvert at the USGS-Menlo Park. The laboratories have identical mass spectrometers and similar extraction lines. Clean 1-5 mg of each biotite separate were packaged in Cu foil and irradiated at the TRIGA reactor at the University of Oregon (Group 1) or USGS-Denver (Group 2). The laboratory equipment used and analytical procedures followed are those described by Hacker and Wang (1995). The mass-spectrometer data were corrected for neutron flux gradient using the sanidine standard 85G003 with assigned age of 27.92 Ma (Group 1) or the sanidine standard TCR-2 with an assigned age of 27.87 Ma. Both standards are calibrated to SB-3 biotite with an age of 162.9 ± 0.9 Ma determined by first principles (Lanphere and Dalrymple, 2000). All the analyses were corrected for decay since irradiation, mass discrimination, and interference of Cl-, Ca-, and K- produced Ar isotopes. Ca corrections were not applied to Group 2 samples due to a nine-month delay between irradiation and analysis. Uncertainties reported are one sigma, determined using the uncertainties in: monitor age, decay rates of ^{37}Ar, ^{39}Ar, and ^{40}Ar, rates of reactor-produced Ar-isotopes, duration of irradiation, time since irradiation, peak heights, blank values, and irradiation parameter J.

Island, and the Chukotka Peninsula. For comparison, we also dated a syenite from Cape Dezhnev, Chukotka Peninsula, Russia (Perchuk, 1965). This rock contains potassium feldspar with accessory biotite, amphibole, pyroxene, and titanite. Biotite from this sample gives a $^{40}Ar/^{39}Ar$ age of 110 ± 1 Ma, and this age is within error of the total fusion age and isochron age (table 6). This pluton intrudes regionally unmetamorphosed Paleozoic carbonate rocks and therefore appears to have been emplaced at high crustal levels. The intrusive age is therefore probably close to the biotite age. We dated two samples from the Sevuokuk pluton on St. Lawrence Island. A granite from the northern part of the pluton has a biotite age of 110 ± 0.6 Ma (table 7), whereas a granodiorite from the southern part of the pluton is 100 ± 0.5 Ma (table 8). This, along with the Sr and Nd isotope data, suggests that this pluton is probably a composite of smaller intrusions. Alternatively, the southern edge may have been reheated by younger plutons such as the Iwoonut pluton, which has a biotite age of 102 Ma (table 9). The Iwoonut pluton is more alkaline than the Sevuokuk pluton but less potassic than the nepheline syenite, so it is interesting that it has a much younger age than the syenite.

DISCUSSION

PETROGENESIS OF THE POTASSIC SUITE

The age and compositional similarities of the nepheline syenites on St. Lawrence Island and Cape Dezhnev suggest that the two plutons are part of the same suite of potassic–ultrapotassic rocks present on the Seward Peninsula and western Yukon–Koyukuk basin (Miller, 1972). The biotite $^{40}Ar/^{39}Ar$ ages of 113 ± 1 Ma (St. Lawrence) and 110 ± 1 Ma (Deznev) reported here probably approximate the intrusive age because in each case, the plutons intrude upper crustal sequences of Paleozoic carbonate rocks. On St. Lawrence Island, the carbonate rocks are contact metamorphosed to marble adjacent to plutons. By contrast, the syenite in the Kigluaik Mountains of the Seward Peninsula intrudes an upper-amphibolite-facies gneissic sequence and is itself pervasively deformed. Thus the U–Pb zircon age of 110 ± 5 Ma on the Kigluaik metasyenite

Table 6. *$^{40}Ar/^{39}Ar$ data from Cape Dezhnev syenite biotite (94DV-1)*

T (°C)	40(mol)	40/39	37/39	36/39	K/Ca	$\Sigma^{39}Ar$	$^{40}Ar^*$	Age (Ma)
550	4.5e15	11.9823	0.0346	0.6013	14	0.000	0.063	91.1 ± 40.2
600	3.4e15	9.1129	0.0841	0.1757	5.8	0.001	0.149	69.7 ± 12.5
650	1.le14	14.0420	0.0718	0.0446	6.8	0.004	0.516	106.3 ± 2.1
675	1.le14	14.5822	0.0515	0.0412	9.5	0.008	0.545	110.3 ± 2.0
700	5.9e14	14.4399	0.0360	0.0305	14	0.029	0.616	109.2 ± 1.1
725	9.5e14	14.5090	0.0137	0.0102	36	0.074	0.828	109.7 ± 1.1
750	1.le13	14.5020	0.0081	0.0033	60	0.131	0.936	109.7 ± 1.1
775	1.7e13	14.5062	0.0046	0.0016	107	0.224	0.968	109.7 ± 1.1
800	2.5e13	14.5082	0.0040	0.0013	121	0.364	0.973	109.7 ± 1.1
825	1.5e13	14.5631	0.0052	0.0010	95	0.446	0.981	110.1 ± 1.1
850	8.5e14	14.5823	0.0081	0.0014	60	0.493	0.973	110.3 ± 1.1
875	7.2e14	14.6276	0.0127	0.0021	39	0.532	0.959	110.6 ± 1.1
900	5.4e14	14.6157	0.0153	0.0022	32	0.561	0.957	110.5 ± 1.1
925	4.8e14	14.5011	0.0180	0.0034	27	0.587	0.936	109.7 ± 1.1
950	5.le14	14.7050	0.0196	0.0044	25	0.614	0.919	111.2 ± 1.1
1000	1.4e13	14.5803	0.0239	0.0035	20	0.687	0.934	110.3 ± 1.1
1025	1.3e13	14.5504	0.0302	0.0015	16	0.760	0.970	110.0 ± 1.1
1050	9.9e14	14.5109	0.0582	0.0015	8.4	0.815	0.971	109.8 ± 1.1
1075	8.4e14	14.5237	0.0963	0.0020	5.1	0.862	0.961	109.9 ± 1.1
1100	9.8e14	14.4775	0.2192	0.0020	2.2	0.916	0.962	109.5 ± 1.1
1300	1.7e13	14.4846	0.2747	0.0087	1.8	1.000	0.850	109.6 ± 1.1

Sample locality: large beach cobble (float) at town of Uelen, just west of Cape Dezhnev massif, at approximately 66° 9.4' N, 169°47.7' W
Total fusion age = 109.89 ± 1.06 Ma (including J)
Weighted mean plateau age = 109.90 ± 1.06 Ma (including J)
Inverse isochron age = 109.99 ± 1.07 Ma. (MSWD = 6.04; $^{40}Ar/^{36}Ar$ = 292.0 ± 2.9)
Steps used: 550, 600, 650, 675, 700, 725, 750, 775, 800, 825, 850, 875, 900, 925, 950, 1000, 1025, 1050, 1075, 1100, 1300, (100% $\Sigma^{39}Ar$)
40(mol) = moles corrected for blank and reactor-produced ^{40}Ar, $\Sigma^{39}Ar$ is cumulative
$^{40}Ar^*$ = radiogenic fraction
J = 0.0043230
Laboratory procedures as in table 5.

Table 7. *Argon data for sample 94StL-19*

T (°C)	40(mol)	40/39	37/39	36/39	K/Ca	S^{39}Ar	^{40}Ar*	Age (Ma)
500	3.76e-16	32.31615	27.67438	0.10748	0.017	1.61e-3	0.84	27.19 ± 17.70
650	2.19e-14	20.32660	5.12577	3.4380e-2	0.095	2.61e-2	0.520	101.70 ± 1.24
750	1.22e-13	12.51290	0.57914	4.1180e-3	0.846	0.15	0.906	108.58 ± 0.39
850	1.93e-13	11.83069	1.04710	1.5499e-3	0.468	0.35	0.967	109.67 ± 0.34
920	1.06e-13	11.93289	4.98020	1.7683e-3	0.098	0.46	0.988	113.18 ± 0.41
1000	1.15e-13	11.95301	1.00848	1.2455e-3	0.486	0.58	0.975	111.61 ± 0.39
1100	3.02e-13	11.53938	1.38319	8.6260e-4	0.354	0.89	0.987	109.12 ± 0.34
1150	9.61e-14	11.57692	2.27252	1.1302e-3	0.215	0.99	0.986	109.44 ± 0.41
1225	6.52e-15	12.97735	24.39807	1.0374e-2	0.020	1.00	0.911	114.92 ± 4.18
1350	2.49e-15	11.80206	185.3965	3.8440e-2	0.002	1.00	0.127	162.02 ± 15.27

Sample locality: 63° 16.62' N, 171° 41.58' W
Total fusion age = 109.7 ± 0.6 Ma (including J)
Weighted mean plateau age = 110.2 ± 0.6 Ma (including J)
Inverse isochron age = 110.6 ± 2.4 Ma (MSWD = 14.6; ^{40}Ar/^{36}Ar = 263.7 ± 51.1)
Steps used: 650, 750, 850, 920, 1000, 1100, 1150, 1225 (99.8% Σ^{39}Ar)
40(mol) = moles corrected for blank and reactor-produced 40Ar
Σ^{39}Ar is cumulative
^{40}Ar* = radiogenic fraction
J = 0.005471887

Steps Used refers to the heating steps used to calculate the plateau age. These spectra do not fit the usual definition of a plateau since the central steps are not within error of each other (McDougall and Harrison, 1988).
Laboratory procedures as in table 5.

Table 8. *Argon data for sample 94StL-8a*

T (°C)	40(mol)	40/39	37/39	36/39	K/Ca	Σ^{39}Ar	^{40}Ar*	Age (Ma)
650	1.04e-14	31.15818	1.24838	7.5904e-2	0.392	5.48e-3	0.283	85.16 ± 2.94
750	1.03e-13	13.21974	0.52390	9.9811e-3	0.935	5.17e-2	0.779	99.06 ± 0.48
825	3.12e-13	10.79145	0.46344	1.4859e-3	1.057	0.19	0.962	99.78 ± 0.31
875	2.22e-13	10.65180	0.62153	9.0939e-4	0.788	0.29	0.979	100.19 ± 0.32
925	1.88e-13	10.62200	0.81480	7.2304e-4	0.601	0.37	0.985	100.58 ± 0.34
975	1.38e-13	10.66914	1.26236	7.1767e-4	0.388	0.43	0.989	101.40 ± 0.38
1050	1.55e-13	10.70268	0.40500	8.9780e-4	1.210	0.50	0.977	100.53 ± 0.36
1125	6.60e-13	10.51632	-0.09828	5.3964e-4	0.000	0.80	0.983	99.37 ± 0.30
1175	4.22e-13	10.48835	0.55611	5.6622e-4	0.881	0.99	0.987	99.56 ± 0.31
1225	2.69e-14	10.76211	-0.36526	8.6065e-4	0.000	1.00	0.973	100.57 ± 1.96
1350	4.13e-15	10.75917	6.74850	4.1824e-3	0.072	1.00	0.934	97.05 ± 12.2

Sample locality: 63° 21.15' N, 171° 38.40' W
Total fusion age = 99.8 ± 0.5 Ma (including J)
Weighted mean plateau age = 100.0 ± 0.5 Ma (including J)
Inverse isochron age = 99.8 ± 0.5 Ma (MSWD = 1.9; ^{40}Ar/^{36}Ar = 289.0 ± 5.6)
Steps used: 750, 825, 875, 925, 975, 1050, 1125, 1175, 1225, 1350 (99% Σ^{39}Ar)
40(mol) = moles corrected for blank and reactor-produced 40Ar
Σ^{39}Ar is cumulative
^{40}Ar* = radiogenic fraction
J = 0.005476958

Steps Used refers to the heating steps used to calculate the plateau age. These spectra do not fit the usual definition of a plateau since the central steps are not within error of each other (McDougall and Harrison, 1988).
Laboratory procedures as in table 5.

Table 9. *Argon data for sample 94StL-1*

T (°C)	40(mol)	40/39	37/39	36/39	K/Ca	Σ^{39}Ar	^{40}Ar*	Age (Ma)
650	4.66e-15	46.72708	5.73365	0.13100	0.085	3.90e-3	0.181	82.09 ± 4.45
750	3.41e-14	19.82766	2.12449	3.2181e-2	0.230	2.70e-2	0.528	100.88 ± 0.90
850	2.17e-13	12.58896	1.07384	6.5598e-3	0.456	0.17	0.852	103.15 ± 0.36
925	2.97e-13	11.19158	0.74873	1.9786e-3	0.654	0.37	0.952	102.48 ± 0.32
975	2.24e-13	10.82400	1.09573	9.0042e-4	0.447	0.52	0.983	102.30 ± 0.33
1025	1.61e-13	10.93029	0.97460	1.1252e-3	0.502	0.62	0.976	102.58 ± 0.36
1075	8.65e-14	11.69304	1.34054	4.0654e-3	0.365	0.68	0.906	101.88 ± 0.51
1150	2.64e-13	12.37750	0.51819	6.1637e-3	0.945	0.86	0.855	101.82 ± 0.36
1200	2.02e-13	11.44704	0.58438	2.9614e-3	0.838	1.00	0.927	102.02 ± 0.35
1250	7.47e-15	12.05182	28.08018	7.0846e-3	0.017	1.00	1.009	118.58 ± 5.38
1350	5.89e-16	17.07258	239.1862	0.10423	0.002	1.00	0.297	58.84 ± 34.7

Sample locality: 63° 20.09'N, 171° 33.44' W
Total fusion age = 102.3 ± 0.5 Ma (including J)
Weighted mean plateau age = 102.3 ± 0.5 Ma (including J)
Inverse isochron age = 102.5 ± 0.5 Ma (MSWD = 1.9; ^{40}Ar/^{36}Ar = 291.4 ± 5.4)
Steps used: 750, 850, 925, 975, 1025, 1075, 1150, 1200, 1250, 1350 (97% Σ^{39}Ar)
40(mol) = moles corrected for blank and reactor-produced ^{40}Ar
Σ^{39}Ar is cumulative
^{40}Ar* = radiogenic fraction
J = 0.005482029
Steps Used refers to the heating steps used to calculate the plateau age.
Laboratory procedures as in table 5.

is probably within error of the intrusive ages of the St. Lawrence and Dezhnev syenites. The apparent eastward younging trend of ages for the rest of the suite is speculative given the uncertainties in the K–Ar dates, but these preliminary data suggest that the entire suite is probably between 105 and 115 Ma (fig. 9).

The initial study of potassic intrusions in the Bering Strait region emphasized that these plutons intruded along a tectonic boundary between the Yukon–Koyukuk basin and Seward Peninsula (Miller, 1972). This boundary is marked by mafic igneous rocks that probably originated as part of an oceanic crustal sequence, and it was subsequently described as a terrane boundary separating the continental Arctic Alaska terrane (including most of northern Alaska, the Seward Peninsula, and probably the Chukotka Peninsula) from the oceanic Angayucham terrane. Many of the potassic plutons of the Yukon–Koyukuk Basin and the eastern Seward Peninsula are located near this boundary. Because the Triassic rocks of St. Lawrence Island have been correlated with the Angayucham terrane, the nepheline syenite of St. Lawrence Island may have been emplaced close to this same boundary although St. Lawrence Island now lies considerably south of the equivalent boundary along the south flank of the Brooks Range. In addition, the Shalaurova granite on Bol'shoi Lyakhov Island in northern Russia is 113 Ma. This was inferred to be a subduction-related intrusion based on trace-element geochemistry, and it is located along the South Anyui suture, which separates Arctic Alaska–Chukotka from the Kolyma–Omolon block (Layer and others, 2001).

These potassic–ultrapotassic plutons are compositionally similar and coeval and therefore serve as a distinctive lithology that correlates across (stitches) the Arctic Alaska–Angayucham terrane boundary. Chukotka Peninsula, St. Lawrence Island, Seward Peninsula, and the Yukon–Koyukuk basin therefore must all have been contiguous since at least Aptian–Albian time. The limited exposures in the Bering Strait region preclude the use of this suite in a rigorous paleo-geographic reconstruction, particularly without knowing whether the plutons had a distribution that was originally linear or curvilinear.

A previous model for the petrogenesis of these potassic–ultrapotassic rocks invoked partial melting of the subcontinental mantle beneath the Seward Peninsula and the western Yukon–Koyukuk basin (Miller, 1972; 1989). This melting event was thought to be related to the same system as the OCVB subduction zone (Miller, 1989) or possibly related to melting of subduction-modified mantle or lower crustal arc rocks in an unspecified tectonic setting (Miller, 1989; Arth and others, 1989).

Current models for potassic and ultrapotassic magmatism invoke mantle metasomatism (Wass and Rogers, 1980; Foley and others, 1987) and small degrees of partial melting of the mantle (Rogers and others, 1985) to produce these unusual compositions. In this region, a Late Jurassic–Early Cretaceous south-dipping subduction zone (present coordinates) was associated with the

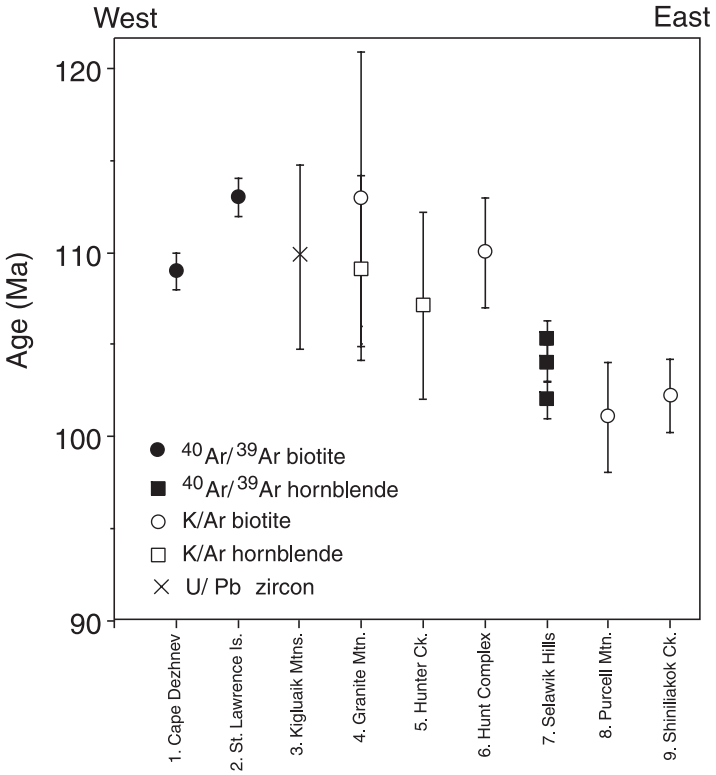

Figure 9. *Summary of geochronology from potassic intrusive rocks in the Bering Strait region. Dates are plotted in relative east–west position (not to scale) projected onto a line at about 65°N latitude. Data sources: 1 and 2, this study; 3, Amato and Wright (1998); 4, Miller (1971) and Patton (1967); 5, Patton (1967); 6, Patton and Miller (1968); 7, Solie and Layer (1993); 8 and 9, Miller and others (1966); see Miller (1989) for a summary of many of these dates.*

collision of the Yukon–Koyukuk arc with the Arctic Alaska terrane (for example, Moore and others, 1994). After collision, a new north-dipping subduction zone developed in this area and created an Albian and younger arc system in the Bering Strait region. The chondrite-normalized trace-element distribution shows a pattern that is similar to most 'orogenic' or subduction-related potassic rocks. This suite of plutons is geochemically similar to the 'Group III' ultrapotassic rocks in the classification of Foley and others (1987), although MgO concentrations tend to be lower in the Bering Strait suite compared to the type examples from the Roman Province of Italy (for example, Peccerillo, 1985). The onset of north-directed (present coordinates) subduction in the Bering Strait region may have produced a low volume of magmatism with compositions resulting from small degrees of partial melting of the mantle. Subsequent magmatism may have been characterized by greater degrees of partial melting with a higher volume of magma that was less potassic than the early phase, but still elevated in potassium relative to typical arc rocks. This association of potassic and subalkaline compositions is also present in the subduction-related Roman province (Peccerillo, 1985). The arc-type chemistry of the plutonic rocks is not likely to be related to partial melting of arc rocks, as has been suggested for some of the plutons in the Yukon–Koyukuk basin (Arth and others, 1989), because the crust on Seward Peninsula and Cape Dezhnev does not originate from an older arc complex.

The major and trace-element geochemistry of the sub-alkaline Cretaceous plutonic rocks and the trachytic volcanic rocks are similar. They display colinear trends on chemical variation diagrams for most elements, with the exception of uniformly higher Y values for the volcanic rocks. Despite the uncertainties regarding the ages of both of these suites of rocks, it appears that they are likely related to the same episode of magmatism in a similar tectonic setting.

Volcanic rocks are found throughout northeastern Russia as part of the subduction-related OCVB. The part of the OCVB nearest St. Lawrence Island is found in the area near the Senyavin Uplift north of Provideniya, Chukotka Peninsula, Russia (for example, Kryukov and Plyasunov, 1987; Calvert, 1999). In this area, a 300- to 500-m-thick section of andesite through rhyolite volcanic and volcaniclastic rocks is present with dips up to 30 degrees due to slip and rotation on normal faults (Calvert, 1999). Thicknesses of 1,850 m are reported for the area (Kryukov and Plyasunov, 1987). The ages of the volcanic rocks were difficult to determine because of reheating by plutons around 90 Ma, but a pre-110 Ma age is suggested on the basis of the age of the oldest crosscutting pluton (Calvert, 1999). Floral assemblages in volcaniclastic rocks are Albian to Cenomanian (112–93 Ma). Although a range of compositions from basalt to rhyolite are reported from the belt, most of the rocks are andesites, with potassic trachytic rocks and shoshonites also reported (Zakharov and Legeydo, 1976). The average

composition is similar to the composition of the andesites from St. Lawrence Island (table 4). The similarities between the volcanic rocks of the OCVB and St. Lawrence Island allow the inference that they both were generated in a convergent margin setting.

Continuous subduction-related magmatism along the paleo-Pacific ocean from 120 to 80 Ma has been well documented in areas such as Russia and Canada. We agree with Rubin and others (1995) that regional relations support continuous subduction beneath the Alaska sector of the belt as well. Cretaceous magmatism on the Seward Peninsula has been interpreted to have occurred within an arc setting (Amato and Wright, 1997). The volcanic rocks and associated subalkaline plutons on St. Lawrence Island are also interpreted as forming in an arc setting based on trace-element geochemistry (fig. 6) and the style of magmatism. The St. Lawrence Island volcanic rocks are linked spatially and temporally to the OCVB. The plutonic rocks on St. Lawrence Island appear to be chemically identical to these volcanic rocks and are therefore also part of the same system. The plutonic rocks on the Seward Peninsula are also chemically and isotopically similar to those on St. Lawrence Island (Amato and Wright, 1997). Thus we conclude that all the mid-Cretaceous igneous rocks of Chukotka Peninsula, St. Lawrence Island, Seward Peninsula, and western Yukon–Koyukuk basin are related to the same subduction system, with the early magmas being more potassic and subsequent magmatism yielding subalkaline compositions. The monzodiorite Iwoonut pluton on St. Lawrence Island can be considered transitional between these two compositional end-members.

DEFORMATION AND TECTONIC IMPLICATIONS

Contrary to previous assumptions that the Cretaceous plutons in Alaska are posttectonic, mid-Cretaceous magmatism in the Bering Strait region was coeval with extensional ductile deformation at depth as shown by relationships on Seward Peninsula and Chukotka Peninsula. On Seward Peninsula, intrusions with ages from 115 to 110 Ma are intensely deformed, whereas the 90-Ma Kigluaik pluton exposed in the core of the Kigluaik gneiss dome is undeformed (Amato and others, 1994). U–Pb monazite ages from similarly deformed metamorphic country rocks in the Kigluaik gneiss dome are 91 Ma. This age has been interpreted as reflecting the time of peak metamorphic temperatures that coincided with significant deformation (Amato and others, 1994). Ductile deformation therefore likely occurred post-110 Ma and pre-90 Ma, possibly culminating around 91 Ma.

In the Koolen metamorphic complex on the Chukotka Peninsula, U–Pb dating of monazite revealed that a 104-Ma pegmatite is deformed, whereas a 94-Ma granite is undeformed (BSGFP, 1997). Tilted Cretaceous volcanic rocks in the Senyavin uplift display a preponderance of northwest-striking beds, that dip northeast (fig. 1; Calvert, 1999). Normal faults have been mapped in the Senyavin area (Calvert, 1999) and the variable dips on the volcanic rocks are likely due to rotation of fault blocks. In the Senyavin Uplift, normal faulting and associated tilting of the OCVB rocks is thought to predate 85 to 95 Ma magmatism. The St. Lawrence Island plutonic rocks are not deformed, and on the basis of structural similarities with rocks from the OCVB, we infer that tilting of the volcanic rocks to dips as steep as 70 degrees likely occurred during this time.

The tectonic setting of Cretaceous deformation on the Seward Peninsula and Chukotka Peninsula has been controversial largely because exhumation of deep levels of the crust has removed upper-crustal brittle structures that may be more diagnostic of extension or contraction at this time. Although different crustal levels are exposed, Seward Peninsula, St. Lawrence Island, and Chukotka all have a similar geologic history that includes potassic magmatism during Aptian–Albian time, and therefore they all probably experienced a common mid-Cretaceous history. The system of normal faults associated with tilted volcanic rocks in the Senyavin uplift may also be responsible for tilting of volcanic rocks on St. Lawrence Island. These structures may represent the typical upper crustal response to extension in the Bering Strait region and were probably coeval with extensional ductile deformation in the Kigluaik Mountains and the surrounding Nome Group rocks (Miller and others, 1992; Amato and others, 1994). Normal faults in the York Mountains and the ≈83-Ma diabase dike swarm in the Kigluaik Mountains (Amato and Wright, 1998) may also indicate extension occurred at this time. Crustal extension above a subduction zone suggests that slab rollback may have been occurring at this time (Rubin and others, 1995; Dumitru and others, 1995; Amato and Wright, 1997).

CONCLUSIONS

On the basis of sparse geochronology, the Cretaceous magmatic history of St. Lawrence Island can be divided into an early phase of potassic plutonism around 113 Ma, coeval with ≈115 to 105 Ma potassic magmatism in the Bering Strait region, and a subsequent phase of larger-volume subalkaline magmatism between 110 and 100 Ma (and possibly younger) based on comparisons with plutonic rocks of similar composition in Russia and Alaska. The potassic pluton is part of a roughly east–west belt of similar alkaline plutons that stretches from Cape Dezhnev, Russia, to the western Yukon–Koyukuk basin. The $^{40}Ar/^{39}Ar$ biotite dates of 113 Ma (St. Lawrence) and

110 Ma (Dezhnev) indicate that these two plutons are coeval with the other plutons in the belt. ε_{Nd} and initial $^{87}Sr/^{86}Sr$ of the plutonic rocks are similar to values reported from the Kigluaik pluton on the Seward Peninsula. A subduction-related origin is proposed for both phases of magmatism on St. Lawrence Island on the basis of trace-element geochemistry and the regional geology. The early potassic plutons may represent small degrees of partial melting of lithosphere during the early phase of magmatism associated with a north-directed subduction system. Younger subalkaline magmatism may represent higher degrees of partial melting of the source region in the same tectonic setting. The tilted volcanic rocks of St. Lawrence Island are similar in lithology, geochemistry, and age to volcanic rocks in the Senyavin uplift of Chukotka and other volcanic rocks in the subduction-related Okhotsk–Chukotsk volcanic belt in Russia. Deformation associated with this magmatism in the Bering Strait region occurred in an extensional regime, possibly linked to slab rollback within the subduction zone.

ACKNOWLEDGMENTS

This project was funded by the Continental Dynamics Division of the National Science Foundation in conjunction with the International Division of the National Science Foundation, as part of award EAR-9317087-005 to E. Miller and S. Klemperer. Field work was carried out by Amato and Miller in 1994. Permission to work and sample on St. Lawrence Island was provided by A. Iwoorrigan and the Board of Directors of Sivuqaq, Inc. Logistical support was provided by J. Slwooko of Gambell, Alaska. The sample of the nepheline syenite on St. Lawrence Island was provided by B. Csejtey, U.S.Geological Survey. XRF data were collected with the assistance of N. McMillan at New Mexico State University. J. Wen helped prepare samples for strontium and neodymium isotopic analysis at Rice University. M. Quinn helped acquire rare-earth-element data at the University of Houston. Reviews by P. Layer and T. Moore were helpful and greatly appreciated.

REFERENCES

Amato, J.M., 1996, New $^{40}Ar/^{39}Ar$ and geochemical data from the mid-Cretaceous potassic intrusive belt in the Bering Strait Region: Syenites from northeastern Russia and St. Lawrence Island, Alaska: Geological Society of America Abstracts with Programs, v. 28, p. 482.

Amato, J.M., and Wright, J.E., 1997, Petrogenesis of the Kigluaik pluton: An isotopic study of Late Cretaceous arc-related potassic magmatism in northern Alaska: Journal of Geophysical Research, v. 102, p. 8065–8084.

Amato, J.M., and Wright, J.E., 1998, Geochronologic investigations of magmatism and metamorphism within the Kigluaik Mountains gneiss dome, Seward Peninsula, Alaska, *in* Clough, J.G., and Larson, Frank, eds., Short Notes on Alaskan Geology 1997: Alaska Division of Geological & Geophysical Surveys Professional Report 118, p. 1–21.

Amato, J.M., Wright, J.E., Gans, P.B., and Miller, E.L., 1994, Magmatically induced metamorphism and deformation in the Kigluaik gneiss dome, Seward Peninsula, Alaska: Tectonics, v. 13, p. 515–527.

Arth, J.G., Criss, R.E., Zmuda, C.C., Foley, N.K., Patton, W.W., Jr., and Miller, T.P., 1989, Remarkable isotopic and trace element trends in potassic through sodic Cretaceous plutons of the Yukon–Koyukuk Basin, Alaska, and the nature of crustal lithosphere beneath the Koyukuk terranes: Journal of Geophysical Research, v. 94, p. 15,957–15,968.

Belyi, V.F., Gelman, M.L., and Paraketov, K.V., 1989, Mesozoic volcanism and structure formation in the north-east USSR: Soviet Geology, v. N4, p. 62–78.

Bering Strait Geologic Field Party (BSGFP), 1997, Koolen metamorphic complex, NE Russia: Implications for the tectonic evolution of the Bering Strait Region: Tectonics, v. 16, p. 713–729.

Calvert, A.T., 1999, Metamorphism and exhumation of mid-crustal gneiss domes in the Arctic Alaska terrane: Santa Barbara, University of California, Ph.D. dissertation, 197 p., 24 figs.

Csejtey, Bela, Jr., and Patton, W.W., Jr., 1974, Petrology of the nepheline syenite of St. Lawrence Island, Alaska: U.S. Geological Survey Journal of Research, v. 2, p. 41–47.

Dumitru, T.A., Miller, E.L., O'Sullivan, P.B., Amato, J.M., Hannula, K.A., Calvert, A.T., and Gans, P.B., 1995, Cretaceous to Recent extension in the Bering Strait region, Alaska: Tectonics, v. 14, p. 549–563.

Evensen, N.M., Carlson, R.W., and O'Nions, R.K., 1978, Rare earth abundances in chondritic meteorites, Geochimica et Cosmochimica Acta, v. 42, p. 1199–1212.

Foley, S.F., Venturelli, G., Green, D.H., and Toscani, L., 1987, The ultrapotassic rocks: Characteristics, classification, and constraints for petrogenetic models: Earth-Science Reviews, v. 24, p. 81–134.

Forbes, R.B., Evans, B.W., and Thurston, S.P., 1984, Regional progressive high-pressure metamorphism, Seward Peninsula, Alaska: Journal of Metamorphic Geology, v. 2, p. 43–54.

Hacker, B.R., and Wang, Q., 1995, Ar/Ar geochronology of ultrahigh-pressure metamorphism in central China: Tectonics, v. 14, p. 994–1006.

Hannula, K.A., and McWilliams, M.O., 1995, Reconsideration of the age of blueschist facies meta-

morphism on the Seward Peninsula, Alaska, based on phengite $^{40}Ar/^{39}Ar$ results: Journal of Metamorphic Geology, v. 13, p. 125–139.

Jones, D.L., Silberling, N.J., Coney, P.J., and Plafker, George, 1987, Lithotectonic terrane map of Alaska (west of the 141st meridian): U.S. Geological Survey Miscellaneous Field Studies Map, MF-1874-A.

Kosygin, Y.A., and Parfenov, L.M., 1981, Tectonics of the Soviet far east, *in* Nairn, E.M., Churkin, M., and Stehli, F.G., eds., The Ocean Basins and Margins, v. 5, p. 377–412.

Kryukov Y.V., and Plyasunov, V.I., 1987, Federal geological map of USSR 1:200 000 scale. Sheet Q-2-XXV, Open-File report. Moscow: MINGEO USSR, 60 p. (in Russian)

Lane, H.R., and Ressmeyer, P.F., 1985, Mississippian conodonts, Lisburne Group, St. Lawrence Island, Alaska: American Association of Petroleum Geologists Bulletin, v. 69, p. 668.

Layer, P.W., Newberry, R.J., Fujita, K., Parfenov, L., Trunilina, V., and Bakharev, A., 2001, Tectonic setting of the plutonic belts of Yakutia, northeast Russia, based on $^{40}Ar/^{39}Ar$ geochronology and trace element geochemistry: Geology, v. 29, p. 167–170.

Le Bas, M.J., Le Maitre, R.W., Streckeisen, A., and Zenettin, B., 1986, A chemical classification of volcanic rocks based on the total alkali–silica diagram: Journal of Petrology, v. 27, p. 745–750.

McDougall, I., and Harrison, T.M., 1988, Geochronology and thermochronology by the $^{40}Ar/^{39}Ar$ method: New York, Oxford University Press, 212 p.

Miller, E.L., and Hudson, T.L., 1991, Mid-Cretaceous extensional fragmentation of a Jurassic–Early Cretaceous compressional orogen, Alaska: Tectonics, v. 10, p. 781–796.

Miller, E.L., Calvert, A.T., and Little, T.A., 1992, Strain-collapsed metamorphic isograds in a sillimanite gneiss dome, Seward Peninsula, Alaska: Geology, v. 20, p. 487–490.

Miller, T.P., 1972, Potassium-rich alkaline intrusive rocks of western Alaska: Geological Society of America Bulletin, v. 83, p. 2111–2128.

———1989, Contrasting plutonic rock suites of the Yukon–Koyukuk Basin and the Ruby Geanticline, Alaska: Journal of Geophysical Research, v. 94, p. 15969–15987.

Miller, T.P., 1994, Pre-Cenozoic plutonic rocks in mainland Alaska, *in* Plafker, George, and Berg, H.C., eds., The Geology of Alaska, The Geology of North America, v. G-1: Boulder, Geological Society of America, p. 535–554.

Moore, T.E., Wallace, W.K., Bird, K.J., Karl, S.M., Mull, C.G., and Dillon, J.T., 1994, Geology of Northern Alaska, *in* Plafker, George, and Berg, H.C., eds., The Geology of Alaska, The Geology of North America, v. G-1: Boulder, Geological Society of America, p. 49–140.

Natal'in, B.A., 1979, The tectonic nature of the metamorphic rock complex on the Chukotskiy Peninsula: Geologiya i Geofizika, v. 20, p. 31–38.

Patrick, B.E., and Evans, B.W., 1989, Metamorphic evolution of the Seward Peninsula blueschist terrane: Journal of Petrology, v. 30, p. 531–555.

Patton, W.W., Jr., and Box, S.E., 1989, Tectonic setting of the Yukon–Koyukuk Basin and its borderlands, western Alaska: Journal of Geophysical Research, v. 94, p. 15,807–15,820.

Patton, W.W., Jr., and Csejtey, Bela, Jr., 1980, Geologic map of St. Lawrence Island, Alaska: U.S. Geological Survey Miscellaneous Investigations Series Map I-1203.

———1971, Preliminary geologic investigations of western St. Lawrence Island: U.S. Geological Survey Professional Paper 664-C, p. C1–C15.

Patton, W.W., Jr., Box, S.E., and Moll-Stalcup, E.J., 1994, Geology of west-central Alaska, *in* Plafker, George, and Berg, H.C., eds., The Geology of Alaska, The Geology of North America, v. G-1: Boulder, Geological Society of America, p. 241–269.

Peccerillo, A., 1985, Roman comagmatic province (central Italy): Evidence for subduction-related magma genesis: Geology, v. 13, p. 103–106.

Perchuk, L.L., 1965, Magmatic replacement of carbonate bodies involving formation of nepheline syenites and other alkalic rocks, with example of Cape Dezhnev massif: International Geology Review, v. 7, p. 280–296.

Plafker, George, and Berg, H.C., 1994, Overview of the geology and tectonic evolution of Alaska, *in* Plafker, George, and Berg, H.C., eds., The Geology of Alaska, The Geology of North America, v. G-1: Boulder, Geological Society of America, p. 989–1022.

Roeske, S.M., Dusel-Bacon, Cynthia, Aleinikoff, J.N., Snee, L.W., and Lanphere, M.A., 1995, Metamorphic and structural history of continental crust at a Mesozoic collisional margin, the Ruby terrane, central Alaska: Journal of Metamorphic Geology, v. 13, p. 25–40.

Rogers, N.W., Keynes, M., Hawkesworth, C.J., Parker, R.J., and Marsh, J.S., 1985, The geochemistry of potassic lavas from Vulsini, central Italy, and implications for mantle enrichment processes beneath the Roman region: Contributions to Mineralogy and Petrology, v. 90, p. 244–257.

Rubin, C.M., Miller, E.L., and Toro, Jaime, 1995, Deformation of the northern circum-Pacific margin: Variations in tectonic style and plate-tectonic implications: Geology, v. 23, p. 897–200.

Sainsbury, C.L., 1969, Geology and ore deposits of the central York Mountains, western Seward Peninsula, Alaska: U.S. Geological Survey Bulletin 1287, 101 p.

Seager, W.R., 1981, Geology of Organ Mountains and southern San Andres Mountains, New Mexico: New Mexico Bureau of Mines and Mineral Resources Memoir 36, 97 pp.

Shuldiner, V.I., and Nedomolkin, V.F., 1976, Kristallicheskiy fundament Eskimosskogo massiva (Crystalline basement of the Eskimos massif): Sovetskaya Geologiya, v. 10, p. 38–47.

Solie, D.N., and Layer, P.W., 1993, Evidence of synmagmatic foliation in the Selawik Hills, northwest Alaska, based on $^{40}Ar/^{39}Ar$ age determinations: Geological Society of America Abstracts with Programs, v. 25, no. 5, p. 149.

Thompson, R.N., 1982, Magmatism of the British Tertiary Volcanic Province: Scottish Journal of Geology, v. 18, p. 50–107.

Till, A.B., and Dumoulin, J.A., 1994, Geology of Seward Peninsula and Saint Lawrence Island, *in* Plafker, George, and Berg, H.C., eds., The Geology of Alaska, The Geology of North America, v. G-1: Boulder, Geological Society of America, p. 141–152.

Ustiev, E.K., 1965, Composition of primary magmas as exemplified by Cretaceous and Paleogene formations of the Okhotsk volcanic belt (in Russian): Dokl. Akad. Nauk. USSR Sr. Geol., v. 3, p. 3–19.

Wass, S.Y., and Rogers, N.W., 1980 Mantle metasomatism—Precursor to continental alkaline volcanism: Geochimica Cosmochimica Acta, v. 44, p. 1811–1823.

Wendt, I., and Carl, C., 1991, The statistical distribution of the mean square weighted deviation: Chemical Geology, v. 86, p. 275–285.

Zakharov, M.N., and Legeydo, V.A., 1976, Geochemical characteristics of Upper Cretaceous and Paleogene magmatic complexes in the transverse Turomchinsk downwarp (Okhotsk–Chukotsk volcanic belt): Geochemistry International, v. 13, p. 22–30.

Zonenshain, L.P., Kuzmin, M.I., and Natapov, L.M., 1990, Geology of the USSR: A plate tectonic synthesis: AGU Geodynamic Series, v. 21, 242 p.

ORE MINERALOGY AND MINERAL COMPOSITIONS FROM GOLDEN ZONE MINE, SOUTHCENTRAL ALASKA

Benjamin G. Gage[1] and Rainer J. Newberry[1]

ABSTRACT

The Golden Zone gold–arsenic–copper breccia pipe developed in a ~70 Ma quartz monzodiorite intrusion with affinities to potassic-reduced Late Cretaceous–early Tertiary magma series of Reed and Lanphere (1973). Mineralization at Golden Zone was coeval with 70-Ma events in southwestern Alaska such as Vinasale Mountain, and Shotgun and Donlin creeks. Mineralization at Golden Zone also bears many similarities with 90-Ma interior Alaska plutonic-related gold deposits, including a wide range of mineralization temperatures, an intimate relationship between gold and bismuth–tellurium minerals, a strong association of gold with arsenopyrite, and evidence for a low to very low oxidation–sulfidation state. Arsenopyrite geothermometry yields a range of temperatures from ~325°C–~500°C, and conditions changed from early, pyrrhotite- and bismuth-stable to later, pyrite-stable. Gold compositions change with time from early, high (>950) fineness to late, low (<500) fineness, but show no systematic pattern with respect to location within the pipe. Sphalerite geobarometry indicates a formation pressure of about 0.9 +/- 0.5 kb, equivalent to a depth of about 2.7 km. This depth is similar to that estimated for shallow Fairbanks-area deposits, but is significantly shallower than those at Fort Knox and Pogo. Major differences between Golden Zone and mid-Cretaceous interior Alaskan gold deposits include abundant copper (seen as chalcopyrite and tetrahedrite) and limited evidence for high-temperature alteration.

INTRODUCTION

The Golden Zone gold–copper–arsenic deposit yielded 1,581 oz gold, 8,617 oz silver, 21 tons copper, and 1.5 tons lead from 1,730 tons of ore mined in 1941–1942 (Hawley, 1974). Recent drilling indicates a resource of about 0.6 million oz gold, grading 0.047 ounces per ton gold (Addwest, 1997). Elements present in anomalous amounts in typical ore include gold, silver, arsenic, copper, bismuth, tellurium, antimony, zinc, and lead, with concentrations of arsenic more than appreciably greater than the others (Hawley and Clark, 1974; Balen, 1990; Gage and others, 1998). Concentra-tions of arsenic exceed that of copper by six times; zinc, lead, and antimony by 15 times, 40 times, and 50 times, respectively; bismuth and silver by 300 times and 430 times; and 1,000 times greater than gold and tellurium.

The deposit is a near-vertical breccia pipe in quartz monzodiorite consisting of altered igneous rock fragments cemented by quartz–carbonate–sulfide (Hawley and Clark, 1974). K–Ar ages of 70.2 to 70.6 Ma for primary biotite and 69.7 Ma for secondary white mica from Golden Zone indicate the mineralization is essentially contemporaneous with plutonism (Swainbank and others, 1977). These ages and the gold–arsenic–copper–bismuth–tellurium metallogeny allow Golden Zone to be grouped with the ~70 Ma plutonic-related gold deposits of southwestern Alaska (fig. 1), which includes Shotgun, Nixon Fork, Vinasale Mountain, and Donlin Creek (Newberry and others, 1995; McCoy and others, 1997). However, Golden Zone lies on the south side of the right-lateral Denali fault and bears an unknown spatial relationship to the other ~70 Ma deposits. Further, the closest analogue deposit of the SW Alaskan deposits, the Vinasale Mountain breccia body, contains almost exclusively sub-micron gold and displays no gold–bismuth relationship, whereas gold at Golden Zone is free-milling and ores contain significant bismuth (Hawley and Clark, 1974). Finally, although published analyses of Golden Zone ores indicate significant concentrations of bismuth and tellurium (Newberry and others, 1995), minerals containing these elements have not been previously identified and there is little published information concerning the ore mineralogy.

The purpose of this study is to characterize, by using petrography and electron microprobe analyses, the ore mineralogy and ore mineral compositions at Golden Zone. We then use this information to estimate the temperature, pressure, and chemical conditions of ore formation at Golden Zone as well as to both compare and contrast Golden Zone with other Cretaceous intrusion-hosted and intrusion-related deposits of Alaska.

SETTING

The Golden Zone deposit lies on the southern flank of the Alaska Range, roughly midway between Anchorage and Fairbanks, 25 km west of the George Parks Highway (fig. 1). A small, 69-Ma (biotite $^{40}Ar/^{39}Ar$, Clautice and others, 1999), subvertical, quartz monzo-

[1]University of Alaska, Department of Geology and Geophysics, PO Box 755780, Fairbanks, Alaska 99775-5780
Email for Benjamin Gage: fsbgg@uaf.edu

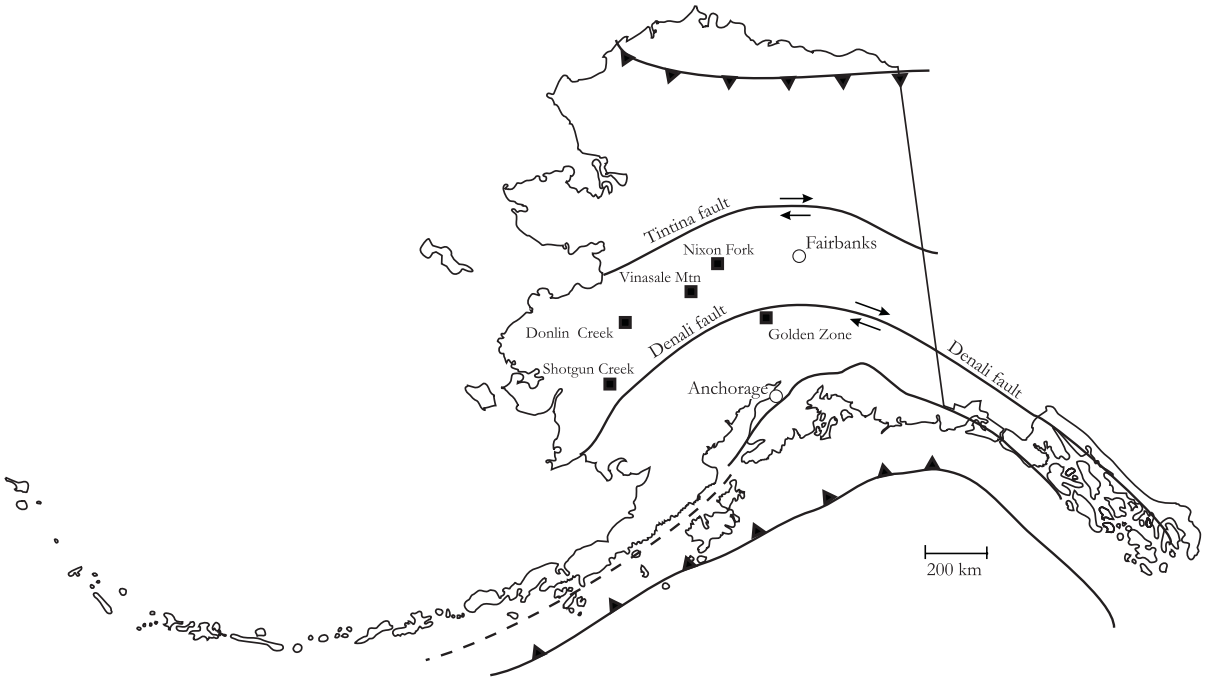

Figure 1. *Location map of gold deposits associated with 70 Ma suite of intrusive plutonic rocks. Modified from Newberry and others (1995).*

diorite porphyry stock hosts most of the mineralization (fig. 2). The location and age of the intrusion and its potassic, reduced nature suggest that it is related to late Cretaceous to early Tertiary plutonism described by Reed and Lanphere (1973). The stock intrudes and hornfelses Permian and Mesozoic volcanic and sedimentary rocks; both the intrusive and hornfels are cut by high-angle faults with both pre-ore and post-ore movement. Within the stock, the most intense mineralization occurs in a quartz–carbonate–sulfide cemented, steeply plunging breccia pipe. C.C. Hawley (written commun., 2000) describes the pipe as follows: "Roughly ovoid (100 m) at the surface, the pipe and host intrusion elongates with depth. At a depth of about 200 m (relative to the top of the pipe), the pipe is about 50 m by 200 m elongated northeast. The pattern of mineralization also changes with depth. Near the surface, maximum extent of sulfide–gold mineralization is as a near peripheral annular ring. The narrowed pipe is largely sulfide-bearing at a depth of 180–200 m. Sparse drilling indicates that the pipe continues to at least 300 m in depth, but its course and extent are uncertain below about 250 m." The clasts within the breccia pipe are subangular to subrounded, strongly quartz–sericite–carbonate altered, and mineralized.

Chalcopyrite, sphalerite, pyrrhotite, and especially arsenopyrite and pyrite are the most abundant sulfides. Overall sulfide content of the pipe exceeds 5 percent; 1-m lengths of drill core commonly contain 20 to 30 percent sulfide. The sulfide minerals are often coarsely crystalline and readily identifiable in hand specimen. Galena, electrum, and tetrahedrite are easily recognized in polished sections of mineralized rock, but not with certainty in hand specimen. Sulfide mineralization occurs in quartz veins and disseminated throughout the stock and adjacent country rock, but is mostly located within the clasts (mainly arsenopyrite and pyrite) and disseminated within the matrix of the breccia pipe. Several high-grade sulfide veins radiate away from the stock, extending up to 500 m into country rocks.

Quartz–sericite–carbonate alteration strongly pervades the intrusive rock, especially near ore (Hawley and Clark, 1974). Even the freshest samples of pluton display some alteration and contain traces of pyrrhotite and chalcopyrite. Goethite and limonite, with lesser malachite, azurite, and scorodite strongly stain the rocks near the surface. Intense supergene alteration is limited to the near-surface environment, except along fractures, where weathering-related clays and supergene copper minerals can be found at nearly 100 m depth.

ANALYTICAL METHODS

Polished thin sections were prepared from 13 ore-bearing drill core samples, representing a variety of locations within a 250-m vertical interval of the Golden Zone breccia pipe. Ore minerals were identified by petrographic techniques and electron microprobe analyses (qualitative and quantitative). Compositions

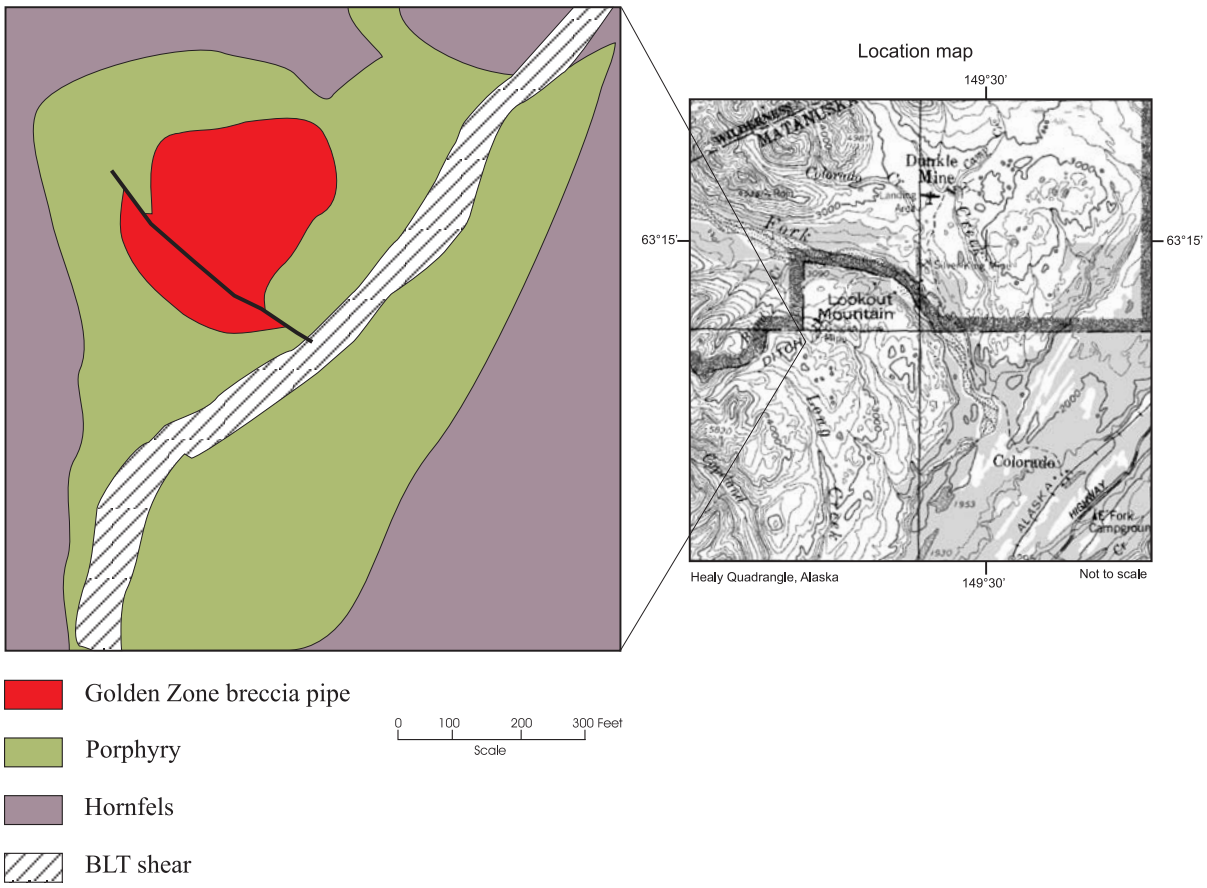

Figure 2. *General geologic map of Golden Zone breccia pipe and quartz monzodiorite porphyry host. Adapted from Addwest (unpub. data, 1997).*

were determined by using a Cameca SX-50 electron microprobe at the Geology and Geophysics Department, University of Alaska Fairbanks, with well-characterized mineral standards. Analytical conditions of 30 to 35 keV, 10 to 15 nA, and 1mm beam size were used with peak counting times of 20 to 60 seconds. Standard ZAF corrections were employed.

PETROGRAPHY

Quartz–sericite–carbonate alteration strongly pervades the intrusive rock and so thoroughly overprints earlier potassic alteration (biotite + K-feldspar) that the extent of the potassic event is difficult to ascertain. Given this problem, it is difficult to determine the sulfide mineralogy associated with early potassic alteration.

Mineralization associated with quartz–sericite–carbonate alteration occurs in veins in country rock and in the intrusion hosting the breccia pipe, and in the sulfide-cemented breccia fragments. Abundant inclusion-free medium-grained arsenopyrite occurs on the margins of quartz–sericite–carbonate-altered monzodiorite clasts. Gold has not been observed in or with this arsenopyrite. In contrast, coarsely crystalline sulfides, including significant amounts of inclusion-bearing arsenopyrite, constitute a major part of the interclast matrix. Minor sulfides identified in reflected light include galena, electrum, bismuthinite, and native bismuth. These minerals were confirmed and the additional phases hedleyite ($Bi_{14}Te_6$), kobellite ($Pb_5(Bi,Sb)_8S_{17}$), maldonite (Au_2Bi), and complex Pb–Bi–Sb and Pb–Sb–Cu–Fe sulfosalts were identified with the electron microprobe.

Native gold, native bismuth, bismuthinite, maldonite, and hedleyite were observed only as inclusions in coarsely crystalline arsenopyrite of interbreccia matrix sulfide. These minerals occurred in combinations as small clusters of anhedral grains, <5mm diameter, usually with coarser, more abundant pyrrhotite and chalcopyrite inclusions. In many cases native bismuth and bismuthinite occur together, but bismuthenite was not observed with either maldonite or hedleyite. This assemblage represents the earliest stage of gold mineralization (fig. 3).

Other sulfides present in the interclast massive sulfide matrix include pyrrhotite, chalcopyrite, tetrahedrite, sphalerite, pyrite, electrum, and galena. Not all

occur in every sample, but pyrite and chalcopyrite are invariably present. The electrum present in this assemblage typically occurs as 10 to 100mm, anhedral grains associated with ankerite, pyrite, chalcopyrite, and tetrahedrite. This electrum represents a second stage of gold mineralization.

The euhedral, coarsely crystalline, matrix arsenopyrite also commonly contains some combination of ankerite, quartz, chalcopyrite, pyrite, tetrahedrite, kobellite, and electrum as fracture fillings. This fracture-related sulfide deposition represents the youngest stage of gold mineralization.

Pyrrhotite, interpreted to have been originally present in much greater quantities in the interclast sulfide matrix, ubiquitously displays partial to complete replacement by a fine-grained mixture of pyrite and marcasite. In hand specimen the secondary FeS_2 appears as an amorphous, anhedral, banded mass, texturally similar to chalcedony. The same amorphous character is evident in reflected light, with very fine grained, anhedral, ragged zones of pyrite intermixed with marcasite containing minor remnant pyrrhotite. The fine grain size and banded morphology of the secondary FeS_2 assemblage is characteristic of supergene destruction of pyrrhotite (for example, Ramdohr, 1980); where such assemblages are present it is common to assume the original mineral was pyrrhotite. This assemblage, labeled in this paper 'secondary py,' is taken to be equivalent to hypogene pyrrhotite.

Electrum was not observed in sulfide veins from outside the breccia pipe. These veins display the same gross mineral assemblage as the breccia-filling sulfide, including bismuth-sulfosalts.

Representative analyses of sphalerite show little compositional variation, whereas arsenopyrite displays significant variation (table 1). All microprobe analyses of sphalerite and arsenopyrite were taken from the edges of crystals to obtain the last equilibrium compositions. Compositions of both minerals were obtained only where an appropriate iron–sulfur 'buffer' assemblage was present, so as to constrain temperature or pressure. Consequently, the analyses presented (table 1) do not necessarily cover the entire range of compositions that occur at the deposit.

Sphalerite analyses presented (table 1) average about 98 total weight percent, which indicates either poor analyses or missing elements. Other analyses (not shown) of Golden Zone sphalerite by the authors indicate 1 to 1.5 wt% cadmium. Cadmium was not analyzed for this study, which most likely accounts for the low totals. Sphalerite analyses with high copper values (>0.5%) represent interference by chalcopyrite, as some sphalerite exhibits 'chalcopyrite disease'. We did not use these high copper analyses for geobarometry.

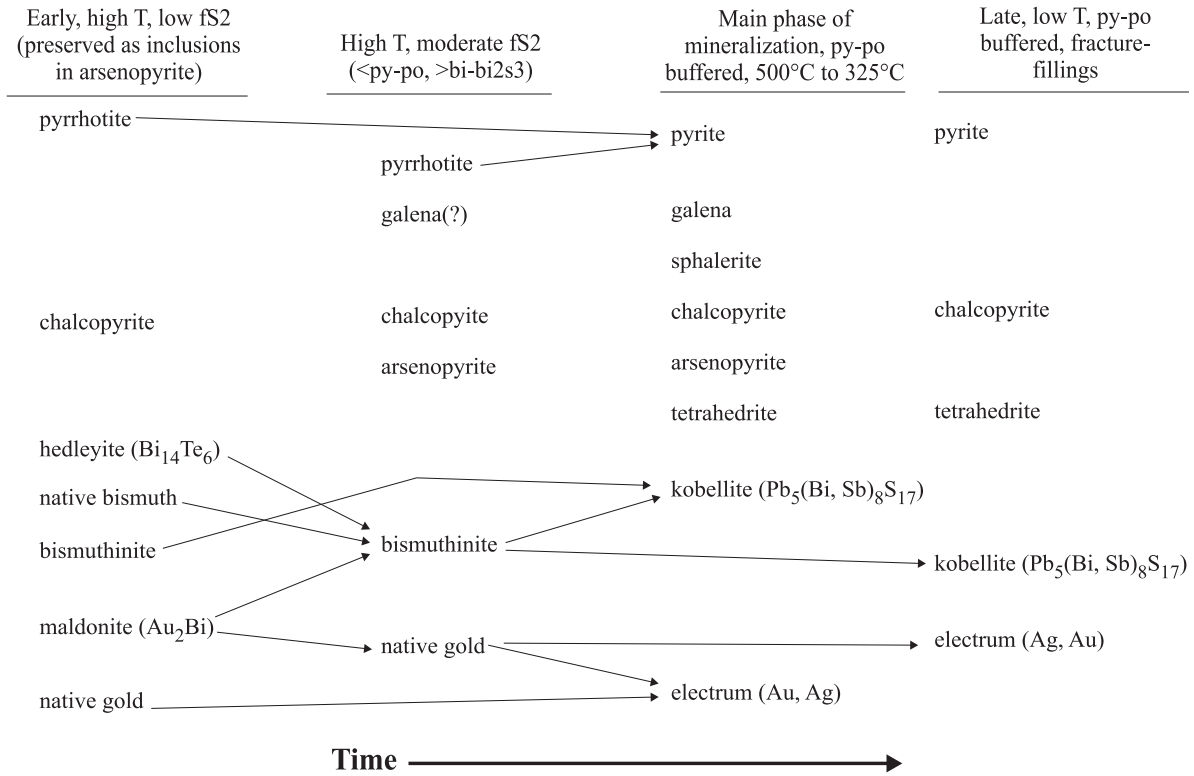

Figure 3. *Paragenesis of ore minerals based on petrographic observations and quantitative electron microprobe analyses. Arrows point from original mineral to its alteration product.*

Arsenopyrite analyses, in contrast, give uniformly high totals (table 1), both for the samples and the secondary arsenopyrite standard (not shown). Because the arsenic–iron–sulfur atomic ratios for the secondary standard closely match the expected values, these analyses were used in geothermometry.

SPHALERITE GEOBAROMETRY

Sphalerite may contain significant amounts of Fe^{2+} depending on the pressure, temperature, and fs_2 of the fluid. However, when sphalerite, pyrite and pyrrhotite coexist in equilibrium, the FeS content of the sphalerite is essentially independent of temperature and depends only on pressure (Barnes, 1997). Pressure is a linear function of mole-percent FeS for the temperature and composition range present (Barnes, 1997). The assemblage pyrite–pyrrhotite–sphalerite is not commonly present at Golden Zone, but the assemblage sphalerite–pyrite–(fine-grained pyrite+marcasite) is common. As the latter mixture is thought to represent hypogene pyrrhotite, compositions of sphalerite from this assemblage as well as from sphalerite–arsenopyrite assemblages were determined (table 1).

Sphalerite compositions (not all of which are shown) range from FeS_{13} to $FeS_{21.2}$; the sphalerite with pyrite and secondary pyrite compositions show a more restricted range, $FeS_{18.8}$ to $FeS_{21.2}$. Sphalerite with FeS greater than 21 percent (within analytical uncertainties) cannot occur in equilibrium with pyrite. All sphalerite compositions are 21 percent or less FeS; hence the compositions indicate equilibrium with pyrite. The most iron-poor sphalerites that occur with arsenopyrite and pyrite have compositions nearly as iron-rich as those present with secondary pyrite (former pyrrhotite), indicating that sphalerite deposition in this assemblage took place at (or very close to) pyrite–pyrrhotite

Table 1 . *Representative electron microprobe analyses of arsenopyrite and sphalerite in weight and atomic percents*

Sample	Mineral	Assemblage	Total weight percent	Atomic percent S	Fe	Zn	As
$GZ13_1$	spl	spl/py/aspy	95.9	50.9	7.8	40.5	- -
$GZ13_2$	spl	spl/py/aspy	97.8	51.1	8.6	40.3	- -
GZ14B	aspy	aspy/py/2py	101.4	36.6	32.4	- -	30.5
GZ14B	aspy	aspy/py/2py	101.8	35.9	32.5	- -	30.9
GZ14A	aspy	aspy/py/2py	102.0	34.8	32.4	- -	32.4
GZ14A	aspy	aspy/py	101.4	35.0	32.6	- -	32.4
BG110	aspy	aspy	102.6	34.6	32.6	- -	32.3
BG110	spl	spl/py/2py	98.1	51.4	9.2	39.3	- -
BG135	aspy	aspy/py/spl	102.0	35.1	32.2	- -	32.1
BG135	spl	spl/py/2py	98.9	50.9	8.5	40.4	- -
BG123	aspy	aspy/py/2py	103.0	34.3	32.8	- -	32.9
BG123	aspy	aspy/py/2py	102.5	34.8	32.5	- -	32.7
BG123	aspy	aspy/py	102.9	34.8	32.5	- -	32.7
BG123	aspy	aspy/py/2py	102.5	35.1	32.6	- -	32.0
BG123	spl	spl in aspy	98.1	50.6	10.0	38.2	- -
BG123	spl	spl/py/2py	97.1	51.2	9.6	39.1	- -
GZ2	aspy	aspy/2py	102.3	35.9	32.4	- -	31.4
GZ2	aspy	aspy/2py	103.0	36.8	32.1	- -	30.7
GZ2	aspy	aspy/py/2py	101.8	37.0	31.9	- -	30.8
GZ7	aspy	aspy/py	103.5	33.0	32.3	- -	34.6
GZ7	aspy	aspy/py	103.1	33.6	32.4	- -	34.0
GZ5	aspy	aspy/py	102.4	35.2	32.3	- -	32.4
GZ5	aspy	aspy/py/2py	102.0	34.9	32.6	- -	32.4
GZ10	aspy	aspy/py	101.9	34.3	32.4	- -	33.2
GZ10	aspy	aspy/py/2py	101.8	34.4	32.1	- -	33.4
GZ10	aspy	aspy/py	102.6	34.1	32.6	- -	33.3
GZ13	aspy	aspy/py/2py?	101.7	36.2	32.8	- -	31.0
GZ13	aspy	aspy/spl/py	101.6	36.7	32.3	- -	30.7
$GZ13_1$	aspy	aspy/py/spl	101.2	36.2	32.3	- -	31.2
$GZ13_2$	aspy	aspy/py/spl	102.2	36.4	32.4	- -	31.2

NOTE: aspy–arsenopyrite, spl–sphalerite, py–pyrite, 2py–py after pyrrhotite. Subscripts denote arsenopyrite–sphalerite pair.
- - Indicates value is below detection limit.

equilibrium conditions. The range of calculated pressures is 0 to 1.6 kb (fig. 4), yielding an average estimated pressure of 0.9 ± 0.5 kb (1s). Most likely the calculated pressure variations represent analytical uncertainties or slight variations from pyrite–pyrrhotite equilibrium conditions, rather than true variations in pressure during sphalerite deposition.

ARSENOPYRITE GEOTHERMOMETRY

The arsenic content of arsenopyrite depends on the temperature and the sulfur fugacity (fs_2) of the precipitating fluid and is nearly independent of pressure (Kretschmar and Scott, 1976; Scott, 1983). Where the fs_2 is buffered by additional sulfide species such as pyrite–pyrrhotite, the arsenopyrite composition yields an estimate of the temperature of precipitation. Similarly, the equilibrium assemblage arsenopyrite–sphalerite yields a deposition temperature estimate that is dependent on the FeS content of sphalerite and the arsenic content of arsenopyrite (fig. 5).

Arsenopyrite present with a buffered sulfide assemblage shows considerable variations in composition (table 1), reflecting significant variations in temperature of deposition. Only arsenopyrite from sample GZ7 was deposited without pyrite present, and its composition (table 1) does not yield a unique tempera-ture. For this early vein there are no necessary limitations on fs_2 beyond the upper stability of arsenopyrite and loellingite; hence the compositions are plotted (fig. 5) as a band yielding temperatures of between 450°C and 500°C.

Other arsenopyrite, with rim compositions of about 30 to 33 atomic percent arsenic, present with pyrite and secondary pyrite or with high-iron sphalerite, indicates arsenopyrite rim deposition at temperatures of ~460°C to 300°C. Arsenopyrite compositional gaps may result from a hiatus in deposition, but more likely from incomplete sampling. Several samples (for example, BG123) have arsenopyrites with significant compositional variations (table 1). Such compositional variations imply temperature variations of up to 60°C during arsenopyrite deposition within a several-square-centimeter area. Samples 14A and 14B, taken 10 cm apart, yield a larger temperature variation (~435°C to 335°C), which is consistent with the pyrite-rich vs arsenopyrite-rich mineralogy of the two. In contrast, samples from simple veins outside of the breccia pipe (for example, GZ2, GZ13) show little composi-tional variability, implying little change in temperature during arsenopyrite deposition.

ANTIMONY- AND BISMUTH-BEARING MINERALS

Analyses of small inclusions were difficult to obtain because of beam spread into the host mineral; this often led to total weight percents different than 100 percent and the presence of elements from the host mineral in the analysis. Most of the analyses of small inclusions were used for mineral identification, rather than any quantitative use. Bismuth minerals that were quantitatively identified include native bismuth, bismuthinite, and maldonite, all of which yielded compositions close to theoretical values, considering their fine-grained nature (table 2). Hedleyite and an unidentified bismuth–arsenic–tellurium mineral are also present.

The major antimony-rich mineral identified is silver-rich tetrahedrite (tables 3, 4), often referred to as 'freibergite' (Ramdohr, 1980). Maximum silver contents of Golden Zone tetrahedrites are close to the upper limit found in nature (~18 weight percent, Ramdohr, 1980), indicating that the fluids were nearly saturated with respect to AgS. Iron and zinc contents of several weight percents are common in tetrahedrite; their presence does not indicate analytical problems. Although tetrahedrite can

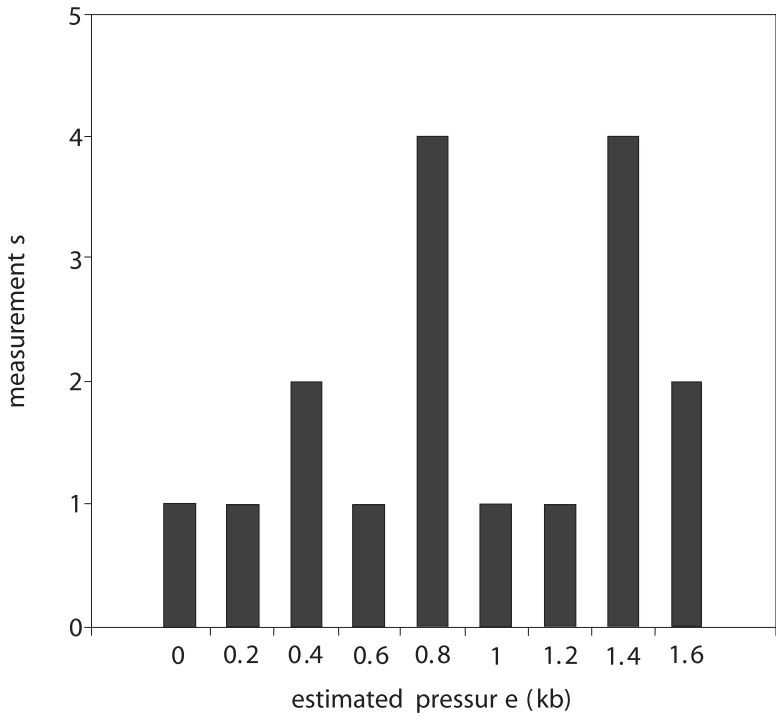

Figure 4. *Histogram of mineralization pressures for the Golden Zone deposit estimated from sphalerite–pyrite–pyrrhotite geobarometry.*

contain appreciable bismuth or mercury, neither is significantly present; arsenic contents vary from below detection to a few weight percents.

A fine-grained anisotropic, moderate reflectivity mineral was identified from microprobe analysis as the sulfosalt kobellite (table 4). Other minerals with major lead–antimony–bismuth–sulfur and lead–antimony–copper–iron–sulfur are present, but could not be conclusively identified from the compositional data.

GOLD AND ELECTRUM

Maldonite and Au–Ag are the only minerals at Gold Zone found to contain detectable gold. An extremely wide range of silver contents are present in the 'gold,' ranging from 5.5 to 55 weight percent (tables 2–4), and the bulk of the 'gold' examined is more properly termed electrum ('gold' with more than 20 percent silver). Because most Au–Ag grains examined were small, the analyses suffer from interference because of host minerals; thus, the arsenic, iron, sulfur, and copper commonly reported are almost certainly not actually present. Tellurium is present at just above detection levels in electrum from sample GZ10 (table 2); no significant concentrations of bismuth, selenium, antimony, or lead were found.

The compositions of Au–Ag vary with paragenesis (fig. 6): earliest-deposited gold (included in arsenopyrite) is silver-poor; latest-deposited (fractures in arsenopyrite) is silver-rich; and free gold grains of intermediate timing possess intermediate compositions. These patterns are exhibited within individual samples, for which the increase of silver with time is particularly striking (fig. 6). Mercury contents also vary significantly and appear to increase with both silver content and time (fig. 7). There

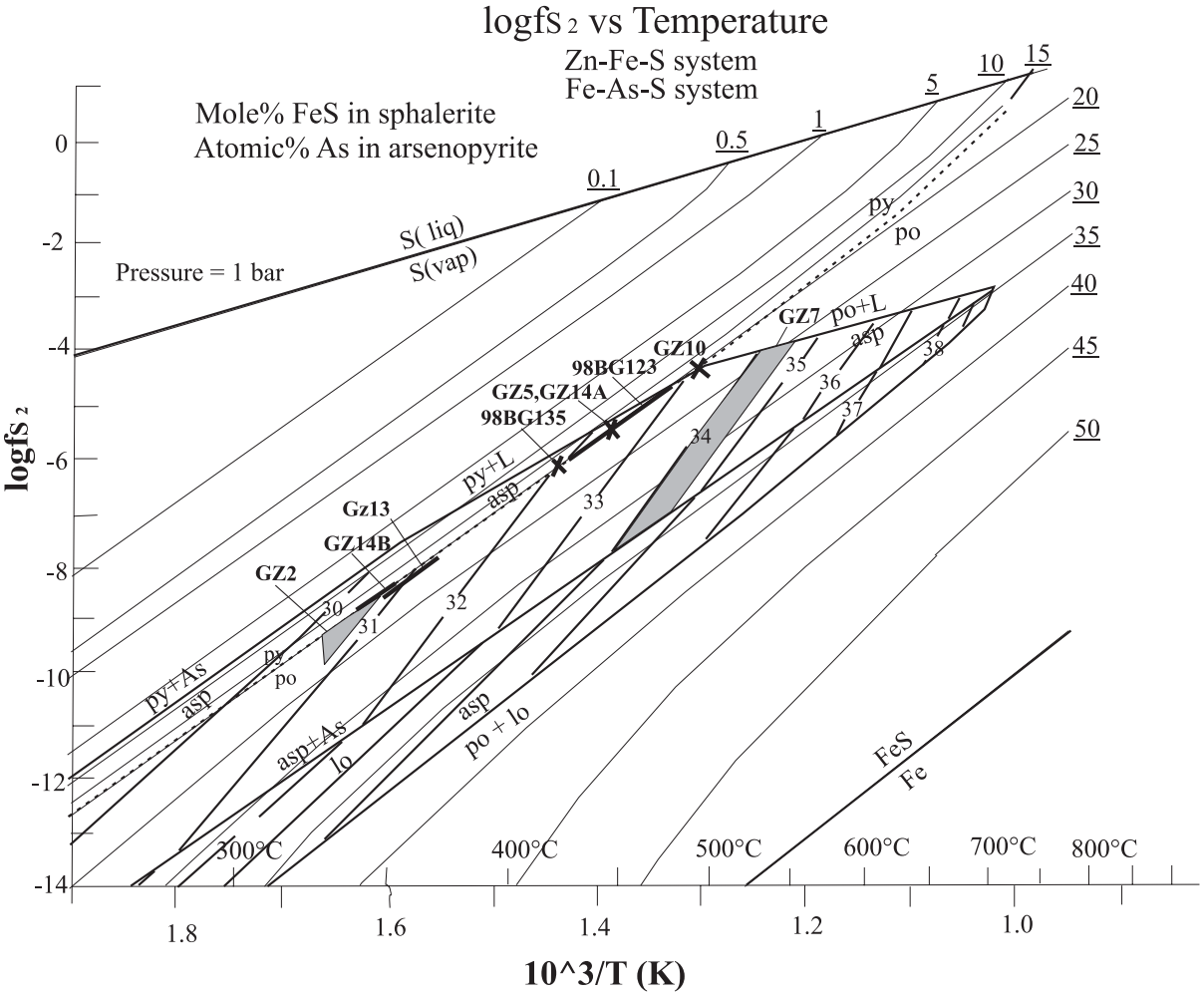

Figure 5. *Log fS2 vs 1/T diagram illustrating major phase boundaries in the iron–arsenic–zinc–sulfur and gold–bismuth–sulfur systems and compositional isopleths for arsenopyrite and sphalerite (underlined), with Golden Zone mineral data. Diagram modified from Scott (1983).*

Table 2. *Electron microprobe analyses of Au- and Bi-bearing minerals present with arsenopyrite in weight percent and atomic percent for selected elements*

Sample	Mineral	Bi	Pb	Hg	Au	As	S	Ag	Te	Total	Description	Bi at%	Au at%	Ag at%	Hg at%	S at%
	LLD	0.3	0.2	0.2	0.2	0.08	0.03	0.1	0.07							
GZ14B	el	- -	0.6	0.0	75.9	2.44	0.4	23.1	0.07	102.6	incl. in aspy	0.0	59.5	33.0	0.0	- -
GZ14B	el	- -	0.0	0.0	70.7	2.74	0.3	26.9	- -	100.7	incl. in aspy	0.0	54.7	38.0	0.0	- -
GZ14B	el	- -	0.3	0.8	71.0	0.30	0.2	28.2	- -	100.9	incl. in aspy	0.1	56.5	41.0	0.6	- -
GZ14B	mal	34.0	0.0	- -	63.0	4.84	0.7	0.0	- -	102.5	incl. in aspy	28.6	56.3	- -	- -	- -
GZ10	bi	99.8	0.0	- -	- -	2.97	0.1	0.1	- -	103.1	incl. in aspy	91.4	0.1	0.2	0.0	- -
GZ10	bi	100.5	0.3	- -	- -	0.89	- -	- -	- -	101.7	incl. in aspy	97.1	0.0	0.0	0.0	- -
GZ10	bism	74.1	2.7	- -	- -	3.21	18.7	- -	- -	98.7	incl. in aspy	35.6	0.0	0.0	0.0	58.7
GZ10	gold	- -	0.0	- -	93.7	0.99	0.2	5.5	- -	100.5	incl. in aspy	0.0	86.9	9.4	0.0	- -
GZ10	el	- -	0.3	1.2	46.5	0.30	0.2	51.7	- -	100.2	in aspy frx	0.0	32.2	65.4	0.8	- -
GZ10	el	- -	0.0	2.3	35.8	0.90	0.3	60.9	0.13	100.3	in aspy frx	0.0	23.3	72.3	1.4	- -
GZ10	el	- -	0.0	1.3	36.8	0.67	0.3	60.4	0.07	99.4	in aspy frx	0.0	24.2	72.7	0.8	- -

Note: LLD–lower detection limits, el–electrum; mal–maldonite; bi–native bismuth; bism–bismuthinite; aspy–arsenopyrite; frx–fracture; incl–inclusion.
- - Indicates value is below detection limit.

Table 3 . *Electron microprobe analyses of electrum and tetrahedrite listed in weight percent and in atomic percent for selected elements*

Sample	Mineral	Fe	Cu	As	S	Ag	Sb	Au	Hg	Bi	Total	Description	Fe at%	Cu at%	S at%	Ag at%	Sb at%	Au at%
	LLD	0.02	0.02	0.05	0.02	0.06	0.04	0.1	0.1	0.3								
98BG135	el	0.41	0.02	- -	0.16	24.98	- -	74.0	0.7	- -	100.3	Free	1.2	0.0	0.8	37.1	0.0	60.3
98BG135	el	0.49	0.3	- -	0.22	25.56	- -	73.0	0.6	- -	100.2	Free	1.4	0.8	1.1	37.5	0.0	58.7
98BG135	el	0.40	0.1	0.50	0.12	26.16	- -	76.1	0.8	- -	104.2	Free	1.1	0.3	0.6	37.2	0.0	59.2
98BG135	tet	4.84	30.3	- -	24.76	10.73	27.9	0.0	0.0	- -	98.6	in aspy frx	5.2	28.6	46.4	6.0	13.8	0.0
98BG135	el	1.24	0.7	- -	0.22	23.54	- -	76.1	0.0	- -	101.8	incl. In cpy	3.4	1.8	1.1	33.8	0.0	59.9
98BG135	el	0.18	0.3	- -	0.20	25.26	- -	77.9	0.2	- -	104.0	incl. In cpy	0.5	0.7	1.0	36.3	0.0	61.4
98BG110	el	0.05	0.00	- -	0.14	29.17	- -	71.9	0.0	- -	101.3	Free	0.1	0.0	0.7	42.2	0.0	56.9
98BG110	el	0.86	0.00	- -	0.19	31.30	- -	70.1	0.4	- -	102.8	Free	2.3	0.0	0.9	43.4	0.0	53.2
98BG110	el	1.07	0.02	- -	0.22	30.87	- -	72.0	0.8	- -	105.0	Free	2.8	0.1	1.0	42.0	0.0	53.6
98BG110	el	0.44	0.00	- -	0.26	28.43	- -	68.8	0.7	- -	98.6	Free	1.2	0.0	1.3	41.7	0.0	55.3

Note: LLD–lower detection limits, el–electrum, tet–tetrahedrite, aspy–arsenopyrite, cpy–chalcopyrite, frx–fracture, incl–inclusion,
- - Indicates value is below detection limit.

Table 4. *Electron microprobe analyses of Au- and Sb-bearing minerals, not present as inclusions, listed in weight and atomic percent*

Sample	Mineral	S	Fe	Cu	Zn	As	Ag	Sb	Au	Hg	Pb	Bi	Total	Description	Ag at%	Au at%	Hg at%
	LLD	0.07	0.04	0.05	0.06	0.1	0.2	0.08	0.2	0.1	0.3	0.3					
GZ14A	el	0.4	0.0	0.0	0.0	- -	23.0	0.0	76.5	0.0	0.0	0.0	100.0	in py frx	34.7	63.1	0.0
GZ14A	el	0.3	0.1	0.0	0.0	0.0	24.3	0.0	74.2	0.4	0.0	0.0	99.4	in py frx	36.6	61.2	0.3
97RN337	kob	21.9	2.7	0.1	0.0	0.0	0.0	25.9	0.0	0.0	38.0	11.0	99.6	free	0.0	0.0	0.0
97RN337	gold	0.1	0.0	0.0	0.0	0.0	16.6	0.1	82.9	0.0	0.0	0.3	100.1	in aspy	26.5	72.4	0.0
97RN337	gold	0.1	0.1	0.0	0.0	0.0	11.3	0.2	87.6	0.1	0.0	0.2	99.5	free	18.8	80.0	0.1
97RN337	gold	0.0	0.0	0.0	0.0	0.1	12.5	0.0	87.6	0.0	0.0	0.0	100.2	w/py/cpy/spl	20.6	79.0	0.0
GZ5	el	0.5	0.2	0.0	0.0	0.0	34.2	0.0	65.7	0.0	0.0	0.0	100.6	w/py/2py	47.4	49.8	0.0
GZ10	el	0.2	0.7	0.0	0.0	2.0	54.8	0.2	39.7	2.8	0.0	0.0	100.6	in aspy frx	65.7	26.1	1.8
98BG110	tet	24.1	5.1	28.0	1.7	0.0	13.9	25.6	0.0	0.1	0.0	0.2	98.7	free	7.8	0.0	0.0
98BG110	el	0.2	0.0	0.0	0.0	0.0	26.6	0.0	74.1	0.0	0.0	0.3	101.3	w/py	39.0	59.5	0.0
98BG110	el	0.2	0.1	0.0	0.0	0.0	27.9	0.1	72.4	0.0	0.0	0.0	100.6	free	40.7	57.9	0.0
98BG135	tet	24.9	4.0	32.0	3.2	0.3	8.4	26.9	0.0	0.2	1.4	0.0	101.3	in aspy frx	4.6	0.0	0.1

Note: LLD–lower detection limits, el–electrum, kob–kobellite, tet–tetrahedrite, aspy–arsenopyrite, py–pyrite, cpy–chalcopyrite, spl–sphalerite, 2py–pyrite after pyrrhotite, frx–fracture, incl–inclusion.
- - Indicates value is below detection limit.

is no apparent lateral or vertical variation in electrum composition within the deposit; rather, there is considerable variation within single samples as a function of paragenesis.

If a fluid is saturated with respect to silver, then the silver content of electrum is a function of the temperature and fs_2 (Barton, 1980). If the fs_2 is also buffered (for example, at pyrite–pyrrhotite), the electrum composition yields a unique temperature (fig. 8). If the system is not saturated with silver (that is, the electrum contains less than maximum silver possible because there simply is not enough silver available), the temperature generated from the electrum composition is a *maximum* estimated temperature. For electrum present with a high-silver tetrahedrite, the condition of silver saturation is approximately met for the highest silver electrum present; in other cases, isolated electrum inclusions in arsenopyrite are likely to not be silver-saturated. Samples meeting both the silver saturation and pyrite–pyrrhotite criteria (fig. 8) yield equilibrium temperatures of ~410°C (free electrum grains) to 260°C (fracture-filling electrum in arsenopyrite). In each case, the temperatures estimated from electrum compositions are less than those estimated from arsenopyrite geothermometry in the same sample.

DISCUSSION

The average formation pressure defined by sphalerite geobarometry (0.9 ± 0.5 kb) corresponds to a depth of about 2.7 ± 1.5 km, at average lithostatic gradient. This pressure is significantly higher than that inferred for the Vinasale Mountain breccia bodies but significantly lower than that determined for nonbreccia deposits such as Fort Knox and Pogo (McCoy and others, 1997, 2000). It is most similar to pressure estimates for 'intermediate depth' deposits such as the Ryan Lode and Dolphin deposits of the Fairbanks district and the Shotgun porphyry gold–arsenic deposit of southwestern Alaska (Rombach, 2000). This depth is well below that considered typical of epithermal deposits and is great enough to allow some thermal and hydrothermal insulation from the paleosurface.

The identification of native bismuth and maldonite at Golden Zone are important because they are only stable under fs_2 conditions much lower than those for pyrite stability (fig. 5); their occurrence as inclusions in arsenopyrite requires that conditions changed during arsenopyrite deposition and that only arsenopyrite rims necessarily equilibrated with pyrite. The ore-forming fluids must have begun at or below the Bi_2S_3–Bi equilibrium (fig. 5) and at temperatures of 500°C (the

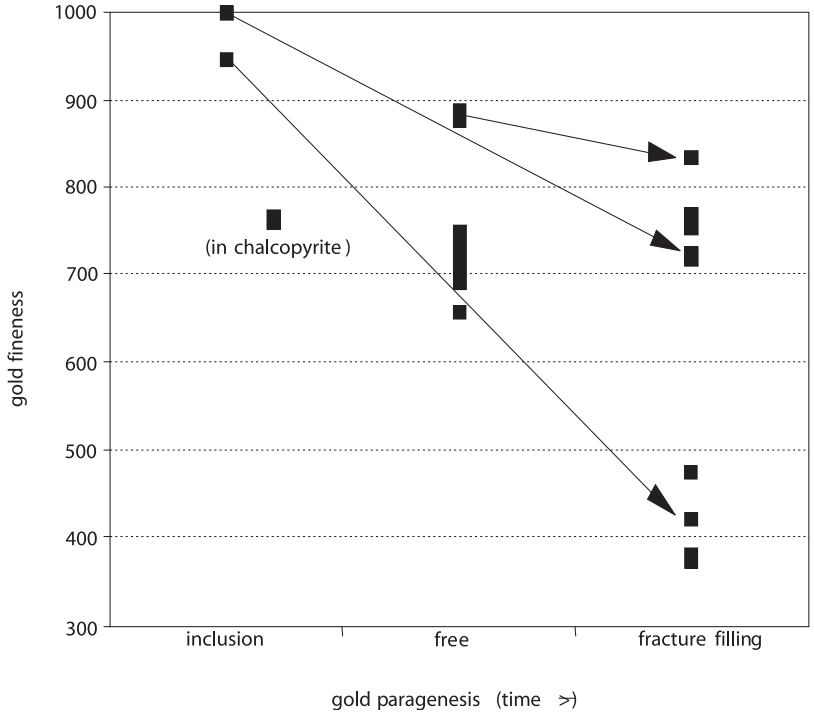

Figure 6. *Fineness (1,000*wt% Au/Ag+Au) for gold and electrum grains, determined by microprobe analysis, vs inferred order of deposition, based on textural criteria for the Golden Zone deposit. Compositional data from tables 2–4.*

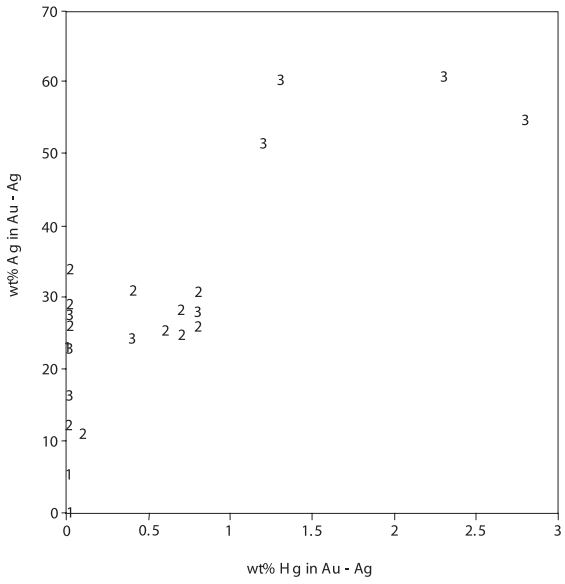

Figure 7. *Weight percent silver vs weight percent mercury, by electron microprobe analyses, for gold and electrum grains, showing change in composition with time. Symbols: 1 = inclusions in arseno-pyrite (1' = in chalcopyrite), 2 = free grains outside of arsenopyrite, 3 = fracture-filling grains in arsenopyrite. Paragenetically 'early' gold is lowest and 'late' gold is highest in mercury and silver. Data from tables 2–4.*

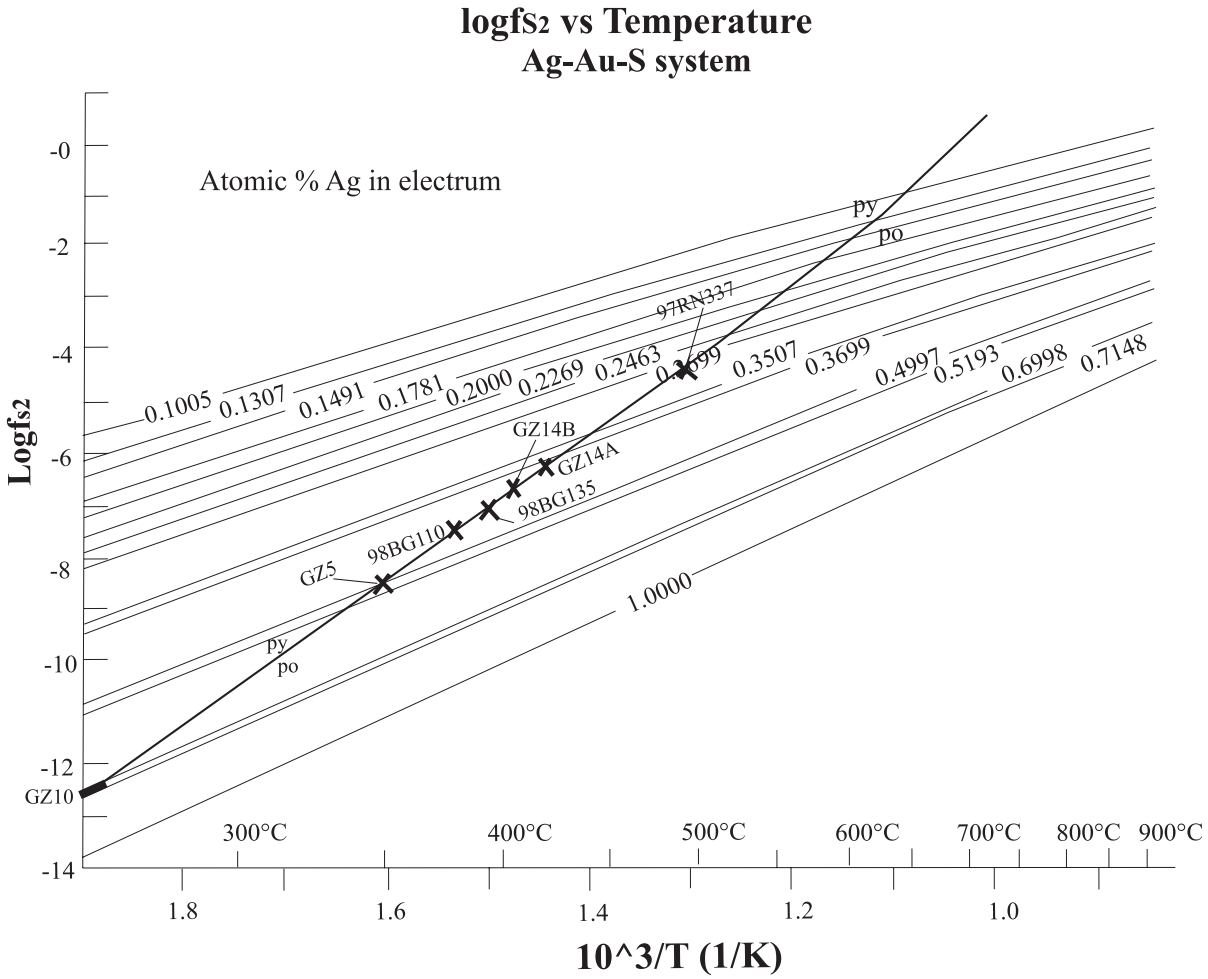

Figure 8. *Log fS2 vs 1/T diagram for the silver–gold–sulfur system, showing gold–silver compositional isopleths for silver-saturated conditions and the pyrite–pyrrhotite equilibrium curve. Electrum compositions plotted are maximum silver contents for a given sample, inferred to be approximately in equilibrium with pyrite–pyrrhotite and saturated with respect to silver.*

maximum temperature determined for arsenopyrite, fig. 5) or greater. Under these conditions and in the presence of excess bismuth, maldonite (Au_2Bi) is stable relative to gold. However, as fs_2 increased, the early formed maldonite would be sulfidized to yield gold + Bi_2S_3 (fig. 5). As maldonite does not contain appreciable amounts of silver, the gold initially reprecipitated from maldonite destruction would be low in silver (fig. 6). Because temperatures within a single sample vary by as much as 100°C (fig. 5), rapid fluid cooling apparently took place during sulfide deposition between breccia fragments. During this time isolated gold grains were deposited, starting at temperatures of about 400°C (fig. 8). Continued cooling and fluid egress led to fracturing of early-formed arsenopyrite and filling with high-silver electrum (fig. 6) at temperatures as low as 260°C (fig. 8).

This gold-compositional paragenesis is identical to that observed at Fort Knox, at Pogo, and in the Fairbanks district as a whole (McCoy, 2000). However, the major distinctions between Golden Zone and these other deposits, are that (a) a significant fraction of the gold was deposited (or redeposited?) at relatively low temperature and (b) the sulfidation state at Golden Zone was buffered to pyrite–pyrrhotite at all but the lowest temperatures, causing high-silver electrum to be stable (fig. 8). Because pyrrhotite was essentially absent in lower-temperature deposits of the Fairbanks district, electrum compositions are necessarily restricted to lower-silver values (fig. 8). Similarly, placer gold derived from (intrusion-related?) pyrrhotite-bearing gold veins of the Kantishna district is of anomalously low (<600) fineness, as is some of the placer gold of the Richardson district (Cobb, 1973; Newberry and others, 1997). Evidently, gold composition is not a reliable guide to deposit origin.

Calculated temperatures in the Golden Zone deposit show considerably more intrasample than intersample variation (fig. 9). Vein samples with carbonate–sericite alteration from outside the pipe (GZ2, GZ13) yield relatively low temperatures; an early, prequartz–carbonate vein from under the pipe (GZ7) yields evidence for high temperature and fs_2 below pyrite–pyrrhotite. Most samples from the pipe yield temperatures greater than 400°C but also less than 400°C, with no obvious change in temperature with depth (fig. 9). Such wide variations in temperature for samples that display no evidence for multiple fluid events (for example, cross-cutting veins) virtually require that mineralizing fluids cooled quickly and in place, without external fluid inputs. Evidently, the deposit formed so quickly that no systematic thermal zoning occurred, with each part of the deposit independently and rapidly cooling.

The Golden Zone deposit thus differs from 'typical' intrusion-related gold deposits of interior Alaska in that (a) mineral deposition was largely confined to the limited 'pipe' volume *per se*, rather than spread out vertically and laterally over large distances and (b) mineral deposition took place over a large range in temperature throughout this restricted volume. Among other implications is the 'telescoping' of elemental and mineral zonation. As higher temperature intrusion-related gold deposits are characterized by anomalous Bi–Te (As) and lower-temperature deposits by anomalous As–Sb–Ag (Zn, Pb, Cu) (McCoy and others, 1997), the bismuth–tellurium–

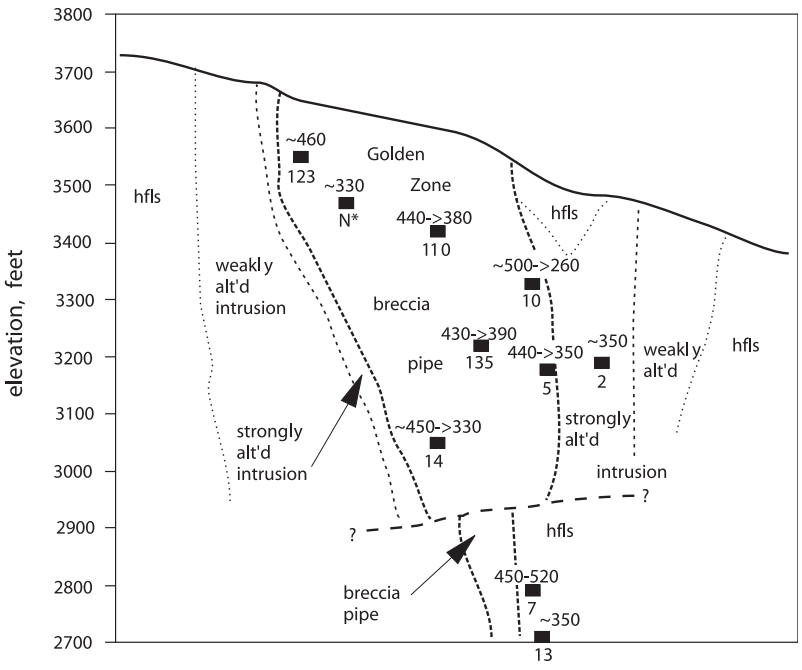

Figure 9. *Simplified cross section through the Golden Zone deposit, showing sample locations and inferred temperatures from gold–silver and arsenopyrite geothermometry. Square = sample location, number above square = estimated temperature (range, if more than one estimation), number below square = sample number (tables 1–4). (N* = sample 97RN337; all others are GZ or 98BG numbers). Abbreviations: hfls = hornfels, alt'd = altered. Note large intrasample variation and general lack of spatial zoning.*

silver–arsenic–antimony–copper–zinc–lead metallogeny of Golden Zone evidently occurred by fluids that cooled rapidly with little lateral or vertical movement. Although the copper contents of Golden Zone ores are anomalously high relative to mid-Cretaceous gold deposits of interior Alaska (which are notoriously copper-poor), such elevated copper contents do appear to be characteristic of the Late Cretaceous deposits as at Shotgun (Rombach, 2000) and Kantishna (McCoy, 2000).

Thus, the major differences in metallogeny, mineralogy, and mineral compositions between Golden Zone and the mid-Cretaceous intrusion-related gold deposits of interior Alaska appear to reflect the mode of deposit formation, rather than either deposit or host rock age. What appears 'unique' about the Golden Zone deposit are the conditions that led to breccia pipe formation (and the resulting 'quenching' of high-temperature hydrothermal fluids) rather than the metal contents of fluids or associated magmas. Golden Zone can thus be viewed as simply another 'variation' on the intrusion-related gold deposit theme, one in which the major characteristics resulted from the abnormally fast cooling of hydrothermal fluids.

ACKNOWLEDGMENTS

We thank Karen Clautice and the Alaska Division of Geological & Geophysical Surveys for funding and field support, without which this study would not have been possible. We are grateful to Chuck Hawley for providing field support, access to materials, and proprietary knowledge, but especially for his insights pertaining to Golden Zone. Reviews by Dan McCoy and Hawley significantly improved this paper.

REFERENCES

Addwest Minerals International, 1997, 1997 Summary Report – Golden Zone Project, AK, unpublished report, 110 p.

Balen, M.D., 1990, Geochemical sampling results from Bureau of Mines Investigations in the Valdez Creek Mining District, Alaska: U.S. Bureau of Mines Open-File Report 34-90, 218 p.

Barnes, H.L., ed., 1997, Geochemistry of Hydrothermal Ore Deposits, 3rd Edition: New York, John Wiley and Sons, Inc. 972 p.

Barton, M.D., 1980, The Ag–Au–S system: Economic Geology, v. 75, p. 303–316.

Clautice, K.H., Newberry, R.J., Pinney, D.S., Blodgett, R.B., Bundtzen, T.K., Gage, B.G., Harris, E.E., Liss, S.A., Miller, M.L., Reifenstuhl, R.R., Clough, J.G., Stone, D.B., and Whalen, M.T., 1999, Preliminary Geologic Map of the Healy A-6 Quadrangle, southcentral Alaska: Alaska Division of Geological & Geophysical Surveys Public-Data File 99-31a, 47 p.

Cobb, E.H., 1973, Placer deposits of Alaska: U.S. Geological Survey Bulletin 1374, 213 p.

Gage, B.G., Chu, P., Liss, S.A., and Clautice, K.H., 1998, Preliminary geochemical and major oxide data: Chulitna project, Healy A-6 Quadrangle and nearby area (1997 and 1998 data): Alaska Division of Geological & Geophysical Surveys Public-Data File 98-36, 48 p., 2 sheets, scale 1:63,360.

Hawley, C.C., and Clark, A.L., 1974, Geology and mineral deposits of the Upper Chulitna district, Alaska: U.S. Geological Survey Professional Paper 758-B, 47 p.

Kretschmar, U.H., and Scott, S.D., 1976, Phase relations involving arsenopyrite in the system Fe–As–S and their application: Canadian Mineralogist, v. 14, p. 364–386.

McCoy, D.T., 2000, Mid-Cretaceous plutonic-related gold deposits of interior Alaska: Metallogenesis, characteristics, gold-associative mineralogy, and geochronology: unpublished Ph.D. Thesis, Fairbanks, Alaska, University of Alaska Fairbanks, 245 p.

McCoy, D.T., Newberry, R.J., Layer, P., DiMarchi, J.J., Bakke, A., Masterman, J.S., and Minehane, D.L., 1997, Plutonic-related gold deposits of interior Alaska: Economic Geology Monograph 9, p. 191–241.

Newberry, R.J., McCoy, D.T., and Brew, D.A., 1995, Plutonic-hosted gold ores in Alaska: Igneous vs metamorphic origins: Resource Geology Special Issue, v. 18, p. 57–100.

Ramdohr, P., 1980, The ore minerals and their intergrowths (2nd edition): New York, Pergamon Press, v. 1, 440 p.

Reed, B.L., and Lanphere, M.A., 1973, Alaska–Aleutian Range Batholith: Geochronology, Chemistry, and Relation to Circum-Pacific Plutonism: Geological Society of America Bulletin, v. 84, p. 2583–2610.

Rombach, C.S., 2000, Genesis and mineralization of the Shotgun Deposit, southwestern Alaska, *in* Tucker, T.L., and Smith, M.T., chairpersons, The Tintina Gold Belt: Concepts, exploration, and discoveries: Special Volume 2, Cordilleran Roundup, Jan. 2000, p. 181–196.

Scott, S.D., 1983, Geochemical behavior of sphalerite and arsenopyrite in hydrothermal and metamorphic environments: Mineralogical Magazine, v. 47, p. 427–435.

Swainbank, R.C., Smith, T.E., and Turner, D.L., 1977, Geology and K–Ar age of mineralized intrusive rocks from the Chulitna mining district, central Alaska. Alaska Division of Geological & Geophysical Surveys Special Report 55, p. 23–28.

STRATIGRAPHY AND GEOCHEMISTRY OF THE RW ZONE, A NEW DISCOVERY AT THE GLACIER CREEK VMS PROSPECT, PALMER PROPERTY, PORCUPINE MINING DISTRICT, SOUTHEASTERN ALASKA

Darwin Green,[1] J. Garfield MacVeigh,[2] Merrill Palmer,[3] David H. Watkinson,[1] and Michael J. Orchard[4]

ABSTRACT

The RW zone is a new zone of polymetallic (Zn–Cu–Pb–Au–Ag) volcanogenic massive-sulfide (VMS) style mineralization discovered recently at the Palmer property, 55 km northwest of Haines, Alaska. The property is located within the Alexander terrane and is underlain by a mafic dominated, rift-related package of submarine volcanic rocks constrained to Late Triassic (Norian to Rhaetian) age based on new conodont data. Rocks on the property have undergone regional greenschist-facies metamorphism and at least three phases of deformation, with the earliest and most evident being a north–south contractional deformation event (D1) that is characterized by slatey to schistose cleavage (S1), and south-vergent folds and thrust faults. S1 foliation is reoriented about north–northwest-plunging, open to tight D2 folds that have no associated fabric. Deformation that postdates the D2 fold event includes rare crenulation fabrics and southwest- to northwest-striking high-angle faults.

The RW zone consists of a body (or bodies) of stratiform sphalerite-, barite-, and chalcopyrite-rich massive sulfide that has a strike length of at least 610 m, a down-dip extent of at least 200 m, and a maximum known thickness of 12 m. Quartz–sericite–pyrite–chlorite-altered rocks in the footwall of the RW zone locally host sphalerite- and chalcopyrite-bearing stockwork. Parts of the RW zone are leached of sulfides and underlain by supergene zinc and copper oxide mineralization.

The RW zone occurs in a panel of moderately north–northeast-dipping strata that forms the hanging wall to a thrust fault that disrupts a tight, overturned anticline. The stratigraphic section preserved in the thrust panel is more than 350 m thick, and hosts stacked stratiform massive-sulfide bodies (RW and Main zones). The section is dominated by massive to pillowed basalt, with subordinate rhyolite, mafic tuff, tuffaceous limestone, trachyandesite, conglomerate, and gabbro. Igneous rocks have a tholeiitic to transitional affinity based on Y vs Zr ratios. Primary variations in the contents and ratios of Zr, TiO_2, and Al_2O_3 permit effective chemical discrimination of volcanic units, and are a useful aid in correlating units across structures and through zones of hydrothermal alteration.

INTRODUCTION AND EXPLORATION HISTORY

This paper focuses on the stratigraphy and chemistry of host rocks at the RW zone, a new zone of polymetallic, volcanogenic massive-sulfide (VMS) style mineralization discovered recently at the Palmer Property, 55 km northwest of Haines, Alaska (fig. 1). VMS mineralization on the property is in Late Triassic rocks of the Alexander terrane, which form a discontinuous belt that contains numerous VMS occurrences, prospects, and deposits throughout southeastern Alaska and northwestern British Columbia, Canada (Taylor, 1997). Major deposits in the belt include the giant Windy Craggy deposit, with reserves of 297.4 million metric tonnes at 1.38 percent copper and 0.07 percent cobalt (Geddes Resources Ltd., 1991), and the precious-metal-rich Greens Creek deposit, which originally contained 11.0 million tons grading 12.8 percent zinc, 4.0 percent lead, 0.12 oz/ton gold, and 13.3 oz/ton silver (Swainbank and others, 2000).

The Palmer property is underlain by a mafic-dominated, bimodal sequence of submarine volcanic rocks that host numerous surface showings of massive sulfide and massive barite associated with zones of

[1]Carleton University, Ottawa, Ontario, Canada K1S 5B6
Email for Darwin Green: darwin@rubiconminerals.com
[2]Rubicon Minerals Corp., Vancouver, British Columbia, Canada V6E 4A6
[3]Alyu Mining Co. and Haines Mining Exploration Co., Haines, Alaska 99827
[4]Geological Survey of Canada, Vancouver, British Columbia, Canada V6B 5J3

intense hydrothermal alteration (fig. 2). Base-metal sulfides and barite were first discovered in 1969 by Merrill Palmer at the Main and Upper Main occurrences in the Glacier Creek prospect area. Early exploration focused on the economic potential of barite at these occurrences, and although tests showed the material to be suitable for production of drilling-mud concentrates, the prospect was never developed. Interestingly, most of the baritic units in the Glacier Creek prospect area are extensively leached of sulfides and it was not until the exploration success at Windy Craggy in the early 1980s and ensuing exploration boom throughout the belt of Late Triassic volcanic rocks of the Alexander terrane that the base-metal potential at Palmer was fully realized. In 1983, high-grade massive-sulfide boulders, such as one with a diameter of 1.8 m grading 33 percent zinc and 2.5 percent copper, were discovered by Merrill Palmer at the toe of a small ice sheet near Mount Henry Clay (Still and others, 1991). Twenty-six additional samples of various boulders collected by the U.S. Bureau of Mines returned an average grade of 19.3 percent zinc, 1.0 percent copper, 0.4 percent lead, 38.2 g/ton silver, 0.22 g/ton gold, and 20.6 percent barium (Still, 1984). Four separate drill programs that totaled 13 holes and 2,958 m of core were unsuccessful in locating the bedrock source of the boulders.

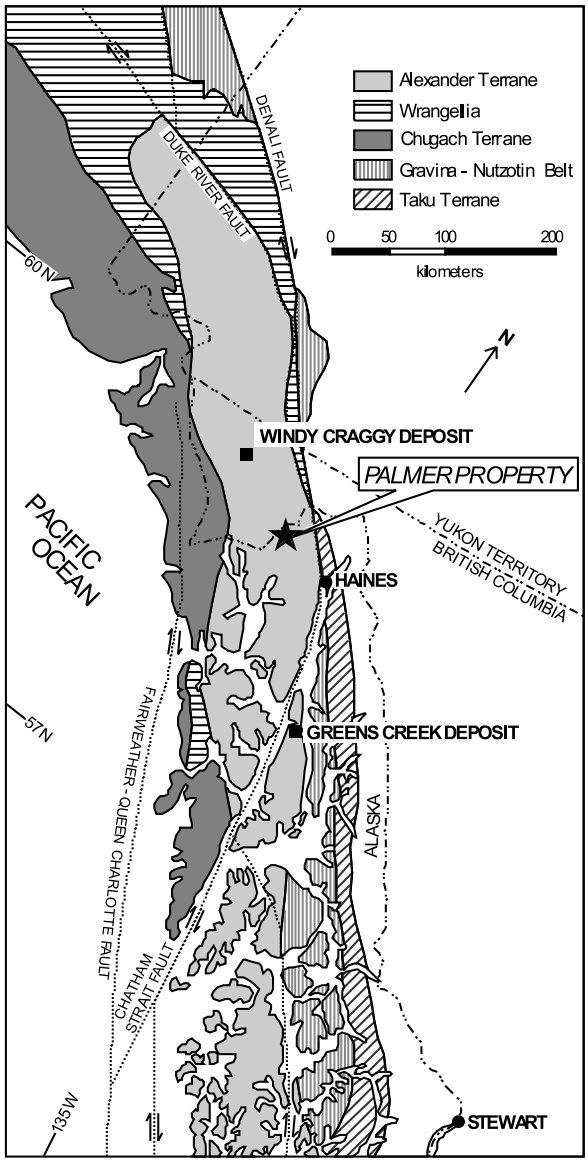

Figure 1. *Location map of the Palmer property, showing tectonostratigraphic terranes and major faults of southeastern Alaska and adjoining parts of Canada. Geology adapted from Gehrels and Berg (1994), and Monger and others (1991).*

In the early 1990s, retreating ice exposed a new outcrop of massive sulfide that became known as the Little Jarvis occurrence. Chip samples at the occurrence yielded assays of 13.0 percent zinc, 7.0 percent copper, 0.02 oz/ton gold, and 7.0 oz/ton silver over 4.6 m (Wakeman, 1995). Rubicon Minerals' 1999 drill hole discovery of the RW zone was based on the interpretation that the Little Jarvis occurrence was correlative with the Upper Main occurrence 610 m to the southeast on the other side of the mountain (figs. 2, 3). Semimassive to massive sulfide (or its leached oxide equivalent) of the RW zone has been intersected in six drill holes and the zone remains open at depth in all directions.

REGIONAL SETTING

The Alexander tectonostratigraphic terrane extends along the coast of northwestern British Columbia northward through the Alaska panhandle into the Saint Elias Mountains of British Columbia and the Yukon, and westward into the Wrangell Mountains of Alaska (Wheeler and McFeely, 1991). According to Gehrels and Berg (1994), the Alexander terrane evolved along a convergent plate margin from Precambrian–Cambrian through Early Devonian time, with deposition of arc-type igneous and sedimentary rocks. These were subsequently deformed and metamorphosed during Middle Cambrian–Early Ordovician and Middle Silurian–earliest Devonian orogenies. The Middle Devonian through Early Permian was marked by relative tectonic stability with deposition of shallow marine carbonate, clastic rocks and subordinate mafic–intermediate volcanic rocks (Gehrels and Saleeby, 1987). Late Triassic, rift-related volcanic and sedimentary rocks were deposited unconformably on the Permian and older rocks (Gehrels and others, 1986). Overprinting deformation and metamorphism occurred mainly during Middle Jurassic through Cretaceous accretion of the Alexander terrane to inboard Cordilleran terranes (Berg and others, 1972; Coney and others, 1980), with further

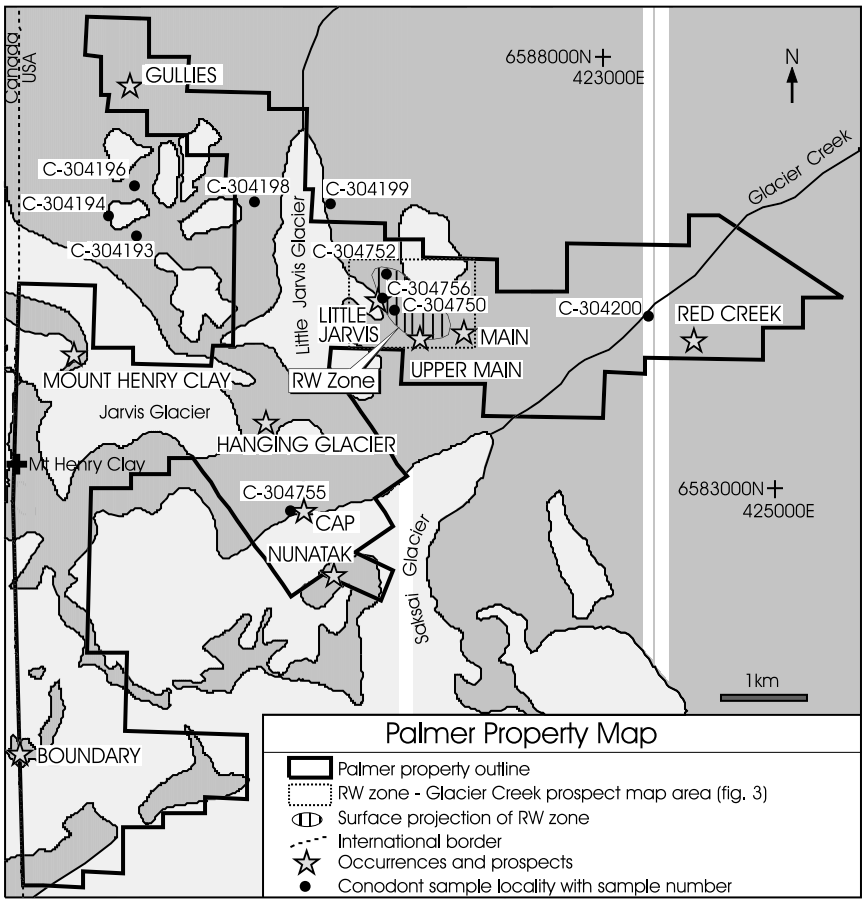

Figure 2. *Property map showing the major mineralized occurrences at Palmer property, new conodont localities, and an outline of the RW zone–Glacier Creek prospect map area.*

dismemberment occurring along regional-scale right-lateral strike-slip faults during Tertiary and Quaternary times.

Regional mapping in the vicinity of the Palmer property indicates that the area is underlain by Paleozoic and lower Mesozoic metasedimentary and metavolcanic rocks that are locally intruded by Cretaceous and Tertiary granitic plutons (Redman and others 1985; McKevett and others, 1974; Campbell and Dodds, 1983). Paleontological data are sparse, and because of structural complexity stratigraphic relationships are poorly understood. Thinly bedded limestone and massive marble that contain fossils of Devonian to Carboniferous age appear to be the oldest rocks in the area and are apparently overlain in depositional contact by pelitic rocks of undetermined age that are referred to as the Porcupine Slate. A dominantly mafic volcanic package, which is host to VMS mineralization at the Palmer property, is the youngest strata in the area, and is locally interfingered with the Porcupine Slate (Redman and others, 1985).

Four new conodont collections from narrow limestone and calcareous siltstone beds intercalated throughout the mafic sequence yield Late Triassic, Norian to Rhaetian ages (fig. 2, table 1), and confirm the suspected age of the rocks reported by MacIntyre (1986), which was based on a single conodont fragment from a sample collected near the Main occurrence. Massive cherty limestone, which is in structural contact with Late Triassic volcanic rocks northwest of the property, yielded a Middle Devonian age, and likely forms part of an overthrust block of Paleozoic basement. Of 27 samples analyzed for microfossils, only ten were productive, and in many of these the fossil populations were either too small or too poorly preserved to permit confident identification or determine tightly bracketed ages.

Late Triassic rocks on the Palmer property are correlative with the Hyd formation in central and southern southeastern Alaska (Loney, 1964; Gehrels and others 1986), as well as with the informally named Tats group, exposed in fault-bounded blocks northwest of the property in the Saint Elias Mountains in British

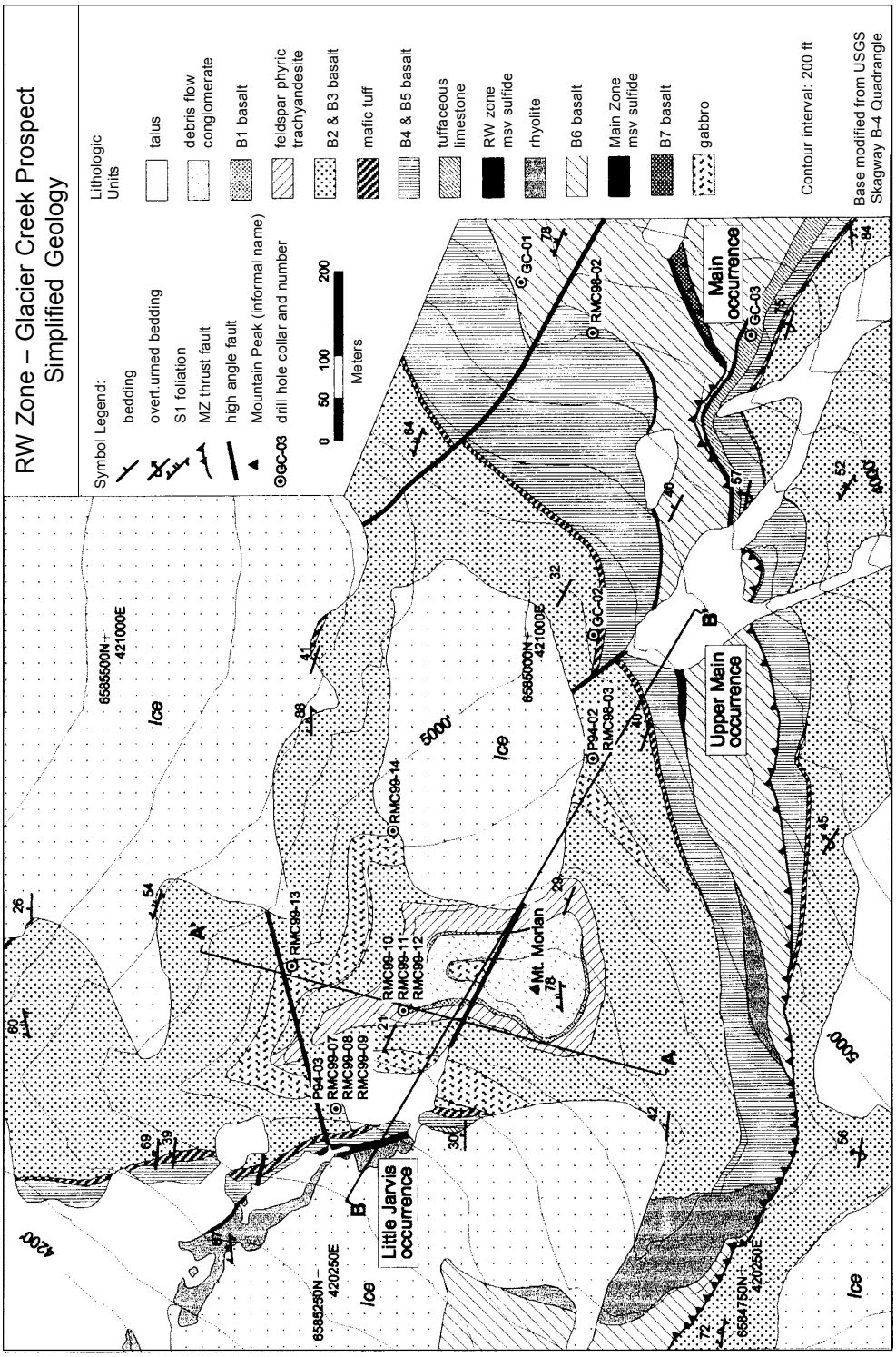

Figure 3. *Simplified geologic map of the RW zone–Glacier Creek prospect area; derived from unpublished mapping by Darwin Green and Jim Oliver.*

Table 1. *New conodont fossil data from the Palmer property and surrounding area*

Sample#	UTM E	UTM N	Zone	Genus	Species	Age	CAI Index
C-304199	419832	6586320	8	*Neogondolella* *Epigondolella*	*sp. indet.* *sp. indet.*	Norian	5
C-304756	420443	6585228	8	*Epigondolella*	*ex gr. bidenata Mosher 1968*	Middle Norian - Rhaetian	3 - 4
C-304196	417555	6586536	8	*Epigondolella*	*bidentata Mosher 1968*	Norian - Rhaetian	5
C-304198	418966	6586337	8	*Epigondolella* *Epigondolella* *Norigondolella*	*bidentata Mosher 1968* *triangularis (Budurov 1972)* *sp. indet.*	Norian - Rhaetian	5.5 - 6.5
C-304200	423535	6585008	8	*Neogondolella*	*sp. indet.*	Permian - Triassic	6.5 - 7
C-304752	420490	6585498	8	*Mesogondolella?*	*sp. indet.* *sp. cf. P. parawebbi*	Permian? (or Triassic)	5
C-304193	417585	6585947	8	*Polygnathus*	*Chatterton 1978*	Middle Devonian	5.5 - 7
C-304194	417262	6586185	8	*Pandorinellina?*	*sp. indet.*	Devonian?	5.5
C-304750	420581	6585085	8	ramiform elements		Ordovician - Triassic	3 - 4
C-304755	419373	6582751	8	ramiform elements		Ordovician - Triassic	7

Columbia (MacIntyre, 1986; Mihalynuk and others, 1993). The Hyd formation hosts the Greens Creek VMS deposit, and the Tats group hosts the Windy Craggy VMS deposit (fig. 1). Restoration of 150 km of Tertiary dextral offset along the Chatham Strait–Denali fault system (Hudson and others, 1982), places the Palmer property less than 30 km from Greens Creek VMS deposit (fig. 1). The Late Triassic proximity of the Palmer property to Greens Creek, in conjunction with similarities such as zinc-rich mineralization and abundance of barite, suggest the two formed in a similar geologic environment.

PROPERTY GEOLOGY

STRUCTURE

Upper Triassic rocks at Palmer record at least three different episodes of deformation, with the earliest and most evident being a north–south contractional event (D1). The D1 deformation is characterized by slatey to schistose cleavage (S1), and south-vergent folds and thrust faults (Lewis, 1998). Fabric intensity is highly variable, reflecting the strong contrast in rheology of the massive basalts and thin-bedded silty rocks making up the section. In most places preservation of primary rock textures is very good, although the rocks are locally deformed beyond recognition of the original protolith. In general, S1 fabric is most strongly developed within sedimentary strata and intensely altered volcanic rocks. Megascopic D1 folds have kilometer-scale wavelengths, closed to tight forms, and are commonly overturned. Mesoscopic D1 folds are scarce and typically restricted to intercalations of sedimentary strata.

The second phase of deformation (D2) is less readily observed and has no associated fabric. It is evidenced by megascopic folds that affect bedding and S1 foliation. The folds are generally tight and have subangular hinges with axes that plunge variably to the northwest. Although important at a property scale, the effects of the D2 deformation event are not apparent in the RW zone–Glacier Creek prospect map area. D3 deformation is manifest by weakly developed northeasterly crenulation fabrics that are present only locally within some of the more schistose rocks (Lewis, 1998). They are interpreted to postdate D2 deformation because the orientation of the crenulation cleavage is independent of position on D2 folds. Regional strain associated with D3 deformation is minor and does not appear to have produced any megascopic structures.

Late southwest- to northwest-striking faults postdate D2 and possibly D3 deformation events. They are brittle, steeply dipping structures that appear to have accommodated both vertical and horizontal movement. Neotectonic structures also appear to have been active at

the Palmer property. Scarps above the Main occurrence area mark the location of large slumps that appear to have displaced stratigraphy by up to 50 m. The fault and slump structures likely contribute to the high permeability and deep oxidation evident in the vicinity of the Main and Upper Main occurrences.

METAMORPHISM

Mineral assemblages and color alteration indices (CAI) of conodonts indicate that rocks at the Palmer property have undergone regional greenschist-facies metamorphism. Mafic rocks outside zones of focused hydrothermal alteration contain plagioclase (albite), chlorite, calcite, magnetite, quartz, epidote, iron carbonate, biotite, and, extremely rarely, actinolite. The scarcity of actinolite (a typical greenschist-facies mineral) suggests a high chemical potential of CO_2, which favors formation of carbonates over calcium-bearing silicates (Miyashiro, 1994).

In general, the CAI values of conodonts at Palmer range from 4 to 6, although a few specimens have values as low as 3 and as high as 7 (table 1). Color alteration index values between 4 and 6 correspond to a range of possible peak temperatures between 190°C and 435°C, when using 1 Ma and 200 Ma as limits on the duration of maximum depth of burial (Epstein and others, 1977; Rejebian and others, 1987). Some of the variation in CAI values is the result of thermal perturbations caused by igneous intrusions and perhaps by the interaction of conodonts with hydrothermal fluids. It is uncertain if there is a correlation at Palmer between stratigraphic position and CAI value or if there is systematic variation in metamorphic mineralogy associated with different CAI values.

Conodonts of known Late Triassic age have an average CAI value of 5 which, when assuming a geologically probable duration of maximum depth of burial between 5 Ma and 50 Ma, indicates peak temperatures between 315°C and 340°C. This temperature range lies in the lower half of the 300°C to 525°C range, under which greenschist-facies minerals typically form (Miyashiro, 1994), suggesting that the regional metamorphism that affected Late Triassic rocks at the Palmer property was lower greenschist facies, rather than upper greenschist facies suggested by Forbes and others (1989).

Contact metamorphism occurs in rocks surrounding intrusions of assumed Cretaceous to Tertiary age. The contact metamorphism is marked by a high modal abundance of biotite in mafic country rocks and by higher-than-average CAI values (for example, CAI=7 in sample C-304755).

GEOLOGY OF THE RW ZONE–GLACIER CREEK PROSPECT AREA

The RW zone is exposed between 1,310 m and 1,525 m in elevation, cropping out in two places on opposite sides of the informally named Mount Morlan (fig. 3). The western exposure is known as the Little Jarvis occurrence, which is separated by 610 m from the exposure on the southeast side of Mount Morlan, known as the Upper Main occurrence. The RW zone occurs in a panel of moderately north–northeast-dipping strata in the hanging wall to the MZ thrust fault. The MZ thrust fault disrupts a tight, overturned anticline, demonstrated by opposing topping directions in correlative pillow basalts on either side of the fault. Magnitude of displacement along the fault appears to be about 200 to 300 m.

The stratigraphic section described herein is 350 m thick and is dominated by massive to pillowed basalt flows, with subordinate impure carbonate rocks, tuff, and felsic volcanic rocks. The rocks were subject to prolonged hydrothermal activity and host stacked zones of massive sulfide. The base of the exposed section is the immediate stratigraphic footwall to massive sulfide at the Main zone, which occurs roughly 90 m stratigraphically below massive sulfide at the RW zone. Unit descriptions are based on examinations of drill core and detailed surface mapping of rocks in the hanging wall to the MZ thrust fault. The same stratigraphic units described in the hanging wall also occur in the overturned footwall to the MZ thrust fault, including leached baritic massive sulfide that occupies the same stratigraphic position as massive sulfide in the RW zone (fig. 3). A generalized strati-graphic section is presented in figure 4, and cross sections through the RW zone are presented in figures 5 and 6.

STRATIGRAPHIC UNITS

B7 BASALT UNIT

The B7 basalt is the lowest unit found in the RW zone–Glacier Creek prospect map area, and is only exposed in the Main occurrence area (fig. 3), where it forms yellow–orange gossanous outcrops in the footwall to leached baritic massive sulfide. It consists of aphyric mafic flows and subordinate tuff that are intensely altered to an assemblage of quartz, sericite, pyrite, and chlorite. Alteration commonly obliterates primary textures and locally makes identification of protolith difficult. Weathered surfaces and fractures are locally coated with secondary zinc and copper oxides, presumably derived from the overlying leached baritic massive sulfide. The B7 basalt unit was not studied in detail and its chemistry has not been characterized.

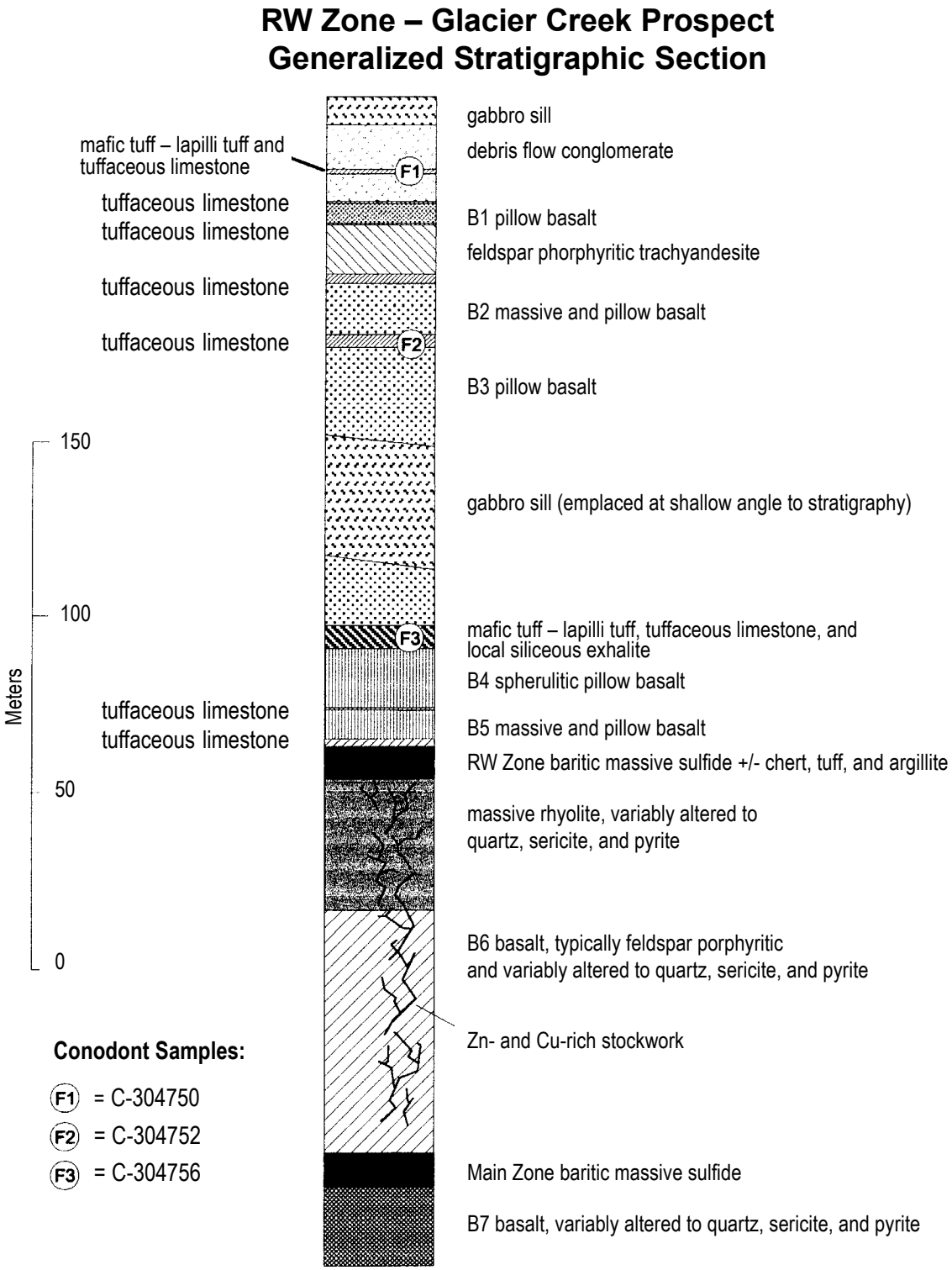

Figure 4. *Generalized stratigraphic section representing approximately 350 m of stratigraphy in the RW zone–Glacier Creek prospect area. Section is based on mapping and drill logs in the hanging wall to the MZ thrust fault. Stratigraphic intervals from which conodont samples were collected are indicated; data for conodont samples is listed in table 1.*

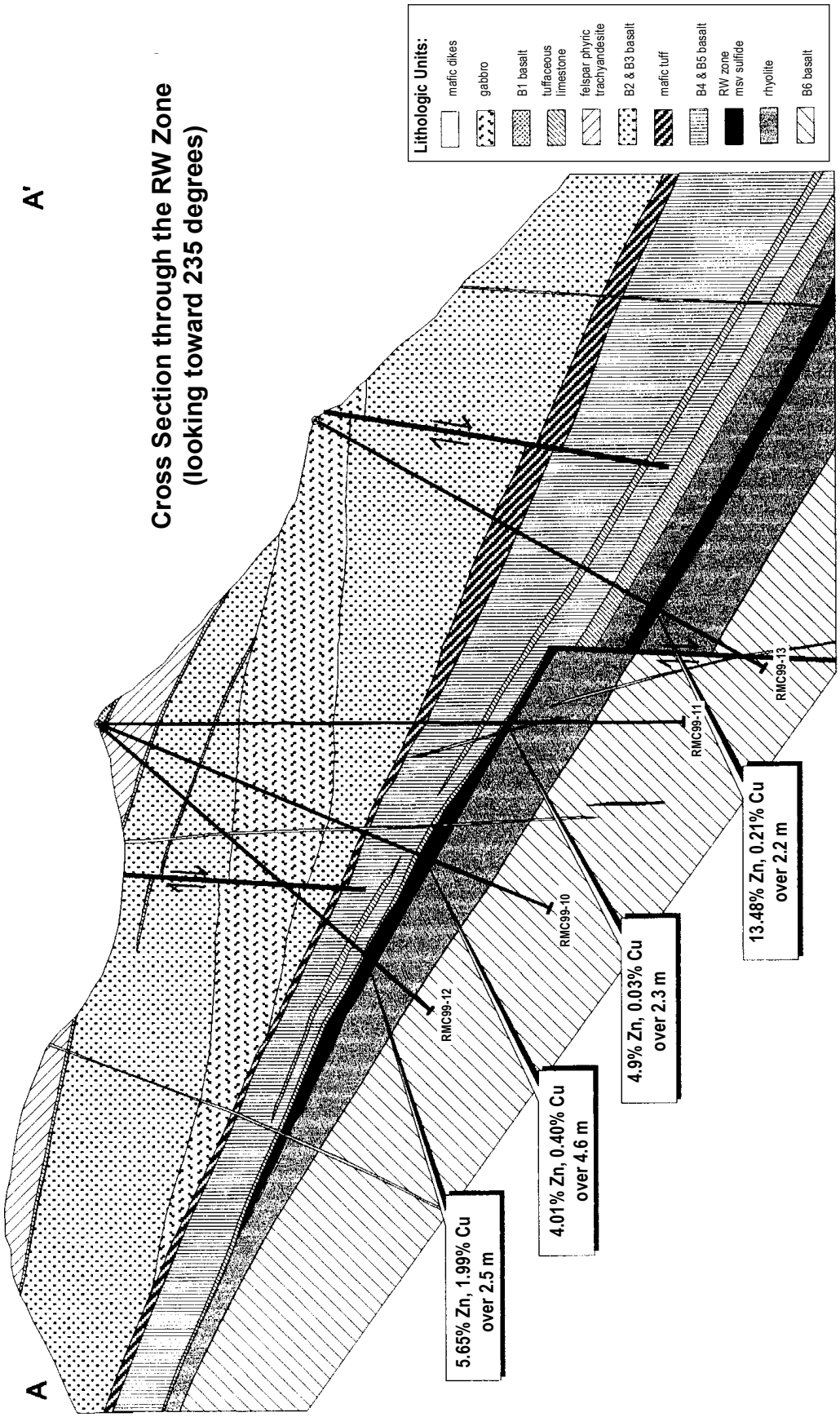

Figure 5. *Cross-section through the RW zone with geologic interpretation. Section is cut roughly perpendicular to strike of stratigraphy; view is toward an azimuth of 285 degrees.*

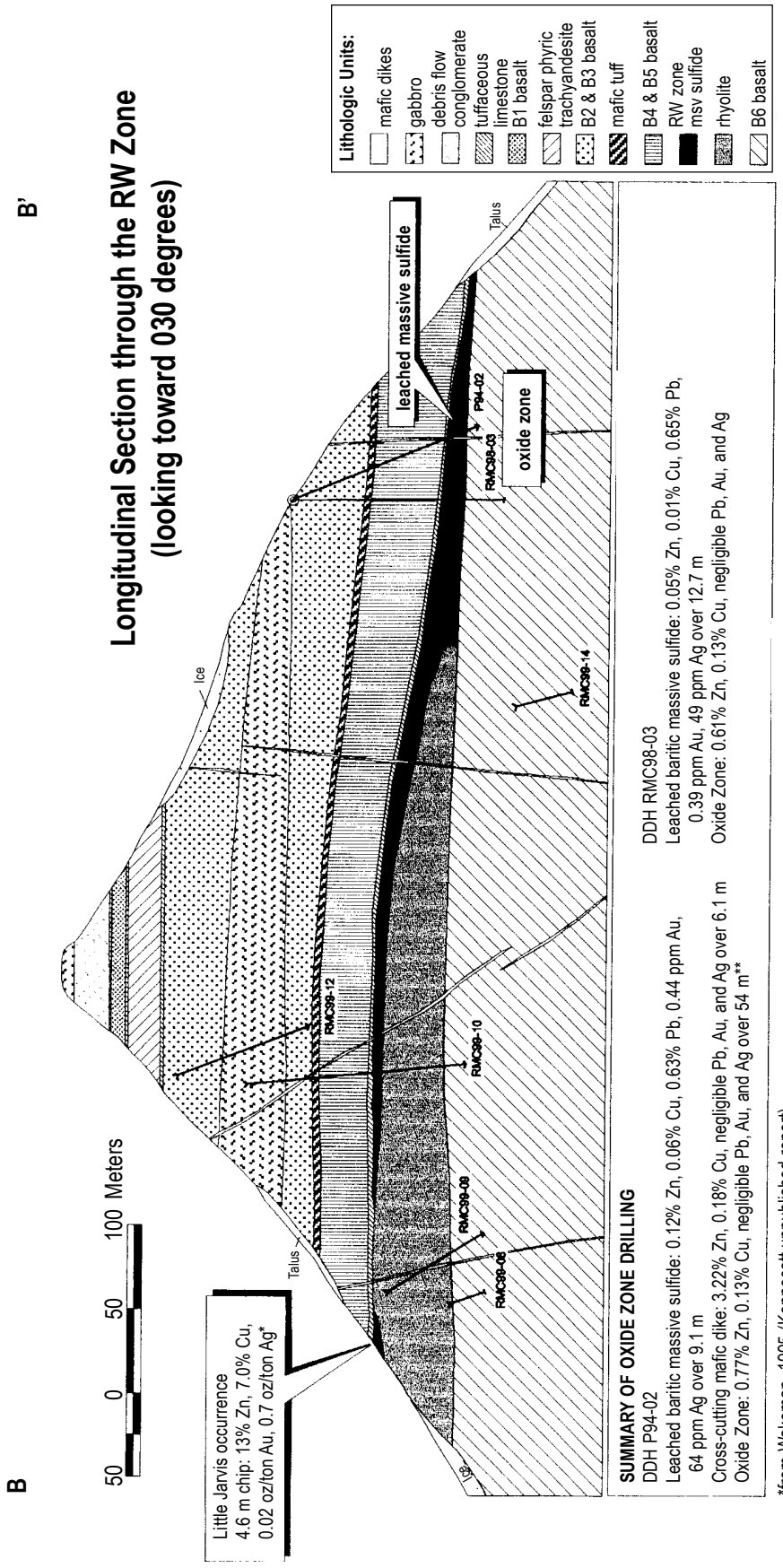

Figure 6. *Longitudinal section showing the RW zone massive-sulfide unit, which is interpreted to extend in a near-continuous manner from the Little Jarvis occurrence in the west to the leached oxide zone near the Upper Main occurrence in the east. View is toward an azimuth of 030 degrees.*

MAIN ZONE MASSIVE-SULFIDE UNIT

The Main zone massive-sulfide unit is exposed at the Main occurrence, where it is 2 to 4 m thick and can be traced along surface for 120 m. It is truncated to the southwest by the MZ thrust fault and appears to pinch out to the northeast into intensely quartz–sericite–pyrite-altered rocks. The unit is typically leached of sulfides and consists of iron-oxide stained, variably siliceous vuggy barite and baritic grus or sand. Primary sulfide mineralogy is preserved in rare weakly oxidized enclaves and includes sphalerite, chalcopyrite, galena, pyrite, and possible sulfosalts. The Main zone massive-sulfide unit has been intersected by only one drill hole (RMC98-02), which cut 4 m of near-surface leached baritic massive-sulfide and footwall zones of supergene copper and zinc oxides. All drill holes that tested the RW zone stopped short of the stratigraphic interval that hosts the Main zone massive-sulfide unit, leaving the subsurface extent of the Main zone virtually untested.

B6 VARIABLY FELDSPAR PORPHYRITIC BASALT UNIT

Overlying the Main zone, and locally forming the immediate footwall to the RW zone, is the B6 basalt unit, which consists of aphyric to feldspar porphyritic, massive and pillowed basalt flows, and minor volcanic breccia. Least altered rocks are blue-gray to olive-green, weakly amygdaloidal, and commonly contain 2 to 8 percent, 2 to 7 mm feldspar phenocrysts. Although the unit exhibits textural variability (aphyric vs porphyritic), it maintains relatively uniform immobile element chemistry, which is characterized by a high Al_2O_3 content (up to 22.06 percent on a LOI-free basis). The lower contact of the B6 basalt unit is exposed only in the vicinity of the Main occurrence. There, it occurs in the immediate hanging wall to the Main zone massive-sulfide unit, is 70 to 90 m thick, and is strongly altered to chlorite, sericite, and pyrite near its base. In areas underlying the RW zone massive-sulfide unit, quartz, chlorite, sericite, and pyrite alteration of the B6 basalt unit is widespread, primary textures are commonly destroyed, and chalcopyrite- and sphalerite-bearing pyritic stringers are common. Near the Main and Upper Main occurrences, most of the quartz–sericite schist described as impure metacherts by Forbes and others (1989) is reinterpreted as intensely altered B6 basalt because the quartz–sericite schist has the same immobile element signature as that of the unaltered B6 basalt unit.

RHYOLITE UNIT

Underlying most of the RW zone massive-sulfide unit is a locally amygdaloidal, generally aphyric, high zirconium (300 to 450 ppm) rhyolite flow unit that averages 30 to 45 m thick. It is only exposed on the south and west sides of Mount Morlan, and forms massive, rounded, yellow to deep-orange gossanous outcrops along the edge of a spur of the Little Jarvis glacier. It is pervasively altered to an assemblage of quartz, sericite, pyrite, and rare chlorite, and locally hosts sphalerite- and chalcopyrite-bearing pyritic stockwork. Amygdules occur in irregular patchy zones and are composed of quartz, pyrite, and sericite. The rhyolite unit typically contains 1 to 8 percent disseminated, very fine grained, euhedral pyrite. Porphyroblasts of iron carbonate occur locally. Most of the rhyolite unit appears to be a single flow with zones of breccia skirting its edge and occurring locally along the upper contact. Generation of minor subsequent flows is indicated by a 12-m-thick intersection of rhyolite in the hanging wall to the RW zone massive-sulfide unit in drill hole RMC99-13 (fig. 5).

RW ZONE MASSIVE-SULFIDE UNIT

The RW zone massive-sulfide unit consists of a body (or bodies) of stratiform zinc- and copper-rich baritic massive sulfide with subordinate chert, altered tuff, and limestone. The body (or bodies) of massive sulfide has a strike length of at least 610 m, a drill-indicated down-dip extent of at least 200 m, and a maximum known thickness of 12 m (figs. 4, 5). Primary mineralogy consists of barite, sphalerite, pyrite, chalcopyrite, quartz, galena, with lesser calcite, magnetite, pyrrhotite, arsenopyrite, and possible sulfosalts. Parts of the massive-sulfide body on the southeast side of Mount Morlan have been extensively leached of sulfides and are underlain by supergene copper and zinc oxides that extend 60 m or more into the footwall. Leached parts of the massive-sulfide body contain negligible copper and zinc, whereas lead, gold, and silver grades remain close to those of non-leached sections of the RW zone. Incipient oxidation persists at considerable depth, as is evident in drill hole RMC99-10, where pyrrhotite in massive sulfide 150 m below surface is replaced by skeletal pyrite and hydrous iron oxide, and covellite rims chalcopyrite grains.

TUFFACEOUS LIMESTONE UNIT

Thin, semi-continuous beds of pale buff to tan or dark gray, silty tuffaceous limestone occur intercalated between most of the major volcanic units in the RW zone–Glacier Creek prospect map area. The beds are finely laminated to massive, and average 1 to 6 m thick. Their composition varies from near pure limestone to pure ash tuff, although they typically are a mixture of carbonate, ash, clay, and silt. Locally the tuffaceous limestone unit contains 1- to 3-m-thick sections of graphitic argillite, and 0.1- to 1-m-thick lenses of chert. Tuffaceous limestone occurring in the immediate hanging wall to RW zone massive sulfide locally has a

component of felsic ash tuff and is variably altered to sericite. Conodonts in sample C-304752, collected from dark gray to black tuffaceous limestone that separates the B3 and B2 basalt units, are loosely constrained to Permian to Triassic age.

B5 massive and pillowed basalt unit

The B5 basalt unit consists of gray–green, weakly to strongly magnetic, weakly to non-amygdaloidal, aphyric, massive to pillowed basalt flows. It locally contains hematite and jasper, and commonly contains carbonate-filled fractures. The unit approaches 30 m in thickness in drill holes near the Upper Main occurrence, although it is either absent or only a few meters thick in drill holes on the west side of the mountain. It was not identified on surface in the area of the Little Jarvis occurrence.

B4 spherulitic pillow basalt unit

The B4 basalt unit consists of dark blue–green, aphyric, moderate to strongly magnetic, amygdaloidal, pillowed basalt flows that commonly exhibit a distinctive spherulitic texture. Spherulites weather pale gray to white, are 0.5 to 10 mm in diameter, and are most conspicuous along dark green, intensely chloritized pillow margins. Amygdules are composed of calcite and are generally 5 to 30 mm in diameter. Flows also commonly contain carbonate in pillow interstices and cooling fractures. At one locality, the flows occur as a series of thin (0.5 to 1 m thick), stacked sheets, suggesting very low viscosity magma. The B4 spherulitic pillowed basalt unit is 15 to 18 m thick above the Little Jarvis occurrence, thickens to the northeast to roughly 30 m in drill hole RMC99-13, and is absent in core from drill holes near the Upper Main occurrence.

Mafic tuff–lapilli tuff, limestone, and siliceous exhalite unit

A 2- to 10-m-thick section of well-bedded tuffaceous rocks forms a good marker bed that is traceable around the mountain and recognized in the overturned footwall to the MZ thrust fault. In the vicinity of the Little Jarvis occurrence the tuff–limestone–exhalite unit consists of alternating layers of pale gray to dark brown variably calcareous fine to coarse ash tuff, and lapilli tuff, capped by a layer of pale buff to tan impure limestone. Minor layers containing rare siliceous lapilli fragments are a distinctive feature of this unit (although overall the tuffaceous rocks are predominantly mafic), and some beds share the same chemical signature as the underlying B4 basalt unit. Conodonts in sample C-304756, collected from the tuff–limestone–exhalite unit in drill hole P94-03, are Middle Norian to Rhaetian age (table 1).

A lens of siliceous exhalite, up to 4.5 m thick and roughly 105 m long, occupies the stratigraphic position of the mafic tuffaceous rocks about 200 m north of the Little Jarvis occurrence. The exhalite consists of massive white, fine-grained silica with local black, strongly magnetic cherty zones, and contains negligible sulfide.

B3 pillow basalt unit

The B3 pillow basalt unit is a 45- to 60-m-thick unit composed of multiple pillowed flows and rare lava tubes or channels. The flows are dark green–brown and commonly contain large (5 to 20 mm) carbonate amygdules densely distributed throughout. They also contain scattered, coarse-grained (up to 15 mm) pyrite cubes in their otherwise aphyric matrix. Near the base of the unit, pockets of carbonate locally form distinctive radial or rosette-like forms that are up to 10 cm in diameter.

B2 massive and pillowed basalt unit

The B2 basalt unit is 12 to 15 m thick and consists of medium to dark green massive to pillowed basalt flows. It is aphyric, weakly magnetic, and contains sparse carbonate amygdules.

Feldspar porphyritic trachyandesite unit

A massive pale green to blue–gray, 10- to 20-m-thick feldspar porphyritic trachyandesite flow is the only volcanic unit encountered in the RW zone–Glacier Creek prospect map area that has an intermediate chemical composition. The rock is variably magnetic, hosts local patches of jasper, and contains scattered pods of carbonate (amygdules?) that are 10 to 40 mm in diameter. Feldspar phenocrysts are up to 5 mm long, and the unit locally contains distinctive euhedral, millimeter-scale iron carbonate porphyroblasts.

B1 pillow basalt unit

The B1 basalt unit is a black, aphyric, nonmagnetic, coarsely amygdaloidal pillowed basalt flow that is 4.5 to 6 m thick. Amygdules are composed of carbonate and are particularly abundant near pillow margins. Chemical composition of the B1 basalt unit is peculiar in that it contains high concentrations of both Zr and TiO_2 (231 ppm Zr and 2.93 percent TiO_2 on a LOI-free basis).

Conglomerate (debris flow) unit

The uppermost stratigraphic unit is a poorly sorted, heterolithic conglomerate that contains angular to rounded granules to boulders of basalt, chert and/or rhyolite(?), and subordinate limestone. It is exposed only near the peak of Mount Morlan and has a minimum thickness of 25 m. The conglomerate occurs in two distinct beds that are separated by 2 to 3 m of mafic ash to lapilli-tuff and tuffaceous limestone, which contain conodonts of undetermined age (sample C-304750,

table1). Its generally massive character, local crude reverse grading, common angular clasts, and poor sorting suggest an origin as a high-density debris flow. Basalt clasts are commonly highly vesicular to scoriaceous, reach up to 1 m in diameter, and in rare cases exhibit the form of pillows and pillow fragments. Siliceous fragments are commonly well rounded and therefore were probably sourced in a subaerial environment. The carbonate-rich matrix weathers recessively, producing a distinctive knobby texture in outcrop.

INTRUSIVE UNITS

GABBRO

A sill-like gabbro body, up to 45 m thick, cuts gently upsection to the northeast in the hanging wall of the RW zone. It is moderately to strongly magnetic, very fine to medium grained (0.2 to 1.5 mm), and contains minor disseminated pyrite and pyrrhotite. Along the contact of a tuffaceous limestone bed, an irregular breccia with a tuffaceous limestone matrix occurs within the gabbro. This contact relationship may indicate that the gabbro intruded sediment that was only partially lithified. A similar gabbro body is exposed near the peak of the mountain, where it overlies the debris-flow conglomerate in a down-dropped fault block. The gabbro has undergone regional greenschist-facies metamorphism, has similar chemistry to the host mafic volcanic rocks, and is assumed to be part of the same overall magmatic system as the host volcanic sequence described above.

MAFIC DIKES

A series of roughly northeast-trending, 0.5- to 3-m-wide basalt and fine-grained diorite dikes cut all other lithologic units. The dikes pinch and swell, have moderate to steep dips and locally form thin sills along tuff and limestone beds. Disseminated fine-grained iron carbonate, which possibly formed during regional metamorphism, is ubiquitous in the diorite dikes. Other dikes include variably altered mafic feeders to the volcanic stratigraphy, some of which can be tied to specific lithologic units on the basis of their chemistry.

CHEMISTRY

ROCK CLASSIFICATION

Compositions of representative samples of the main igneous units are recorded in table 2. Classification of rock units was based on the immobile elements zirconium, titanium, aluminum, niobium, and yttrium. Diagrams that rely on concentrations of potassium and sodium are not used here because of the potential mobility of these elements in environments of hydrothermal alteration and greenschist-facies metamorphism.

A bimodal grouping for the majority of the volcanic units is clearly displayed on the Zr/TiO_2 vs Nb/Y diagram (fig. 7A;Winchester and Floyd, 1977). Most mafic rocks plot in the sub-alkaline basalt field or are transitional between the sub-alkaline basalt and andesite/basalt fields. Felsic rocks all plot well within the rhyolite field. The only intermediate composition comes from a feldspar porphyritic unit that falls on the edge of the trachyandesite field. On the SiO_2 vs Zr/TiO_2 diagram (Winchester and Floyd, 1977), samples cluster in similar fields but have a marked vertical spread because of addition and depletion of silica during alteration (fig. 7B). The effects of alteration are most pronounced in rocks in the footwall and immediate hanging wall to the RW zone massive sulfide, with rocks shifting out of the fields to which they are classified based on immobile element chemistry alone. With the Y vs Zr diagram of Barrett and MacLean (1994), most of the igneous rocks cluster in the tholeiitic field, although the data show a fair degree of spread and a few of the samples lie within the transitional field (fig. 8).

GEOCHEMISTRY OF VOLCANIC UNITS

Each of the major volcanic units forms a tight cluster on a Zr/TiO_2 vs Zr/Al_2O_3 diagram (fig. 9A), which permits effective geochemical discrimination of the units. This type of geochemical signature is extremely useful on the structurally complex Palmer property, where different mafic units are commonly very similar in physical appearance. It allows for confident identification of units in areas of intense hydrothermal alteration, supports the correlation of strata in the hanging wall to the MZ thrust fault with strata in the overturned footwall to the fault, and aids in the correlation of the RW zone–Glacier Creek prospect area with occurrences elsewhere on the property.

A linear distribution of lithologic unit data points on the Al_2O_3 vs Zr diagram (fig. 9B) and the TiO_2 vs Zr diagram (fig. 9C) is interpreted to reflect mass gains and mass losses due to alteration. The linear trends are most apparent in the rhyolite and B6 basalt units, which form the highly altered footwall to the RW zone mineralization. In general, strongly altered rocks are depleted in Na_2O, CaO and locally SiO_2, and enriched in Fe_2O_3, K_2O, and SiO_2.

SUMMARY AND DISCUSSION

The RW zone is a new zone of VMS-style mineralization discovered recently at the Palmer property, near Haines, Alaska. It is hosted by a mafic-dominated bimodal section of tholeiitic to transitional volcanic rocks that are Late Triassic (Norian to Rhaetian) age and correlative with the host rocks at the Greens Creek and Windy Craggy VMS deposits. After restoration of 150 km of Tertiary dextral offset along the Chatham Strait–Denali fault system, the Palmer property would be

Table 2. *Chemical composition of igneous units in the RW zone–Glacier Creek prospect area. Shown is a 44-sample subset of the 100 samples used in figures 7–9. All samples were analyzed by X-ray fluorescence at Chemex Laboratories in Vancouver, British Columbia, Canada.*

Sample	Unit	Al_2O_3 (%)	CaO (%)	Cr_2O_3 (%)	Fe_2O_3 (%)	K_2O (%)	MgO (%)	MnO (%)	Na_2O (%)	P_2O_5 (%)	SiO_2 (%)	TiO_2 (%)	LOI (%)	Total (%)	Ba ppm	Rb ppm	Sr ppm	Nb ppm	Zr ppm	Y ppm
RMR30279	B1 basalt	14.81	3.68	<0.01	14.19	0.33	7.86	0.11	3.13	0.93	44.80	2.67	6.30	98.81	485	12	96	30	210	46
RMC60504	Trachyandesite	14.90	4.60	<0.01	6.37	2.17	6.73	0.06	4.13	0.12	51.86	0.47	8.21	99.62	1045	38	246	24	168	38
RMR30280	Trachyandesite	14.97	4.35	<0.01	7.50	0.98	8.99	0.08	3.13	0.10	50.02	0.52	8.93	99.57	600	20	182	20	153	30
RMC60505	B2 basalt	14.21	9.91	<0.01	11.76	1.59	6.84	0.21	1.52	0.18	41.20	1.04	9.64	98.10	8370	26	232	10	66	18
RMR30296	B2 basalt	15.80	6.48	<0.01	11.99	1.64	6.06	0.14	2.12	0.20	45.15	1.24	8.16	98.98	2580	22	130	14	81	22
RMR30295	B3 basalt	12.51	12.03	<0.01	10.21	0.27	5.00	0.11	4.18	0.15	42.08	0.66	12.18	99.38	140	12	318	10	60	22
RMR31802	B3 basalt	14.74	7.89	0.03	8.98	0.22	6.98	0.13	4.60	0.18	44.35	0.82	10.30	99.22	560	12	380	8	81	18
RMC60560	B3 basalt	14.57	6.61	0.03	10.07	0.72	4.38	0.11	5.87	0.23	48.51	0.89	6.91	98.90	320	26	234	10	75	24
RMC60506	B3 basalt	13.69	8.75	<0.01	9.63	1.86	5.38	0.14	4.36	0.16	45.38	0.73	8.96	99.04	610	36	264	10	63	22
RMC60548	B3 basalt	13.88	7.52	<0.01	10.40	0.46	5.81	0.14	4.46	0.13	46.69	0.73	9.34	99.56	305	20	200	12	69	24
RMC60511	B3 basalt	13.04	9.50	0.01	9.65	1.97	3.92	0.13	3.96	0.17	43.10	0.65	13.54	99.64	505	44	192	12	69	28
RMR30271	B4 basalt	13.04	8.07	<0.01	12.54	0.06	5.98	0.14	3.94	0.18	44.89	1.14	8.57	98.55	110	8	208	12	87	24
RMR30283	B4 basalt	12.71	8.02	<0.01	11.16	0.64	5.28	0.16	3.81	0.28	46.10	1.10	9.56	98.82	1170	20	218	12	84	22
RMR30298	B4 basalt	13.46	11.73	<0.01	10.36	0.15	5.47	0.16	3.61	0.27	40.73	1.25	12.25	99.44	810	8	220	10	96	22
RMR31806	B4 basalt	12.92	10.72	0.02	11.61	0.08	5.32	0.17	3.92	0.22	41.63	1.14	11.39	99.14	85	12	206	10	84	22
RMR31813	B4 basalt	13.82	7.96	0.05	19.18	0.08	11.38	0.20	0.55	0.22	32.38	1.69	11.51	99.02	90	16	168	10	120	22
RMR31820	B4 basalt	14.32	7.19	0.02	11.28	0.07	5.88	0.13	3.99	0.25	45.84	1.46	8.80	99.23	130	10	174	14	108	20
RMC60562	B5 basalt	13.69	7.94	0.01	14.48	0.17	5.08	0.17	4.41	0.31	43.25	1.75	8.50	99.76	485	18	162	10	90	26
RMC60563	B5 basalt	12.73	7.54	<0.01	15.46	0.22	5.04	0.20	3.15	0.25	45.16	1.66	7.66	99.07	2100	18	206	10	84	24
RMC60191	B5 basalt	13.31	7.95	<0.01	15.48	0.16	4.69	0.19	3.81	0.25	43.05	1.78	8.33	99.00	480	14	172	10	90	22
RMC60541	B5 basalt	13.52	6.79	<0.01	15.14	0.06	6.28	0.18	3.15	0.26	42.75	1.87	8.95	98.95	95	10	122	14	93	28
RMC60514	B5 basalt	13.69	7.18	<0.01	15.38	0.06	5.50	0.15	2.82	0.31	43.44	1.72	9.33	99.58	55	12	140	12	90	22
RMC60522	B5 basalt	13.49	6.53	<0.01	14.97	0.16	4.86	0.16	3.78	0.28	46.17	1.73	7.45	99.58	135	12	152	12	93	26
RMR30273	Rhyolite	11.91	1.56	<0.01	2.81	2.63	1.79	0.05	1.28	0.03	73.19	0.23	3.05	98.53	4300	54	44	46	345	98
RMR30286	Rhyolite	9.70	0.05	<0.01	3.42	3.00	0.40	0.01	0.13	0.03	79.43	0.18	2.78	99.13	1455	60	20	44	294	72
RMR30290	Rhyolite	12.57	0.44	<0.01	5.84	3.02	3.10	0.06	0.33	0.05	69.37	0.23	3.97	98.98	1695	62	22	44	375	96
RMR30291	Rhyolite	11.57	0.03	<0.01	4.18	2.87	2.11	0.03	0.16	0.03	74.80	0.22	3.26	99.26	1985	56	12	44	357	88
RMR30299	Rhyolite	10.87	0.16	<0.01	1.30	3.46	0.54	0.01	0.08	0.02	79.99	0.20	1.87	98.50	3440	64	10	38	327	82
RMC60537	Rhyolite	13.64	1.15	0.01	5.04	2.50	3.12	0.08	1.65	0.03	67.33	0.25	3.32	98.12	3030	52	88	52	423	105
RMC60385	Rhyolite	13.58	0.26	<0.01	3.35	3.61	1.63	0.07	0.57	0.05	72.57	0.24	3.14	99.07	2750	74	36	44	396	115
RMC60321	Rhyolite	12.55	0.63	<0.01	2.91	3.81	0.77	0.04	0.14	0.05	73.76	0.23	3.77	98.66	3730	74	38	48	381	115
RMC60374	Rhyolite	11.09	0.36	<0.01	4.50	3.17	0.97	0.04	0.10	0.01	74.93	0.19	3.42	98.78	5110	58	24	42	315	72
RMC60524	Rhyolite	14.13	0.71	<0.01	4.73	2.57	3.01	0.08	1.35	0.05	68.85	0.28	3.14	98.90	2140	54	80	50	405	92

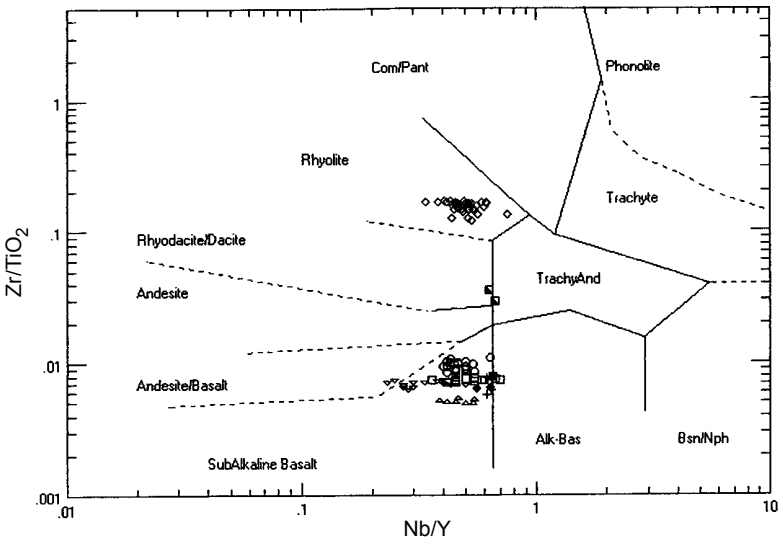

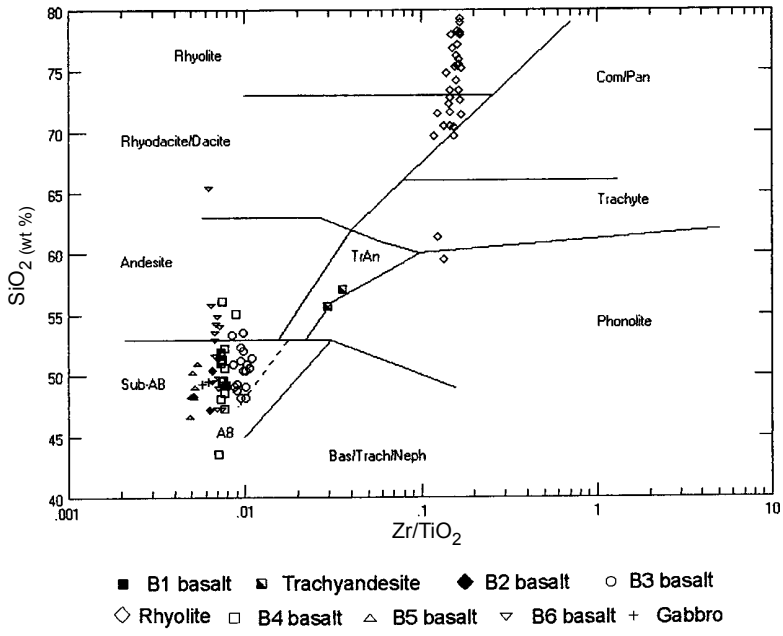

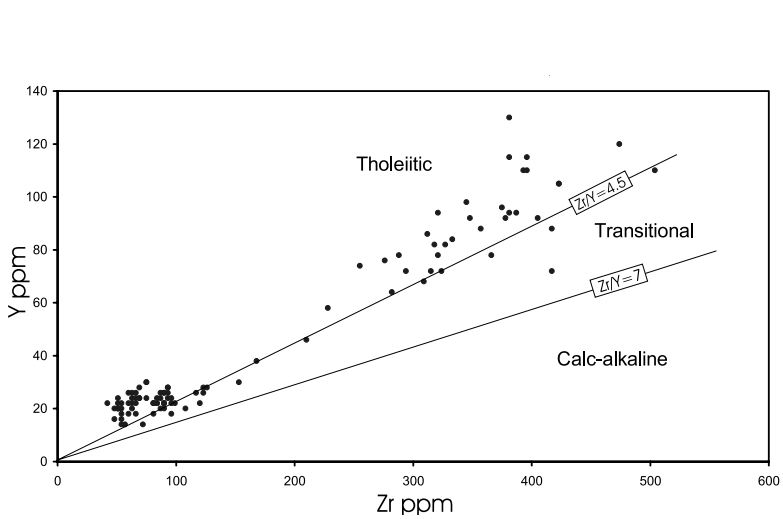

Figure 7. *Plots of (A) Zr/TiO_2 vs Nb/Y, and (B) SiO_2 vs Zr/TiO_2 (after Winchester and Floyd, 1977) for 100 rock samples from the RW zone–Glacier Creek prospect area. The vertical spread in data points in figure 7b is largely a function of alteration. Data are presented on a LOI-free basis.*

Figure 8. *Y vs Zr magmatic affinity plot for 100 rock samples from the RW zone–Glacier Creek prospect area (fields after Barrett and MacLean, 1994).*

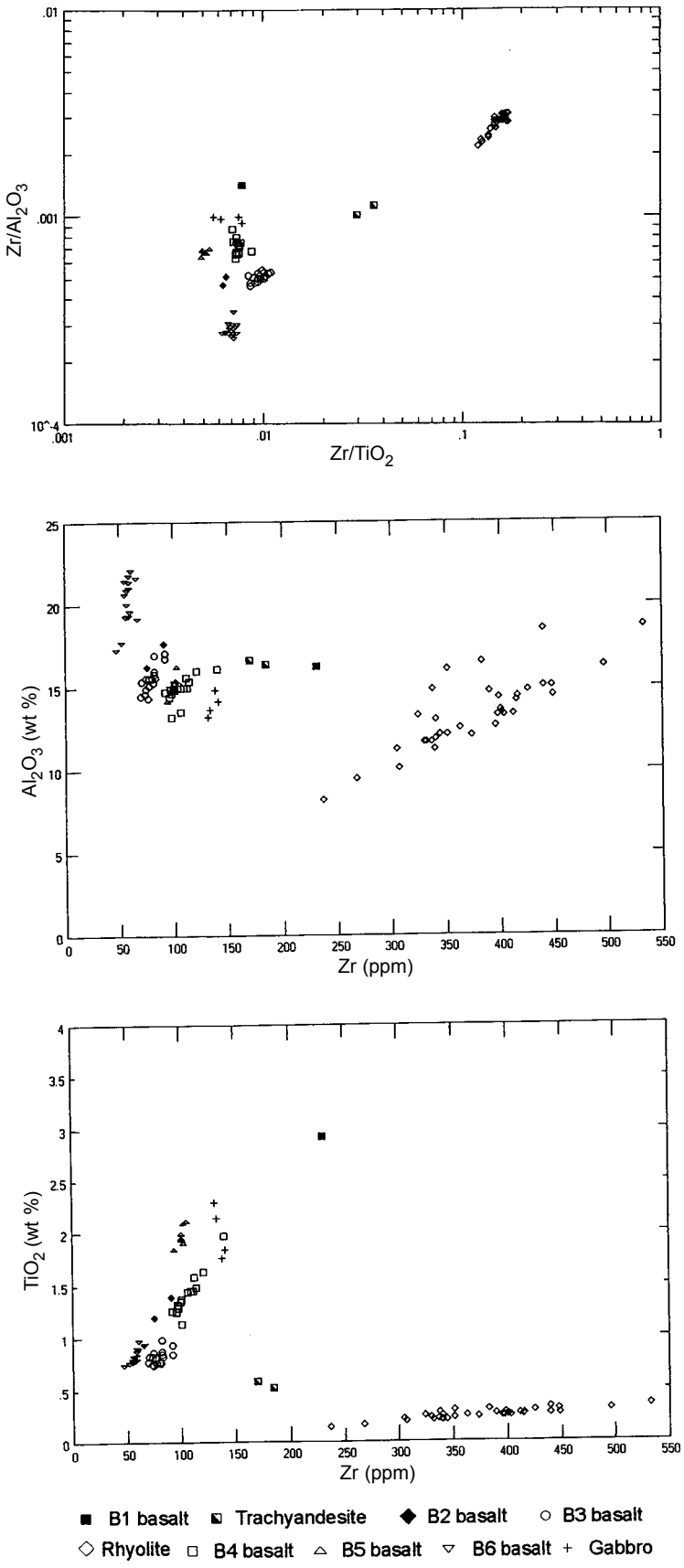

Figure 9. *Plots of (A) Zr/Al_2O_3 vs Zr/TiO_2, (B) Zr vs Al_2O_3, and (C) Zr vs TiO_2 for 100 rock samples from the RW zone–Glacier Creek prospect area. Note how each of the different lithologic units in figure 9A plots in its own unique space. The effects of mass change during alteration can be seen in the linear distribution of data points for individual lithologic units in figures 9B and 9C. Data are presented on a LOI-free basis.*

located less than 30 km from the Greens Creek mine. The Late Triassic proximity of the Palmer property to the Greens Creek VMS deposit in conjunction with similarities such as zinc-rich mineralization and the abundance of barite suggest the two formed in a similar geologic environment.

Rocks on the property have undergone regional greenschist-facies metamorphism and at least three phases of deformation, with the earliest and most evident being a north–south contractional deformation event (D1) that is characterized by slatey to schistose cleavage (S1) and south-vergent fold and thrust structures. S1 foliation is reoriented around north–northwest-plunging, open to tight D2 folds that have no associated fabric. Deformation postdating D2 includes rare crenulation fabrics and steep southwest- to northwest-striking faults.

The RW zone occurs in a panel of moderately north–northeast-dipping strata that forms the hanging wall to the MZ thrust fault. The rocks were subject to prolonged hydrothermal activity and host stacked zones of massive sulfide. The stratigraphic section preserved in the thrust panel is more than 350 m thick and is dominated by massive to pillowed basalt, with subordinate rhyolite, mafic tuff, tuffaceous limestone, trachyandesite, conglomerate, and gabbro. Volcanic units have distinct immobile element signatures, permitting effective geochemical discrimination of units. This provides a tool that aids in the correlation of units across structures and through zones of hydrothermal alteration.

The RW zone consists of a body (or bodies) of stratiform sphalerite-, barite-, and chalcopyrite-rich massive sulfide that has a strike length of at least 610 m, a down-dip extent of at least 200 m, and a maximum known thickness of 12 m. The zone is underlain by intensely quartz–sericite–pyrite–chlorite-altered rocks that locally host sphalerite- and chalcopyrite-rich stockwork. The Main zone, which sits roughly 90 m stratigraphically below the RW zone, consists of similar stratiform mineralization. It has only been intersected in one drill hole and its subsurface extent remains virtually untested. Supergene processes have played an important role in modifying both the RW and Main zones. Along the southeastern side of Mount Morlan, barite-rich massive-sulfide bodies have been extensively leached of sulfides and are underlain by zinc and copper oxide enrichment zones. Previous work on the property failed to recognize that iron-oxide stained, variably siliceous vuggy barite and barite grus, or sand, in both outcrop and drillcore was leached massive sulfide, resulting in the underevaluation of the property's potential to host significant massive-sulfide mineralization.

ACKNOWLEDGMENTS

This paper is based on data collected during the 1998, 1999, and 2000 field seasons and summarizes results of ongoing M.Sc. thesis research by Darwin Green. The research was made possible by financial assistance from Rubicon Minerals Corp., the Natural Sciences and Engineering Research Council of Canada, and the Society of Economic Geologists Foundation (Hickok–Radford Grant). Peter Lewis, Jim Oliver, Katherine Bull, Peter Daubeney, David Adamson, and Michael Gray contributed to the understanding of the property geology. We also appreciate the insights of the late Richard Walker, after whom the new discovery at Palmer was named. Thanks are extended to Charles Greig for editorial comments, and to Jeanine Schmidt and Thomas Bundtzen for their critical reviews of the manuscript.

REFERENCES

Barrett, T.J., and MacLean, W.H., 1994, Chemostratigraphy and hydrothermal alteration in exploration for VHMS deposits in greenstones and younger volcanic rocks, *in* Lentz, D.R., ed., Alteration and alteration processes associated with ore-forming systems: Geological Association of Canada, Short Course Notes, v.11, p. 433–467.

Berg, H.C., Jones, D.L., and Richter, D.H., 1972, Gravina–Nutzotin belt–Tectonic significance of an upper Mesozoic sedimentary and volcanic sequence in southern and southeastern Alaska: U.S. Geological Survey Professional Paper 800D, p. D1–D24.

Campbell, R.B., and Dodds, C.J., 1983, Geology of the Tatshenshini River map area (114P), British Columbia: Geological Survey of Canada Open-File Report 926, 1 sheet, scale 1:125,000.

Coney, P.J., Jones, D.L., and Monger, J.W.H., 1980, Cordilleran suspect terranes: Nature, v. 288, p. 329–333.

Epstein, A.G., Epstein, J.B. and Harris, L.D., 1977, Conodont color alteration – an index to organic metamorphism: U.S. Geological Survey Professional Paper 995, 27 p.

Forbes, R.B., Gilbert, W.G., and Redman, E.C., 1989, Geologic setting and petrology of the metavolcanic rocks in the northwestern part of the Skagway B-4 Quadrangle, southeastern Alaska: Alaska Division of Geological & Geophysical Surveys Public-Data File 89-14, 46 p.

Geddes Resources Ltd., 1991, Third quarter report to shareholders, November 18, 1991, 6 p.

Gehrels, G.E., and Berg, H.C., 1994, Geology of southeastern Alaska, Chapter 13, *in* Plafker, George, and Berg, H.C., eds., The Geology of Alaska; The Geology of North America: Geological Society of America, v. G-1, p. 451–467.

Gehrels, G.E., and Saleeby, J.B., 1987, Geologic framework, tectonic evolution, and displacement history of the Alexander Terrane: Tectonics, v. 6, no. 2, p. 151–173.

Gehrels, G.E., Dodds, C.J., and Campbell, R.B., 1986, Upper Triassic rocks of the Alexander terrane, southeastern Alaska, and the Saint Elias Mountains of B.C. and Yukon: Geological Society of America Abstracts with Programs, v. 18, no. 2, p. 109.

Hudson, Travis, Plafker, George, and Dixon, Kirk, 1982, Horizontal offset history of the Chatham Strait fault, *in* Coonrad, W.L., ed., United States Geological Survey in Alaska; Accomplishments during 1980: U.S. Geological Survey Circular 844, p. 128–132.

Lewis, P., 1998, Palmer project preliminary field report: structural and stratigraphic setting of mineral occurrences, Glacier and Jarvis Creek area, Haines, Alaska Rubicon Minerals Corporation, unpublished report, 11 p.

Loney, R.A., 1964, Stratigraphy and petrography of the Pybus–Gambier area, Admiralty Island, Alaska: U.S. Geological Survey Bulletin 1178, 103 p.

MacIntyre, D.G., 1986, The geochemistry of basalts hosting massive sulphide deposits, Alexander terrane, northwest British Columbia: British Columbia Ministry of Energy, Mines and Petroleum Resources, Geological Fieldwork 1985, p. 197–210.

MacKevett, E.M., Jr., Robertson, E.C., and Winkler, G.R., 1974, Geology of the Skagway B-3 and B-4 quadrangles, southeastern Alaska: U.S. Geological Survey Professional Paper 832, 33 p.

Mihalynuk, M.G., Smith, M.T., MacIntyre, D.G., and Deschenes, M., 1993, Tatshenshini project, northwestern British Columbia (114P/11, 12, 13, 14; 114O/9, 10, 14, 15 & 16), Part A, Overview; Part B, Stratigraphic and magmatic setting of mineral occurrences, *in* Grant, B., and Newell, J.M., eds., Geological fieldwork 1992; a summary of field activities and current research: British Columbia Ministry of Energy, Mines and Petroleum Resources Geological Fieldwork 1993-1, p. 189–229.

Miyashiro, Akiho, 1994, Metamorphic Petrology: New York, Oxford University Press, 404 p.

Monger, J.W.H., Wheeler, J.O., Tipper, H.W., Gabrielse, H., Harms, T.A., Struik, L.C., Campbell, R.B., Dodds, C.J., Gehrels, G.E., and O'Brien, J., 1992, Upper Devonian to Middle Jurassic assemblages; Cordilleran terranes, Chapter 8, *in* Gabrielse, H., and Yorath, C.J., eds., Geology of the Cordilleran Orogen in Canada: Geological Survey of Canada, The geology of North America, v. G-2, no. 4, p. 281–317.

Redman, E.C., Gilbert, W.G., Jones, B.K., Rosenkrans, D.S., and Hickok, B.D., 1985, Preliminary bedrock-geologic map of the Skagway B-4 Quadrangle, Alaska: Alaska Division of Geological & Geophysical Surveys Report of Investigations 85-6, 1 sheet, scale 1:40,000.

Rejebian, V.A., Harris, A.G., and Huebner, J.S., 1987, Conodont color and textural alteration: an index to regional metamorphism, contact metamorphism, and hydrothermal alteration: Geological Society of America Bulletin, v. 99, no. 4, p. 471–479.

Still, J.C., 1984, Stratiform massive sulfide deposits of Mount Henry Clay area, southeast Alaska: U.S. Bureau of Mines Open-File Report 118-84, 10 p.

Still, J.C., Hoekzema, R.B., Bundtzen, T.K., Gilbert, W.G., Weir, K.R., Burns, L.E., and Fechner, S.A., 1991, Economic geology of the Haines–Klukwan–Porcupine area, southeastern Alaska: Alaska Division of Geological & Geophysical Surveys Report of Investigations 91-4, 156 p.

Swainbank, R.C., Szumigala, D.J., Henning, M.W., Pillifant, F.M., 2000, Alaska's Mineral Industry 1999: Alaska Division of Geological & Geophysical Surveys Special Report 54, 73 p.

Taylor, C.D., 1997, An arc-flank to back-arc transect: Metallogeny of Late Triassic volcanogenic massive sulfide occurrences of the Alexander Terrane, southeast Alaska and British Columbia [extended abs.] *in* SEG Neves Corvo Field Conference Abstracts and Program: p. 68.

Wakeman, B., 1995, Summary marketing document: Kennecott unpublished company report, 12 p.

Wheeler, J.O, and McFeely, P. (comp.), 1992, Tectonic assemblage map of the Canadian Cordillera and adjacent parts of the United States of America: Geological Survey of Canada Map 1712A, 3 sheets, scale 1:2,000,000.

Winchester, J.A., and Floyd, P.A., 1977, Geochemical discrimination of different magma series and their differentiation products using immobile elements: Chemical Geology, v. 20, p. 325–343.

A PERMIAN COOL-WATER LIMESTONE FROM THE CHULITNA TERRANE, SOUTHCENTRAL ALASKA

Simone Montayne[1] and Michael T. Whalen[1]

ABSTRACT

Recent studies contrast facies assemblages typical of cool-water carbonate environments with those typical of warm-water settings. The differences between warm- and cool-water carbonate facies assemblages allow for more refined environmental interpretations of ancient limestones than would otherwise be possible. Photosynthetic carbonate-producing organisms, abundant lime mud and nonskeletal carbonate grains, and little mechanical compaction due to early cementation characterize warm-water carbonate facies. Cool-water carbonates are dominated by heterotrophic carbonate-producing organisms, have few nonskeletal carbonate grains, little or no lime mud, and commonly compact to a greater degree than warm-water lithofacies. Petrographic examination of Permian limestones from the Chulitna terrane reveals features that are characteristic of cool-water deposition. Heterotrophic bryozoans and echinoderms dominate the biotic assemblage to the exclusion of phototrophic carbonate-producing organisms. Planispiral forams, echinoid spines, a solitary rugose coral, spicule molds, and fragments of brachiopods and bivalves occur in minor amounts. The assemblage lacks nonskeletal grains, contains little carbonate mud, lacks evidence of former aragonitic components, and contains mechanical compaction features. Triassic limestones from the Chulitna terrane contain facies indicative of a low-latitude tropical to subtropical environment. Accumulation of cool-water carbonate facies during Permian time followed by deposition of warm-water facies during the Triassic requires a change in latitude, climate, or oceanography. Differentiation of warm- and cool-water depositional regimes in Permian and Triassic limestones of other North American Cordilleran accreted terranes will generate new insight into the paleogeographic setting of the terranes, and provide information about the distribution of calcareous organisms throughout the ancestral Pacific Ocean.

INTRODUCTION

Carbonate-producing organisms are particularly sensitive to climate and oceanographic conditions and therefore are significant indicators of biogeography, paleogeography, and oceanography. Studies over the past three decades have revealed that cool-water carbonate environments, with water temperatures generally colder than 20°C, are characterized by different facies associations than those found in modern warm-water settings (Lees and Buller, 1972; Lees, 1975; Nelson, 1988; James, 1997). Nelson (1988) and James (1997) propose that differences between warm- and cool-water carbonates have existed throughout Phanerozoic time.

A variety of different associations of carbonate grain types are documented in warm- and cool-water settings but the major difference between them appears to be a preponderance of phototrophic and heterotrophic carbonate-producing organisms in warm- and cool-water environments, respectively. James (1997) proposed the terms photozoan and heterozoan to describe the associations of different carbonate grain types in warm- and cool-water carbonate sediments. The dominant skeletal grains in these associations have changed through the Phanerozoic, with Cenozoic heterozoan facies characterized by foraminifera, red calcareous algae, molluscs, bryozoans, and barnacles and pre-Cenozoic examples typified by echinoderms, brachiopods, and bryozoans (Lees and Buller, 1972; Nelson, 1988; James, 1997). In addition to a lack of phototropic organisms, cool-water carbonate assemblages are also distinguished by the presence of mechanical compaction and a scarcity of nonskeletal grains and carbonate mud (Lees and Buller, 1972; Nelson, 1988; James, 1997).

Much of the Pacific Rim, including most of North America west of the Rocky Mountains, is made up of a series of allochthonous accreted terranes (Coney and others, 1980; Jones and others, 1977, 1986; Howell and others, 1985). North American Cordilleran accreted terranes contain Paleozoic and Mesozoic carbonate rocks with numerous paleogeographic affinities (Jones and others, 1977; Coney and others, 1980; Stanley and Senowbari-Daryan, 1986; Newton, 1987, 1988; Stanley and Whalen, 1989; Belasky and Runnegar, 1993; Blodgett and Boucot, 1999). Difficulties in establishing the distribution of carbonate depositional environments throughout the ancestral Pacific Ocean are linked to our current inability to determine the paleogeographic positions of these accreted terranes (Flügel, 1994). Determination of paleolatitude through paleomagnetic studies has been instrumental in helping to decipher the tectonic history of the Peninsular, Wrangellia, and

[1]Department of Geology and Geophysics, University of Alaska Fairbanks, Fairbanks AK 99775-5780
Email for Simone Montayne: simone_montayne@dnr.state.ak.us

Alexander terranes in Alaska (Packer and Stone, 1972, 1974; Hillhouse, 1977; Van der Voo and others, 1980). Recent analysis of coral biogeography resulted in a proposed method to estimate paleolongitude as well (Belasky and Runnegar, 1993). However, these techniques require either documentation of primary magnetization of sedimentary or igneous rocks or detailed data on the diversity and distribution of specific fossil taxa. In many accreted terranes this information is lacking and their paleogeographic history remains obscure. Additional insights into the paleogeography of Late Paleozoic and Mesozoic accreted terranes in western North America have also been gleaned from carbonate facies and fossil assemblages (Stanley and Senowbari-Daryan, 1986; Newton, 1987, 1988; Whalen, 1988; Stanley and Whalen, 1989). Also, transitions between cool and warm-water limestone facies have been used to document changes in ancient climate, oceanography, and paleogeography (for example, Beauchamp and Desrochers, 1997).

Detailed stratigraphic and sedimentologic analysis of carbonate rocks will broaden our understanding of the paleogeography and history of accreted terranes. Identification of the transition between cool- and warm-water depositional environments in Late Paleozoic and Early Mesozoic carbonate strata from the accreted terranes of the North American Cordillera can provide information important to understanding the paleogeographic evolution, oceanographic circulation patterns, and faunal distribution of the ancestral Pacific Ocean. This investigation is a petrographic analysis of samples collected from Permian carbonate strata in the Chulitna terrane of southcentral Alaska that appear to represent a cool-water depositional setting (fig. 1; Blodgett and Clautice, 1998, 2000; Whalen and others, 1999). We describe the carbonate microfacies of this Permian limestone, interpret its depositional history, and discuss the importance of this unit in deciphering the geologic history of the Chulitna terrane.

GEOLOGIC BACKGROUND

Southern Alaska is a mosaic of fault-bounded, stratigraphically distinct lithotectonic fragments that are thought to have accreted to the North American craton during the late Mesozoic (Coney and others, 1980; Jones and others, 1982, 1986; Plafker and Berg, 1994). The Chulitna terrane crops out in the southcentral Alaska Range (fig. 1) as a small nappe-like structure that overlies Mesozoic flysch (Jones and others, 1980; Clautice and others, 2001). Its strata include a Devonian ophiolite suite, an Upper Paleozoic succession of interbedded volcaniclastic rocks, chert, argillite, flysch, and limestone, Lower Triassic limestone, and Upper Triassic and Jurassic limestone, volcanics, and redbeds (fig. 2; Jones and others, 1980). Structural and stratigraphic relations within the terrane are complex and poorly understood. This research resulted from a collaboration with an Alaska Division of Geological & Geophysical Survey mapping project (Clautice and others, 2001) to help define the geology of the Chulitna area.

Prior to docking with the North American continent, Chulitna's paleogeographic relationship with coeval terranes in southern Alaska and with the ancient North American craton is enigmatic. A paleomagnetic study of Upper Triassic basalts from the Chulitna terrane demonstrated that they are strongly overprinted by a secondary magnetization and the original paleolatitude could not be determined (Hillhouse and Gromme, 1980). Paleomagnetic data have, so far, been inconclusive in establishing constraints on the paleogeographic evolution of the Chulitna terrane; however, carbonate facies and fossilized organisms provide some data about changes in the terrane's pre-accretion paleoenvironment.

STRATIGRAPHY

Many details of the stratigraphy of the Chulitna terrane remain to be determined, but recent mapping has clarified some stratigraphic relationships (fig. 2; Blodgett and Clautice, 1998; Clautice and others, 2001). Basal volcanic rocks, chert, and tuff of the Chulitna terrane include units as old as Late Devonian and as young as Mississippian (Blodgett and Clautice, 1998; Clautice and others, 2001). Pennsylvanian(?) and Permian rocks include volcaniclastic conglomerate, sandstone, and siltstone overlain by chert and thin-

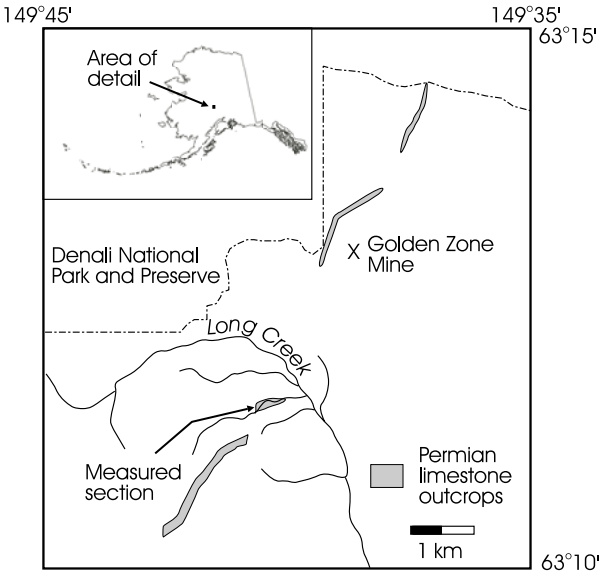

Figure 1. *Map illustrating the location of Permian limestone outcrops (after Clautice and others, 2001) and the measured section for this study in the southcentral Alaska Range.*

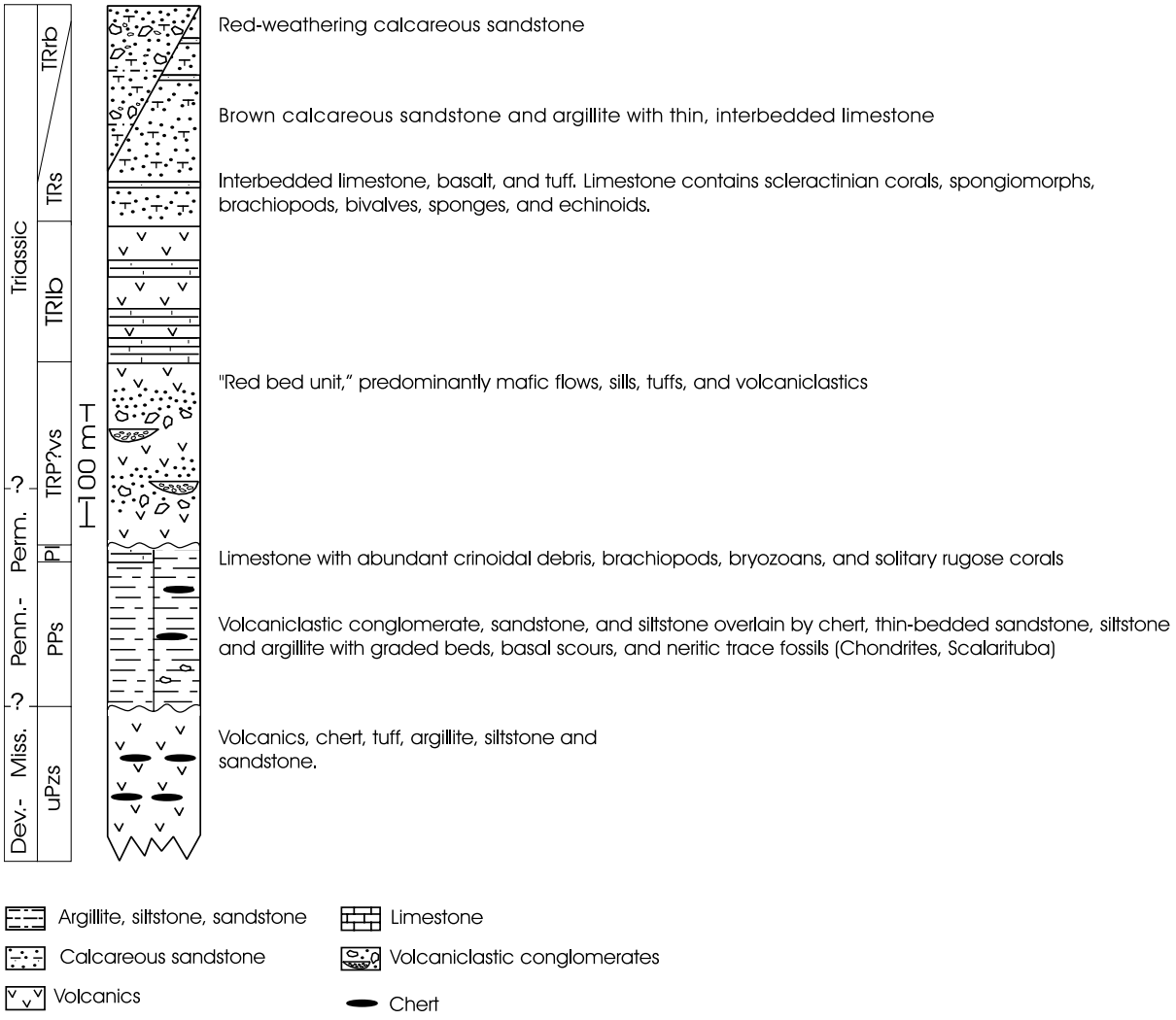

Figure 2. *Composite schematic stratigraphic section of the upper Paleozoic through Triassic of the northern Chulitna terrane, compiled from units exposed in several isolated fault-bounded packages (Modified from Jones and others, 1980; Clautice and others, 2001). The Permian limestone (Pl) is underlain by Pennsylvanian and Permian siliciclastic rocks (PPs) and overlain by Permian(?) and Triassic volcanic and volcaniclastic rocks.*

bedded sandstone, siltstone and argillite with graded beds, flutes, and abundant neritic trace fossils including *Chondrites* and *Scalarituba* (fig. 2; Blodgett and Clautice, 1998, 2000; Whalen and others, 1999).

The Permian argillites are overlain by Late Permian limestone (Clautice and others, 2001). Argillite deposits exposed just upstream from the Permian limestone were originally thought to overlie it (Blodgett and Clautice, 1998); however, subtle flute structures within the argillites (fig. 3) indicate that they are overturned and actually underlie the Permian limestone (fig. 2; Whalen and others, 1999; Clautice and others, 2001). The limestone occurs as a series of coarsening-upward packages that record an increase in siliciclastic and possibly volcaniclastic input (fig. 4). The megafauna in the limestone is of an 'Arctic Permian' type and contains abundant echinoderms and bryozoans and the brachiopods *Spiriferella, Spiriferellina, Horridonia, Lioproductus,* and *Krotovia* (Blodgett and Clautice, 1998, 2000; Clautice and others, 2001). The upper contact of the Permian limestone is not exposed but appears to grade into an overlying heterogeneous Permian(?) to Triassic unit that includes mafic volcanic flows, sills, tuffs, redbed volcaniclastic rocks, and Lower Triassic limestone (fig. 2; Clautice and others, 2001). Overlying this heterogeneous assemblage are interbedded Upper Triassic limestone–basalt and limestone–sandstone strata (fig. 2; Jones and others, 1980; Clautice and others, 2001). These in turn are overlain by brown calcareous Triassic sandstone, argillite, and limestone that is, at least partly, equivalent to a redbed sandstone and conglomerate unit (fig. 2;

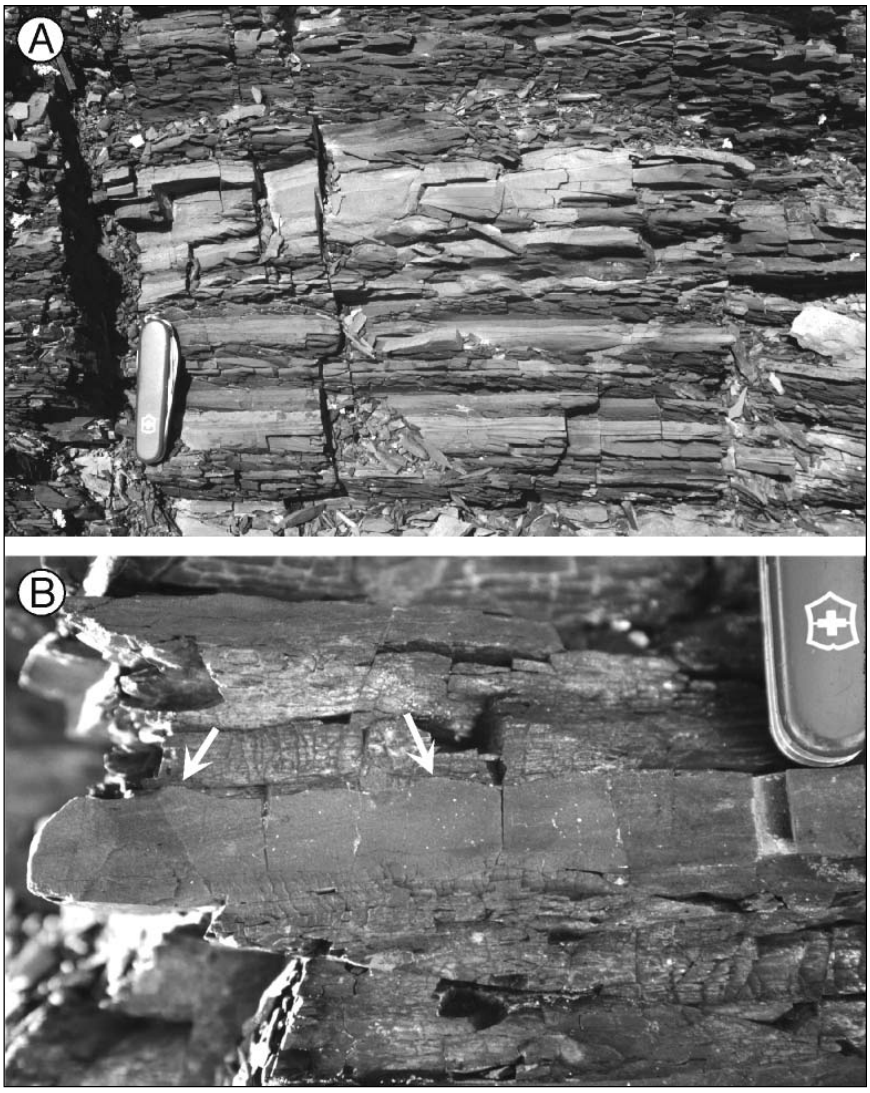

Figure 3. *Overturned Permian argillite that underlies the Permian limestones. (A) Outcrop illustrating the thinly bedded argillites that grade from medium-brown siltstones to dark gray to black mudstones. (B) Overturned graded siltstone bed with basal flute marks indicating stratigraphic up direction.*

Jones and others, 1980; Blodgett and Clautice, 1998; Clautice and others, 2001). The Triassic units are unconformably overlain by Jurassic and Cretaceous argillite, sandstone, chert, and thin limestone followed by a thick Cretaceous flyschlike assemblage (Clautice and others, 2001).

The Triassic limestones of the Chulitna terrane uniformly record warm-water depositional environments (Nichols and Silberling, 1979; Blodgett and Clautice, 1998; Whalen and others, 1999; Yarnell and Stanley, 2000). The Lower Triassic limestone contains ammonites found to have equatorial affinities and exhibit acicular isopachous carbonate cement fringes, an early diagenetic feature limited to warm-water environments (Nichols and Silberling, 1979). A 15- to 20-m-thick Upper Triassic limestone unit, composed of shelf-margin and upper-slope bioclastic rudstone and grainstone, grades upward into biostromal beds with laminar spongiomorphs and thickets of branching scleractinian corals (Whalen and others, 1999; Yarnell and Stanley, 2000). A tropical to subtropical fauna of corals, spongiomorphs, *Spondylospira* and other brachiopods, alatoform bivalves, sponges, and echinoids and lithologic characteristics of this limestone imply warm-water, regressive deposition (Whalen and others, 1999). These limestones and lithologically and faunally similar limestones interbedded with basalt, tuff, and volcanically derived sandstone are Norian (fig. 2;

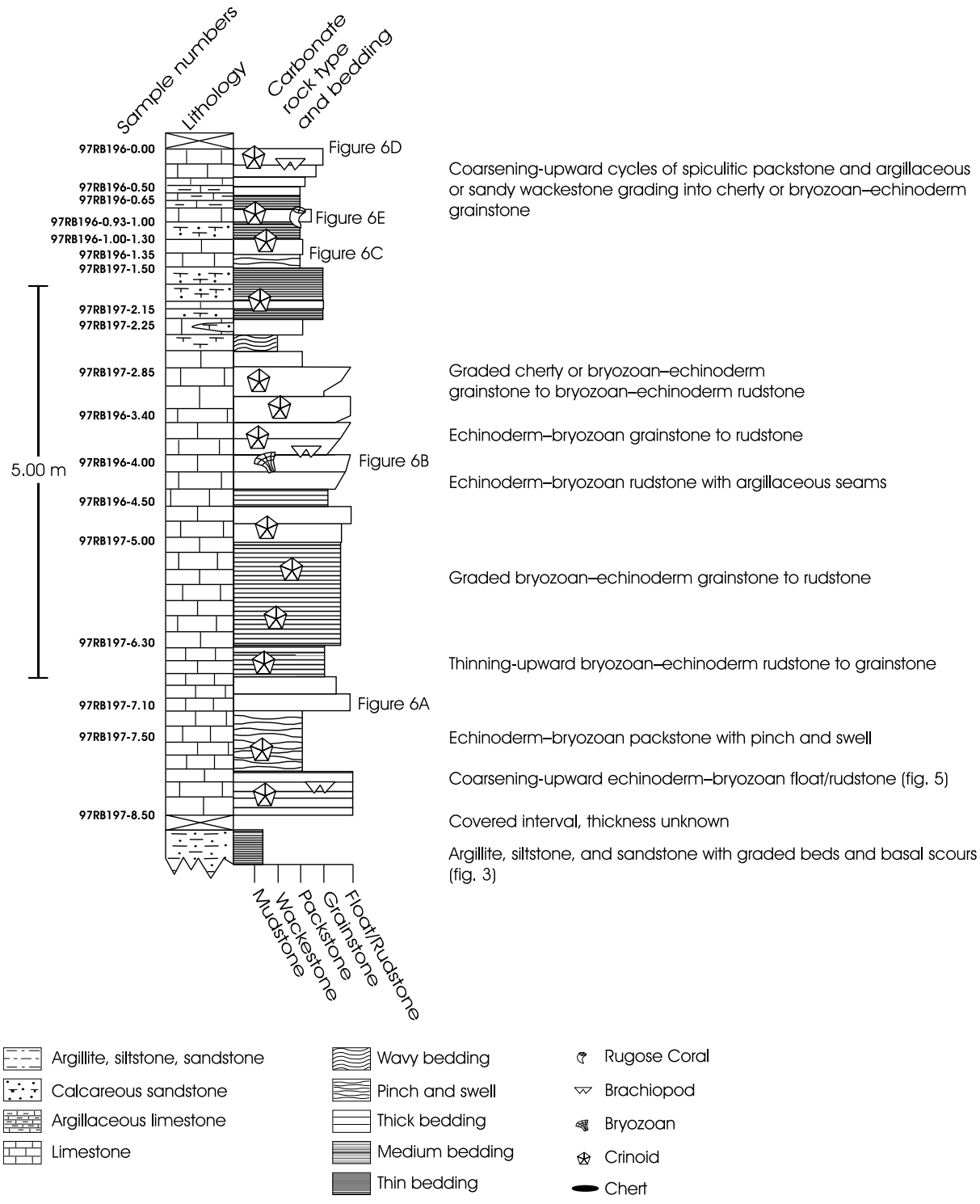

Figure 4. *Measured section through overturned Permian limestone from the northern Chulitna terrane. Figure illustrates lithostratigraphy, carbonate rock types, fauna, and sample number and location. Stratigraphic section measured by M.T. Whalen, J.G. Clough, and R.B. Blodgett.*

Jones and others, 1980; Yarnell and Stanley, 2000; Clautice and others, 2001).

LITHOFACIES ANALYSIS

Our study investigates samples collected from an outcrop in an overturned section that is exposed along Long Creek, about 4 km southwest of Golden Zone Mine (fig. 1). The stratigraphic section was measured with a jacob staff. Seventeen samples were collected at approximate 0.5-m intervals and at obvious textural transitions (fig. 4; Whalen and others, 1999). The samples were thin-sectioned and optically examined by using standard petrographic techniques. Textural and biotic characteristics were used to group the samples into representative lithofacies that are classified according to Dunham (1962) and Embry and Klovan (1972). Representative samples were stained with Alizarin Red S, and X-ray diffractometry was performed to differentiate calcite and dolomite.

Average grain size, bioclast ratios, compaction features, calcite cement morphology, and noncarbonate mineralogy define the lithofacies. In facies dominated by bryozoan and echinoderm grains, the ratio of these grains is implied by the nomenclature; that is, the first modifier describes the most prevalent grain type. Calcite cements are either syntaxial overgrowths on echinoderms, drusy spar, equant pseudospar (10–50 μm), or microspar (4–10 μm). The noncalcite mineralogy includes varying amounts of carbonate fluorapatite, quartz sand, microcrystalline quartz (chert), and opaque material, some of which is recognizable as pyrite by its blocky outline. The rocks exhibit both mechanical and chemical compaction features. Fractured grains indicate mechanical compaction, whereas stylolites and sutured grain contacts imply chemical compaction and dissolution.

The rocks weather light to medium brown and are medium to dark gray on fresh surfaces. The most common grains in all samples are echinoderm and bryozoan fragments. Most echinoderm fragments can be generally identified only to the level of phylum, although some can be identified specifically as crinoid ossicles or echinoid spines. Planispiral forams, small gastropods, echinoid spines, and fragments of brachiopods and bivalves occur in minor amounts in many of the samples. Subangular to subrounded, fine-to-medium quartz sand grains are rare to common in many facies and increase in abundance upsection. Thin calcite veins, oriented approximately perpendicular to bedding, are common.

BRYOZOAN–ECHINODERM RUDSTONE

The bryozoan–echinoderm rudstone facies (fig. 6A) is supported by randomly oriented medium sand-sized bryozoan grains. Very coarse sand-sized echinoderm grains are also abundant. The stratigraphically lowest sample of this facies contains a single small rugose coral. Quartz sand, carbonate fluorapatite, and opaque grains are common. The bryozoans exhibit a wide range of skeletal morphologies and are surrounded by equant or drusy calcite cement. Fractured grains, sutured grain contacts, and stylolites are common.

ECHINODERM–BRYOZOAN RUDSTONE

The echinoderm–bryozoan rudstone facies (figs. 5, 6B) is distinguished by an abundance of randomly oriented, very coarse sand- to granule-sized echinoderm grains. Medium sand-sized bryozoan fragments are also common. Opaque minerals and quartz are rare. Echinoderm grains are surrounded by extensive syntaxial cement that differentiates this facies from the bryozoan–echinoderm rudstone. The bryozoans are usually associated with drusy or equant calcite cement and minor amounts of carbonate fluorapatite. Compaction features are limited to fractured grains.

Figure 5. *Outcrop photograph of echinoderm–bryozoan rudstone. Note the large crinoid ossicles, some of which are partially articulated (for stratigraphic position see fig. 4).*

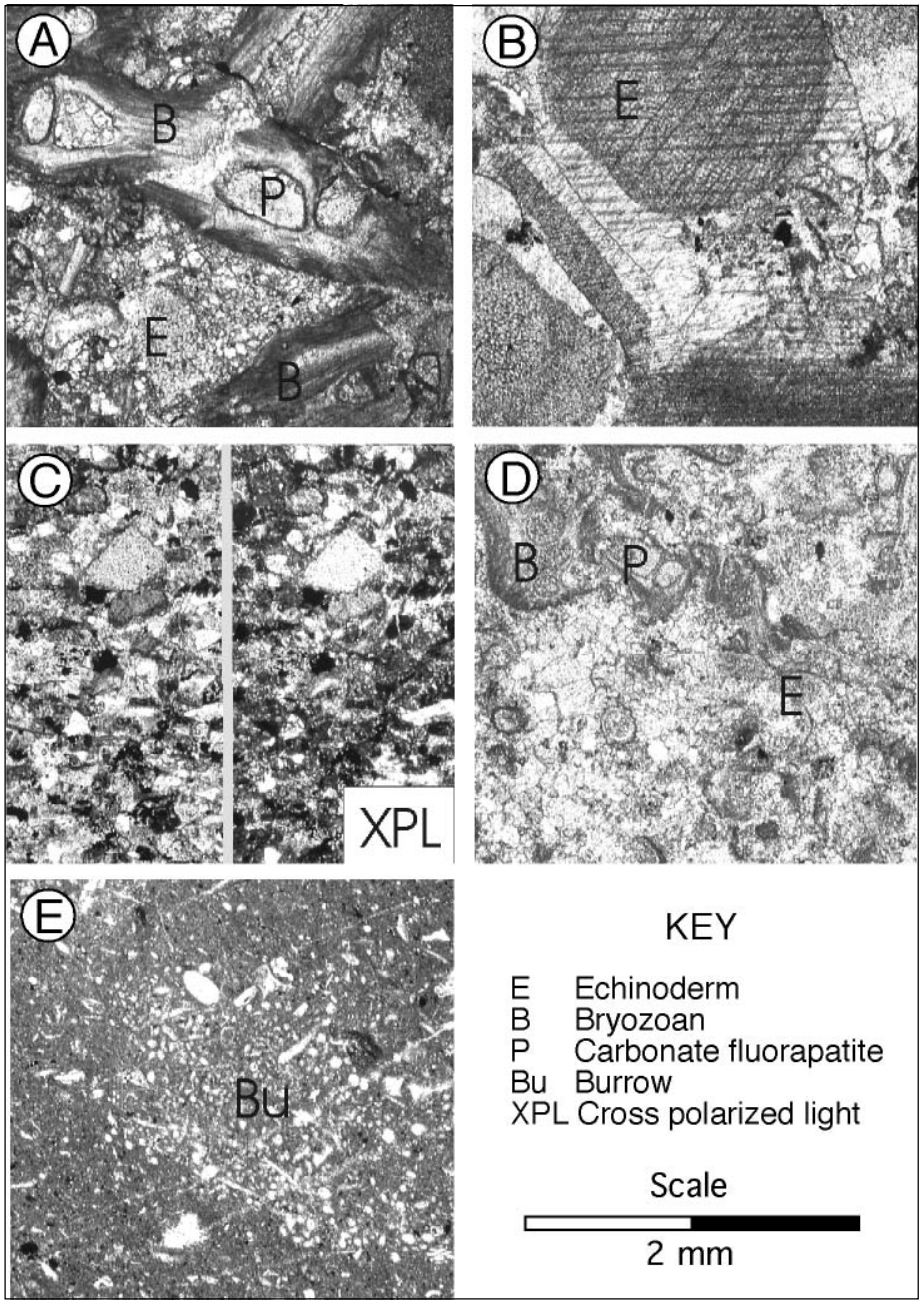

Figure 6. *Photomicrographs of representative lithofacies from the Permian limestone. Numbers in parentheses correspond to sample numbers in figure 4. (A) Bryozoan–echinoderm grainstone (97RB197-7.10) with sand-size bryozoan and echinoderm fragments and carbonate fluorapatite pore filling cement. (B) Cherty grainstone (97RB196-4.00) in plane polarized (left) and cross polarized (XPL, right) light. Note the large echinoderm fragment in the top center of the photo and siliceous cement visible under XPL. (C) Spiculitic packstone (97RB196-1.35) with spicules concentrated within a burrow. (D) Bryozoan–echinoderm rudstone (97RB196-0.00) with sand- to granule-size skeletal fragments. Note the carbonate fluorapatite pore filling cement within bryozoan zooecia. (E) Echinoderm–bryozoan rudstone (97RB196-0.93-1.00) with sand- to granule-size skeletal fragments. Key to labels: B = bryozoan, E = echinoderm, P = carbonate fluorapatite pore filling cement, Bu = burrow.*

CHERTY GRAINSTONE

Well sorted medium sand-sized bryozoan and echinoderm fragments surrounded by a phosphatic, microcrystalline quartz matrix characterize the cherty grainstone facies (fig. 6C). Fine laminations in the samples are defined by sutured grain contacts and thin, parallel dissolution seams. The calcite grains appear brown under cross-polarized light. Echinoderm grains exhibit thin rims of syntaxial cement. This facies is abruptly to gradationally interbedded with the bryozoan–echinoderm grainstone facies on a centimeter scale.

BRYOZOAN ECHINODERM GRAINSTONE

The bryozoan echinoderm grainstone facies (fig. 6D) is distinguished by an abundance of medium sand-sized bryozoan and echinoderm fragments. The grains exhibit subparallel orientation and lack compaction features. Most intergranular and intragranular spaces are filled by equant pseudospar, drusy spar, syntaxial calcite cement, carbonate fluorapatite, or microcrystalline quartz. Microspar is rare and occurs only around a few bryozoan grains, suggesting that it is cement rather than neomorphosed mud.

SPICULITIC PACKSTONE

The spiculitic packstone (fig. 6E) occurs in only one sample and is characterized by a micritic matrix surrounding sponge spicule molds filled by calcite spar. The matrix is homogeneous with regard to crystal size but occurs in irregularly elongate light and dark patches. In the lighter colored areas the spicules tend to be aligned with the patch edges, suggesting that the patches are burrows. The sample contains gastropods, forams, a few echinoderm and bryozoan fragments, several spiny brachiopod fragments, and disseminated fine sand-sized pyrite nodules. Quartz or calcite has replaced most of the forams. The darker matrix areas have been partially phosphatized and silicified and the sample lacks compaction features.

FACIES INTERPRETATION AND DEPOSITIONAL HISTORY

The facies described above indicate dominantly subtidal deposition in an open-shelf environment. The predominance of stenohaline bryozoa and echinoderms argues for normal marine conditions and there are no sedimentologic indications of peritidal or deep-water deposition. The lack of wave- or current-generated structures (other than graded bedding) either implies deposition below fairweather wave base or thorough bioturbation in shallower water environments. The normally graded rudstone and grainstone facies commonly have sharp bases and are most likely storm-influenced deposits, although deposition by turbidity currents cannot be ruled out. The general facies distribution records a progressive decrease in grain size, indicating waning energy within successive depositional environments. The change in grain size and spiculitic packstones near the top of the package implies that the facies represent a deepening upward sequence.

DISCUSSION AND CONCLUSIONS

Bryozoans and echinoderms dominate the biotic assemblage in these Permian carbonates. Planispiral forams, echinoid spines, a solitary rugose coral, spicule molds, and fragments of brachiopods and bivalves occur in minor amounts. The assemblage lacks nonskeletal grains such as ooids, oncoids, peloids, or aggregate grains and contains little carbonate mud. No evidence of early marine cementation was observed and grains fractured by mechanical compaction indicate that these facies were not cemented prior to compaction. Syntaxial, equant and drusy calcite cements, such as those observed here, do not provide unequivocal evidence of genesis but all have been documented from burial environments (Bathurst, 1975; Tucker and Wright, 1990). The biotic and textural characteristics exhibited by the Permian Chulitna limestones are identical with those characterized by Lees and Buller (1972), Lees (1975), Nelson (1988), and James (1997) as typical of cool-water carbonate depositional environments.

Unlike warm-water carbonate facies, cool-water carbonate deposition can occur at any latitude as long as terrigenous clastic input is low (Nelson, 1988). Cool-water carbonate facies are present at low latitudes in regions where low salinity, upwelling, and cool water transported by oceanic gyres inhibit deposition of warm-water carbonate facies (Lees and Buller, 1972; Lees, 1975; Whalen, 1995; James, 1997). This implies that Permian Chulitna strata could have been deposited at high latitudes. However, low-latitude deposition in a region exposed to open ocean circulation or upwelling is also a possibility. Although identification of cool-water carbonate facies during Permian time does not provide latitudinal constraints, the warm-water facies deposited during the Triassic (Nichols and Silberling, 1979; Blodgett and Clautice, 1998; Whalen and others, 1999) require a change in latitude, climate, or oceanography.

Identification of cool-water carbonate depositional environments throughout the rock record allows us to make more refined environmental interpretations than would otherwise be possible. While the paleogeographic history of the Chulitna terrane remains enigmatic, identification of Permian cool-water carbonate deposition and recognition of a change to more tropical conditions during the Triassic significantly adds to what is known about the geologic history of this poorly understood region. Further documentation of the

paleogeographic and paleoceanographic affinities of Permian and Triassic limestones in other Cordilleran accreted terranes will provide insight into terrane evolution and the tectonic history of the western margin of North America.

ACKNOWLEDGMENTS

The Alaska Division of Geological & Geophysical Surveys supported fieldwork for this project. We thank Karen Clautice for facilitating helicopter access to remote exposures in the Alaska Range. We thank James G. Clough and Robert B. Blodgett for their collaboration in the field portion of this study and for insightful reviews that significantly improved the manuscript. Robert B. Blodgett and George D. Stanley, Jr., deserve thanks for Permian and Triassic fossil identification, respectively. We thank Rainer Newberry for insightful input on the geology of the Chulitna area. The Department of Geology and Geophysics, University of Alaska Fairbanks, assisted with the cost of manuscript preparation.

REFERENCES

Bathurst, R.G.C., 1975, Carbonate sediments and their diagenesis: New York, Elsevier, 658 p.

Beauchamp, B., and Desrochers, A., 1997, Permian warm- to very cold-water carbonates and cherts in northwest Pangea, *in* James, N.P., and others, eds., Cool-Water Carbonates: SEPM (Society for Sedimentary Geology) Special Publication 56, p. 327-348.

Belasky, P., and Runnegar, B., 1993, Biogeographic constraints for tectonic reconstructions of the Pacific region: Geology, v. 21, p. 979-982.

Blodgett, R.B., and Boucot, A.J., 1999, Late Early Devonian (Late Emsian) eospiriferinid brachiopods from Shellabarger Pass, south-central Alaska, and their biogeographic importance: further evidence for a Siberian origin of the Farewell and allied Alaskan accreted terranes: Senckenbergiana lethaea, v. 79, p. 209-221.

Blodgett, R.B., and Clautice, K.H., 1998, New insights into the stratigraphy and paleontology of the Chulitna terrane and surrounding area, Healy A-6 quadrangle, south-central Alaska: *in* Karl, S.M., ed., The Alaska Geological Society 1998 Science and Technology Conference, 'Cutting Edge in Alaska,' 2 p.

———2000, Fossil locality map for the Healy A-6 Quadrangle, southcentral Alaska: Alaska Division of Geological & Geophysical Surveys Report of Investigations 2000-5, 41 p.

Clautice, K.H., Newberry, R.J., Blodgett, R.B., Bundtzen, T.K., Gage, B.G., Harris, E.E., Liss, S.A., Miller, M.L., Reifenstuhl, R.R., Clough, J.G., and Pinney, D.S., 2001, Bedrock geologic map of the Chulitna mining district, southcentral Alaska: Alaska Division of Geological & Geophysical Surveys Report of Investigations 2001-1A, 31 p., 1 sheet, scale 1:63,360.

Coney, P.J., Jones, D.L., and Monger, J.W.H., 1980, Cordilleran suspect terranes: Nature, v. 288, p. 329-333.

Dunham, R.J., 1962, Classification of carbonate rocks according to depositional texture: *in* Ham, W.E., ed., Classification of carbonate rocks—A symposium: American Association of Petroleum Geologists Memoir 1, p. 108-121.

Embry, A.F., and Klovan, J.E., 1972, Absolute water depth limits of Late Devonian paleoecological zones: Geologische Rundschau, v. 61, p. 672-686.

Flügel, E., 1994, Pangean shelf carbonates, *in* Klein, G.B., ed., Pangea: Paleoclimate, tectonics, and sedimentation during accretion, zenith, and breakup of a supercontinent: Geological Society of America Special Paper 288, p. 248-266.

Hillhouse, J.W., 1977, Paleomagnetism of the Triassic Nikolai Greenstone, McCarthy Quadrangle, Alaska: Canadian Journal of Earth Sciences, v.14, p. 2578-2592.

Hillhouse, J.W., and Gromme, S., 1980, Paleomagnetism of Triassic red beds and basalt in the Chulitna terrane, south-central Alaska: U.S. Geological Survey Open-File Report 80-368. 12 p.

Howell, D.G., Jones, D.L., and Schermer, E.R., 1985, Tectonostratigraphic terranes of the circum-Pacific region, *in* Howell, D.G., ed., Tectonostratigraphic terranes of the Circum-Pacific region: Circum-Pacific Council for Energy and Mineral Resources Earth Science Series, no. 1, p. 3-30.

James, N.P., 1997, The cool-water carbonate depositional realm, *in* James, N.P., and others, eds., Cool-water carbonates, SEPM (Society for Sedimen-tary Geology) Special Publication 56, p. 1-20.

Jones, D.L., Silberling, N.J., and Hillhouse, J.W., 1977, Wrangellia—A displaced terrane in northwestern America: Canadian Journal of Earth Sciences, v. 14, p. 2565-2577.

Jones, D.L., Silberling, N.J., Csejtey, B., Jr., Nelson, W.H., and Blome, C.D., 1980, Age and structural significance of ophiolite and adjoining rocks in the upper Chulitna district, south-central Alaska: U.S. Geological Survey Professional Paper 1121-A, 21 p.

Jones, D.L., Silberling, N.J., Gilbert, W.G., and Coney, P.J., 1982, Character, distribution, and tectonic significance of accretionary terranes in the central Alaska Range: Journal of Geophysical Research, v. 87, p. 3709-3717.

Jones, D.L., Silberling, N.J., and Coney, P.J., 1986, Collision tectonics in the Cordillera of western North America: Examples from Alaska, *in* Coward, M.P.,

and Ries, A.C., eds., Collision tectonics: Geological Society of London Special Publication 19, p. 367-387.

Lees, A., 1975, Possible influences of salinity and temperature on modern shelf carbonate sedimenta-tion: Marine Geology, v. 19, p. 159-198.

Lees, A. and Buller, A.T., 1972, Modern temperate-water and warm-water shelf carbonate sediments contrasted: Marine Geology, v. 13, p. 1767-1773.

Nelson, C.S., 1988, An introductory perspective on non-tropical shelf carbonates: Sedimentary Geology, v. 60, p. 3-12.

Newton, C.R., 1987, Biogeographic complexity in Triassic bivalves of the Wallowa Terrane, northwest United States: oceanic islands, not continents, provide the best analogues: Geology, v. 15, p. 1126-1129.

———1988, Significance of "Tethyan" fossils in the American Cordillera: Science, v. 242, p. 385-391.

Nichols, K.M., and Silberling, N.J., 1979, Early Triassic (Smithian) ammonites of paleoequatorial affinity from the Chulitna terrane, south-central Alaska: U.S. Geological Survey Professional Paper 1121-B, 5 p.

Packer, D.R., and Stone, D.B., 1972, An Alaskan Jurassic palaeomagnetic pole and the Alaskan orocline: Nature, v. 237, p. 25-26.

———1974, Paleomagnetism of Jurassic rocks from southern Alaska, and the tectonic implications: Canadian Journal of Earth Sciences v. 11, p. 976-997.

Plafker, G., and Berg, H.C., 1994, Overview of the geology and tectonic evolution of Alaska, *in* Plafker, G., and Berg, H.C., eds., The Geology of Alaska: Boulder, Colorado, Geological Survey of America, The Geology of North America, v. G-1, p. 989-1021.

Stanley, G.D., Jr., and Senowbari-Daryan, B., 1986. Upper Triassic Dachstein-type reef limestone from the Wallowa Mountains, Oregon: first reported occurrence in the United States: Palaios, v. 1, p. 172-177.

Stanley, G.D., Jr., and Whalen, M.T., 1989, Upper Triassic corals and spongiomorphs from Hells Canyon, Wallowa terrane, Oregon: Journal of Paleontology, v. 63, p. 800-818.

Tucker, M.E., and Wright, V.P., 1990, Carbonate sedimentology: Malden, Maine, Blackwell Science, 482 p.

Van der Voo, R., Jones, M., Gromme, C.S., Eberlein, G.D., Churkin, M., Jr., 1980, Paleozoic paleomagnetism and northward drift of the Alexander terrane, southeastern Alaska: Journal of Geophysical Research, v. 85, p. 5281-5296.

Whalen, M.T., 1988, Depositional history of an Upper Triassic drowned carbonate platform sequence: Wallowa terrane, Oregon and Idaho: Geological Society of America Bulletin, v. 100, p. 1097-1110.

———1995, Barred basins: A model for eastern ocean basin carbonate platforms: Geology, v. 23, p. 625-628.

Whalen, M.T., Clough, J.G., Blodgett, R.B., Stanley, G.D., Clautice, K., and Newberry, R., 1999, Late Paleozoic and Early Mesozoic carbonate rocks and depositional history of the Chulitna terrane: Alaska Geological Society Science and Technology Conference, April 23-24, Fairbanks, Alaska.

Yarnell, J.M., and Stanley, G.D., Jr., 2000, Two Triassic reef faunas from terranes in Alaska and Yukon and their paleogeographic significance: Geological Society of America Abstracts with Programs, v. 32, p. A12.

MINERALIZATION AND STRUCTURAL CONTROLS IN THE KENSINGTON MINE AND BERNERS BAY AREA, SOUTHEASTERN ALASKA

Earl Redman,[1] Stan Caddey,[2] Dave Harvey,[3] and Mike Jaworski[4]

ABSTRACT

Gold deposits at Berners Bay, Alaska, are mesothermal quartz–carbonate–pyrite vein complexes formed in structural dilations. The district displays an asymmetric metal zonation pattern with gold in gold–silver tellurides and trace base metals in the Kensington area that grade southeastward into free gold associated with silver–gold tellurides, base metals, and molybdenite in the Jualin–Comet area.

The Kensington deposits consist of multiple mineralized zones and formed in extensional structural dilations between conjugate fault–shears in competent diorite. The fault–shears were formed by lateral compression and right-lateral reverse wrenching. Mineralization consists of numerous, narrow, discontinuous vein swarms that fill a penetrative system of extensional joint sets.

On the basis of 3,000 structural measurements, four tectonic events (D1–D4) are recognized, beginning with ductile deformation, passing through a brittle–ductile transition, and terminating in the brittle structural regime. Gold mineralization began in D3–when Kensington formed–and ended late in D4.

INTRODUCTION

The Kensington project is located at the north end of the Juneau gold belt, 45 mi northwest of Juneau, in southeastern Alaska. Coeur became the full owner and operator of the Kensington project in July 1995, and began a review of the project to develop a 4,000 ton/day underground mine. The identified gold mineral resource for the Kensington vein system is 17.9 million tons at a grade of 0.144 ounces/ton gold (by the authors).

The present report is based on work done by the authors between 1994 and 1999. This work included: (1) a comprehensive structural analysis of the Kensington mine and the Berners Bay district, based on the collection of over 3,000 structural measurements; (2) a complete remapping of all accessible mine workings in the district and extensive remapping of surface geology, which resulted in the identification of major new structural features in the district; (3) the creation of a new genetic model for ore body formation and control; (4) 57,000 ft of new core drilling; (5) a district-wide evaluation of mineral zonation patterns; (6) the relogging of old Kensington and Jualin core in light of new geologic structural analysis; and (7) the creation of a 3-dimensional geologic model based on all available data. Also included in this report is new district-wide mineralogical information from Gramstad (2000).

REGIONAL GEOLOGIC SETTING

The northern half of the Berners Bay district is underlain by an upright sequence of Triassic metabasalts and gray phyllite of the Wrangellia terrane (fig. 1). The elongate Jualin diorite was intruded at 105 Ma (unpublished information cited in Kistler and others, 1993; Miller and others, 1995; Gehrels, 2000) along the contact between the metabasalts and phyllite. Unconformably overlying the Jualin diorite and the Triassic rocks is a metamorphosed sequence of conglomerates, volcaniclastic sedimentary rocks, and felsic volcanic rocks that grade upward into black phyllite (Redman, 1984). Gold deposition in the Berners Bay district (as well as the entire Juneau gold belt) occurred 55 to 57 Ma (Miller and others, 1995).

BERNERS BAY STRUCTURAL SETTING

Two major northwest-trending shear zones, the Gastineau shear zone and the Kensington megashear zone (fig. 1), transect the area and, according to structural data collected by the authors, controlled the formation and direction of the regional foliation. The shear zones roughly parallel the Jualin pluton. Conjugate shears originating from the Kensington megashears control all the mineralization in the Berners Bay district.

[1]Alaska House, Urney Lane, Ballinagh, Co. Cavan, Ireland
Email for Earl Redman: killydoon@eircom.net
[2]16 Cedar Canyon, Littleton, Colorado 80127
[3]Coeur Rochester Group, P.O. Box 1057, Lovelock Nevada 89419
[4]941 Calle Mejia, Apt 101, Santa Fe, New Mexico 97501

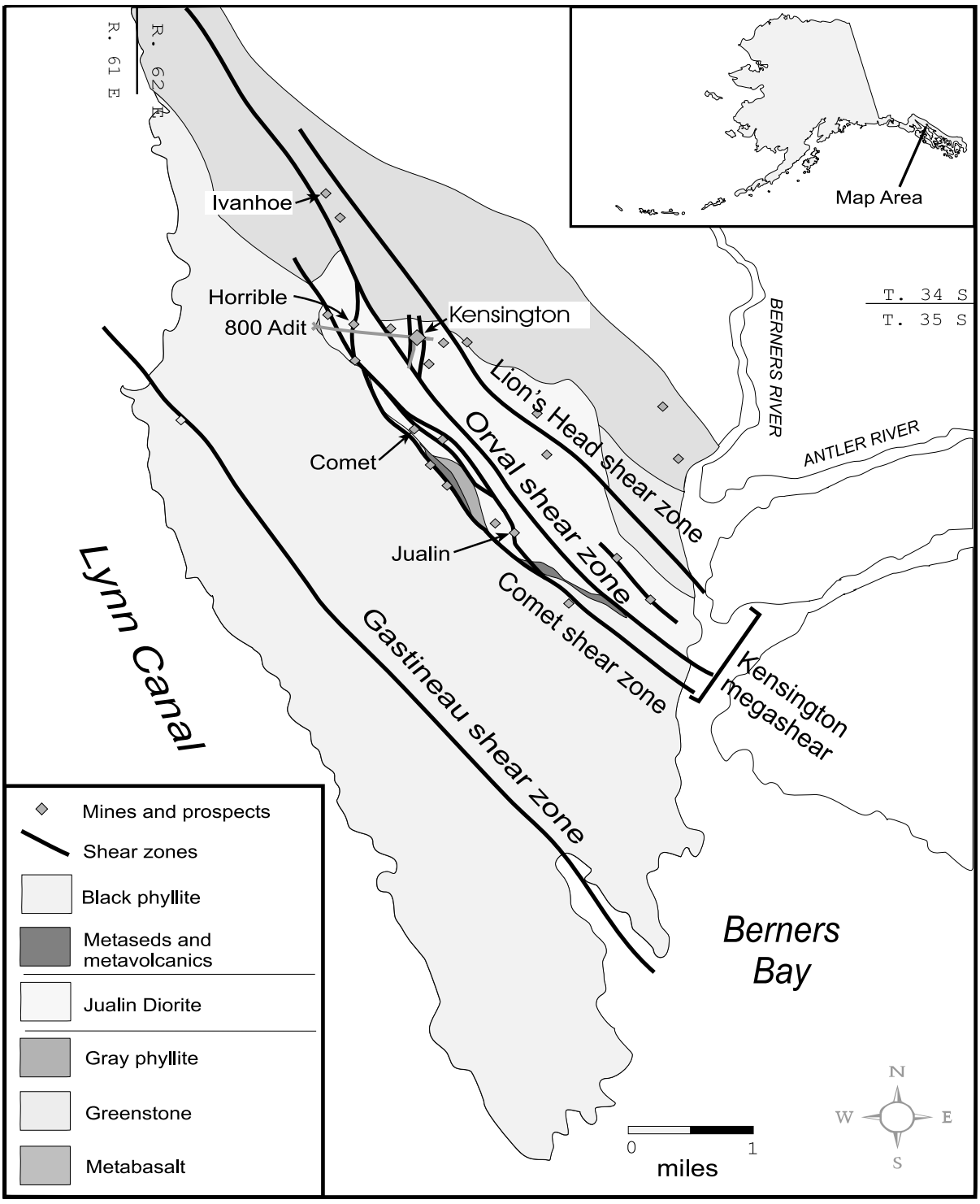

Figure 1. *Structural geology and mineral deposits of the Berners Bay district.*

The Gastineau structure is marked by a 50- to >100-ft-wide zone of penetrative shear foliation, local mylonite, and an anastomosing system of chlorite shears. The shear strikes N35°–40°W and dips 70°–85°NE. Kink and drag folds are common and demonstrate right-lateral reverse movement along the structure.

The Kensington megashear is about 1 mi wide and contains three major structures, the Orval, Comet, and Lion's Head shear zones (fig. 1). The largest structure is the Orval shear zone, which varies from 100 ft wide at its northwesternmost exposure to over 1,000 ft wide at its southeastern exposures. Where the shear zone is widest, it contains up to 50 percent lens-shaped blocks of unsheared diorite. The Comet and Lion's Head shear zones are 15 to 50 ft wide.

MINERALIZATION AND ORE CONTROLS

The gold deposits in the Berners Bay area are mesothermal vein systems formed largely within the brittle–ductile transition. They represent the composite development of vein patterns related to four pulses of compressive tectonic activity (Caddey and others, 1995). Fracture patterns are complex, biaxial, systematic, and repeated at all scales. Individual precious-metal deposits in the region have large vertical extents, low trace-metal contents and, within each deposit, consistent metallurgical characteristics (Redman and others, 1998).

The Berners Bay district is unique within the Juneau gold belt because all deposits contain telluride minerals (Redman and others, 1992). The district displays an asymmetric thermal and metal zonation pattern, in which the Kensington deposit forms the higher temperature core, with gold–silver tellurides (calaverite), minute grains of free gold, and trace base metals. Outwardly, mineralization grades into lower temperature silver–gold tellurides (petzite, hessite), coarser gold, electrum, more abundant copper, lead and zinc, and molybdenite, such as at the Jualin deposit (Gramstad, 2000).

At Kensington, gold grades are directly proportional to pyrite concentration (Redman and others, 1998). More than 90 percent of the gold occurs as calaverite ($AuTe_2$) inclusions in anhedral pyrite. Rare native gold occurs as minute particles (less than 50 ì diameter) on the surfaces of—or in fractures within—pyrite grains. Trace occurrences of other tellurides (petzite, coloradoite, and altaite) have been identified. There are also trace amounts of chalcopyrite, sphalerite, galena, and pentlandite (Gramstad, 2000; Redman and others, 1998).

In the Jualin–Comet area, most gold is free and associated with chalcopyrite, galena, sphalerite, and the gold–silver tellurides hessite and petzite with traces of sylvanite (Gramstad, 2000; Redman and others, 1998).

THE KENSINGTON DEPOSIT

Mineralized zones at Kensington have the geometric form of large, north-trending ladder veins (fig. 2) that are tabular to sigmoidal in cross-section (fig. 3) and not commonly bounded by obvious contacts, but characteristically show continuous veining across the entire width with minor intervening, weakly veined, or barren intervals. An abundance of closely spaced faults is important to ore control within dilation zones. The diffusion of gold-bearing fluids in the dilation zones was constrained by available open fractures. Closely spaced active faults continually rebroke the intervening rock (as shown by cross-cutting veins with differing mineralogies) and allowed more gold to be deposited. Where faults are more widely spaced, only the fault and adjacent wallrock were mineralized. Hanging-wall and footwall limits of the ore zones are determined by a decrease in quartz-carbonate vein density and a corresponding decrease in pyrite and gold. All mineralized zones terminate at the contact with the metavolcanic rock.

Zone 10 is the largest and most continuous mineralized zone in the deposit (figs. 2, 3). The zone dips 55 degrees to 65 degrees east, has about 1,500 ft of strike length, and 2,600 ft of dip length. Width varies from 50 to 150 ft.

Zone 41 is a smaller, but high-grade, sigmoid-shaped ladder vein positioned beneath the apex of the Ramp and Zone 44 shear intersection and immediately above Zone 10 (fig. 3). The zone lies within a structurally dilated zone formed by right-lateral oblique–slip thrust faulting, and consists of three massive quartz–pyrite veins with dense swarms of veinlets and hydrothermal, quartz–pyrite-healed breccias on the hanging wall and footwalls. In its central portion, Zone 41 dips 26 degrees to 43 degrees northeast; at the upper and lower extents, dip increases to 65 degrees.

Four stages of vein emplacement at Kensington have been recognized by the writers. The first vein stage predated gold mineralization. Two stages of gold-bearing veins followed. Early ore stage vein sets contained varying amounts of quartz, chlorite, calcite, pyrite, and some gold, whereas later sets contained variable quartz, ankerite, pyrite, gold, and tellurides. The final stage, consisting largely of ankerite, postdated gold mineralization (Redman and others, 1998).

Veins typically form narrow, discontinuous veinlets only a few inches in width. Extensional, ladder, and "centipede" structures are most common. Ladder veins formed because of extension adjacent to a shear or between two shears in a shear couple, and generally form en-echelon vein sets. Centipede structures formed when swarms of extensional or release fractures (or both) were intersected and rotated by active right-lateral–reverse oblique–slip shear faults as the structures were being

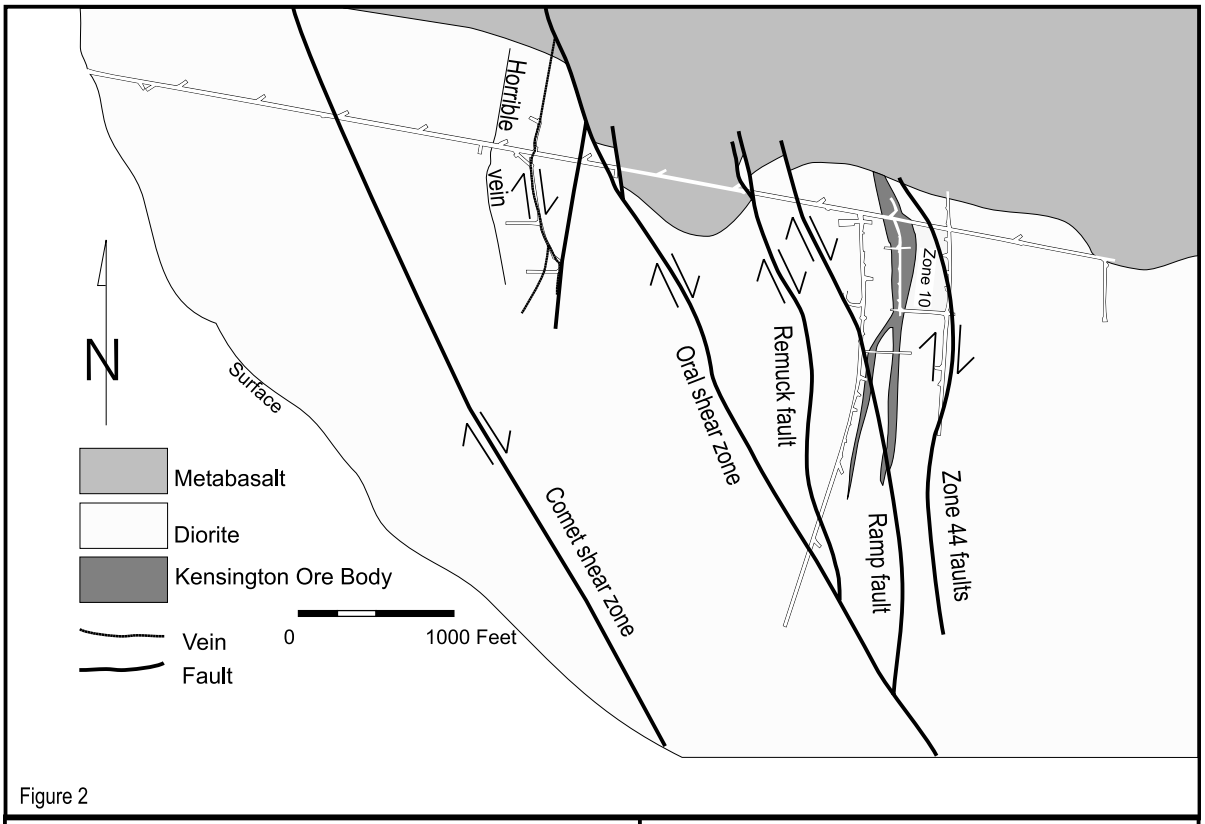

Figure 2

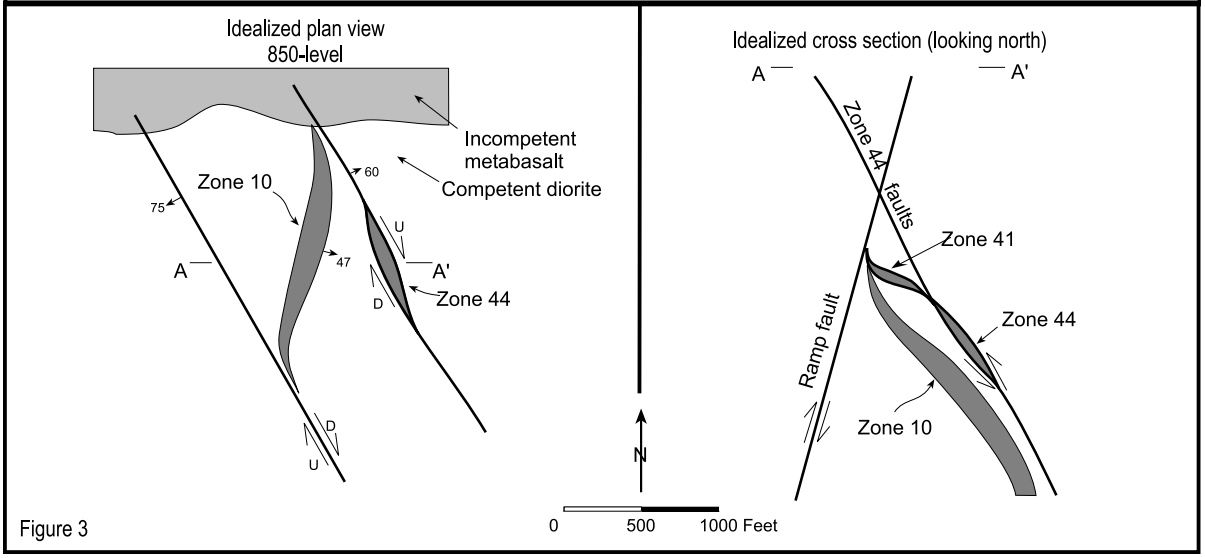

Figure 3

Figure 2 (above). *Geologic plan map of the 850 level.*
Figure 3 (above). *The relationship of dilation zones and the major faults in the Kensington area.*
Figure 4 (right). *Wulff nets of the deformational events.*
Figure 5 (right, inset). *Average orientations of district mesothermal vein systems, Berners Bay district.*

Ductile plain strain
N18°W, 40°N,
70°N, 80°S, 20°S
N
N72°E
S72°W
Master shear thrusts
F1axial plane
Subordinate reverse faults
Regional thrust faulting
S1
S2
S3
F1
Preliminary Deformation D1 (>110 Ma)
Average vein orientations
Ductile biaxial strain
N18°W, 70°N,
70°S
N45°W, 72°N,
72°S
N81°W, 79°N,
79°S
N45°E, 82°N, 82°S
Juneau master shears
Berners Bay master shears
Premineral Deformation D2 (105 Ma)
Structural geometry/kinematic plan
Brittle-ductile transition biaxial strain
N16°W, 57°N
N47°W, 65°N
N19°E, 59°S
Ore Stage Deformation D3a (55-57 Ma)
Average orientations of mesothermal
Qtz-Py-Au vein sets
Brittle plane strain
N4°W, 43°N
N8°W, 73°N
N16E, 15S
Ank-Qtz-Py veins
Ore Stage Deformation D4b (53 Ma)
Reverse-thrust, dip-slip
Master shear
Extension fractures
Conjugate shear
Release fracture
Average poles
Figure 4
Master shear - Empire, Gold King, Fremming, DZ, Greek Boy
Extension fractures - Kensington Zone 10, Comet, Johnson, Jualin
Conjugate shear - Elmira, Eureka, Northern Belle, Horrible
Release fracture - Hope
Average poles
Figure 5

mineralized. Extensional and release fractures are locally drag folded adjacent to the shears.

Vein orientations form in well defined groups. Nearly all the pregold veins and most of the gold-bearing quartz–pyrite–calcite veins dip west. In contrast, most of the later gold-bearing quartz–ankerite–pyrite veins dip east. Vein sets commonly overprint each other, resulting in a swarmlike appearance. Swarms typically contain en-echelon veins in ladderlike, centipede-like, or subparallel stringer geometric forms.

Four types of hydrothermal alteration within and adjacent to the mineralized zones have been identified: (1) propylitic assemblages of carbonate+epidote+sericite that replace plagioclase adjacent to the zones; (2) pronounced chlorite replacement of mafic minerals by chlorite±magnetite±rutile±quartz±carbonate±sphene; (3) brownish carbonate alteration of the diorite; and (4) sericitic alteration within the mineralized zones developed immediately adjacent to the veins.

DEFORMATIONAL EVENTS

Caddey and others (1995) collected over 3,000 structural measurements from which they identified four major tectonic events (D1–D4) at the Kensington deposit (fig. 4):

D1

The first tectonic event occurred before 110 Ma and was characterized by N72°E–S72°W compression associated with crustal shortening and uplift. The event was premineral, ductile plane strain, and regional. Thrust faults and asymmetric regional fold sets were formed along roughly north–south trends.

D2

The second tectonic event occurred about 105 Ma and was characterized by N45°E–S45°W compression associated with crustal shortening and metamorphism to greenschist facies. It was premineral, ductile biaxial strain, and regional. Early shears generated in the Kensington area include the Orval, Ramp, Zone 44, and Remuck shear zones.

D3

The third tectonic event consisted of at least four individual pulses (D3a, D3b, D3c, and D3d) between 55 and 57 Ma. It was intramineral, early ore stage and characterized by lateral compression and extension, followed by brief periods of relaxation. The tectonic style was in the brittle–ductile transition, and biaxial. The principal stress was oriented about N12°W–S12°E in D3a but rotated clockwise to N24°E–S24°W in D3c. This generated an oblique-slip system of wrench faults that were right-lateral reverse. Shear couples generated between master shears initiated development of structural dilation zones, such as Zone 10 at Kensington. Early veins consisted of calcite–quartz–chlorite with or without pyrite and probably no gold. Later veins were filled with quartz–chlorite–calcite–pyrite and quartz–pyrite, both containing gold. The later vein compositions contained abundant pyrite and high-grade gold. Quartz–carbonate mineralization filled closely spaced extensional joints (fig. 5).

D4

The fourth tectonic event, which ended about 53 Ma, consisted of six recognizable brittle plane strain pulses (D4a–D4f) and represents a major change in the stress field to east–west compression and vertical extension. Small-scale ladder veins and centipede vein structures formed throughout the Kensington deposit. Vein compositions slowly changed from: (1) quartz–chlorite–pyrite to quartz–pyrite, to (2) quartz–ankerite–pyrite, to (3) ankerite–quartz–pyrite, to (4) ankerite with or without quartz. All vein compositions except for late monomineralic ankerite phase contain gold. Mineralization ended late in D4f. This was a period of thrusting and reverse faulting.

ACKNOWLEDGMENTS

The authors thank Coeur D'Alene Mines for permission to publish the information in this paper. We also thank Karen Clautice for her helpful comments on preparation. This paper was reviewed by D.A. Brew and R.J. Newberry.

REFERENCES

Caddey, S.W., Harvey, D., Burton, C., Cato, K., 1995, Structural analysis of the Kensington gold deposit; deformation history, deposit formation, ore controls, and exploration guides, Juneau, Southeast Alaska; Confidential report prepared for Coeur D'Alene Mines Corporation, Juneau, Southeast Alaska, 15 p.

Gehrels George, 2000, Reconnaissance geology and U–Pb geochronology of the west flank of the Coast Mountains between Juneau and Skagway, southeastern Alaska, *in:* Stowell, H.H., and McClelland, W.C., eds., Tectonics of the Coast Mountains, southeastern Alaska and British Columbia, Geological Society of America Special Paper 343, p. 213–233.

Gramstad, S.D., 2000, Mineralogy and Stable Isotope Geochemistry of Gold–Silver Telluride Mineralization in the Berners Bay District, Alaska: Ames, Iowa, M.S. thesis, Iowa State University, 117 p.

Kistler, R.W., Newberry, R.J., Brew, D.A., 1993, Rubidium–strontium isotopic systematics of vein minerals in the Juneau gold belt, Alaska, *in* Dusel-

Bacon, Cynthia, and Till, A.B., eds., Geologic studies in Alaska by the U.S. Geological Survey, 1992: U.S. Geological Survey Bulletin 2068, p. 236–240.

Miller, L.D., Goldfarb, R.J., Snee, L.W., Gent, C.A., Kirkham, R.A., 1995, Structural geology, age, and mechanisms of gold vein formation at the Kensington and Jualin deposits, Berners Bay district, Southeast Alaska: Economic Geology, v. 90, no. 2, p. 343–368.

Redman, Earl, 1984, An unconformity with associated conglomeratic sediments in the Berners Bay area of Southeast Alaska, *in* Short Notes on Alaskan Geology, 1983, Alaska Division of Geological & Geophysical Surveys Professional Report 86, p. 1–4.

Redman, E.C., Caddey, S.W., Harvey, D., 1998, Mineralization and structural controls in the Berners Bay district and the Kensington mine; Confidential report prepared for Coeur D'Alene Mines Corporation, Juneau, Southeast Alaska, 41 p.

Redman, E.C., Maas, K.M., Kurtak, J.M., Miller, L.D., 1992, Bureau of Mines mineral investigations in the Juneau mining district, Alaska, 1984–1988: U.S. Department of the Interior, section D, v. 2, Juneau gold belt subarea, 424 p.

PRELIMINARY PETROGRAPHIC STUDY OF 11 MISSISSIPPIAN TO TERTIARY AGE SANDSTONES, SAGAVANIRKTOK QUADRANGLE, BROOKS RANGE FOOTHILLS AND NORTH SLOPE, ALASKA

Rocky R. Reifenstuhl[1] and Alexis E. Reifenstuhl[2]

ABSTRACT

A preliminary petrographic study of 11 sandstones from the eastern North Slope and Brooks Range foothills, Alaska, sheds light on the tectonic setting of the source area and to a limited degree, the depositional basins where the sands accumulated. The sandstones are from outcrops of the Brookian, Beaufortian, Ellesmerian, and Franklinian sequences. The 11 samples, from nine rock formations of Mississippian to Tertiary age, were systematically point-counted to determine framework grain types, grain boundary relationships, and cement and matrix composition. Framework grain composition of sandstones (average: $Quartz_{89}$ $Feldspar_{1}$ $Lithic_{10}$), combined with porosity, matrix, and cement data, can be a predictor of petroleum reservoir potential. Sandstone provenance is a significant tool in petroleum exploration for reconstructing, in a general sense, the geologic history of both the sediment source area and the depositional basin. Grain totals were plotted on ternary diagrams to discriminate between provenance and tectonic setting. The ternary diagrams indicate that the North Slope samples are composed predominantly of monocrystalline quartz, suggesting that the framework grains of the Kekiktuk, Ivishak, and Kemik Formations and the Franklin Bluff Member (of the Sagavanirktok Formation) have undergone more than one erosional cycle. All 11 samples plot within the following four provenance fields: (a) 'transitional recycled' (five from Prince Creek, Sagavanirktok, Schrader Bluff, Canning Formation, Nanushuk Group, White Hills gravel Sagavanirktok Formation); (b) 'quartzose recycled' (three from Kemik Sandstone and Kekiktuk Conglomerate, Franklin Bluff Member Sagavanirktok Formation); (c) 'craton interior' (two from Ivishak and Kekiktuk Formations); or (d) 'lithic recycled' (Prince Creek Formation). This preliminary petrographic study shows a trend toward increasing proportions of monocrystalline quartz with increasing age.

INTRODUCTION

This paper presents results from a petrographic study of 11 outcropping North Slope sandstones collected in the Sagavanirktok Quadrangle (figs. 1, 2). Samples were collected during the 1999 Alaska Division of Geological & Geophysical Surveys (DGGS) North Slope field-season. The samples represent nine formations that range in age from Mississippian to Tertiary (fig. 3). The sandstone compositions (Folk, 1968) include quartz arenite, subarenite, and litharenite.

Sandstone petrography is a critical tool in petroleum exploration, sedimentary basin analysis and evaluation, provenance determination, and petroleum reservoir-rock assessment. Thin sections of sandstones were point counted with a standard petrographic microscope equipped with a mechanically advancing stage that automatically moves the predetermined skip distance. This method allows for accurate and reproducible determination of sandstone composition. The framework grain compositions are used here to determine the original tectonic setting of 11 North Slope sandstones. Point-count results plotted on ternary diagrams with quartz–feldspar–lithic grains as apexes (fig. 4) portray relative grain abundances and similarities between samples. Up to 10 provenance fields have been identified on the standard quartz–feldspar–lithic ternary diagram (or variants of this diagram) that are related to the tectonic setting of the source terrane and, in some cases, the tectonic setting of the depositional basin (Dickinson, 1970; Dickinson and Suczek, 1979; Dickinson and others, 1983; Leeder, 1999). These environmental settings are: continental block provenances (CBP), magmatic arc provenances (MAP), and recycled orogen provenances (ROP). Figure 5 shows the subdivisions of these major environmental settings.

CBP is the ancient (generally Precambrian) granite central part of many continents worldwide; MAP consists of volcanic and plutonic rocks that occur adjacent to subduction zones, and ROP consists of different types of pre-existing sedimentary rocks, uplifted, eroded (recycled), and deposited in new environments. For each North Slope sandstone, one of these three general provenance types will be indicated. The provenance type of a particular sandstone is one predictor of its suitability as a potential petroleum reservoir rock. The highest

[1]Alaska Division of Geological & Geophysical Surveys, 794 University Ave., Suite 200, Fairbanks, Alaska 99709-3645
Email for Rocky Reifenstuhl: rocky@dnr.state.ak.us
[2]Department of Geology, Portland State University, Portland, Oregon 97201

reservoir potential for siliciclastic rocks is commonly in the monocrystalline quartz-rich part of the recycled orogen provenance.

The North Slope rock samples examined for this study and their ages (fig. 3) are: Kekiktuk (Early Mississippian), Ivishak (Triassic), Nanushuk Group (Early Cretaceous to early Late Cretaceous), Schrader Bluff (Late Cretaceous), Canning Formation (Late Cretaceous to early Tertiary), Sagavanirktok Formation (early to middle Tertiary), and Franklin Bluff Member of the Sagavanirktok Formation (middle Tertiary).

Previous petrographic studies of North Slope sandstones include Reifenstuhl and others (1997), Wartes and Reifenstuhl (1997), and Reifenstuhl (1991, 1995).

METHODS

Samples included in this study were collected from Mississippian to Tertiary rocks on the North Slope. With a petrographic microscope, 100 framework grains were counted from each standard-size thin section. Thin sections were stained for plagioclase feldspar and potassium feldspar. The Gazzi-Dickinson protocol was used, in which categories were based on subgrains larger than 63 microns. This protocol helped to normalize for compositional differences that were purely a function of grain size (Dickinson, 1970; Gazzi, 1966; Gazzi and Zuffa, 1970). On average, the sandstones were upper fine to medium grained, with a mean grain size of about 0.25 mm. Also counted were accessory minerals, matrix type, cement, rare minerals, grain sorting, rounding, and sphericity; this counted nonframework grain information was in addition to the 100 framework grains counted for each thin section.

Point counting on a grid with a fixed skip distance results in the random selection of points to be counted. This counting process achieves reproducible results and uses a mechanical, stage-mounted device that moves the thin section the prescribed skip distance after each count. For statistical reliability the skip distance selected was greater than the grain size of 95 percent of the apparent diameter of grains in a thin section (Decker, 1985). After all thin sections were point counted and the counts totaled, the results were plotted on ternary diagrams. SigmaPlot, a commercial computer program, was used to normalize the data and create ternary plots. Data from this study were compared with published sandstone compositions from known tectonic environments (Dickinson and Suczek, 1979; Dickinson and others, 1983).

Sandstone compositions from different types of basins are a function of rock types in the source area, which are strongly controlled by the plate tectonic environment (Dickinson and Suczek, 1979; Dickinson and others, 1983). Certain exceptions have been noted in the relationship between plate tectonics and sandstone compositions by Mack (1984), including recycling, long transport distances, or tropical weathering. All these factors tend to increase the quartz content of the detritus relative to most other grains, consequently distorting provenance interpretations. However, since the vast majority of sandstones addressed in the current study are exceedingly quartz rich, the influence of these factors is here considered as minor.

RESULTS

Point-count data from the 11 North Slope samples were plotted on five complementary ternary diagrams (figs. 4–8), which indicate source-terrane composition and allow inferences regarding the tectonic setting. Four of the five plots discriminate between different provenances (figs. 4–6); each diagram displays a different group of grain populations. Point-count data on figures 4–8 do not include the amount of cement, matrix, and pore space (table 1) but only framework grains.

Q–F–L (quartz–feldspar–lithics)

Figure 4 shows total quartz (monocrystalline, polycrystalline, and chert) vs feldspar vs lithics. All 11 samples, from the nine eastern North Slope formations, fall in the quartz-rich area of the diagram. Two samples (Kekiktuk and Ivishak) plot in the craton interior. The remaining nine lie in one of the subdivisions of the recycled orogen provenance.

Qm–F–Lt (quartz, monocrystalline–feldspar–lithics, including chert)

Figure 5 is a slightly altered version of figure 4 in that the quartz apex is restricted, encompassing the monocrystalline quartz variety only, and polycrystalline quartz and chert grains are moved to the lithics component. Because the feldspar component is small, all 11 samples plot on, or close to, the line between quartz and lithics. Figure 5 graphically displays the monocrystalline quartz component in these rocks. As in figure 4, most of the samples (nine) are located in the recycled orogen provenance field. The remaining two are again located in the craton interior. The shift of position for an individual sample within the triangular plots (figs. 4, 5) in most samples is a function of the abundance of the chert component. The polycrystalline quartz component typically is low, except in the Schrader Bluff Formation (22 percent) and one of the Kekiktuk samples (21 percent; table 1). Consequently, the 11 samples spread along the quartz–lithics join, denoting an increase of lithic component as they plot within the quartzose-recycled, transitional-recycled, and lithic-recycled fields.

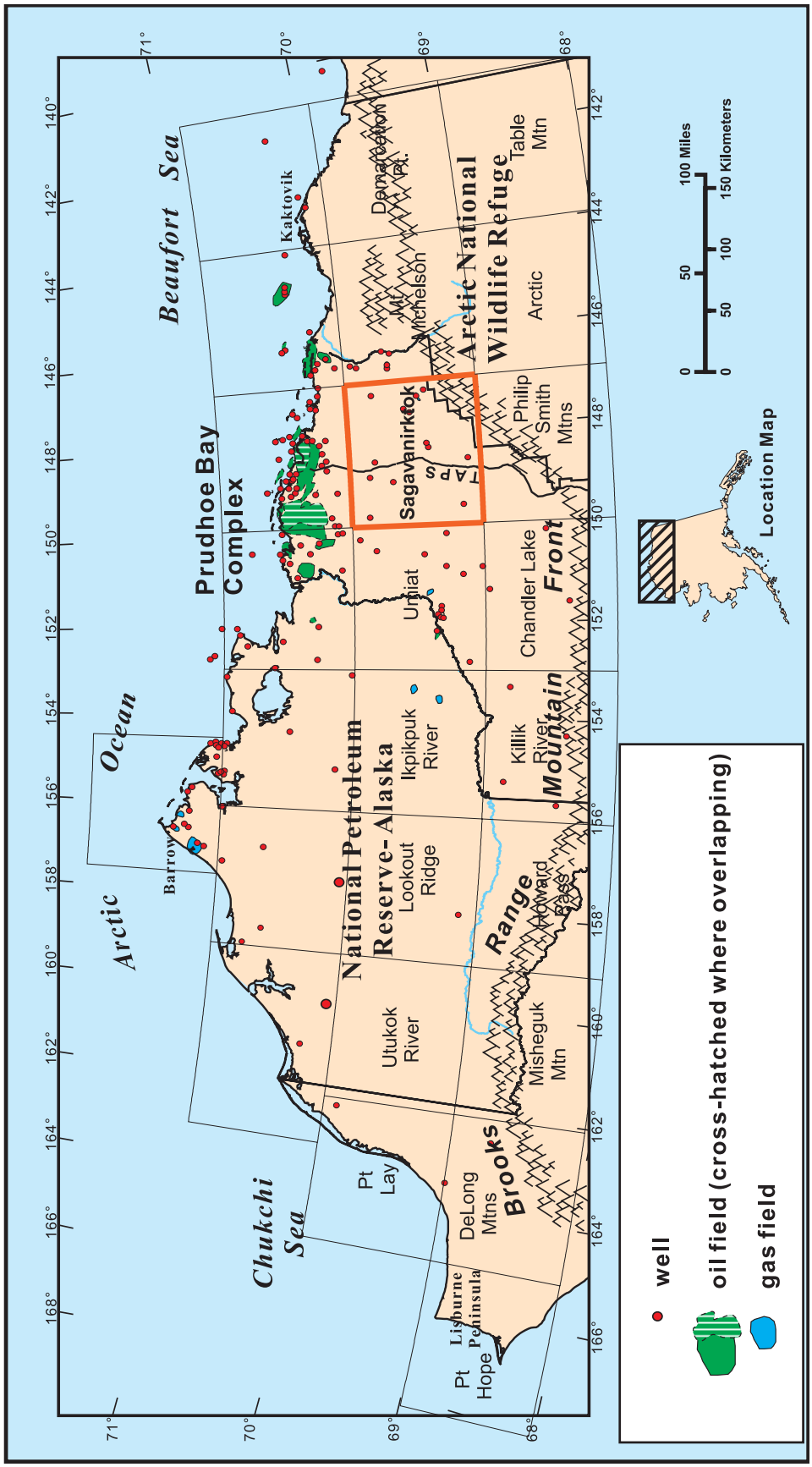

Figure 1. *North Slope, northern Brooks Range, and Sagavanirktok Quadrangle location map, with North Slope basin wells, petroleum fields, and quadrangle index.*

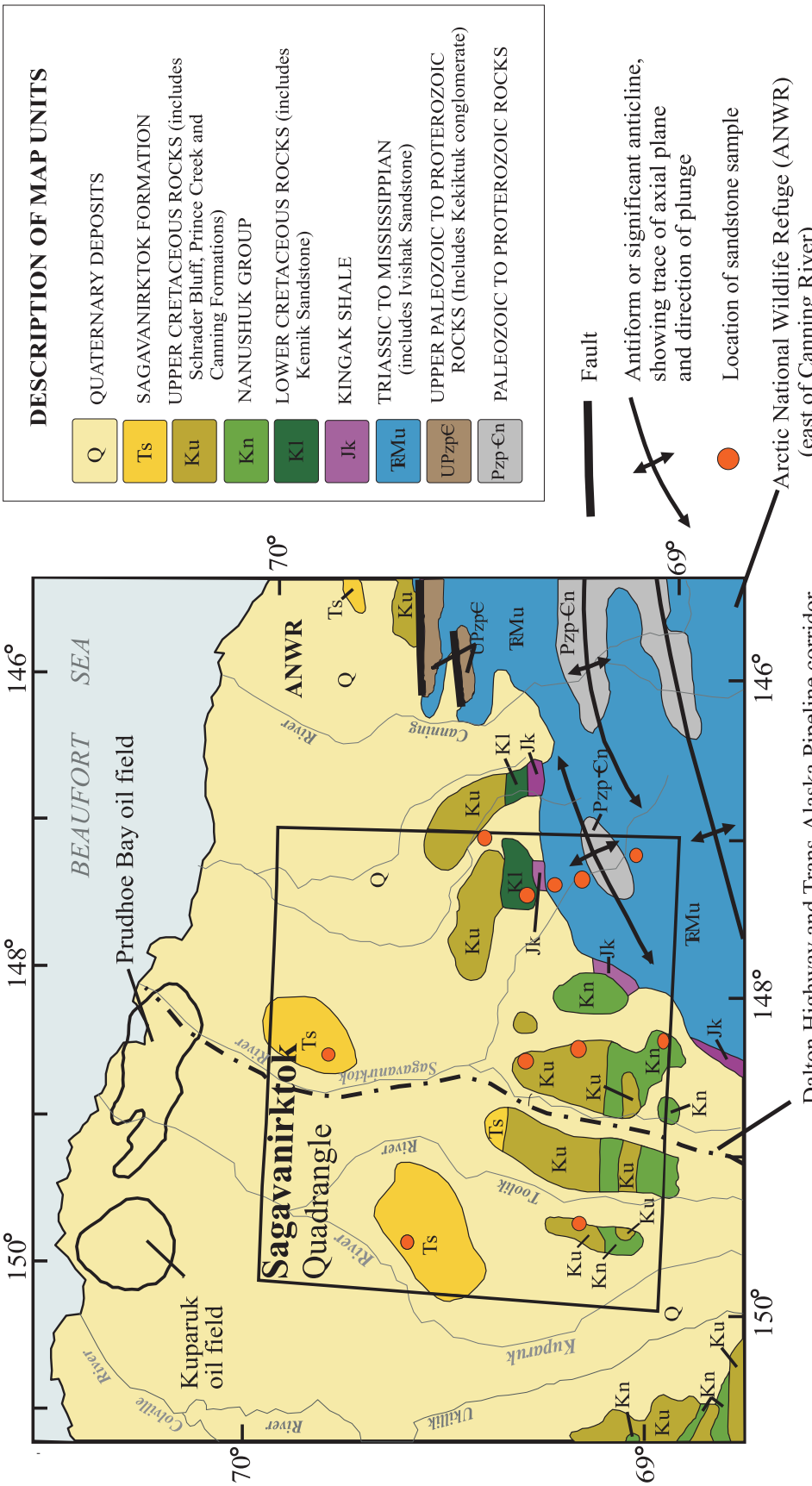

Figure 2. *General geologic map (1:250,000-scale) of the Sagavanirktok Quadrangle and surrounding area, showing locations of sandstone samples.*

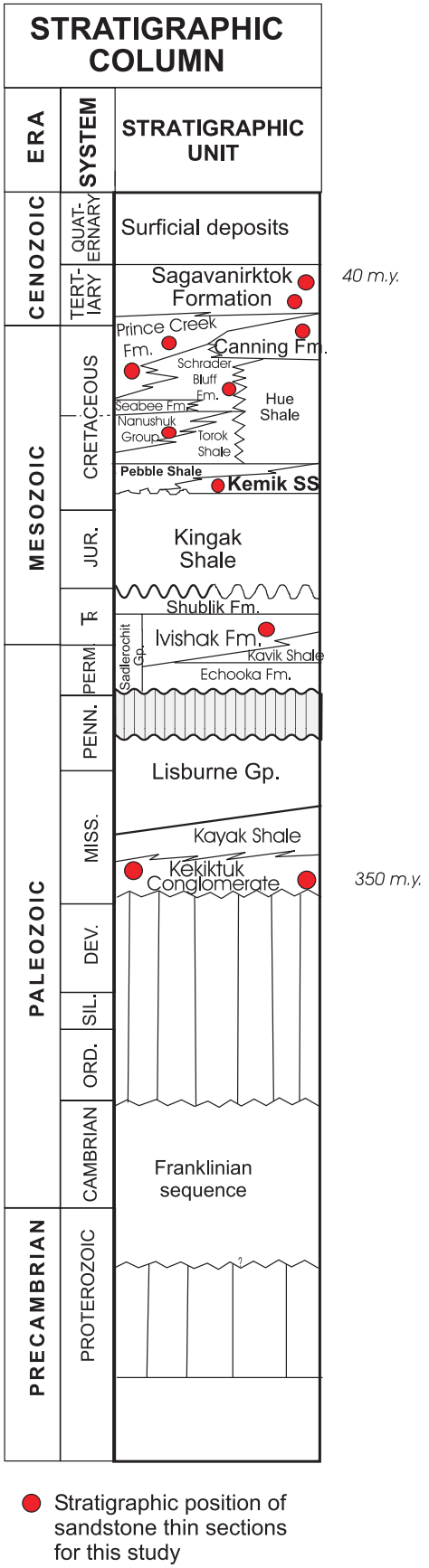

Qp–Lv–Ls (quartz, polycrystalline+chert–lithics, volcanic–lithics, sedimentary)

Figure 6 shows a generally low amount of volcanic lithic fragments and sedimentary lithic fragments in all formations. Again, all samples fall closest to the quartz apex of the plot and display their quartz-rich compositions.

Qm–Pf–Kf (quartz, monocrystalline–plagioclase feldspar–potassium feldspar)

Figure 7 incorporates plagioclase feldspar and potassium feldspar into the plot, with the third apex being monocrystalline quartz. Only five of the 11 samples contain any feldspar, and only one sample (Nanushuk; 99RR97A) has both plagioclase and potassium feldspar (table 1).

I–M–S (igneous–metamorphic–sedimentary)

Figure 8 shows igneous, metamorphic, and sedimentary rock fragments. The points are spread across the diagram and indicate no relative abundance of one particular lithic grain type over another. The total amount of each of these individual components as a percent of the total amount of framework grains averages only about 3 percent (table 1).

DISCUSSION

Of all the significant framework grains, mono-crystalline quartz is the most resistant to all types of weathering, followed by chert, followed by polycrystalline quartz (Leeder, 1999; Miall, 1990). Rocks containing a large percentage of quartz are generally better reservoir rocks, whereas rocks with large quantities of framework grains (for example, feldspar and sedimentary lithics) that alter to clays are not generally good reservoir candidates. This is because clays commonly become incorporated into the rock matrix, reducing porosity and permeability, and consequently restrict fluid flow and decrease pore volume (Mann and others, 1997). Therefore, of the 11 samples in this pilot study, the rocks composed of framework grains with the best reservoir character plot closest to the monocrystalline quartz apex on figure 5. Other important considerations include, for example, the timing of the clay diagenesis, cement diagenesis, and burial history of the sandstone. In the case of the Kekiktuk samples, diagenesis produced secondary quartz grain overgrowths. But, more importantly, locally deep burial created a quartzite with virtually no porosity. Consequently, the Kekiktuk samples from the northern Brooks Range indicate no reservoir potential. In sharp contrast is the Kekiktuk sandstone within the subsurface Endicott Field, some 150 km northwest. Here the Kekiktuk of the Endicott Group forms an excellent petroleum reservoir because of a much different burial history, diagenesis, and location, which is well north of the fold and thrust-belt mountain front.

Figure 3. *Generalized stratigraphic column for the eastern North Slope and northeastern Brooks Range, Alaska. Circles show stratigraphic position of thin sections from sandstones analyzed for this study.*

Table 1. *Petrographic point-count data from 11 eastern North Slope- and Brooks Range foothills sandstones. One hundred framework grains are counted from each thin section. Sandstones are all upper fine grained to medium grained, and average 0.25 mm grain diameter.*

Rock unit	**Prince Creek**	**Prince Creek**	**Schrader Bluff**	**Canning**	**Kemik**	**Sagava-nirktok**	**Kekiktuk**	**Nanushuk**	**Kekiktuk**	**Ivishak**	**Franklin Bluff**	**Average**
Sample	99RR71C	99RR80B	99RR61A	99RR85A	99RR24A	99RR90A	99RR91A	99RR97A	99RR94A	99RR95A	99RR67C	
Quartz Polycrystalline	5	5	22	10	10	11	21	9	4	0	1	9
Quartz Monocrystalline	24	33	47	56	70	38	79	49	96	90	81	60
Chert	56	48	18	21	17	37	0	2	0	0	16	20
Potassium Feldspar	0	1	1	0	0	0	0	0	0	0	0	0
Plagioclase Feldspar	0	0	0	0	0	0	0	0	0	1	1	0
Sedimentary	8	4	7	4	0	0	0	2	0	0	0	2
Metamorphic	2	1	3	1	2	1	0	25	0	0	0	3
Volcanic/Igneous	4	7	2	8	2	12	0	7	0	0	0	4
White Mica	0	1	0	0	0	0	0	4	0	0	0	0
Zircon	0	0	0	0	0	0	0	0	0	0	1	0
Glauconite	0	0	14	0	0	0	0	0	0	0	0	1
Cement total	19	62	0	2	0	0	1	0	38	37	2	15
Carbonate CaCO3	0	11	0	0	0	0	1	0	25	34	0	6
Silica SiO2	0	15	0	0	0	0	0	0	6	3	0	2
Iron-oxide FeO2	0	31	0	0	0	0	0	0	7	0	2	4
Matrix	1	0	0	0	9	0	4	0	0	0	0	1
Porosity	1	0	18	10	0	0	5	0	0	0	0	3
Lithics total	**14**	**13**	**12**	**13**	**4**	**13**	**0**	**38**	**0**	**9**	**0**	11
Quartz total	**85**	**86**	**87**	**87**	**97**	**86**	**100**	**60**	**100**	**90**	**98**	89
Feldspar total	**0**	**1**	**1**	**0**	**0**	**0**	**0**	**2**	**0**	**1**	**1**	1

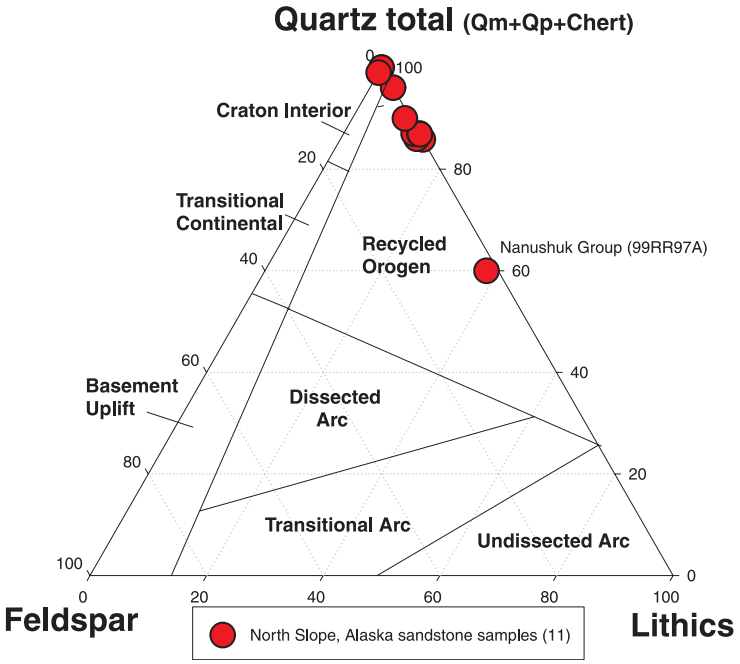

Figure 4. *Plot of total quartz–total feldspar–lithics of 11 North Slope sandstones. Nanushuk Group sample (99RR97A) contains a significant percentage of lithic framework grains, lies notably closer to the lithics apex than other samples, and is therefore labeled on diagram. Fields from Dickinson and others (1983).*

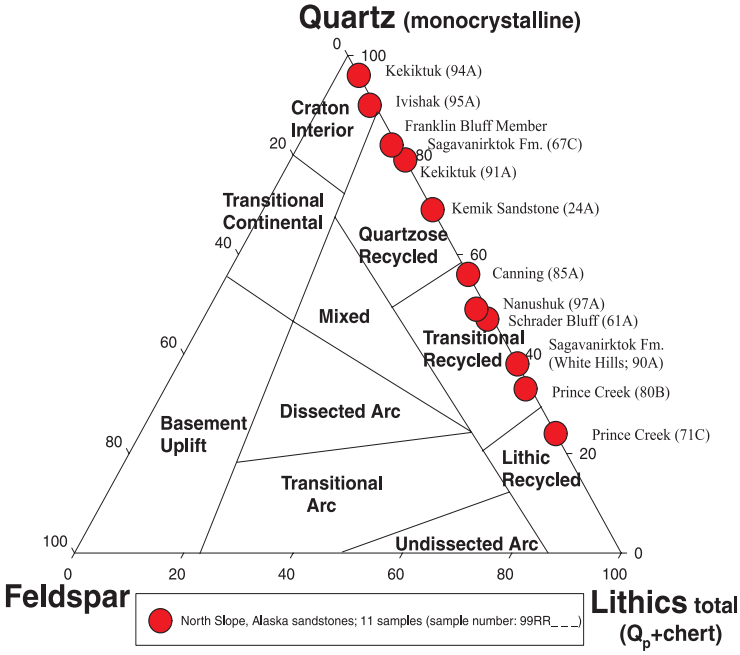

Figure 5. *Quartz (monocrystalline) vs feldspar vs total lithics (including polycrystalline quartz and chert) for 11 sandstones from the Sagavanirktok Quadrangle, eastern North Slope, Alaska (sample locations, fig. 2; stratigraphic position, fig. 3). One hundred framework grains counted per thin section. Fields are from Dickinson and others (1983).*

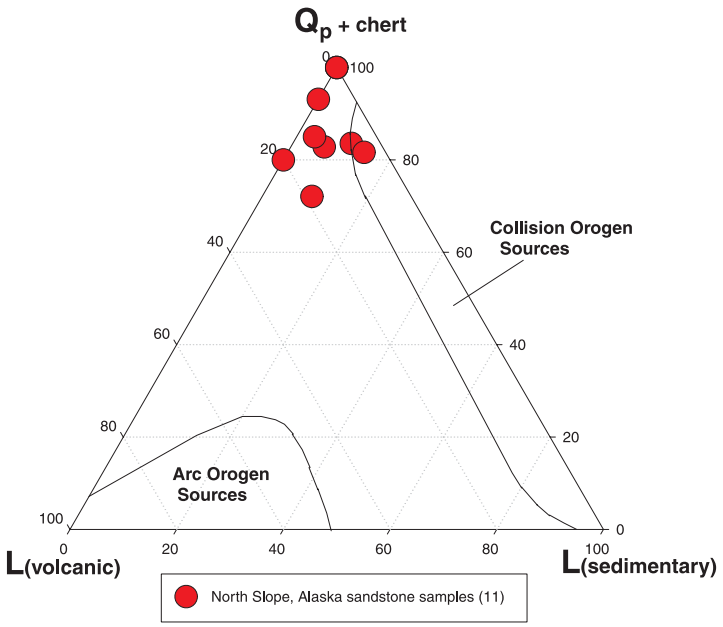

Figure 6. *Plot of quartz plus polycrystalline quartz (chert) vs volcanic lithics vs sedimentary lithics shows predominance of quartz components, and slightly more volcanic grains relative to sedimentary grains. The more volcanic-rich rock units include: Sagavanirktok, Canning, Nanushuk, and Prince Creek. Fields from Dickinson and Suczek (1979).*

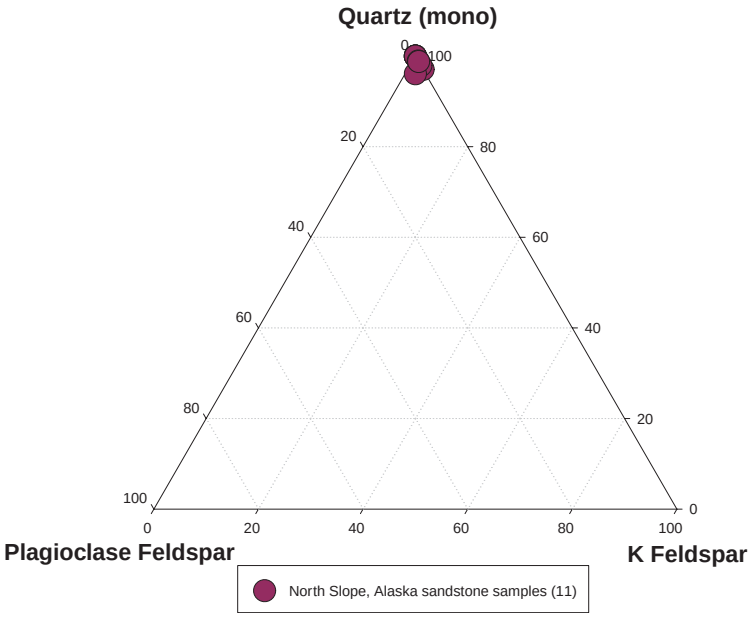

Figure 7. *Quartz (moncrystalline) vs potassium feldspar vs plagioclase feldspar. Eleven samples from nine eastern North Slope rock units ranging in age from Mississippian to Tertiary; 100 framework grains counted from each thin section.*

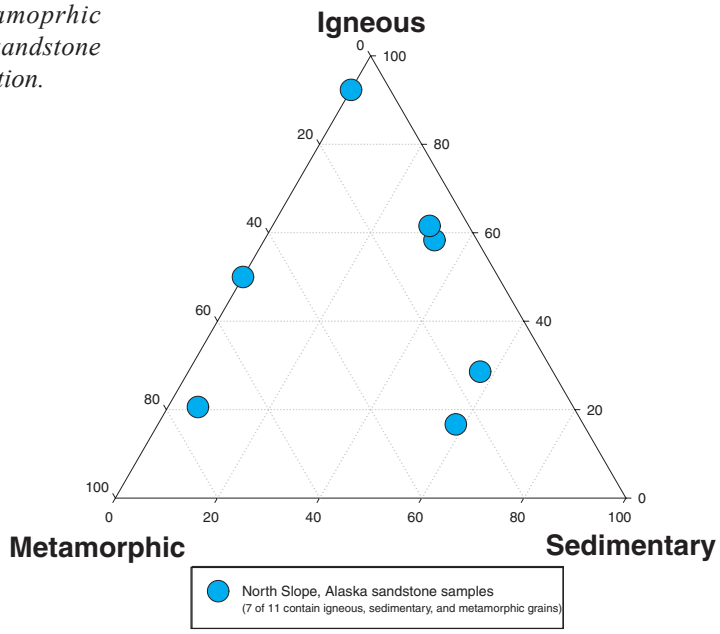

Figure 8. *Igneous vs. sedimentary vs metamoprhic ternary plot of 11 North Slope, Alaska, sandstone samples; 100 grains counted per thin section.*

The Prince Creek Formation (Late Cretaceous to early Tertiary age) has well-developed porosity locally (fig. 9B). The rock is predominantly chert (56 percent) and quartz (29 percent), with a much smaller lithic component (15 percent). Of note are the rare carbonate framework grains (fig. 9A). An early carbonate cement has been dissolved locally, creating significant secondary porosity (figs. 9A, 9B). Globally, however, carbonate cements are volumetrically the most abundant and detrimental to porosity of sandstone reservoirs, in which they commonly create barriers to fluid flow (dos Anjos and others, 2000).

Counting significantly more framework grains from each thin section (from 100 to 400 total points, for example) can significantly increase the accuracy of components that compose less than 10 percent of the rock (Van der Plas and Tobi, 1965). However, the plotted positions of the 11 samples in the study on the main ternary diagrams (figs. 4-7) would not change significantly because these components (lithics and quartz types) constitute such a large percentage of the total framework grain population. However, the accuracy (Van der Plas and Tobi, 1965) of the igneous–metamorphic–sedimentary component plot (fig. 8) is low because these grains make up only about 3 percent of the total of all framework grains (table 1).

CONCLUSIONS

The composition of sandstone is influenced by the composition of rocks in the source terrane(s) from which they are derived. Figure 5 shows that all but two samples fall within the recycled orogen field. Sandstones plotting in this part of the diagram have more quartz than any other framework grain type and are similar to most known petroleum-bearing siliciclastic sandstones on the North Slope. Figure 4 displays the abundance of quartz and the relative lack of lithic fragments. The clear exception is the Nanushuk Group sample (97A), in which the lithic component is 40 percent of the framework grain population. Generally, the more quartz-rich a rock unit, the better suited it is as a petroleum reservoir. The framework grains of quartz-poor rocks readily deform and either reduce or destroy their original porosity during compaction. Lithic grains are soft and upon only moderate burial become crushed and flattened, thereby eliminating much original sandstone porosity.

Within the recycled orogen field, sediment sources are sedimentary rocks and subordinate volcanic rocks, in part metamorphosed, exposed to erosion by uplift in mountain belts (Dickinson and others, 1983). In a very general sense, petrographic study of this suite of North Slope sandstone samples shows a trend of increasing monocrystalline quartz in stratigraphically older units (fig. 5). This is not purely a function of geologic age; rather, it has to do with the geology of the various source terranes, depositional environments, and other factors.

The two samples plotting closest to the quartz apex lie in the craton interior. The sample from the Mississippian-age Kekiktuk contains about 96 percent monocrystalline quartz. The second sample that plots within the craton interior (fig. 5) is the Triassic-age Ivishak Sandstone. Both samples suggest derivation from a low-relief, relatively quartz-rich cratonic interior.

Figure 6 aids in refining the provenance and in differentiating between volcanic and sedimentary

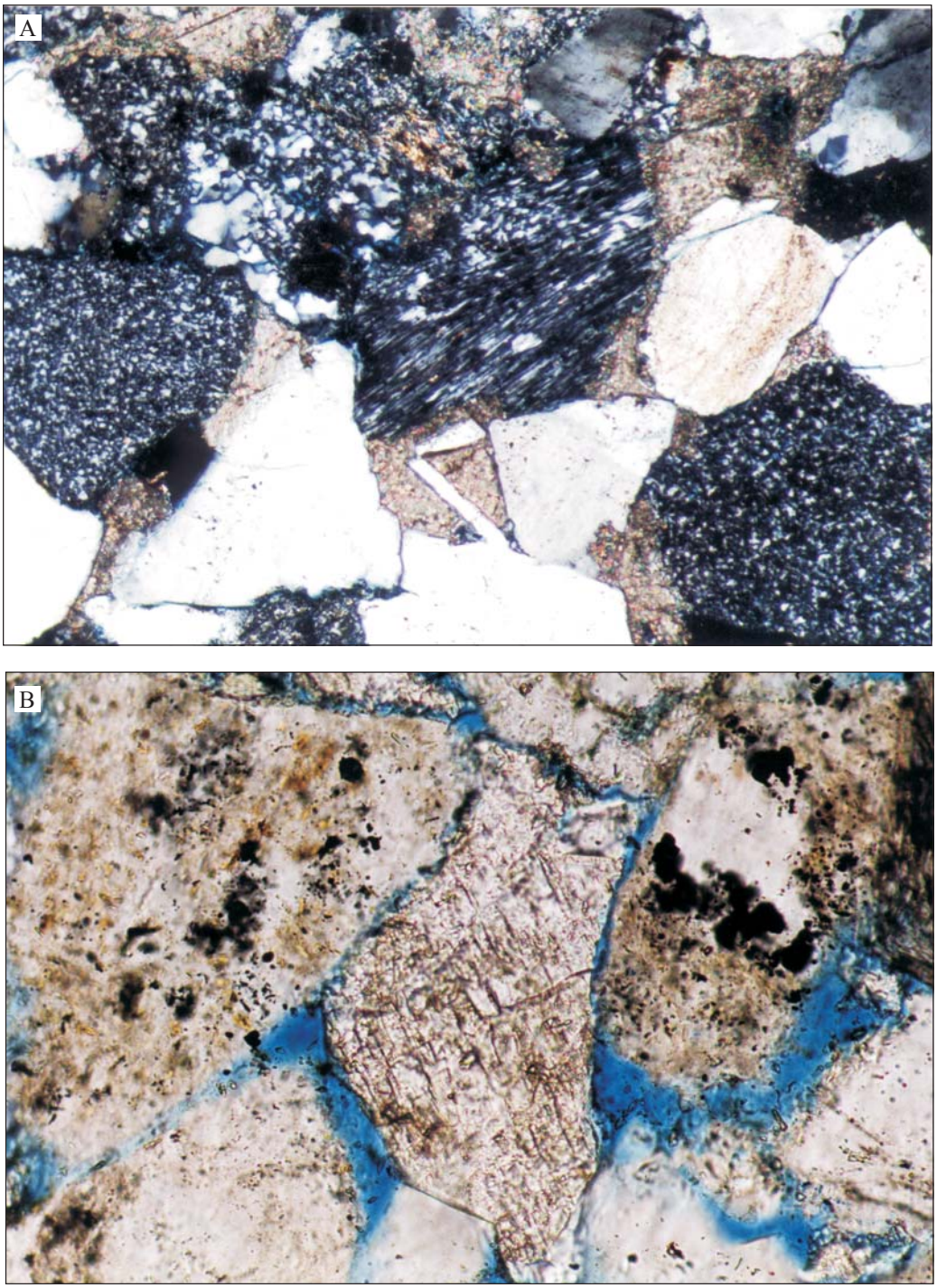

Figure 9. *Photomicrographs of Prince Creek Formation, Sagavanirktok Quadrangle, North Slope, Alaska. (A) Sample 99RR80B (Toolik River, 100X magnification; about 3 mm across bottom of photo) shows foliated chert (at center), microcrystalline chert (lower right and center left), monocrystalline quartz (white-appearing, at bottom), and interstitial calcium carbonate cement. (B) Sample 99RR71C (Echooka River, 250X magnification; about 1 mm across bottom of photo) shows monocrystalline quartz (bottom left, right, and center), carbonate grain (center), and interstitial porosity.*

orogenic environments. Feldspar framework grains are minor components in all the rocks studied. Figure 6 suggests that the provenance from which these sandstones were derived did not contain igneous rocks as a significant component. Figure 7 does not differentiate between different provenance and basin types. This plot shows the relative abundance of sedimentary, igneous, and metamorphic clasts, and does not include in the diagram any quartz (monocrystalline or polycrystalline) or chert clasts; the predominance of polycrystalline quartz is shown.

Petrography makes it possible to decipher a sandstone's provenance (fig. 5) and predict its reservoir characteristics. This study does not address other critical components of the petroleum system: generation, migration, source rock, trapping mechanism, timing, diagenetic history, and thermal maturity, but merely addresses whether the sandstones have some of the important characteristics of a siliciclastic petroleum reservoir.

ACKNOWLEDGMENTS

For reviewing and improving earlier drafts of this paper, thanks to Dave LePain, Paul McCarthy, and Cyndie Beale. Funding for this research was provided by Alaska Division of Geological & Geophysical Surveys, Anadarko Petroleum Corporation, Phillips Petroleum Company, and BP Exploration (Alaska).

REFERENCES

Anjos, S.M.C. dos, De Ros, L.F, de Souza, R.S., de Assis Silva, C.M., and Sombra, C.L., 2000, Depositional and diagenetic controls on the reservoir quality of Lower Cretaceous Pendencia sandstones, Portiguar rift basin, Brazil: American Association of Petroleum Geologists, v. 84, no. 11, p. 1719–1742.

Decker, John, 1985, Sandstone modal analysis procedure: Alaska Division of Geological & Geophysical Surveys Public-Data File 85-3 p. 1–35.

Dickinson, W.R., 1970, Interpreting detrital modes of graywacke and arkose: Journal of Sedimentary Petrology, v. 40, p. 695–707.

Dickinson, W.R., and Suczek, C.A., 1979, Plate tectonics and sandstone compositions: The American Association of Petroleum Geologists, v. 63, no. 12, p. 2164–2182.

Dickinson, W.R., Beard, L.S., Brakenridge, G.R., Erjavic, J.L., Ferguson, R.C., Inman, K.F., Knepp, R.A., Lindberg, F.A., and Ryberg, P.T., 1983, Provenance of North American Phanerozoic sandstones in relation to tectonic setting, Geological Society of America, v. 94, p. 222–235.

Folk, R.L., 1968, Petrology of sedimentary rocks: Austin, Texas, Hemphill's, 170 p.

Gazzi, P., 1966, Le arenarie del flysch sopracretaceo dell'Appennino moderese; correlazioni con il flysch di Monghidoro, Mineralogica et Petrographica Acta, v. 12, p. 69–97.

Gazzi, P., and Zuffa, G.G., 1970, Le arenarie paleogniche dell'Appennino emiliano, Mineralogica et Petrographica Acta, v. 16, p. 97–137.

Leeder, M.R., 1999, Sedimentology and sedimentary basins: from turbulence to tectonics: Malden, Massachusetts, Blackwell Science Ltd., 592 p.

Mack, G.H., 1984, Exceptions to the relationship between plate tectonics and sandstone composition: Journal of Sedimentary Petrology, v. 54, no. 1, p. 0212–0220.

Mann, U., Hantschel, T., Schaefer, R.G., Krooss, B., Leythaeuser, D., Little, R., and Sachsenhofer, R.F., 1997, Petroleum migration: mechanisms, pathways, efficiencies and numerical simulations, *in* Welte, D.H., Horsfield, B., and Baker, D.R., eds., Petroleum and basin evolution, New York, Springer-Verlag, p. 405–520.

Miall, A.D., 1990, Principles of sedimentary basin analysis, New York, Springer-Verlag, 668 p.

Reifenstuhl, R.R., 1991, Gilead sandstone, northeastern Brooks Range, Alaska: an Albian to Cenomanian marine clastic succession, *in* Reger, R.D., ed., Short notes on Alaskan geology 1991, Alaska Division of Geological & Geophysical Surveys Professional Report 111, p. 69–76.

Reifenstuhl, R.R., 1995, Lithofacies, petrology, and petrophysics of the Kemik Sandstone (Lower Cretaceous), eastern Arctic Slope, Alaska: *in* Combellick, R.A. and Tannian, Fran, eds., Short notes on Alaska geology 1995, Alaska Division of Geological & Geophysical Surveys Professional Report 117, p. 53–67.

Reifenstuhl, R.R., Wilson, M.D., and Mull, C.G., 1997, Petrography of the Tingmerkpuk Sandstone (Neocomian), northwestern Brooks Range, Alaska: A preliminary study, *in* Clough, J.G., and Larson, Frank, eds., Short notes on Alaska geology 1997, Recent research on Alaska geology, Alaska Division of Geological & Geophysical Surveys Professional Report 118, p. 111–124.

Van der Plas, L., and Tobi, A.C., 1965, A chart for determining the reliability of point counting results: American Journal of Science, v. 263, p. 87–90.

Wartes, M.A., and Reifenstuhl, R.R., 1997, Preliminary petrography on the provenance of six Neocomian to Albian sandstones, northwestern Brooks Range, Alaska, *in* Clough, J.G., and Larson, Frank, eds., Short notes on Alaska Geology 1996, Alaska Division of Geological & Geophysical Surveys Professional Report 118, p. 131–140.

GASTROPOD OPERCULA FROM THE SILURIAN AND DEVONIAN OF ALASKA

David M. Rohr[1] and Robert B. Blodgett[2]

ABSTRACT

Silurian and Devonian gastropod opercula from Alaska are described for the first time. The opercula probably belong to the family Omphalocirridae Wenz, 1938, or Oriostomatidae Munier-Chalmas, 1876.

INTRODUCTION

A single unsilicified operculum was recovered from an unnamed white, bioclastic limestone in the Taylor Mountains D-2 Quadrangle. Locality 84TNS-45 (=USGS 11948-SD) is in the SW¼ SW¼ NE¼ SW¼ sec. 4, T10N, R24W (see Adrain and others, 1995, fig. 1, for location). This locality yielded richly diverse trilobite fauna of late Llandovery (Telychian) age (Adrain and others, 1995).

Twenty-eight silicified opercula were recovered from an unnamed Lower Devonian (Emsian) limestone unit exposed on the south flank of Limestone Mountain, west-central Alaska. The limestone also contains an abundant and diverse gastropod fauna. Locality 83RB9 is in the SW¼ NE¼ sec. 26, T26S, R23E, Medfra B-4 Quadrangle, at latitude 63º16'01"N, longitude 154º32'44"W. Blodgett and Rohr (1989, fig. 1) provide details on this location.

The specimen numbers are those of the University of Alaska Museum (UAM), Fairbanks, where the specimens illustrated are deposited.

GASTROPOD OPERCULA

Silurian–Devonian gastropods known to have calcified opercula were reviewed by Yochelson and Linsley (1972) and Forney and others (1981). The opercula are similar to those associated with the oriostomatids and omphalocirrids, which typically have counterclockwise multispiral ornament on the exterior and a paucispiral interior surface (Rohr and Boucot, 1985; Checa and Jiménez-Jiménez, 1998). Forney and others (1981) compiled an extensive list of Silurian–Devonian occurrences of *Oriostoma*. The genus is relatively common in eastern North America and Europe, but no opercula of *Oriostoma* have been reported from western North America.

Australonema lilydalensis (Etheridge, 1891) from the Lower Devonian of Victoria, Australia, has a round, paucispiral operculum. Lindström (1884) illustrated a variety of Silurian multispiral opercula from Gotland, some of which are tabular and others are bullet shaped.

Operculum type 1
fig. 1.1

Description—Circular (28 mm in diameter), concentric, symmetric operculum with slightly concave outer surface; concentric rings relatively wide, only four rings present, each ring with an angular crest; slightly over half of each previous ring overlapped. Thickness unknown.

Discussion—Only the exterior of the operculum is known. It is unique among Silurian–Devonian opercula because of its coarse, concentric growth pattern. Other opercula, discussed below, have a fine, multispiral external ornament.

Occurrence—Locality 84TNS-45 (=USGS11948-SD), unnamed white, bioclastic limestone, Taylor Mountains D-2 Quadrangle. Silurian (late Llandovery, Telychian).

Operculum type 2
figs. 1.2–1.5

Description—Circular (3–11 mm in diameter), disc-shaped operculum with slightly concave outer surface; fine, counterclockwise spiral growth lines on exterior; interior surface nearly planar to convex with a shallow depression in the center; raised, rounded rim around edge; some specimens show a weak, counterclockwise paucispiral pattern on the interior; largest specimen, 11 mm in diameter, is 3 mm thick and has a slight inward tapered margin.

Discussion—Members of the Omphalocirridae Wenz, 1938, including *Liomphalus northi* (Etheridge, 1890) have a circular multispiral operculum. The operculum is close to that of *L. northi* as illustrated by

[1]Department of Earth and Physical Sciences, Sul Ross State University, Alpine, Texas 79832
Email for David Rohr:drohr@sulross.edu
[2]Department of Zoology, Oregon State University, Corvallis, Oregon 97331

Yochelson and Linsley (1972, pl. 2) from the Lower Devonian of Victoria, Australia. The Alaskan operculum is also similar to a single unnamed specimen illustrated by Spitz (1907, pl. 14, fig. 1a–c) from the Lower Devonian (Emsian) of the Carnic Alps. Opercula of the Silurian *Oriostoma coronatum*, described by Lindström (1884, pl. 17), also have similar features, including a convex to obtusely conical outer surface and a rimmed planar to convex paucispiral interior. Isolated specimens from the Silurian (Llandovery of Quebec) described by Rohr and Boucot (1985) as from *Oriostoma* have the same ornament but a convex exterior.

Occurrence—Locality 83RB9, unnamed Lower Devonian limestone unit, south flank of Limestone Mountain, Medfra B-4 Quadrangle, Lower Devonian (Emsian).

CONCLUSIONS

It is impossible to assign these unusual Alaska fossils generically. Because so few Silurian–Devonian opercula are known and in-place opercula so rare, it is difficult to determine which, if any, features are diagnostic. The shape of the opercula indicates they correspond to shells with a circular whorl profile. Very similar opercula occur

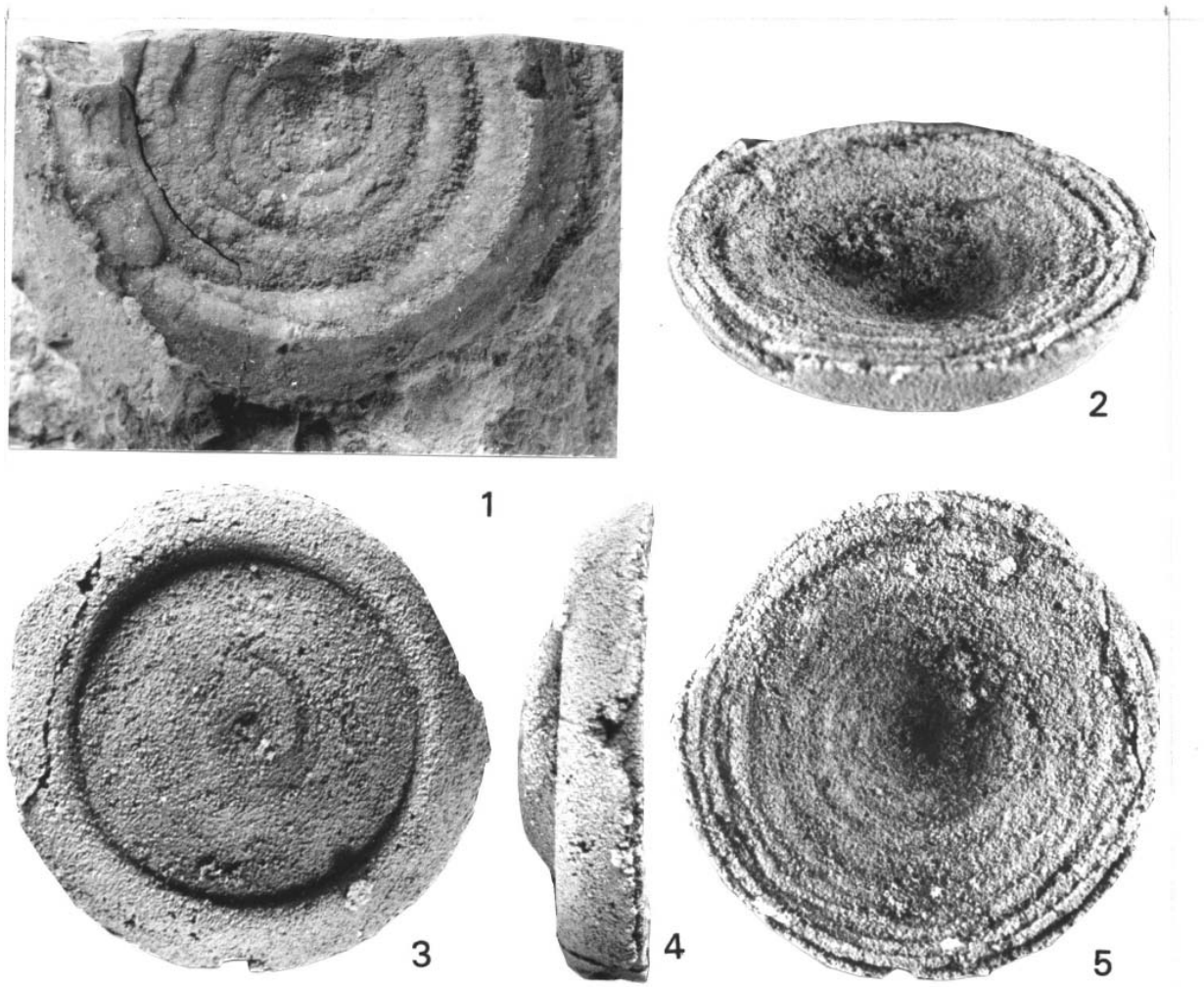

Figure 1. *Silurian and Devonian gastropod opercula. Specimen numbers are those of the University of Alaska Museum (UAM).*

1. Operculum type 1, exterior view of specimen in matrix, x3. Note coarse, concentric growth lines. UAM 2584. Locality 84TNS-45 (=USGS11948-SD), Taylor Mountains D-2 Quadrangle, Silurian (late Llandovery, Telychian).

2-5. Operculum type 2, oblique exterior, interior, side, and exterior view of silicified specimen; x6. UAM 2585. Locality 83RB9, south flank of Limestone Mountain, Medfra B-4 Quadrangle, Lower Devonian (Emsian).

in-situ from two families of gastropods, the Omphalocirridae and the Oriostomatidae. It is uncertain if this shared morphology is derived from a common lineage or if it is due to convergence.

ACKNOWLEDGMENTS

The specimen from the Taylor Mountains D-2 Quadrangle was collected by T.N. Smith of the Alaska Division of Geological & Geophysical Surveys. Rohr was supported in part by a Sul Ross State University, Research Enhancement Grant. We are grateful to A.J. Boucot, Department of Zoology, Oregon State University, for helpful comments on the manuscript and the use of acid etching facilities. We are also grateful to E.L. Yochelson, National Museum of Natural History, for his comments on the manuscript.

REFERENCES

Adrain, J.M., Chatterton, B.D.E., and Blodgett, R.B., 1995, Silurian trilobites from southwestern Alaska: Journal of Paleontology, v. 63, p. 723–736.

Blodgett, R.B., and Rohr, D.M., 1989, Two new Devonian spine-bearing pleurotomariacean gastropod genera from Alaska: Journal of Paleontology, v. 63, p. 47–53.

Checa, A.G., and Jiménez-Jiménez, A.P., 1998, Constructional morphology, origin, and evolution of the gastropod operculum, Paleobiology, v. 24, p. 109–132.

Etheridge, Robert, Jr., 1890, Descriptions of Upper Silurian fossils from the Lilydale Limestone, Upper Yarra District, Victoria: Records of the Australian Museum, v. 1, p. 60–67.

Etheridge, Robert, Jr., 1891, Further descriptions of Upper Silurian fossils from the Lilydale Limestone, Upper Yarra District, Victoria: Records of the Australian Museum, v. 1, p. 125–130.

Forney, G.G., Boucot, A.J., and Rohr, D.M., 1981, Silurian and Lower Devonian zoogeography of selected molluscan genera, *in* Gray, J., Boucot, A.J., and Berry, W.B.N., eds., Communities of the past: Stroudsberg, Pennsylvania, Hutchinson Ross Publishing Company, p. 119–164.

Lindström, G., 1884, On the Silurian Gastropoda and Pteropoda of Gotland: Kongliga Svenska Veternskap-Akademiens Handlinger, Bandt 19, no. 6, 250 p.

Munier-Chalmas, E., 1876, Mollusques nouveaux des terrains paléozoiques des environs de Rennes: Journal de Conchyliologie, 3^{e} série, v. 16, p. 102–109.

Rohr, D.M., and Boucot, A.J., 1985, Observations on the operculum of Oriostoma (Silurian Gastropoda): Canadian Journal of Earth Sciences, v. 22, p. 294–296.

Spitz, A., 1907, Die Gastropoden des karnischen Unterdevon: Beiträge zur Paläontologie und Geologie Österreich-Ungarns und des Orients, v. 20, p. 115–190.

Wenz, Wilhelm, 1938, Gastropoda, Teil 1: Allgemeiner Teil und Prosobranchia, *in* Schindewolf, O.H., ed., Handbuch der Paläozoologie: Band 6, Gebrüder Borntraeger, Berlin, p. 1–240.

Yochelson, E.L., and Linsley, R.M., 1972, Opercula of two gastropods from the Lilydale Limestone (Early Devonian) of Victoria, Australia: Memoirs of the National Museum of Victoria (Melbourne), v. 33, p. 1–14.

NEW SILURIAN MURCHISONIID GASTROPODS FROM ALASKA AND A REVIEW OF THE GENUS *COELOCAULUS*

David M. Rohr[1], Robert B. Blodgett[2], Jiøí Frýda[3]

ABSTRACT

Medfracaulus cooki n. gen., n. sp. and *Coelocaulus karlae* n. sp. are described from the Upper Silurian of west-central and southeastern Alaska, respectively. *Coelocaulus* is redefined to limit the content to selenizone-bearing murchisoniids with a deep, straight-walled umbilicus and without a columellar flange. The presence of a deep umbilicus in high-spired shells cannot be used alone as a diagnostic character of *Coelocaulus*, as on this basis many other non-murchisoniid species (mainly based on steinkerns) have erroneously been attributed to the genus. Establishment and recognition of these unusually large, deeply umbilicate murchisoniid shells is important for the Silurian biostratigraphy of Alaskan terranes. Both genera are abundant and are characteristic of Upper Silurian strata of west-central Alaska (Nixon Fork subterrane of the Farewell terrane) and southeastern Alaska (Alexander terrane). Similar morphotypes are unknown from rocks located undoubtedly on the North American continent (Laurentia) during the Late Silurian.

INTRODUCTION

Unusually large, deeply umbilicate murchisoniid gastropod shells are both abundant and characteristic of Upper Silurian strata of Alaskan accreted terranes. These include occurrences in Nixon Fork subterrane of the Farewell terrane of west-central Alaska and the Alexander terrane of southeastern Alaska. Similar morphotypes are not known from Upper Silurian strata in North America (Laurentia) except from exotic terranes. Thus, these forms provide excellent guide fossils for mapping purposes within Alaska, and their description is deemed important for future biostratigraphic studies of shallow-water platform carbonate environments in the Upper Silurian of Alaska. Similar forms occur in Lower Devonian rocks of Alaska, but they are considerably smaller.

Abundant silicified specimens occur in the Medfra B-3 Quadrangle, west-central Alaska, in thin beds of an unnamed, southwest-dipping, platy limestone unit at 63°18.56' N, 154°34.97' W. The beds also contain the Silurian-age (early Ludlow to early Pridoli) conodont *Ozarkodina confluens* (Savage and others, 1995). Gastropods from this locality were collected by J.T. Dutro, Jr., and W.W. Patton, Jr., in 1979 (field locality 79APa82b of W.W. Patton, Jr.) and later by two of the authors (Rohr and Blodgett) in 1994. Other less abundant silicified megafossils from the lime mudstone include the brachiopod *Meristina* sp. and the gastropod *Murchisonia* sp.

Non-silicified *Coelocaulus* occur in southeastern Alaska. The specimens were collected by E. Kirk in 1917 and bear the label, "993, Small island lying off northeast end of Willoughby Island, Glacier Bay, Alaska." Examination of Kirk's collection indicates that the species was part of a large-shelled molluscan assemblage that included *Euomphalopterus liratus* (Kirk, 1928), *Holopea* sp. and a large unnamed pleurotomaroid shell.

Specimen numbers with a USNM prefix are from the National Museum of Natural History, Washington, D.C.; UAM numbers indicate the specimens deposited at the University of Alaska Museum, Fairbanks.

Superfamily MURCHISONIOIDEA Koken, 1896
Family MURCHISONIIDAE Koken, 1896

Discussion—Despite the common occurrence of murchisonoidean gastropods within Paleozoic gastropod communities, their higher systematic position is still uncertain. Knight and others (1960), following Wenz (1938), placed Murchisonioidea Koken, 1896, within Archaeogastropoda into the suborder Murchisoniina Cox and Knight, 1960. The latter suborder was considered to be a transition between the Archaeogastropoda and the more advanced Caenogastropoda group. For this reason the Murchisonioidea were placed in the subclass Caenogastropoda in some recent gastropod classifications (*e.g.*, Ponder and Warén 1988). The discovery of a caenogastropod-type protoconch in Carboniferous '*Murchisonia*' (Bandel 1994) was considered to be further evidence for the latter placement. However, the discovery of an archaeogastropod-type protoconch in several Early Devonian murchisoniids (Frýda and Manda 1997, Frýda 1999), including the type genus *Murchisonia*, suggests that at

[1]Department of Earth and Physical Sciences, Sul Ross State University, Alpine, Texas 79832
Email for David Rohr:drohr@sulross.edu
[2]Department of Zoology, Oregon State University, Corvallis, Oregon 97331
[3]Czech Geological Survey, Klárov 3/131, 118 21 Praha 1, Czech Republic

least some of the Devonian murchisoniids belong to the Archaeogastropoda. Knight and others (1960) placed only two families in the superfamily Murchisonioidea: Murchisoniidae and Plethospiridae. Recently, an archaeogastropod-type protoconch was also discovered in some Devonian plethospirids including *Diplozone* Perner, 1907 (Frýda, unpublished data). Thus, the archaeogastropod-type protoconch is the only protoconch type known in Siluro–Devonian members of the Murchisonioidea. At present, there is no reason to presume that the Siluro–Devonian murchisonoideans, including the taxa described herein, belong to Caenogastropoda. Data on the protoconch of *Coelocaulus* and closely related genera are unknown, and uncertainty must remain as to their higher systematic placement.

Genus COELOCAULUS Oehlert and Oehlert, 1888

Type Species—Murchisonia davidsoni Oehlert, 1877, from the Lower Devonian (Emsian) of France.

Emended diagnosis—High-spired, slowly expanding gastropods with moderately to weakly convex outer whorls, very deep, tapering, straight-walled umbilicus, columellar flange absent, and a selenizone near or slightly below midwhorl. Medium to large size, growth lines prosocline above selenizone, opisthocline below.

Discussion—Coelocaulus Oehlert and Oehlert, 1888, is a distinctive, high-spired murchisoniid genus characterized by its many whorls and continuous, narrow umbilical perforation. The umbilicus is produced when the rate of expansion of the whorl is relatively small compared to the increase in the radius of the spiral around the axis of coiling. In some murchisoniids this relationship produces a thick columella, but in *Coelocaulus*, a void, the umbilicus, is produced. Established as a subgenus of *Murchisonia* by Oehlert and Oehlert (1888), *Coelocaulus* was more widely used as a genus by Bassler (1915), but later was relegated as a synonym of *Michelia* Roemer, 1852, by Knight and others (1960) in the Treatise on Invertebrate Paleontology.

In the original description of the type species *Murchisonia davidsoni*, Oehlert (1877, p. 587) described the shell with a "bande du sinus," and the band, "...est large, à peine visible." Their illustrations show this weak band. Knight (1941, p. 81) stated that the type species lacks a selenizone. Later in the same paragraph, Knight describes an "obscure selenizone-like band" on the shell. Neither Knight nor we examined the type material, but we conclude that a weak selenizone is present on the type species.

Closely related, but distinct, genera include the Early Devonian-age *Ptychocaulus* Perner, 1907, and *Barroisocaulus* Gubanov and others, 1995, both with a columellar flange. *Coelidium* Clarke and Ruedemann, 1903, is a junior objective synonym of *Coelocaulus* (Knight, 1941).

Previously *Coelocaulus* has included any high-spired gastropods of Ordovician to Carboniferous age with a deep umbilicus. Such overidentification continued until recently (*i.e.* Blodgett and others [1988], where the generic concept was used to include any Lower Devonian forms with a deeply umbilicate, high-spired shell, regardless of external ornament). We restrict the usage to those umbilicate forms that have a selenizone. It is uncertain if *Michelia* Roemer, 1852, has a selenizone. Knight (1941) noted the absence of the feature on the holotype of the type species, *M. cylindrica* Roemer, 1852, from the Eifelian of the Harz Mountains of Germany. Another deeply umbilicate genus (originally designated as a subgenus of the Tertiary genus *Niso*) is *Vetotuba* Etheridge, 1890, based on *N. (V.) brazieri* Etheridge, 1890, from the Lower Devonian Lilydale Limestone of Victoria, Australia. *Vetotuba* was recognized to be a junior subjective synonym of *Coelocaulus* by Chapman (1916) and Knight (1944). Subsequently, it was placed in synonymy with the genus *Michelia*. However, Knight (1941) and Tassell (1977) described a selenizone or "pseudoselenizone" in this species, although this feature is not clearly visible on any of the illustrations provided in either paper. If a selenizone is truly present in the type species of *Vetotuba*, judging by the external shell form it would be reasonable to consider it synonymous with *Coelocaulus*, rather than *Michelia*, as the latter genus lacks this feature.

Age range—Late Silurian to Early Devonian (Emsian). Ordovician reports of the genus are based on a misunderstanding of the generic features. *Coelocaulus neglectus* Ulrich and Scofield, 1897 (Edenian) is based on a single internal mold, has rounded whorls, and was apparently included because of the presence of an umbilicus. *Coelocaulus oehlerti* Ulrich and Scofield, 1897 (Shermanian) has a slow rate of expansion and deep umbilicus, but it is based on rare internal molds and the exterior is unknown. Bassler (1915) assigned the Middle Ordovician *Murchisonia linearis* Billings, 1859, to *Coelocaulus*, but the shell is poorly known. *Coelocaulus delicatus* Butts, 1941, from the Lower Ordovician is based on poorly preserved specimens, and the presence of an umbilicus is unknown. *Coelocaulus neglectus* var. *major* Troedsson, 1929, is umbilicate, but has a high rate of translation along the vertical axis.

Perner (1907) considered *Coelocaulus* to be a subgenus of *Murchisonia,* and he noted the following Silurian (Ludlow–Pridoli) species from Bohemia: *C. cybele* Barrande *in* Perner, 1907, *C. latona* Barrande *in* Perner, 1907, *C. contracta* Barrande *in* Perner, 1907, *C.*

zonaria Perner, 1907, *C. argolis* Perner, 1907, *C. alceste* Perner, 1907, *C. clavata* Barrande *in* Perner, 1907, and *C. pollens* Barrande *in* Perner, 1907. The shells of *Coelocaulus cybele* are relatively variable. Perner noted four varieties of this species but all of them are morphologically far removed from the type species of *Coelocaulus, C. davidsoni* (Oehlert, 1877). In contrast to the type species, the whorls in *C. cybele* are very low and the lateral sides of the whorls are flat. The very deep, tapering, straight-walled umbilicus in *C. cybele* is much wider than that in the type species of *Coelocaulus*. Thus, shells of *C. cybele* resemble Early Devonian *Ptychocaulus* rather than *Coelocaulus* in the above-mentioned shell characters.

The shells of *C. latona* Barrande *in* Perner, 1907 also have low whorls and a wide umbilicus (see Perner, 1907, plate 99, figs. 5, 9–12) and seem to be closer to *Ptychocaulus*. The presence of a columellar ridge is considered to be an important diagnostic feature of the latter genus. However, such ridge is not present in the Silurian species (*C. cybele* and *C. latona),* and therefore their generic position is unclear. The low, flat-sided whorls distinguish *C. clavata* Barrande *in* Perner, 1907 (see plate 97, fig. 46–47) from the type species of *Coelocaulus*. On the other hand, pupiform shells of the latter species having flat whorl sides and almost parallel shell sides distinguish *C. clavata* from the morphological range of *Coelocaulus*. Similarly, very high whorls in *C. argolis* make its placement to *Coelocaulus* unacceptable. The Late Silurian *C. contracta* Barrande *in* Perner, 1907, and *C. pollens* Barrande *in* Perner, 1907, are poorly known because their types were based on imperfectly preserved specimens (internal molds). The general shell morphology in the Silurian *C. zonaria* Perner, 1907, and *C. alceste* Perner, 1907 (see pl. 99, figs. 1–4) seems to be close to that of the type species, *Coelocaulus oehlerti* from the Devonian. In summary, Perner (1907) placed Silurian species with considerably different morphologies in *Coelocaulus*. At the present, it is difficult to reevaluate their relationships to the type species of *Coelocaulus* because a revision of generic diagnoses of the closely related genera *(Ptychocaulus, Hormotoma, Barroisocaulus, Michelia, Catozone*, and *Cerithioides*) is needed. On the other hand, closely similar shell morphologies of some Silurian species as *C. pollens* Barrande *in* Perner, 1907 (pl. 100, figs. 52–54), '*Murchisonia' compressa* (Lindström, 1884, pl. XII, figs. 15–19), and *Coelocaulus karlae* n. sp. unite them into one morphological group.

Horný (1952, 1953) assigned two Silurian (Ludlow) species from Bohemia to *Coelocaulus* on the basis of the asymmetrical arch of the whorl profile and the position of the selenizone below midwhorl. *Coelocaulus concinnus* has a narrow, spiral umbilicus, and *C. chlupaci* has no umbilicus. We remove them both from *Coelocaulus* and place them in *Murchisonia*.

Several Silurian species that have previously been included in the genus are removed until such time as the presence of a selenizone can be demonstrated. Bassler (1915) included *Murchisonia bivittata* Hall, 1852, *M. longispira* Hall, 1852, *M. turritiformis* Hall, 1852, and *M. terebralis* Hall, 1852, in *Coelocaulus*, although none preserve the external surface. *Murchisonia bivittata* Hall, 1852, has a double spiral fold on the columella, suggesting that it is related to *Ptychocaulus*. *Murchisonia macrospira* Hall, 1852 (=*M. logani* Hall, 1852) and *M.* cf. *vitellia* Billings, 1865 were included in *Coelidium* by Clarke and Ruedemann, 1903, on the basis of the narrow umbilicus. The cross sections show rounded to oval whorls with a rate of expansion more like *Murchisonia*; the exteriors are unknown.

In the Lower Devonian *Coelocaulus barroisi* Oehlert and Oehlert, 1888, *C. procera* Oehlert and Oehlert, 1888, and the type species *C. davidsoni* Oehlert, 1877, occur in France. A single Lower Devonian species from Bohemia is *C. decipiens* Perner, 1903.

Lower Devonian species tentatively removed from the genus because of the lack of an observed selenizone include *Coelocaulus rodneyi* Rohr, 1980, from northern California and *C.* sp. Gubanov and others, 1995, from Kyrgyzstan. Undescribed umbilicate internal molds are known from the Lower Devonian (Emsian) of Kasaan Island, southeastern Alaska and the Receptaculites Limestone of Australia.

Donald (1892) placed her Carboniferous species *Murchisonia (Coelocaulus) tuedia* tentatively in *Coelocaulus*. Absence of any data about the shell base or the umbilicus makes the assignment to the latter genus very uncertain.

Geographic range—North America (Alaska), Europe (France, Bohemia, Sweden), and Australia? (Victoria).

COELOCAULUS KARLAE n. sp.
Figure 1.4–1.7

Diagnosis—Large shells with a deep, tapering straight-walled umbilicus and a selenizone at midwhorl, outer whorl surface broadly convex.

Types—Holotype USNM specimen 511815, paratype USNM 511816.

Etymology—Named in honor of Susan M. Karl, U.S. Geological Survey, Anchorage, Alaska.

Description—Large (12 cm high), high-spired (apical angle 35 degrees), deeply phaneromphalous gastropods with band at midwhorl; suture impressed, right and left shoulders convex, band slightly raised. Growth lines poorly known, prosocline above band.

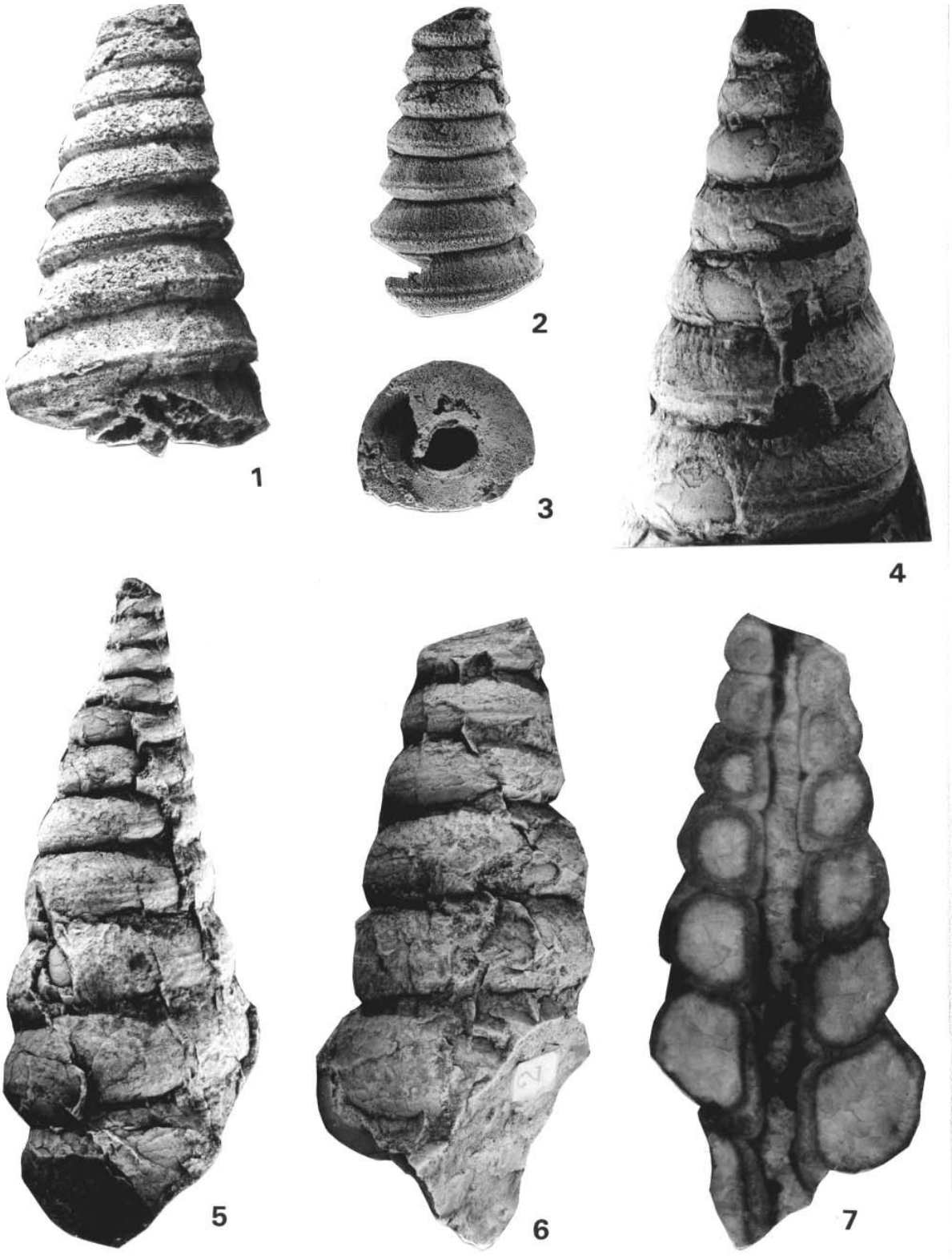
1
2
3
4
5
6
7

Base of whorl convex, sharp, circumumbilical angulation, umbilicus deep, flat walled. Whorl profile D-shaped, in sawn section, the umbilical width is seen to increase at a slower rate than the width of a single whorl (fig. 1.7); in earlier stages the umbilicus is about equal to the whorl width, and in later stages about half the width.

Discussion—In addition to its much larger size, this species can be distinguished from *C. davidsoni* by its lower rate of translation along the axis of coiling and its flatter whorls. It has a much wider umbilicus than Clarke and Ruedemann's (1903) Silurian occurrences of *Coelidium macrospira* (Hall, 1852) and *C.* cf. *vitellia* (Billings, 1865).

With its low whorls and wide umbilicus, the shell of *Coelocaulus karlae* resembles some Silurian species of *Coelocaulus* from the Prague Basin. *C. pollens* is the most similar of the Bohemian species to *Coelocaulus karlae* (see Perner 1907, pl. 100, figs. 52–54). Both species have the same general shape, relative width of umbilicus, and shell size. Unfortunately, *Coelocaulus pollens* is based on an internal mold, so more detailed comparison of both species is impossible. The relatively wide umbilicus as well as low whorls unite some species of *Coelocaulus*, including *C. karlae*, in well-defined morphological groups. Relationship of the latter group to the late Early Devonian type species of *Coelocaulus* needs clarification and further study. Existence of some transitional shell forms such as the Silurian *Murchisonia (Hormotoma) sana* Barrande *in* Perner, 1907, complicates such a revision.

Occurrence—Kirk's locality 993, "small island lying off northeast end of Willoughby Island," Glacier Bay, southeastern Alaska. This locality is within the Willoughby Limestone of Rossman (1963).

MEDFRACAULUS n. gen.

Diagnosis—Slowly expanding, high-spired gastropod with deep, tapering, straight-walled umbilicus; selenizone below midwhorl, whorl above selenizone very broadly convex, growth lines nearly orthocline above selenizone.

Comparison—Medfracaulus is distinguished from *Coelocaulus* by a selenizone below midwhorl.

Type species—Medfracaulus cooki n. sp.

Etymology—Genus named after the Medfra Quadrangle, where the specimens were discovered. Species named in honor of Alex G. Cook, Queensland Museum, Brisbane, Queensland, Australia.

Included species—Medfracaulus cooki.

Known stratigraphic range—Silurian (Ludlow or Pridoli)

Known geographic range—West-central Alaska (Nixon Fork subterrane of the Farewell terrane).

MEDFRACAULUS COOKI n. sp.
Figure 1.1–1.3

Types—Holotype UAM 2586, paratype UAM 2587.

Description—Moderate size (up to 6 cm in height), slowly expanding, high-spired (22–35 degrees), some specimens slightly coeloconoid, deeply phanerompha-lous gastropods with slit band at periphery slightly below midwhorl, each whorl embraces previous whorl just below periphery. Suture angular and impressed, upper whorl surface nearly planar to slightly convex, selenizone bordered above and below by cord. Whorl profile D-shaped with upper and lower part of 'D' sloping downward toward axis of coiling. Growth lines faint, slightly sigmoid. Base of whorl convex, periphery of umbilicus angular; deep umbilicus, flat walled, umbilical sutures impressed. Width of umbilicus equal to width of whorl on large and small specimens.

Comparison—In general shell shape, whorl profile, and shape and relative width of the umbilicus, the Silurian *Coelocaulus contracta* Barrande *in* Perner, 1907 (see pl. 102, figs. 40–42), resembles *Medfracaulus cooki*. Unfortunately, *Coelocaulus contracta* is based on an imperfectly preserved specimen (internal mold), so its placement in *Medfracaulus* is tentative.

Occurrence—Rohr's locality 94R-3 (field locality 79APa82b of W.W. Patton, Jr.), early Ludlow to early Pridoli, Medfra B-3 Quadrangle, west-central Alaska.

ACKNOWLEDGMENTS

Specimens from the Medfra Quadrangle were collected by Rohr, Blodgett, and E.A. Measures with support from National Geographic Society grant 5188-94. We are grateful to A.J. Boucot, Department of Zoology, Oregon State University, for helpful comments on the manuscript and the use of acid etching facilities.

Figure 1 (left). *1–3.* Medfracaulus cooki *n. gen., n. sp. Locality 94R-3 of Rohr (=locality 79APa82b of W.W. Patton, Jr.), Medfra B-3 Quadrangle, west-central Alaska. 1, side view x2, holotype UAM 2586. 2–3, side and umbilical views x1.5, paratype, UAM 2587.*

4–7. Coelocaulus karlae *n. sp., E. Kirk collection 993, "small island lying off northeast end of Willoughby Island," Glacier Bay, southeastern Alaska. 4, side view highlighting selenizone and growth lines, x2; and 5, side view of entire shell, x1, USNM 511815. 6, 7, exterior and interior showing deep umbilicus, x1.5, USNM 511816.*

We are also grateful to E.L. Yochelson, National Museum of Natural History, for his comments on the manuscript.

REFERENCES

Bandel, Klaus, 1994, Comparison of Upper Triassic and Lower Jurassic gastropods from the Peruvian Andes (Pucara Group) and the Alps (Cassian Formation): Palaeontographica, Abteilung A, v. 233, p. 127–160.

Bassler, R.S., 1915, Bibliographic index of American Ordovician and Silurian fossils: Bulletin of U.S. National Museum, v. 92, 1,521 p.

Billings, Elkanah, 1859, Fossils of the Chazy Limestone with descriptions of new fossils: Canadian Naturalist and Quarterly Journal of Science, p. 426–470.

———1865, Palaeozoic fossils, Volume 1: Geological Survey of Canada, 426 p.

Blodgett, R.B., Rohr, D.M., and Boucot, A.J., 1988, Lower Devonian gastropod biogeography of the western hemisphere, *in* McMillan, N.J., Embry, A.F., and Glass, D.J., eds., Devonian of the world: Canadian Society of Petroleum Geologists Memoir 14, v. 3, p. 285–305.

Butts, Charles, 1941, Geology of the Appalachian Valley in Virginia, part 2; Fossil plates and explanations: Virginia Geological Survey Bulletin, v. 52, p. 271.

Chapman, Frederick, 1916, New or little-known Victorian fossil in the National Museum: Proceedings of the Royal Society of Victoria, N.S., v. 29, p. 75–103.

Clarke, J.M., and Ruedemann, Rudolf, 1903, Guelph fauna in the State of New York: Memoir of the New York State Museum and Science Service, v. 5, 195 p.

Donald, J.T., 1892, Notes on some new and little-known species of Carboniferous *Murchisonia*: Quarterly Journal of the Geological Society of London: v. 68, p. 562–575.

Etheridge, Robert, Jr., 1890, Descriptions of Upper Silurian fossils from the Lilydale Limestone, Upper Yarra District, Victoria: Records of the Australian Museum, v. 1, p. 60–67.

Frýda, Jiøí, 1999, Higher classification of the Paleozoic gastropods inferred from their early shell ontogeny: Journal of the Czech Geological Society, v. 44, p. 137–153.

Frýda, Jiøí, and Manda, Stepan, 1997, A gastropod faunule from the *Monograptus uniformis* graptolite biozone (Early Lochkovian, Early Devonian) in Bohemia: Mitteilungen aus dem Geologisch-Palaeontologischen Institut der Universität Hamburg, v. 80, p. 59–122.

Gubanov, A.P., Blodgett, R.B., and Lytochkin, V.N., 1995, Early Devonian (Pragian) gastropods from Kyrgyzstan (central Asia): Journal of Paleontology, v. 69, p. 431–440.

Hall, James, 1852, Descriptions of the organic remains of the lower middle division of the New York system: Paleontology of New York, v. 2, 362 p.

Horný, Radvan, 1952, Dva noví zástupci èeledi Murchisonidae Koken (Gastropoda)ze stœdoèeského siluru: Rozpravy Ústœdního ústavu geologického, v. 19, p. 209–228.

———1953, Nekolik nových gastropodu ze stœdoèeského siluru: Rozpravy Ústœdního ústavu geologického, v. 20, p. 189–211.

Kirk, Edwin, 1928, *Bathmopterus*, a new fossil gastropod genus from the Silurian of Alaska: Proceedings of the United States National Museum, v. 74, article 18, p. 1–4.

Knight, J.B., 1941, Paleozoic gastropod genotypes: Geological Society of America Special Paper 32, 510 p.

———1944, Paleozoic Gastropoda, *in* Shimer, H.W., and Shrock, R.R., eds., Index Fossils of North America: New York, John Wiley & Sons, p. 437–479.

Knight, J.B., Batten, R.L., Cox, L.R., Keen, A.M., Robertson, Robert, and Yochelson, E.L., 1960, Systematic descriptions, *in* Moore, R.C., ed., Treatise on invertebrate paleontology, Part I, Mollusca 1: Lawrence, KS, Geological Society of America and University of Kansas Press, p. I169–I324.

Koken, Ernst, 1896, Die Leitfossilien: Leipzig, C.H. Tarchnitz, 848 p.

Lindström, G., 1884, The Silurian Gastropoda and Pteropoda of Gotland: Kongliga Svenska Vetenskaps Akademiens Handlingar, 250 p.

Oehlert, D., 1877, Sur les fossiles dévoniens du département de la Mayenne: Bulletin de la Société Géologique de France, 3e série, v. 5, p. 578–603.

Oehlert, D., and Oehlert, P., 1888, Descriptions de quelques espèces dévoniennes du département de la Mayenne: Bulletin de la Société d'Études Scientifique d'Angers, v. 1887, p. 65–120.

Perner, J., 1903, Gastéropodes, Tome 1, *in* Barrande, J., ed., Systême silurien du centre de la Bohême 4, Prague, 164 p.

———1907, Gastéropodes, Tome 2, *in* J. Barrande, Systême silurien du centre de la Bohême 4, Prague, 380 p.

Ponder, W.F., and Warén, Anders, 1988, Classification of the Caenogastropoda and Heterostropha—a list of the family-group names and higher taxa, *in* Ponder, W.F., ed., Prosobranch Phylogeny, Malacological Review Supplement, p. 288–326.

Roemer, F.A., 1852, Beiträge zur geologischen Kenntnis des nordwestlichen Harzgebirges: Palaeontographica, v. 3, p. 69–111.

Rohr, D.M., 1980, Ordovician–Devonian Gastropoda from the Klamath Mountains, California: Palaeontographica, Abteilung A; Palaeozoologie–Stratigraphie, v. 171, p. 141–210.

Rossman, D.L., 1963, Geology of the eastern part of the Mount Fairweather Quadrangle, Glacier Bay, Alaska: U.S. Geological Survey Bulletin, 1121-K, 57 p., 2 pl.

Savage, N.M., Rohr, D.M., and Blodgett, R.B., 1995, Late Silurian conodonts from the Medfra B-4 Quadrangle, west-central Alaska: Geological Society of America, Abstracts with Programs, v. 27, no. 5, p. 76.

Tassell, C.B., 1977, A revision of the gastropod fauna of the Lilydale Limestone (Early Devonian) of Victoria: Memoirs of National. Museum of Victoria, v. 37, p. 1–22.

Troedsson, G.T., 1929, On the Middle and Upper Ordovician faunas of northern Greenland, Part 2: Meddelelser om Grønland, v. 72, p. 1–197.

Ulrich, E.O., and Scofield, W.H., 1897, The Lower Silurian Gastropoda of Minnesota, The Geology of Minnesota: Paleontology, v. 3, pt. 2, p. 813–1081.

Wenz, Wilhelm, 1938, Gastropoda, Teil 1: Allgemeiner Teil und Prosobranchia, *in* Schindewolf, O.H., ed., Handbuch der Paläozoologie: Band 6, Gebrüder Borntraeger, Berlin, p. 1–240.

ALASKADISCUS, A NEW BELLEROPHONTOIDEAN GASTROPOD FROM THE UPPER ORDOVICIAN OF THE YORK AND FAREWELL TERRANES OF ALASKA

David M. Rohr[1], Jiří Frýda[2], and Robert B. Blodgett[3]

ABSTRACT

Alaskadiscus donensis, a new Late Ordovician genus and species of tropidodiscid gastropod, is known only in two areas in Alaska: (1) the Seward Peninsula (York terrane), and (2) the Lone Mountain area, McGrath Quadrangle, west-central Alaska (Nixon Fork subterrane of the Farewell terrane). The genus is similar to *Tropidodiscus* Meek and Worthen, 1866, but in *Alaskadiscus* the interior surface has a distinctive, raised, flat-topped ridge. The unusual morphology of the internal whorl space in *Alaskadiscus donensis* is interpreted as evidence for the presence of bilaterally symmetrical, paired organs.

INTRODUCTION

An unusual tropidodiscid gastropod, originally included in *Tropidodiscus* Meek and Worthen, 1866, occurs in abundance in Late Ordovician (Ashgillian) age rocks in two areas of Alaska (fig. 1). This gastropod was first illustrated by Rohr (1988) and was based on specimens from the Port Clarence Limestone on the Seward Peninsula. Several hundred silicified specimens were collected from three localities on the Seward Peninsula (Rohr, 1988, fig. 1) by ARCO Alaska geologists in the 1980s.

Blodgett and others (1992; 2002) mentioned that the same species occurs in an unnamed limestone in the Lone Mountain area, west-central Alaska. Locality 89ABd27 consists of small outcrop and surrounding rubble-crop zone (about 10 ft wide) containing abundant silicified gastropods, corals, and the pentameroid brachiopod *Tcherskidium*. The locality is along the ridge crest at an elevation of about 1,500 ft and is situated in the NW¼ NW¼ NW¼ SE¼ sec. 9, T28N, R30W, McGrath C-4 Quadrangle (fig. 2). This locality is within the same general stratigraphic level but slightly beneath USNM locality 32023 (=Blodgett field localities 81RB13 and 89ABd28), which yielded the silicified gastropod fauna described in Rohr and Blodgett (1985). Beds at this locality strike N10°E and dip 80°NW.

Specimen numbers with a USNM prefix are those deposited in the National Museum of Natural History, Washington, D.C., and the UAM numbers indicate specimens deposited in the University of Alaska Museum in Fairbanks.

BIOGEOGRAPHY

At present, the genus is known only from two areas (fig. 1) within Alaska: (1) in the Upper Ordovician Port Clarence Limestone near the Don River, western Seward Peninsula (part of the York terrane), and (2) in unnamed Upper Ordovician shallow-water carbonate rocks that form part of the Nixon Fork subterrane of the Farewell terrane (locality 89ABd27) exposed in the hills west of Lone Mountain, McGrath C-4 Quadrangle, west-central

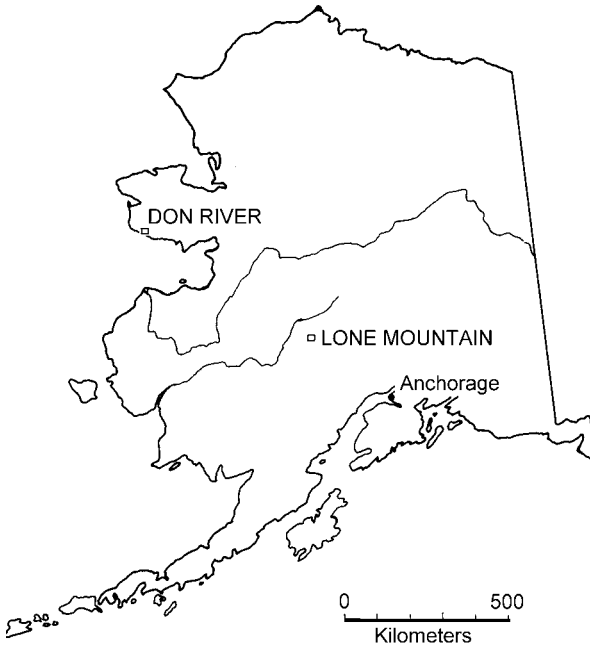

Figure 1. Alaskadiscus *n. gen. occurs in the Don River area of the Seward Peninsula and the Lone Mountain area, McGrath C-4 Quadrangle, west-central Alaska.*

[1]Department of Earth and Physical Sciences, Sul Ross State University, Alpine, Texas 79832
Email for David Rohr:drohr@sulross.edu
[2]Czech Geological Survey, Klárov 3/131, 118 21 Praha 1, Czech Republic
[3]Department of Zoology, Oregon State University, Corvallis, Oregon 97331

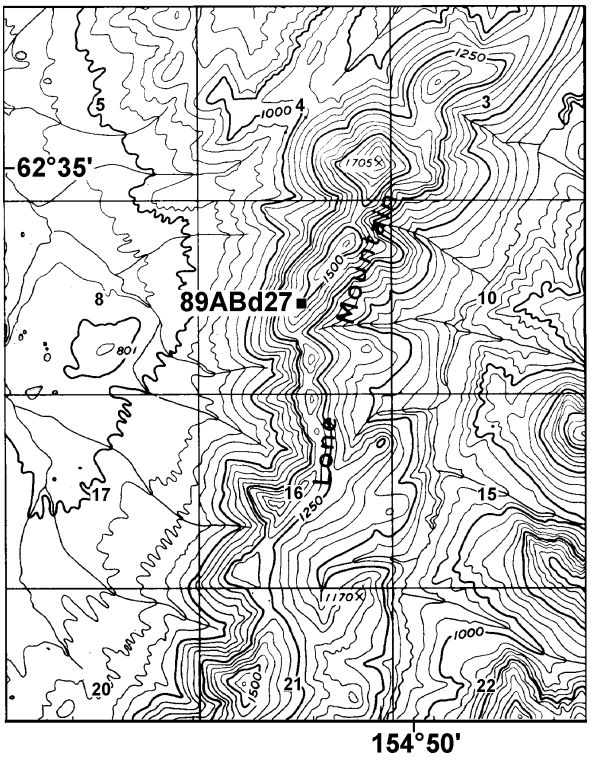

Figure 2. *Map showing location of fossil locality 89ABd27 in the Lone Mountain area, McGrath C-4 Quadrangle, west-central Alaska. Numbered squares are sections, one mile square.*

Alaska. The occurrence of this distinctive genus has previously been referred to in Blodgett and others (1992; 2002) as an unnamed "new genus aff. *Tropidodiscus.*"

SYSTEMATIC PALEONTOLOGY

Superfamily BELLEROPHONTOIDEA M'Coy, 1851

Family TROPIDODISCIDAE Knight, 1956

Discussion—Knight (1956) erected the subfamily Tropidodiscinae within the family Bellerophontidae, but Golikov and Starobogatov (1975) and Wahlman (1992) elevated the Tropidodiscinae to family level. The family contains *Tropidodiscus* Meek and Worthen, 1866, *Phragmolites* Conrad, 1838; *Temnodiscus* Koken, 1896, *Chalarostrepsis* Knight, 1948, *Groomodiscus* Rohr and Yochelson, 1990, and *Alaskadiscus* n. gen. Other genera previously placed in the family include the synonyms of *Tropidodiscus*: *Tropidocyclus* De Koninck, 1882, and *Oxydiscus* Koken, 1889.

The tropidodiscids are known to range from the Early Ordovician to the Late Devonian.

Genus ALASKADISCUS n. gen.

Diagnosis—Compressed lenticular, phaneromphalous, planispiral shells with angular keel; adaxial interior surface with a raised, flat-topped ridge formed where it overlaps the keel of the previous whorl.

Etymology—Genus name derived from the combination of Alaska and the Latin word *discus* (from the Greek *diskos*, meaning flat or circular plate).

Type species—*Alaskadiscus donensis* n. sp.

Included species—Only the type species is known.

Known stratigraphic range—Upper Ordovician (Ashgillian).

Known geographic range—Alaska.

ALASKADISCUS DONENSIS n. sp.
Figure 3

Tropidodiscus aff. *subacutus* (Ulrich). Rohr, 1988, p. 552, figs. 2.1–2.3.

Diagnosis—By monotypy, same as the genus.

Types—Holotype UAM 2582, paratypes UAM 2583, USNM 422307, 422308.

Etymology—Species name from the Don River on the Seward Peninsula.

Description—Small (4–7 mm), relatively thick-shelled, compressed lenticular, planispiral shells with open umbilici and acutely angular keel; whorl heart-shaped in cross section, umbilical angulation sharp, sutures incised; shell surface apparently smooth; final whorl of mature specimens in contact with previous whorl; aperture slightly flared and thickened at edges. Outer edge of aperture not preserved, slit not observed but probably present (see below). Faint sigmoid growth lines on some specimens (see Rohr, 1988, fig. 2.2) indicate a tangential aperture.

Discussion—Typically *Tropidodiscus* has an acute keel, and the adaxial interior surface has a low angular ridge formed as it overlaps the keel of the previous whorl (for example, Wahlman, 1992, pl. 41, figs. 9–13). In *Alaskadiscus* the interior surface has a distinctive, raised flat-topped ridge.

The presence of a slit is unknown because the outer edge of the aperture is not preserved. This consistent breakage suggests that part of the shell was weakened by the presence of a slit.

Thickening of the apertural area has been reported in other planispiral gastropods, and is interpreted to better balance and stabilize the shell (Wahlman, 1992).

Occurrence—USNM localities 36394, 36405, and 36406, are from the Port Clarence Limestone and situated in sec.14, T1N, R40W, Teller B-4 Quadrangle,

Seward Peninsula (see Rohr, 1988, fig 1, for their location). Locality 89ABd27, in an unnamed limestone, NW¼ NW¼ NW¼ SE¼ sec. 9, T28N, R30W, McGrath C-4 Quadrangle, west-central Alaska (fig. 2).

Figured specimens—UAM 2582 and 2583 from USNM loc. 36404 (=323-1).

HIGHER TAXONOMIC POSITION OF TROPIDODISCIDAE

Because of the lack of any data on their anatomy, protoconch morphology and shell structure are the only characters that can help to determine the higher taxonomic position in fossil gastropods. Unfortunately, our knowledge of these shell features in all six genera (*Tropidodiscus, Phragmolites, Temnodiscus, Chalarostrepsis, Groomodiscus*, and *Alaskadiscus*) placed in the family Tropidodiscidae is very poor. There are no data about the shell structure in any of these genera. An internal mold of a juvenile shell identified as *Tropidodiscus* sp. from the Early Ordovician of Sweden (Dzik, 1981) represents the only published information on the protoconch morphology in tropidodiscids. However, such a type of preservation is not helpful. The figured juvenile shell of *Tropidodiscus* sp. shows that its protoconch was bilaterally symmetrical and relatively large (diameter of the first whorl is about 300 μm). Similar protoconch morphology was also found by one of us (Frýda) in the Early Devonian *Tropidodiscus pragensis* Horný, 1962, from the Prague Basin (Czech Republic). Unfortunately, no boundary line between protoconch and teleoconch was observed in either species. For this reason, the total number of protoconch whorls is unknown. These facts make a comparison of the protoconch morphology in tropidodiscids with those in other gastropods, as well as an evaluation of its significance for their higher taxonomic position, difficult.

The teleoconch morphology of the type genus of the Tropidodiscidae, *Tropidodiscus*, is very stable through its whole stratigraphic range (Early Ordovician [Arenig]–Middle Devonian [Givetian]). Moreover, *Tropidodiscus* has a wide geographical distribution (it is known from sedimentary rocks of all the present continents), and its species inhabited a relatively large range of marine environments from the cold water, clastic to the tropical reefal facies. These facts evidence a successful life strategy for this genus. Peel (1977) pointed out that micromorphic *Tropidodiscus arisaigensis* from the Silurian of Nova Scotia can be considered as a possible foliage dweller. Occurrence of clusters of many shells

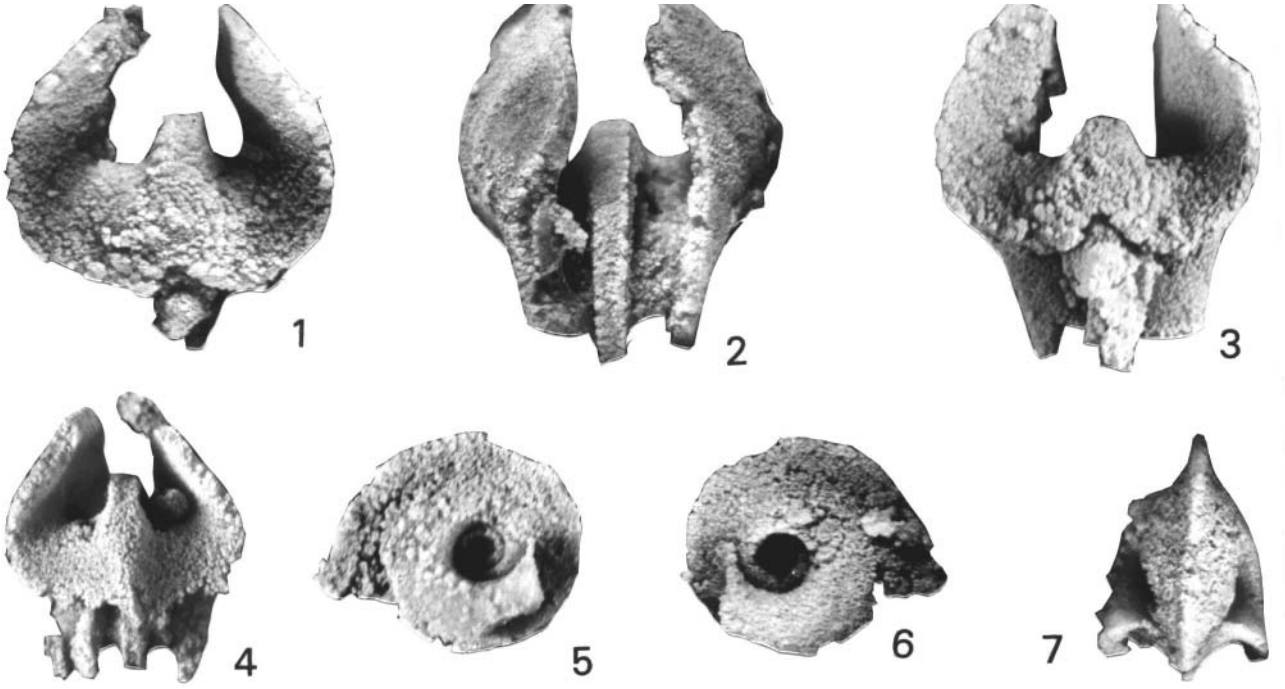

Figure 3. Alaskadiscus donensis *n. gen., n. sp. USNM loc. 36404, Port Clarence Limestone, Seward Peninsula. All views x8. UAM numbers indicate the University of Alaska Museum, Fairbanks.*
1–3. Views showing the apertural lip covering the flat-topped ridge, holotype, UAM 2582
4–7. Apertural, umbilical, and abapertural views of the lenticular shell, paratype, UAM 2583.

belonging to *Tropidodiscus pusillus* (Perner) in the Middle Ordovician Sarka Formation of the Prague Basin suggests such a mode of life. The dominance of *Tropidodiscus pragensis* Horný within the Early Devonian *Palaeozygopleura–Boucotonotus* gastropod community of the Prague Basin seems to be consistent with an interpretation of *Tropidodiscus* as an herbivorous grazer amongst algal foliage. On the other hand, the stratigraphic as well as geographic ranges of the remaining tropidodiscid genera are much narrower, and no data are available on their mode of life. Openly coiled gerontic whorls in some tropidodiscids (*Temnodiscus, Chalarostrepsis*, and *Groomodiscus*) indicate their limited mobility at least in the final growth stages. Thus, the family Tropidodiscidae unites species of the successful, widespread genus *Tropidodiscus* on the one hand, and relatively highly specialized taxa (Late Cambrian *Chalarostrepsis*, Middle Ordovician *Groomodiscus*, and Middle Ordovician–Silurian *Temnodiscus*) on the other. Monophyly of the family Tropidodiscidae should be tested.

The tropidodiscids have been considered to be related to bellerophontids and have been placed in the superfamily Bellerophontoidea (see Knight and others, 1960). Opinions on the higher taxonomic position of the latter group are contradictory (see Yochelson, 1967; Horný, 1992; Peel, 1991a,b; Wahlman, 1992; and Frýda, 1999a for review). Finding of a non-archaeogastropod-type protoconch in *Bellerophon* was interpreted as evidence for the independent position of the Bellerophontoidea within the class Gastropoda (Frýda, 1999a). However, quite different protoconch morphology in the main groups of bellerophontiform molluscs suggests that Paleozoic bellerophontiform molluscs represent a polyphyletic group (Frýda, 1999b). Discovery of fossilized intestinal contents in the Lower Ordovician *Cyrtodiscus nitidus* (Perner) introduced important anatomical data (Horný, 1998). The latter species was interpreted according to its geometry as a typical member of Class Tergomya (in the sense of Peel, 1991b; and Horný, 1996, 1998). The latter group has been interpreted as an independent molluscan class uniting untorted molluscs (Peel, 1991a,b). However, geometry of the fossilized intestinal contents in *Cyrtodiscus nitidus* fits well with its interpretation as a torted mollusc and, by extension, as a member of the Class Gastropoda. In summary, our anatomical knowledge of the bellerophontiform molluscs (including tropidodiscids) is still poor, and their higher taxonomic position(s) is open.

Finding of a flat-topped ridge within the aperture of *Alaskadiscus donensis* (fig. 3) brings new, important data on the morphology of its internal organs. The flat-topped ridge divides the internal whorl space into two equivalent, bilaterally symmetrical parts. This fact suggests that the internal organs in *Alaskadiscus donensis* were also bilaterally symmetrical. Moreover, the presence of bilaterally symmetrical, very complex shell structures within the aperture of the Silurian genus *Liljevallospira* Knight, 1945, may be interpreted in the same way. Both genera, belonging to different families, Tropidodiscidae and Bellerophontidae, may have a similar anatomy, characterized by the presence of bilaterally symmetrical, paired organs. On the other hand, there are many examples of modern gastropods with bilaterally symmetrical shells, but asymmetrical anatomy. However, none of these have the internal whorl space divided into two equivalent, bilaterally symmetrical parts like the above-mentioned bellerophontoidean genera. This fact makes a test of the hypothesis on symmetry of the internal organs in tropidodiscids very difficult.

ACKNOWLEDGMENTS

Specimens from the Seward Peninsula were collected by A.W. Potter and S. Reusing of ARCO, Alaska. Field work by RBB in the McGrath Quadrangle was supported by the Alaska Division of Geological & Geophysical Surveys. We are grateful to A.J. Boucot, Department of Zoology, Oregon State University, for his review of the manuscript and for the use of acid etching facilities. N.M. Savage, Department of Geological Sciences, University of Oregon, also reviewed the manuscript.

REFERENCES

Blodgett, R.B., Rohr, D.M., and Clough, J.G., 1992, Late Ordovician brachiopod and gastropod biogeography of Arctic Alaska and Chukotka: International Conference on Arctic Margins, Anchorage, Alaska, September 2–4, 1992, Abstract Volume, p. 11.

Blodgett, R.B., Rohr, D.M., and Boucot, A.J., 2002, Paleozoic linkages among some Alaskan accreted terranes and Siberia based on megafossils, *in* Miller, Elizabeth, Grantz, Art, and Klemperer, Simon, eds., Tectonic evolution of the Bering Shelf–Chukchi Sea–Arctic Margin and adjacent landmasses: Geological Society of America Special Paper 360, p. 273-290.

Conrad, T.A., 1838, Report on the palaeontological department of the survey: New York, New York Geological Survey, Annual Report 2, p. 107–119.

Dzik, Jerzy, 1981, Larval development, musculature, and relationships of *Sinuitopsis* and related Baltic bellerophonts: Norsk Geologisk Tidsskrift, v. 61, p. 111–121.

Frýda, Jiří, 1999a, Higher classification of the Paleozoic gastropods inferred from their early shell ontogeny: Journal of the Czech Geological Society, v. 44, p.137–153.

Frýda, Jiøí, 1999b, Suggestions for polyphyletism of Paleozoic bellerophontiform molluscs inferred from their protoconch morphology: Pittsburgh, 65th Annual Meeting, American Malacological Society, Abstracts Volume, p. 30.

Golikov, A.N., and Starbogatov, Y.I., 1975, Systematics of prosogranch gastropods: Malacologia, v. 15, p. 185–232.

Horný, Radvan, 1962, New genera of Bohemian Lower Paleozoic Bellerophontina: Vestník Ústøedního ústavu geologického, v. 27, p. 473–476.

———1992, Vývoj názoru na klasifikaci cyklomyarnich mekkýšu (Mollusca, Monoplacophora): Èasopis Národního Muzea, Øada pøírodovedná, v. 157 (1-4), p. 13–50.

———1996, Retractor muscle scars in *Gamadiscus* (Mollusca, Tergomya): Vestník Ústøedního ústavu geologického, v. 71, p. 243–247.

———1998, Fossilized intestinal contents in the Lower Ordovician *Cyrtodiscus nitidus* (Mollusca, Tergomya) from the Barrandian Area (Bohemia): Vestník Ústøedního ústavu geologického, v. 73, p. 211–216.

Knight, J.B., 1945, Some new genera of Paleozoic gastropods: Journal of Paleontology, v. 19, p. 573–587.

———1948, The application of opinion 138 to some recently published names: Journal of Paleontology, v. 22, p.107–110.

———1956, New families of Gastropoda: Journal of the Washington Academy of Sciences, v. 46, p. 41–42.

Knight, J.B., Batten, R.L., Cox, L.R., Keen, A.M., Robertson, R., and Yochelson, E.L., 1960, Systematic descriptions [Archaeogastropoda], p. I169–I310, *in* Moore, R.C., ed., Treatise on invertebrate paleontology—Part I, Mollusca 1: Lawrence, Kansas, Geological Society of America and University of Kansas Press.

Koken, E., 1889, Über die Entwickelung der Gastropoden vom Cambrium bis zur Trias: Neues Jahrbuch für Mineralogie, Geologie, und Palaeontologie, Beilageband 6, p. 305–484.

———1896, Die Leitfossilien: C.H. Tarchnitz, Leipzig, 848 p.

Koninck, L.G. de, 1882, Notice sur la famille des Bellerophontidae suivie de la description d'un nouveau genre de cette famille: Annales Societé Géologique de Belgique, v. 9, p. 72–90.

M'Coy, F., 1851, On some new Silurian Mollusca: Annals and Magazine of Natural History, including zoology, botany, and geology, 2nd Series, p. 45–63.

Meek, F.B., and Worthen, A.H., 1866, Descriptions of invertebrates: Illinois Geological Survey, Paleontology, v. 2, 339 p.

Peel, J.S., 1977, Systematics and palaeontology of the Silurian gastropods of the Arisaig group, Nova Scotia: Det Kongelige Danske Videnskabernes Selskab, Biologiske Skrifter, v. 21, 89 p.

———1991a, Functional morphology of the class Helcionelloida nov., and the early evolution of the Mollusca, *in* Simonetta, A., and Conway, M.S., eds., The early evolution of Metazoa and the significance of problematic taxa: Cambridge, England, Cambridge University Press, p. 157–177.

Peel, J.S., 1991b, The classes Tergomya and Helcionelloida, and early molluscan evolution: Bulletin Grønlands Geologiske Undersogelse, v. 161, p. 11–65.

Rohr, D.M., 1988, Upper Ordovician gastropods from the Seward Peninsula, Alaska: Journal of Paleontology, v. 62, p. 551–566.

Rohr, D.M., and Blodgett, R.B., 1985, Upper Ordovician Gastropoda from west-central Alaska: Journal of Paleontology, v. 59, p. 667–673.

Rohr, D.M., and Yochelson, E.L., 1990, An unusual new bellerophontacean gastropod from the Ordovician (Whiterockian) of Nevada: Journal of Paleontology, v. 64, p. 956–960.

Wahlman, G.P., 1992, Middle and Upper Ordovician symmetrical univalved mollusks (Monoplacophora and Bellerophontina) of the Cincinnati Arch region: U.S. Geological Survey Professional Paper 1066-O, p. O1–O203.

Yochelson, E.L., 1967, Quo Vadis, *Bellerophon*? *in* Teichert, K., and Yochelson, E.L., eds., Essays in paleontology and stratigraphy: Kansas, University of Kansas Department of Geology, R.C. Moore Commemorative Volume, Special Publication 2, p. 141–161.

NEW MAPPING NEAR IRON CREEK, TALKEETNA MOUNTAINS, INDICATES PRESENCE OF NIKOLAI GREENSTONE

Jeanine M. Schmidt,[1] Melanie B. Werdon,[2] and Bruce Wardlaw[3]

ABSTRACT

Detailed geologic mapping in the Iron Creek area, Talkeetna Mountains B-5 Quadrangle, has documented several intrusive bodies and rock units not previously recognized and has extended the geologic history of the area through the Mesozoic and into the Tertiary era. Greenschist-facies metabasalt and metagabbro previously thought to be Paleozoic are intruded by Late Cretaceous to Paleocene dioritic to granitic plutons. The metabasalts are massive to amygdaloidal, commonly contain abundant magnetite, and large areas are patchily altered to epidote ± quartz. They host numerous copper oxide–copper sulfide–quartz–hematite veins and amygdule fillings. These lithologic features, recognized in the field, suggested a correlation of the metamafic rocks with the Late Triassic Nikolai Greenstone, which had not previously been mapped in the Iron Creek area. Thin, discontinuous metalimestones that overlie the metabasalt sequence had previously been assigned a Pennsylvanian(?) and Early Permian age on the basis of correlation with marbles to the north, which yielded Late Paleozoic or Permian macrofossils, or both. Three new samples from the metalimestones near Iron Creek yielded Late Triassic conodonts, which confirms the correlation of the underlying metamafic rocks with Nikolai Greenstone. These new data extend the occurrence of Nikolai Greenstone about 70 km southwest of its previously mapped extent.

Five to 10 km north of the conodont sample localities, numerous microgabbro and diabase sills intrude siliceous and locally calcareous metasedimentary rocks of uncertain age. These sills probably represent feeder zones to the Nikolai Greenstone. In the Mt. Hayes quadrangle 150 km to the northeast, large sill-form mafic and ultramafic feeders (for example, the Fish Lake complex) to the Nikolai Greenstone in the Amphitheatre Mountains host magmatic sulfide nickel–copper–platinum-group-element (PGE) mineralization. This new recognition of Nikolai Greenstone and possible magmatic feeders in the Iron Creek area suggests a much greater potential for large PGE, copper, or nickel deposits in the Talkeetna Mountains than previous mineral resource appraisals of the area have suggested, and requires reevaluation of large-scale tectonic models for the area.

INTRODUCTION

The Iron Creek geophysical tract is a kidney-shaped section of the central Talkeetna Mountains, Alaska, and includes parts of seven 15' (1:63,360-scale) quadrangles (fig. 1). An airborne geophysical (aeromagnetic and resistivity) survey of the Iron Creek tract was flown in 1998 under contract to the Alaska Division of Geological & Geophysical Surveys (DGGS Staff, 1998). Geologic field work was carried out by the DGGS and USGS in July 1999 to provide ground truth over one part of the geophysical tract and to allow further evaluation of the mineral potential of the area. This joint state–federal cooperative mapping project concentrated on the eastern part of the Talkeetna Mountains B-5 Quadrangle, including the middle and east forks of Iron Creek (fig. 1). About 100 square miles were mapped at a scale of 1:63,360 during the 15-day project.

Elevations in the Iron Creek area range from 1,000 to 5,700 ft. Lowlands are heavily tree-covered, and cut by steep canyons and braided rivers. Rubble and moderate outcrop occur on the higher plateaus and steep ridgelines. Generally, there is a poor correlation between color, weathering style, and rock type. In particular, it is not possible to discriminate between mafic metavolcanic rocks and intermediate composition plutonic rocks from even a few meters distance, which severely limits field interpolation between stations and across drainages.

During the 1999 mapping, samples were collected for microfossil (conodont) identification and for $^{40}Ar/^{39}Ar$ dating, rock geochemical analyses (major and minor oxide, trace, and rare earth elements), and petrographic studies. The preliminary geologic map of the south-eastern B-5 quadrangle (Werdon and others, 2002) incorporates results from available geochemical analyses (Werdon and others, 2000) and interpretations of the magnetic and resistivity data. $^{40}Ar/^{39}Ar$ dating studies are currently in review (Drake and Layer, 2001).

[1]U.S. Geological Survey, 4200 University Drive, Anchorage, Alaska 99508
Email for Jeanine Schmidt: jschmidt@usgs.gov
[2]Alaska Division of Geological & Geophysical Surveys, 794 University Avenue, Suite 200, Fairbanks, Alaska 99709-3645
[3]U.S. Geological Survey, MS 926A, 12201 Sunrise Valley Dr., Reston, Virginia 20192

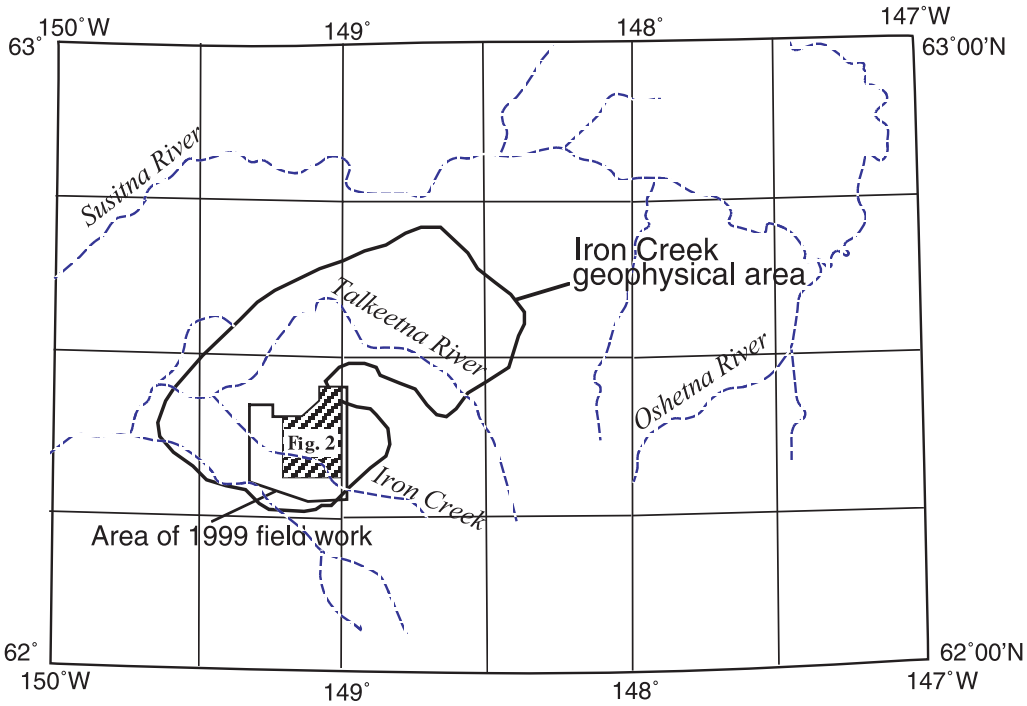

Figure 1. *Index map of the Talkeetna Mountains Quadrangle, Alaska, showing the area mapped in 1999 and the location of figure 2.*

PREVIOUS WORK

Csejtey and others (1978) previously mapped the Iron Creek area at a reconnaissance scale. The area was thought to be predominantly underlain by a 5-km-thick marine volcanic assemblage (Pzv of Csejtey and others, 1978) of Pennsylvanian(?) and Early Permian age. This assemblage was described as comprising basaltic to andesitic flows and tuffs, with subordinate mafic volcaniclastic rocks, mudstone, and phyllite. The assemblage was interpreted to have been regionally metamorphosed to greenschist or lower facies and complexly deformed during Jurassic or Cretaceous time or both (Csejtey and others, 1978). Minor thin, locally bioclastic, limestone and marble lenses were differentiated from the volcanic sequence (unit Pls of Csejtey and others, 1978). The age of the Pzv (volcanic) unit was interpreted to be similar to, and possibly older than, that of the limestones, which contain Late Paleozoic or Early Permian macrofossils or both (brachiopods and crinoid columnals) 30 to 75 km north of the Iron Creek map area.

Regionally, the Pzv unit was interpreted (Csejtey and others, 1978) as a marine volcanic arc that unconformably underlies Triassic Nikolai Greenstone within the Wrangellia terrane in the Talkeetna Mountains. In this interpretation, the Pzv unit would be correlative to the Skolai volcanic arc (Tetelna Volcanics and Station Creek Formation), which underlies the Late Triassic Nikolai Greenstone type section in the Wrangell Mountains 400 km to the east (Nokleberg and others, 1994). Chalcopyrite- and hematite-bearing copper prospects hosted by the Pzv unit within the Iron Creek area have previously been interpreted as porphyry copper, volcanic-hosted copper, and (or) polymetallic vein deposits (Riehle, 1998).

On the eastern boundary of the Iron Creek geophysical tract, Csejtey and others (1978) mapped undifferentiated Jurassic plutonic and metamorphic rocks and minor Tertiary volcanic rocks. Several small plutons of granodioritic, granitic, and tonalitic composition mapped throughout the Iron Creek map area were interpreted to be of Tertiary or Cretaceous age (Csejtey and others, 1978).

DESCRIPTION OF MAP UNITS

Geologic mapping around Iron Creek (Talkeetna Mountains B-5 Quadrangle) in 1999 (fig. 2) identified a wide range of intrusive, volcanic, and sedimentary rock types within the area previously mapped as Pzv (Csejtey and others, 1978). Two types of metamafic rocks underlie about 50 percent of the area. The first group consists of magnetite-rich, epidote-bearing amygdaloidal basalt and microgabbro and rare volcanic breccias. Epidote-altered rocks commonly host small hematite–chalcopyrite–bornite–pyrite occurrences. These rocks bear a strong physical resemblance to the Late Triassic Nikolai Greenstone, whose type section is mapped in the Wrangell Mountains about 400 km southeast of the Iron Creek

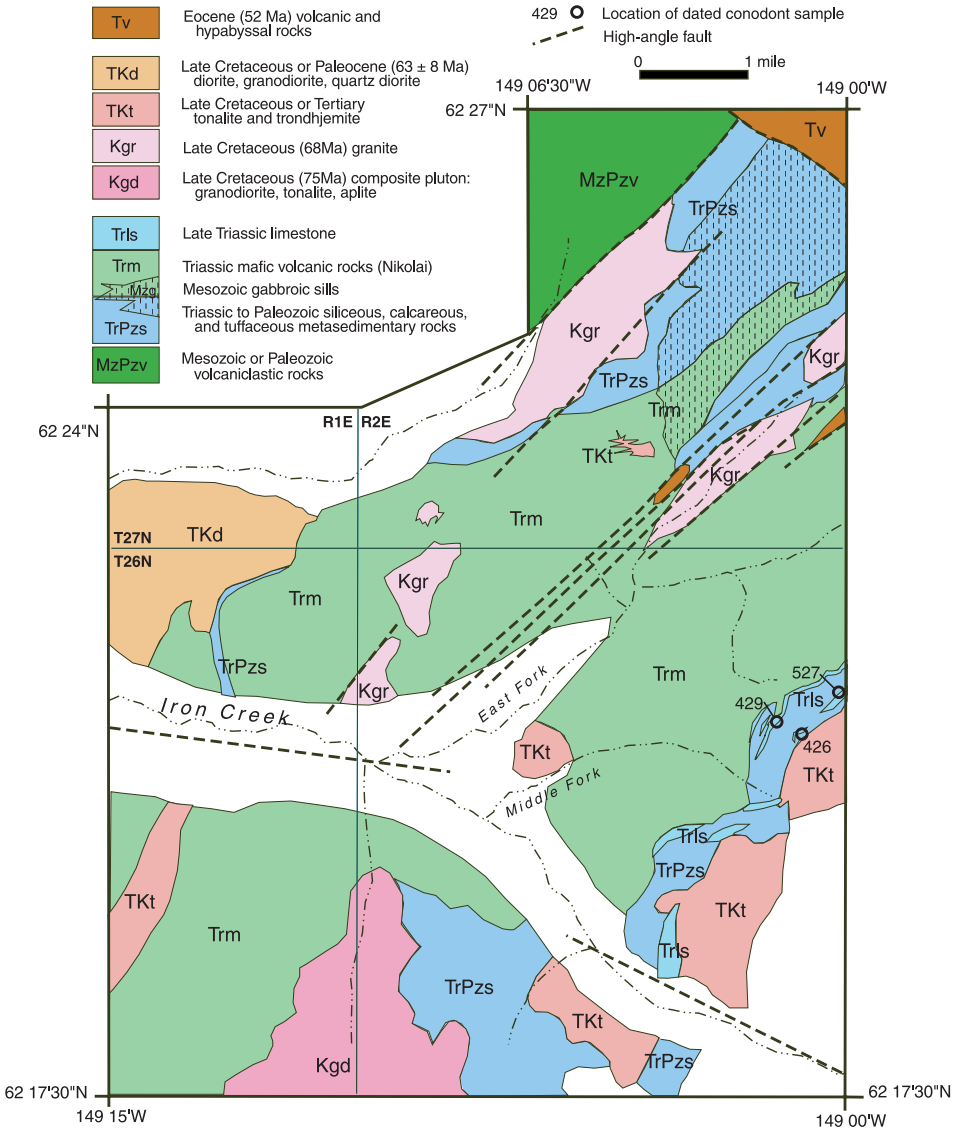

Figure 2. *Simplified geologic map of the northeastern part of the Iron Creek map area (modified from Werdon and others, 2002). Numbers 426, 429 and 527 are the locations of samples 99MBW426, 99MBW429 and 99MBW527, respectively, which yielded identifiable conodonts.*

study area. A thick sequence of Nikolai Greenstone is also present in the southern Alaska Range, 180 km northeast of Iron Creek. The second type of metamafic rocks that occurs in the B-5 map area is massive, usually nonmagnetic, aphanitic metabasalt and microcrystalline greenstone. Both types of mafic rocks are metamorphosed to lower greenschist facies and contain epidote, chlorite, actinolite, clinozoisite, pumpellyite, calcite, relict clinopyroxene and plagioclase, and minor quartz, albite, and opaques. The most common relict texture is subophitic, but porphyritic and glomeroporphyritic textures are also present. Because these two types of metamafic rocks are intercalated on a small scale and have similar compositions and mineralogy, they have been mapped as a single mafic unit (Trm; fig. 2).

Metasedimentary rocks (TrPzs; fig. 2) compose about 25 percent of the area previously mapped as Pzv (Csejtey and others, 1978) and occur in two main areas of the B-5 map (fig. 2). All units mapped as TrPzs include metalimestones, which are too thin and discontinuous to differentiate at this scale. Some parts of the TrPzs unit were indicated as lenses of Pls on the Csejtey and others (1978) map. In the northern part of the B-5 map area, siliceous metasiltstone is the dominant lithology. It is interbedded with minor metalimestone and possible chert. These bedded rocks are near vertical, and intruded

by numerous fine-grained, equigranular diabase and microgabbro sills and dikes (Mzg; fig. 2) of probable Triassic age. In the southern and eastern map area, the metasedimentary rocks (TrPzs) include metalimestone, chloritic and graphitic phyllite, and banded calcsilicate-bearing light gray-green rocks interpreted as metatuffs. Steep dips and isoclinal folds in the southern metasedimentary rocks indicate that they have been deformed, but no crosscutting gabbros have been recognized.

Plutonic rocks compose the remaining 25 percent of the B-5 map area previously interpreted as Pzv (Csejtey and others, 1978). Roof pendants are common within the intrusions and several plutons are unroofed only in cirque valleys whose walls and ridgelines are composed entirely of metamafic and metasedimentary rocks. Several distinct ages and compositions of plutons have been identified. A large composite pluton of biotite- and hornblende-bearing granodiorite, quartz diorite, tonalite, and diorite (Kgd; fig. 2) south of Iron Creek has yielded an $^{40}Ar/^{39}Ar$ hornblende age of 75.5 ± 0.6 Ma (Drake and Layer, 2001). Quartz-rich biotite granite intrusions (Kgr; fig. 2) elongate along and bounded by northeast-trending high-angle faults are latest Cretaceous (68.5 ± 0.6 Ma) (K-feldspar $^{40}Ar/^{39}Ar$ age; Drake and Layer, 2001). A large intrusive body (Tkd; fig. 2) in the western part of the map area is composed of separate diorite, granodiorite, and quartz diorite phases. Coarse hornblendite associated with the diorite yielded a poorly constrained (63.0 ± 8.4 Ma; Drake and Layer, 2001) age near the Cretaceous–Paleocene boundary. Biotite–granodiorite immediately west of the area shown in figure 2 is earliest Paleocene (57.7 ± 0.05 Ma) in age (hornblende $^{40}Ar/^{39}Ar$ date; Drake and Layer, 2001). A trondhjemite(?) sill and several tonalite and trondhjemite intrusions (TKt; fig. 2) in the southern part of the map area are undated but assumed to be Late Cretaceous or early Tertiary.

Rare Eocene rhyodacitic and basaltic dikes along northeast-trending high-angle faults are coeval (52.1 Ma; Drake and Layer, 2001) with mafic flows mapped by Csejtey and others (1978) capping ridges in the northern Iron Creek map area (Tv; fig. 2). These volcanic and hypabyssal rocks are part of a prominent northwest-trending Eocene magmatic field that crosscuts the predominant northeasterly lithologic and structural grain of the region.

The wide variety of plutonic types present in this small map area and their distinct ages are not predicted by simple models of subduction along the southern Alaska margin. Additional mapping and radiometric dating are required to understand the tectonic framework of this area and the complex relationship between magmatism and the formation of northeast-trending structures during a transition to Eocene extensional volcanism.

LIMESTONES AND CONODONTS

All metalimestones mapped in the Iron Creek map area are similar in color, lithology, and grain size and differ mainly in their associated interbeds. Along the eastern border of the mapped area, several thin limestone beds (Trls; fig. 2) overlie the metamafic rocks (fig. 3A) with apparent conformity. These limestones are platy weathering (fig. 3B), with millimeter- to centimeter-scale partings, and are rarely color laminated. Individual beds are a few meters to tens of meters thick. Rare collapse(?) breccia textures occur, but other sedimentary structures are notably absent. The metalimestones are recrystallized, finely granular (=2mm), and light colored (pale to medium gray or buff). None are fetid. They contain minor organic matter, trace pyrite, and rare calc-silicate minerals (tremolite and epidote). They are interbedded to the east (stratigraphically upward?) with phyllite, chloritic phyllite, gray quartz–mica schist, and metatuff (unit TrPzs) of uncertain age and origin.

South of Iron Creek, bedded rocks of the TrPzs unit occur as kilometer-sized roof and wall pendants around Cretaceous and Tertiary plutons. Lenses of light-gray metalimestone tens of meters thick are intercalated with banded calc-silicate-bearing metatuffs(?) and with bright orange-weathering dark-gray to black phyllite of unknown age. In the northeastern part of the map area, platy-weathering, light-gray metalimestones form a very minor part of the TrPzs unit, which is composed mainly of fine-grained siliceous metasedimentary rocks (metasiltstones?; fig. 3C). The metalimestones in this area are generally fine grained; a few retain a rough weathering surface preserving outlines of crinoid and coral fossil debris (fig. 3D). The metasedimentary rocks (TrPzs) in this northern area are presumed to be mainly pre-Triassic because they are intruded by numerous gabbroic sills and dikes of similar composition to the metabasalts.

Eleven limestones from all exposures of the TrPzs metasedimentary rock unit at Iron Creek were sampled for conodonts. Four of these samples were lost in the mail; and four were barren. The three samples that yielded conodonts (table 1) are all from the eastern exposure of TrPzs, where limestones and associated metasedimentary rocks overlie the metamafic sequence in apparent conformity.

Conodonts from all three limestones are Late Triassic (table 1), with an age range of late Carnian to Norian. Because these limestones lie directly above the metamafic sequence, they provide an upper age limit for the mafic rocks. The type section of the Nikolai Greenstone is Ladinian (late Middle Triassic) to Carnian (early Late Triassic) (Nokleberg and others, 1994), on the basis of the occurrence of fossiliferous units both below and above it. Thus, the metamafic rocks in the Iron Creek

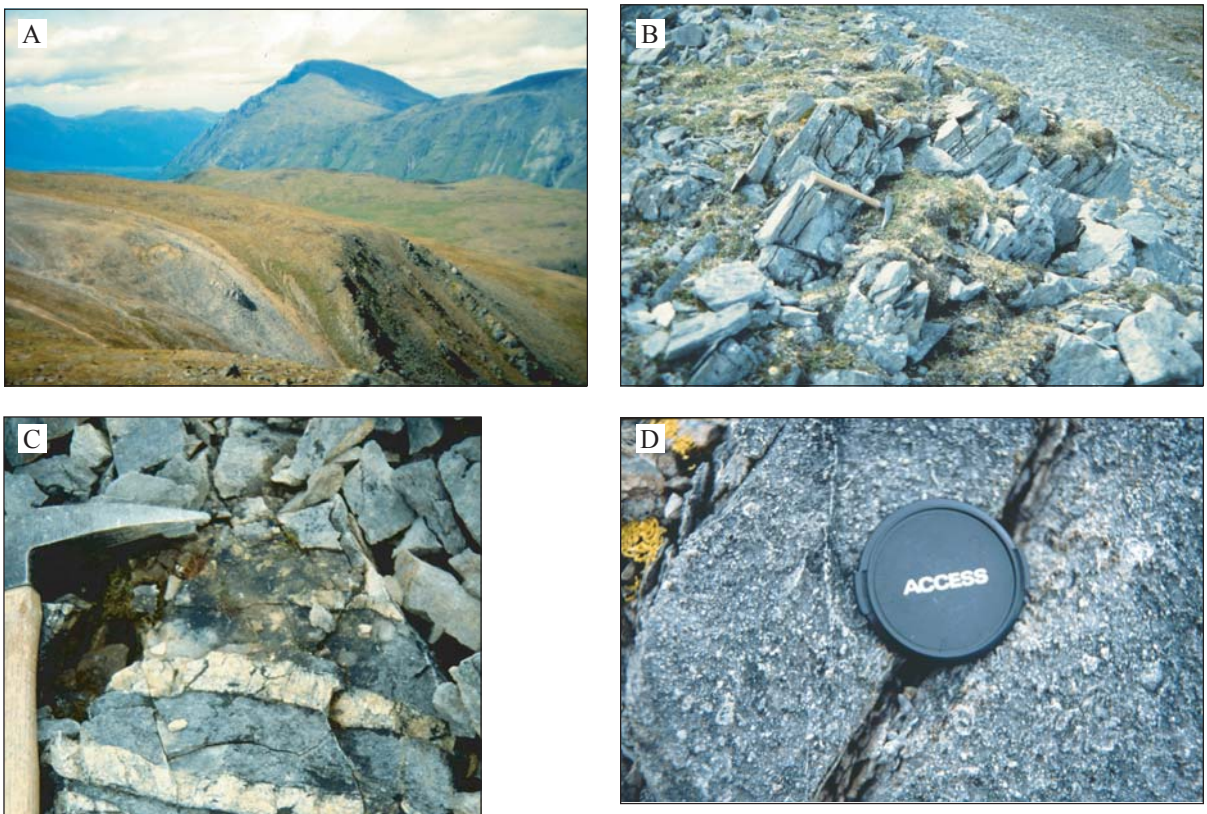

Figure 3. *Photographs of metalimestones from the Talkeetna Mountains B-5 Quadrangle. (A) View westward toward the East Fork of Iron Creek, showing outcrop of Triassic metalimestone (Trls) in mid-ground, overlying dark-weathering mafic metavolcanic rock (Trm). (B) Platy weathering light-gray metalimestone. This unit is the one sampled at location 99MBW426.(C) Bedded metalimestone and fine-grained siliceous metasediments (metasiltstone) from the northern part of the map area. These metasedimentary rocks are crosscut by abundant gabbroic sills and are probably pre-Triassic.(D) Rough weathering surface of metalimestone containing relict fossil debris, from within the dominantly siliceous metasedimentary unit .*

area are correlative in age as well as being mineralogically and lithologically similar to the Nikolai Greenstone.

The very high CAIs (6–8) of these conodonts may result from their proximity to a large number of Cretaceous to early Tertiary plutons. The apparent high temperatures reached (360°C–800°C; Rejebian and others, 1987) and poor development of foliation in most of the metasedimentary rocks suggest a relatively high temperature, short-lived, static (contact or hornfels) metamorphism, such as that within a plutonic aureole.

DISCUSSION

Detailed geologic mapping in the Iron Creek area, Talkeetna Mountains B-5 Quadrangle, has documented several intrusive bodies and rock units not previously recognized and has extended the geologic history of the area through the Mesozoic and into the Tertiary era.

Metasedimentary rocks in the southern Iron Creek area include thin upper Carnian to Norian metalimestone beds that occur above a sequence of greenschist-facies metabasalt and metagabbro. The basalts, which are

Table 1. *Samples collected for conodont identification from the Iron Creek area, Talkeetna Mountains B-5 Quadrangle, Alaska*

Sample No.	Location	Sample Lithology	Unit Description	CAI[a]	Conodont Fauna	Age
99MBW426	62° 21.10' N 149°1.38' W T26N R2E Sec. 11 Elev. 5000'	Mottled light gray–tan platy weathering imestone; some brecciated. Sparse (<0.5%) disseminated py-rite to 1 mm. Limestone is finely crystalline (=40µ), with ovoids (to 1.4 mm) of partially recrystallized do-lomite(?). Minor stylolites.	1.5 m-wide-zone of rubble between fractured, fine grained metagabbro to the east, and a fissile, variably iron-stained gray tuff(?) to the west.	8	*Epigondolella bidentata* (Mosher, 1968). 7 Pa elements *Metapolygnathus* sp. one Pa element	Late Triassic, middle Norian (*bidentata* and *andrusovi* zones)
99MBW429	62° 21.16' N 149°1.54' W T26N R2E Sec. 11 Elev. 4950'	Pale-gray fissile limestone with 1–6 mm bedding. Micrite (~20µ) contains trace quartz, opaques, and calcite veinlets.	5- to 10-m-wide zone of limestone rubble in sharp contact with dark-green, very fine grained gabbro(?) to east, and foliated, medium green metabasalt to west.	6-7	*Metapolygnathus nodosus* (Hayashi). 28 complete to broken Pa elements. Fragments: 34	Late Triassic, late Carnian to earliest Norian (*nodosus* to earliest *spatulata* zones)
99MBW527A	62° 21.43' N 149°0.29' W T26N R2E Sec. 12 Elev. 4950'	Pale-gray to tan mottled to thinly color-banded lime-stone; micrite with sparse grains to 2 mm; contains trace quartz (<2%), white mica (<2%), opaques (<1%), minor calcite vein-lets and poorly developed stylolites.	>60-m-thick unit in sharp conformable contact over dark-green chlorite phyllite; locally internally folded.	7-8	*Epigondolella* sp. 6 Pa element juveniles and fragments with affinities to the *E. abneptis, E. postera* and *E. bidentata* lineage. *Metapolygnathus* sp. 2 Pa element fragments. Indeterminate fragments: 14	Late Triassic, Norian
99ARj030	62°20'10"N 149°03'45"W T26N R23 Sec. 22 Elev. 4900'	Thinly laminated gray lime-stone with silty partings.	Interlayered with minor tuffaceous siltstone.		Two poorly preserved ichthyolith fragments.	
99ARj061	62°20'20"N 149°01'44" T26N R2E Sec. 14 Elev. 3200'	Thinly laminated, alterna-ting dark-gray and pale-yellow limestone.	Steeply bedded, interlayered with phyllite.		Barren	
99MBW531	62°21'35"N 149°00'31"W T26N R2E Sec. 12 Elev. 4500'	Pale tan and gray, blocky weathering, mottled pale gray and tan micritic limestone. Orange-tan bands may contain minor dolomite.	In conformable(?) contact with siliceous, pyritic metavolcanic(?) rock to SE. Uncertain contact with chloritic phyllite to NW.		Barren	
99MBW541	62°22'11"N 149°12'56"W T26N R1E Sec. 2 Elev. 4550'	Pale gray to white blocky weathering; white, medium grained (1-3mm) crystal-line limestone.	In uncertain contact with fine-grained hornblendite/ greenstone to west.		Barren	

[a]Color alteration index

commonly amygdaloidal and often magnetic and epidote altered, strongly resemble the Middle to Late Triassic (Ladinian to Carnian) Nikolai Greenstone whose type section is in the Wrangell Mountains, about 400 km to the east. Our new conodont ages support this correlation, and extend the occurrence of Nikolai Greenstone about 70 km southwest of its previously mapped extent. Ongoing mapping by the USGS along a transect to the northeast (Schmidt and Riehle, 2000) suggests that a near-continuous belt of Nikolai Greenstone exists between the Iron Creek area and exposures previously mapped in the Mt. Hayes Quadrangle. The extent of the Nikolai Greenstone southwestward from Iron Creek is unknown, but there may be significant amounts of it within the belt of rocks previously mapped as Paleozoic arc volcanics (Pzv).

The presence of Nikolai Greenstone in the Talkeetna Mountains is significant for both tectonic and metallogenic reasons. Late Triassic basalts of the Karmutsen Formation on Vancouver Island, which are correlative to the Nikolai, have been interpreted to be derived either by initiation of a mantle plume (Richards and others, 1991) or within a back-arc rift setting (Barker and others, 1989) on older oceanic crust. In the Talkeetna Mountains, the recently recognized Nikolai Greenstone has no apparent association with an older or age-equivalent volcanic arc, and may provide evidence to discriminate between alternative tectonic hypotheses.

Nikolai Greenstone in the Iron Creek area hosts numerous occurrences of copper oxides, copper sulfides, and hematite as veins, pods, and amygdule fillings, generally associated with epidote alteration within the magnetite-bearing amygdaloidal basalts. These occurrences indicate some potential for basaltic-hosted copper deposits within the Nikolai Greenstone itself. Five to 10 km north of the conodont sample localities, siliceous metasedimentary and some metamafic rocks are intruded by numerous gabbroic sills, which may represent magmatic feeders to the Nikolai volcanic rocks. This setting, of mafic magmatic chambers below an active flood basalt province, is a likely target for magmatic nickel–copper and platinum-group-element (PGE) sulfide deposits. Sill-form ultramafic intrusions beneath Nikolai Greenstone in the Mt. Hayes Quadrangle 150 km northeast of Iron Creek host PGE mineralization of this type, and the setting mirrors that of world class nickel–copper–PGE deposits in the Norils'k district associated with the Siberian-traps flood basalts (Hulbert, 1997).

The recognition of Nikolai Greenstone and possible magmatic feeders in the Iron Creek area suggests a much greater probability of large, undiscovered copper, nickel, or PGE deposits in southcentral Alaska than previous mineral resource appraisals of the area have suggested, and may require reevaluation of large-scale tectonic models as well.

ACKNOWLEDGMENTS

Jim Riehle (USGS, retired), Rainer Newberry (University of Alaska Fairbanks), and Gar Pessel (DGGS, retired) were integral members of the field party that produced the Talkeetna Mountains B-5 map, and their geologic discussions contributed greatly to the recognition of the Nikolai Greenstone in this area. We thank Gary Brogdon of Maritime Helicopters for his excellent piloting skills and enthusiasm for rainy weather. Julie Dumoulin and Marti Miller reviewed earlier versions of the manuscript and contributed greatly to its clarity.

REFERENCES

Barker, F., Sutherland Brown, A., Budahn, J.R., and Plafker, George, 1989, Back-arc with frontal-arc component origin of Triassic Karmutsen basalt, British Columbia, Canada: Chemical Geology, v. 75, p. 81–102.

Csejtey, Bela, Jr., Nelson, W.H., Jones, D.L., Silberling, N.J., Dean, R.M., Morris, M.S., Lanphere, M.A., Smith, J.G., and Silberman, J.L., 1978, Reconnaissance geologic map and geochronology, Talkeetna Mountains quadrangle, northern part of Anchorage quadrangle, and southwest corner of Healy quadrangle, Alaska: U.S. Geological Survey Open-File Report 78-558-A, scale 1:250,000, 1 sheet, 62 p.

DGGS Staff, 1998, CD-ROM containing profile and gridded data and section lines of 1997 geophysical survey data for Iron Creek area, Talkeetna Mountains Quadrangle, southcentral Alaska: Alaska Division of Geological & Geophysical Surveys Public-Data File 98-9, 1 CD-ROM.

Drake, Jeff, and Layer, Paul, 2001, $^{40}Ar/^{39}Ar$ analyses from the Iron Creek area, Talkeetna Mountains Quadrangle, Alaska: Alaska Division of Geological & Geophysical Surveys Raw Data File 2001-3, 12 p.

Hulbert, L.J., 1997, Geology and metallogeny of the Kluane mafic–ultramafic belt, Yukon Territory, Canada: eastern Wrangellia – a new Ni-Cu-PGE metallogenic terrane: Geological Survey of Canada Bulletin 506, 265 p.

Mosher, L.C., 1968, Triassic conodonts from western North America and Europe and their correlation: Journal of Paleontology, v. 42, no. 4, p. 895–946.

Nokleberg, W.J., Plafker, George, and Wilson, F.H., 1994, Geology of south-central Alaska, Chapter 10, *in* Plafker, George, and Berg, H.C., eds., The Geology of Alaska: Boulder, Colorado, Geological Society of

America, The Geology of North America, v. G-1, p. 311–366.

Rejebian, V.A., Harris, A.G., and Huebner, S.J., 1987, Conodont color and textural alteration: An index to regional metamorphism, contact metamorphism and hydrothermal alteration: Geological Society of America Bulletin, v. 99, p. 471–479.

Richards, M.A., Jones, D.L., Duncan, R.A., and DePaolo, D.J., 1991, A mantle plume initiation model for the Wrangellia flood basalt and other oceanic plateaus: Science, v. 254, p. 263–267.

Riehle, J.R., 1998, Talkeetna Mountains quadrangle Alaska resource data file: U.S. Geological Survey Open-File Report 98-473, 173 p.

Schmidt, J.M., and Riehle, J.R., 2000, What's new in the northern Talkeetna Mountains: an investigation of the docking of Wrangellia [abs]: Alaska Geological Society and Geophysical Society of Alaska 2000 Science and Technology Program with Abstracts, April 13, 2000, Anchorage Alaska, p. 21.

Werdon, M.B., Riehle, J.R., Schmidt, J.M., Newberry, R.J., and Pessel, G.H., 2000, Major oxide, minor oxide, trace element, and geochemical data from rocks collected in the Iron Creek area, Talkeetna Mountains B-5 Quadrangle, Alaska in 1999: Alaska Division of Geological & Geophysical Surveys Raw Data File 2000-2, 31 p., 2 sheets, scale 1:63,360.

———2002, Geologic map of the Iron Creek area, Talkeetna Mountains B-5 Quadrangle, Alaska: Alaska Division of Geological & Geophysical Surveys Preliminary Interpretive Report 2002-4, 1 sheet, scale 1:63,360.

NEW PALEONTOLOGICAL INVESTIGATIONS OF TRIASSIC CARBONATE ROCKS IN THE UPPER CHULITNA DISTRICT (CHULITNA TERRANE), SOUTHCENTRAL ALASKA

George D. Stanley, Jr.[1] and Jeannette M. Yarnell[2]

ABSTRACT

A field visit and paleontological study of an unnamed Upper Triassic carbonate rock unit in the Upper Chulitna district (Chulitna terrane), southcentral Alaska, have revealed previously unknown fossil corals, spongiomorphs, chaetetid sponges, and other shallow-water, tropical invertebrate assemblages. These occur within part of a thicker interval of interbedded limestone and pillow basalts of the Chulitna terrane. The limestone contains abundant scleractinian corals, rarer spongiomorph hydrozoans, abundant chaetetid sponges, and a variety of other invertebrate shelly biotas. These fossils occur in a 15- to 20-m-thick interval of pure to impure bedded limestone exposed along Long Creek. Although the sequence has some reefal characteristics, it is much thinner and, because of its bedded characteristics, lack of mound-like characteristics, and locally extensive coral and sponge framework, we interpret it as a biostromal deposit. Large laminar to domate chaetetid sponges are important in producing reefal thickenings in the upper parts of the carbonate interval. Six taxa of corals and a new species of large chaetetid sponge have been identified from the carbonate interval. The corals are conspecific with Norian–Rhaetian taxa from the Northern Limestone Alps in central Europe and other regions of the former western Tethys. In addition to a variety of brachiopods, molluscs, and echinoderms, we also report the occurrence of large alatoform bivalves belonging to the recently designated family Wallowaconchidae. The corals and wallowaconchid bivalve can be compared with coeval biotas known from other American terranes, including the Luning Allochthon of Nevada; the Antimonio terrane of Sonora, Mexico; and the Wallowa, Stikine, and Quesnel terranes. Statistical analysis of the faunal composition of the corals occurring in these terranes appears useful, not only for helping to reconstruct the Late Triassic biogeography, but also in testing some ideas about the Chulitna terrane and its tectonic relationship with other terranes of the Cordilleran region.

INTRODUCTION

Upper Triassic reef and reef-related carbonate deposits are widespread and becoming well known in the American Cordillera, where they occur within island-arc settings of many terranes. Most of these Late Triassic deposits are Norian, which appears to have been a 'turn-on' time for widespread deposition of reefs and carbonates in both the Cordilleran region and the Tethys. This phenomenon appears connected with widespread sea-level rise coupled with a warming trend during the Norian (Flügel, 1994). The Late Triassic carbonate deposits contain abundant and diverse marine invertebrates including thalamid sponges, scleractinian corals, spongiomorphs, molluscs, and calcareous algae. Stanley (1996) summarized past paleontological studies and problems of the early Mesozoic North American Cordillera. To date, Triassic sites of reef faunas have been identified from ten different North American terranes (fig. 1). Inboard terranes such as the western Great Basin of Nevada; the Antimonio terrane of Sonora, Mexico; Quesnellia; and Stikinia have yielded distinctive, chambered thalamid sponges. Norian carbonates from other terranes such as the Antimonio, Wallowa, and Stikinia (Reid, 1985) have also yielded an equally distinctive fauna of large alatoform bivalves known as wallowaconchids (Yancey and Stanley, 1999). These faunas differ from those of more outboard terranes such as Wrangellia. Yarnell (2000) concentrated on a description and paleogeographic interpretation of Upper Triassic (Norian) corals, spongiomorphs, and giant alatoform bivalves from the Whitehorse Trough (Lewes River Group), Yukon, and the Upper Chulitna district, Alaska.

The diverse, shallow-water faunas characterizing these early Mesozoic reefs and carbonate buildups have tropical origins, and correct paleontological identification appears especially useful for paleogeo-graphic analyses. A major thrust of geologic studies among Cordilleran terranes has addressed the tectonic evolution and attempted to resolve the ambiguities of their tectonostratigraphic settings, particularly the timing and history of accretion and subsequent displacement of terranes along the Pacific margin during Permian to Jurassic time. As apparent with the tropical reef and reef-related Triassic sites (fig. 1), the faunas show great

[1]Department of Geology, The University of Montana, Missoula, Montana 59812
Email for George D. Stanley: fossil@selway.umt.edu
[2]SLR Alaska, 2525 Blueberry Road, Suite 206, Anchorage, Alaska 99503

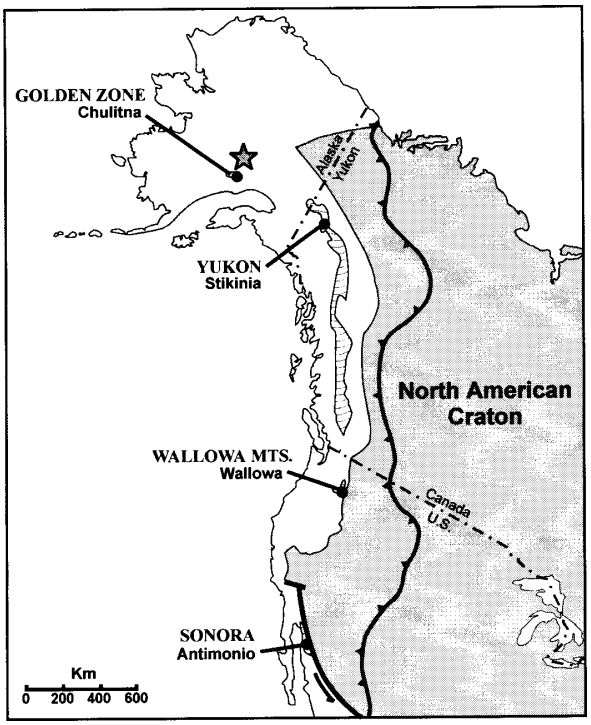

Figure 1. *North American terrane map showing the Chulitna terrane and some other terranes discussed in the text. Large shaded area is Stikinia.*

latitudinal breadth in terms of present-day geography. Together, ranging from southcentral Alaska to Mexico, they present a particularly wide latitudinal range, most likely not reflective of their original tropical distributions. Many of these ambiguities are explained by post-early Mesozoic tectonic displacements, which characterize much of the western Cordillera.

Among the numerous tectonostratigraphic terranes of Alaska and the North American Cordillera, the Chulitna terrane (fig. 1) stands out. It is distinguished by both its small size (about 400 square km), and its unique stratigraphic characteristics, which include rare Early Triassic limestone (Nichols and Silberling, 1979), interbedded Upper Triassic limestone and pillow basalts, and tuffs associated with unique marine redbeds (Hawley and Clark, 1974; Jones and others, 1980; Whalen and others, 1999). Some of the ammonoid faunas have been reported and described, but relatively little is known about the Upper Triassic shallow-water faunas.

The paleontological collections come from two different localities in the Upper Chulitna district: (a) along the region of Little Shotgun Creek and adjacent areas to the southern part of the map area, and (b) along the upper drainage of Long Creek, located farther north (fig. 2). The Upper Chulitna region lies along the south flank of the central Alaska Range, in southcentral Alaska, just outside the southeast boundary of Denali National Park and about 225 km north of Anchorage. The area is obstructed by the Chulitna River and access is best made by helicopter from the Colorado Station on the Alaska Railroad. The limestone outcrops of the Long Creek locality lie within, and a few meters northwest of, the stream cut of Long Creek, which is about 2 km west of the Golden Zone Mine camp (fig. 2).

At Long Creek, the Upper Triassic carbonate interval is part of a unit of limestone and basalt found within the larger stratigraphic sequence now recognized in the Upper Chulitna district (fig. 3).

Paleontological investigation of the Chulitna terrane occurred at two different localities in the Upper Chulitna region of Alaska: Long Creek (1997 collections of Schlichtholz and Blodgett; 1998 collections of Stanley and Yarnell) and from Shotgun Creek and adjacent areas (1997 collections of Blodgett, Schlichtholz, and Clautice). The fossil corals were the subject of a graduate thesis in paleontology (Yarnell, 2000).

The Shotgun Creek locality contains massive beds of Upper Triassic limestone that form ridges located almost 20 km southwest from the Golden Zone Mine camp (fig. 2).

THE LONG CREEK LOCALITY

Along the upper reaches of Long Creek, there is fairly continuous exposure of limestone along the creek bed (fig. 4) and some isolated exposures along the sides of the drainage. Interest in the site was produced by fossil collections referred to us by Karen H. Clautice, Sarah Schlichtholz, and Robert Blodgett (field nos. 97RB187; 97RB188=97SS2). An invitation to the present authors to visit the site at Long Creek (June 28–30, 1998) allowed us the opportunity to collect additional fossils and to complete a measured section along Long Creek (fig. 5). These fossils became the subject of further investigation by Yarnell as part of a graduate thesis at the University of Montana. All fossils are curated in the University of Montana Paleontology Collections, where each specimen was designated an UMIP number. The fossils were collected at two sites in the Healy A-6 Quadrangle, 63°11'–12' N lat., 149°41'–42' W long.; along the north side of Long Creek (NE¼ NW¼ sec. 8,T20S, R11W) and from beds along the opposite side of the creek.

The site at Long Creek along the creek bed (fig. 4), is located at 3,700 to 3,750 ft elevation and presents an excellent exposure of bedded biostromal limestone, rich in dendroid–phaceloid scleractinian corals (fig. 6). The upper part of the exposure contains an abundance of large, laminar to domate colonies of massive chaetetid sponges in thin-bedded pure to slightly impure limestone. Beds are 10 to 50 cm thick with regular argillaceous partings. Bafflestone to framestone textures (mostly

bioclastic), produced by the abundant reefal organisms, predominate. Beds are steeply dipping, 85°–90°, and strike N15°E but dip and strike change along the section because of the presence of several thrust faults and at least two volcanic dikes or sills (fig. 5).

A detailed section measured along the creek bed (fig. 5) reveals at least three distinct lithofacies. These yield three general carbonate lithologies: (a) an upper interval of light-colored, bioclastic impure limestone (packstone and micrite), with abundant calcite veins, and rich in corals and molluscs, including alatoform wallowaconchid bivalves; (b) a darker, impure bedded limestone interval rich in corals, including a framestone characterized by some large, in-place thickets of phaceloid–dendroid coral colonies (fig. 6); and (c) an upper interval of purer, more massive limestone composed predominantly of large colonies of chaetetid sponges.

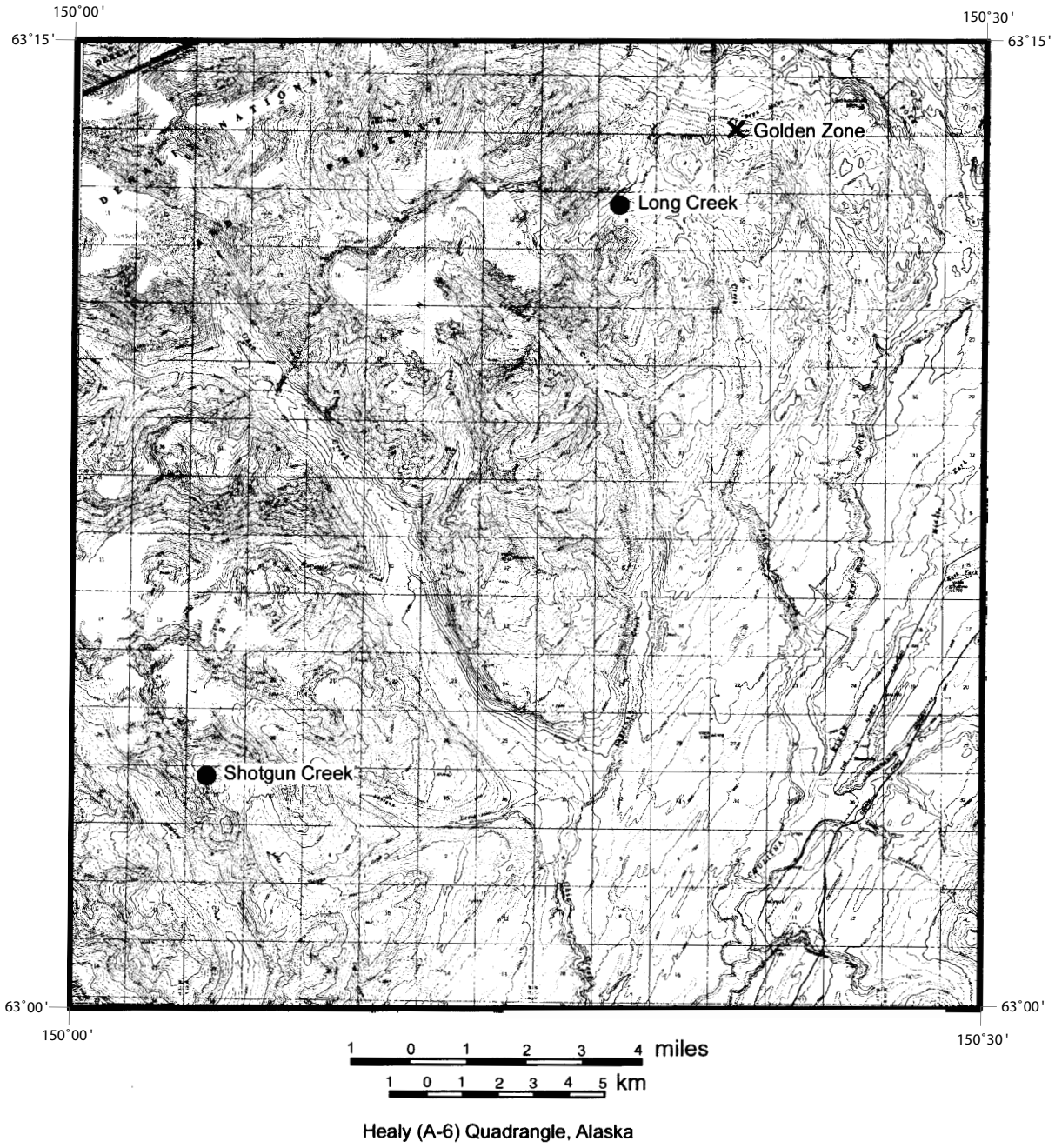

Figure 2. *Locality map (geologic) of the region showing both Long Creek and Shotgun Creek.*

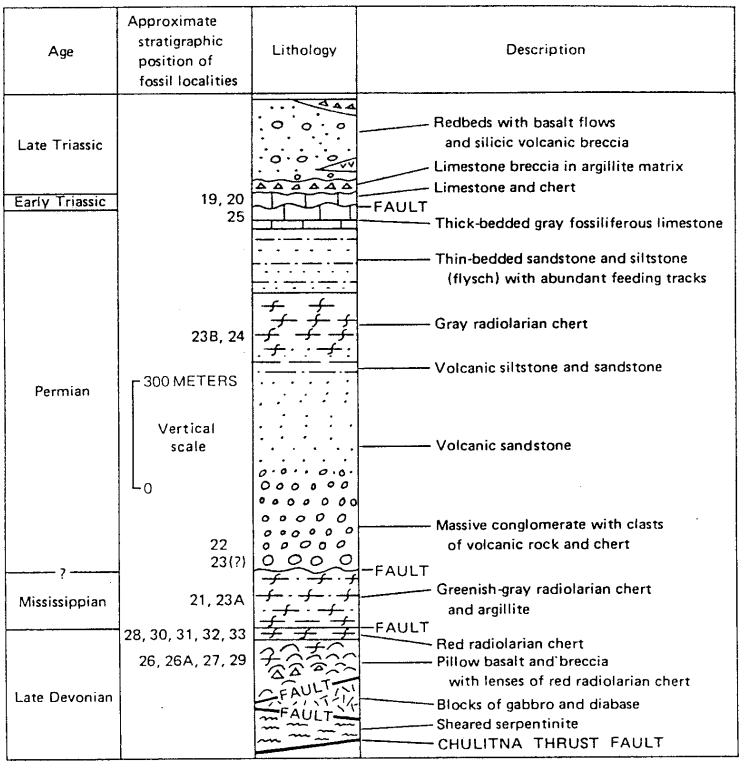

Figure 3. *General stratigraphy of the mid-Paleozoic to Triassic unnamed units of the Chulitna terrane (from Jones and others, 1980). Fossils discussed come from the Triassic redbeds and basalt flows (upper part).*

Collections made in 1998 were complemented by those made the previous year. A full report on the systematic positions of the corals currently is in preparation by the authors. In addition to corals and spongiomorphs, spiriferid and terebratulid brachiopod specimens were collected and are currently under study by Michael Sandy (University of Dayton) (Stefanoff and Sandy, 1999). They include *Spondylospira lewesensis,* a taxon typical of Norian strata throughout the Cordilleran region of both North and South America. Also present are alatoform bivalves belonging to the family Wallowaconchidae. Included among the fauna are indeterminate bivalves and gastropods, echinoid tests and spines, and crinoid ossicles.

The limestone interval is dated by the discovery of conodonts in strata nearby on the eastern side of the creek, at the base of the cliff (locality 97RB152). The latter area yielded the conodont *Epigondolella bidentata*, a taxon characterizing the Bidentata zone of uppermost Norian (roughly equivalent to the Cordilleranus ammonoid zone). This date is compatible with the taxa of sponges, corals, and spongiomorphs.

Rather than a bioherm (reef), we interpret the deposit exposed at Long Creek as a biostrome composed of bioclastic debris, in-place coral thickets, and large chaetetid colonies. Although some large phaceloid–dendroid coral colonies occur (fig. 6), they do not form extensive framework and much of the coral limestone is bioclastic, being composed of reworked or broken fragments. Unlike a reef, all the strata are bedded and the limestone is impure. The darker carbonate rocks have a petroliferous odor and locally contain iron pyrite, some of which fills small excavated cavities within the corals. The most reeflike aspect of the carbonate interval is in the upper part (fig. 5), which is dominated by abundant, large chaetetid sponges. These individual sponge colonies reach several meters in diameter and through massive laminar to hemispherical growth, locally are important builders of the limestone.

OTHER CHULITNA FOSSIL SITES

On the basis of fossils referred to us, other Upper Triassic (Norian) sites in the Upper Chulitna district have yielded the distinctive spherical hydrozoan, *Heterastridium conglobatum* (fig. 7). This taxon most likely followed a planktonic ecology and attained a paleogeographic distribution that is nearly global with respect to marine environments. It occurs throughout the Eurasian Tethys and in many of the Cordilleran terranes, including central Alaska, the Canadian Cordillera, and as far south as Sonora, Mexico (Stanley and Senowbari-Daryan, 1999). Because this hydrozoan is restricted to the middle to upper Norian and basal Rhaetian, it is useful for general biostratigraphic dating. Although not fully tested, it appears that the average diameter of *Heterastridium* is directly correlated with stratigraphic age, as this taxon appears to undergo size increases during the course of its evolution in the Triassic.

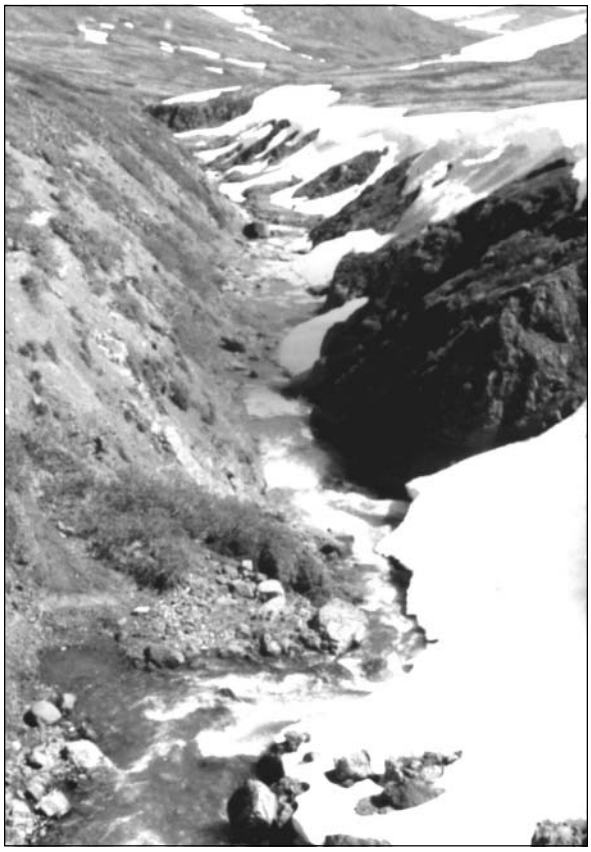

Figure 4. *Some steeply dipping limestone in partially snow-covered Long Creek. In the foreground are units 1–4 (see fig. 5).*

Heterastridium (previously reported by Jones and others, 1980) occurs on a ridge in the upper drainage of Little Shotgun Creek (section 31, T21S, R12W, Healy A-6 Quadrangle) in marine sandstone and siltstone, and in an impure limestone unit above a redbed unit (fig. 2). These localities were cited in an Alaska Division of Geological & Geophysical Surveys report (Blodgett and Clautice, 2000) with fossil-locality map numbers. The size range of *Heterastridium* (23.5 to 31.4 mm) indicates an age range of uppermost Norian to lowermost Rhaetian (Cordilleranus to Amoenum zones). In the stratigraphic succession of Upper Shotgun Creek, corals and reefal facies are absent. Depositional environments, rock types, and fossils from these sites, while about the same age as those at Long Creek, are of completely different composition. *Heterastridium* is not present in the coral–chaetetid carbonate facies but these spherical hydrozoans are common at the other sites. Mostly they occur in concentrated beds, of possible deeper water facies, which most likely represent storm deposits (fig. 7). With the exception of gastropods, corals and abundant shallow-water shelly faunas have not been found in this interval. Localities reported in Blodgett and Clautice (2000) containing *Heterastridium* include fossil locality map numbers 53, 117, 120, 136, 140–146, and 150.

THE INVERTEBRATE FAUNAS

The principal fossils found at Long Creek include solitary and colonial scleractinian corals and laminar and massive hydrozoans, all of which are the primary focus of the study. Also present are spiriferid and terebratulid brachiopods (Blodgett and Clautice, 2000; Stefanoff and Sandy, 1999), indeterminate bivalve and gastropods,

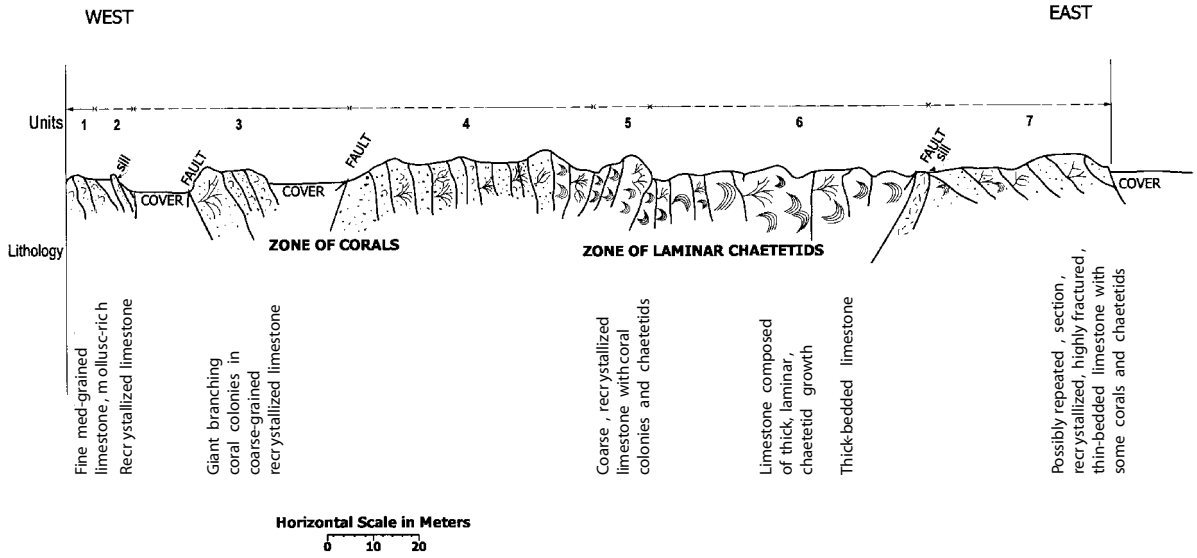

Figure 5. *Stratigraphic section measured from west to east along Long Creek, showing the various units and characteristic fossils.*

echinoid spines and tests, and crinoid ossicles. Our report focuses primarily on the corals, hydrozoans, and the chaetetid sponges.

Compared with other Norian–Rhaetian reef localities in Europe and a reef complex known from the Whitehorse Trough in Yukon, Canada (Reid, 1985; Yarnell, 2000), the diversity of the Long Creek fauna is relatively low. Also, unlike many Triassic reef localities, most of the coral taxa are dominated by solitary or pseudocolonial corals. The low diversity may indicate that the site has not been adequately sampled, but more likely the lower diversity might indicate nonreef settings and depositional environments less suitable to the growth of the corals.

The chaetetid sponges (currently under study by the authors) all represent *Pseudoseptifera*. However, they are exceedingly abundant. In some parts of the studied interval (unit 6, fig. 5), massive, tabular to slightly domate colonies constitute the bulk of the stratified limestone. Chaetetid sponges are known from other regions of the Tethys but have not been previously reported from North America.

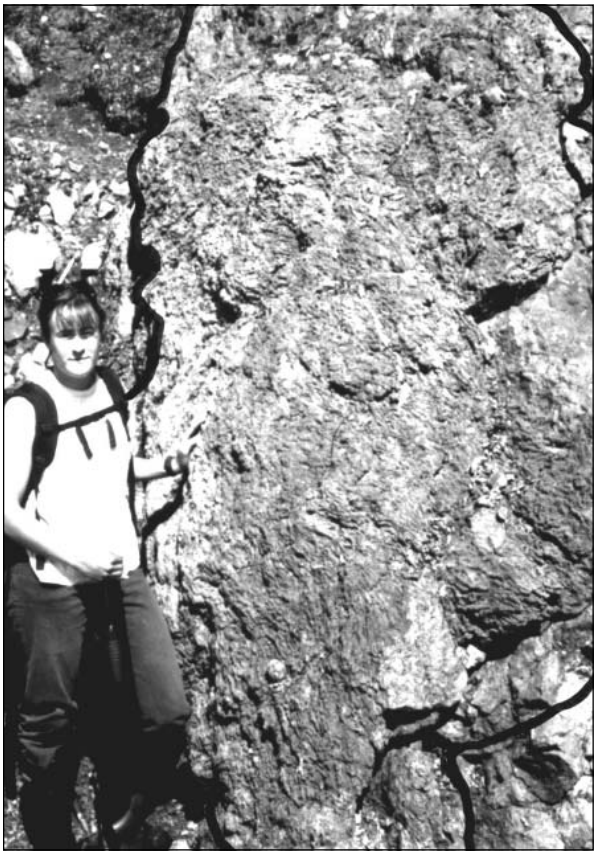

Figure 6. *Large in-place colony of* Retiophyllia*, a phaceloid colonial coral from unit 3 (shape traced in black).*

LONG CREEK

Scleractinian corals (in preparation for publication elsewhere)

- *Distichophyllia norica* (Frech, 1890)—solitary, common to abundant
- *Distichophyllia marmorea* (Frech, 1890)—solitary, rare
- *Retiophyllia* cf. *R. norica* (Frech, 1890)—phaceloid, abundant
- *Alpinophyllia flexuosa* (Roniewicz, 1989)—cerioid to meandroid, rare
- *Astraeomorpha crassisepta* (Reuss, 1854)—thamnasterioid, rare to common
- *Parastraeomorpha miniscula* (Roniewicz, 1989)—branching thamnasterioid, rare

Spongiomorphs

- Small branching *Spongiomorpha ramosa*

Chaetetid Sponges

- Large domate to laminar forms assignable to *Pseudoseptifera* (taxonomy currently under study)

The coral fauna is typical of other Upper Triassic, Norian coral localities in the American Cordillera. All six coral species are conspecific with those of the former Tethys region (Roniewicz, 1989). Unlike other localities, Long Creek is dominated by large solitary or pseudocolonial corals. Among these, *Distichophyllia norica* is the most geographically ubiquitous, occurring in most of the island-arc terranes of the American Cordillera and in the Tethys. While this species is usually solitary, it is known to laterally bud, producing pseudocolonial forms capable of producing small-scale framework as in both the Wallowa terrane of Oregon and in the Austrian Alps (Stanley and Senowbari-Daryan, 1986). *Distichophyllia marmorea* is a large solitary coral characterized by an abundance of fine septa. First described in central Europe, this taxon also occurs in west-central Nevada in great abundance in the Luning Allochthon and in the Wallowa terrane, Oregon (study in prep.). *Parastraeomorpha miniscula,* though rare at Chulitna, occurs as a slender branching form. It was known previously from the Northern Limestone Alps of central Europe (Roniewicz, 1989), and the discovery at the Chulitna site constitutes the first occurrence in North America. *Retiophyllia* cf. *R. norica* and *Alpinophyllia flexuosa* are both known from North America, occurring together in the Luning Allochthon and Antimonio terrane and individually among other inboard terranes such as Stikinia and Wallowa, and Quesnellia, respectively. Finally, *Astraeomorpha crassisepta*, a thamnasterioid hemispherical coral, is found in the Alexander and Wallowa terranes of the Cordillera, but also is known from the Koryak terrane in Siberia.

PALEOGEOGRAPHIC IMPLICATIONS OF THE LONG CREEK FAUNA

The scleractinian coral fauna assemblage from Long Creek, although low in diversity, is significant for reconstructing the paleogeography of the Chulitna terrane. Yarnell (2000) performed a statistical analysis in which the corals from Long Creek (except *Parastraeomorpha miniscula*) were compared, on the basis of general similarity or dissimilarity, to coral faunas from eight other Cordilleran terranes and one Siberian terrane. Although results varied slightly, one prevalent outcome was the apparent geographic closeness of Chulitna to inboard terranes of the American Cordillera, particularly Stikinia (fig. 1). In a cluster analysis of coral assemblages, the Chulitna terrane clustered with inboard terranes Stikinia, Quesnellia, Luning Allochthon, and Antimonio. In another method that uses parsimony analysis to build a phylogeny, the Chulitna terrane appears on an ancestral branch related to a grouping of the Stikine, Quesnel, and Antimonio terranes. Finally, a third statistical analysis produced a faunal similarity matrix. This shows the Chulitna terrane to have a significant similarity with Stikinia, indicating possible 'sharing' of faunas and thus implying geographic proximity (Yarnell and Stanley, 2000).

The presence of wallowaconchid bivalves at Long Creek also may have some significance for the paleogeographic reconstruction of terranes. Wallowaconchid bivalves also are known from the Stikine, Wallowa, and Antimonio terranes, but no real geographic connection between these terranes has yet been established. Specimens of wallowaconchids from Long Creek are similar, mainly on the basis of size, to those found far to the south, in the Antimonio terrane (fig. 1), whereas larger sized bivalves are found in Stikinia and the Wallowa terranes. This phenomenon suggests possible paleogeographic relationships among these terranes to the south and invites continued investigation of other North American terranes to search for more fossil evidence to test paleogeographic and tectonic hypotheses.

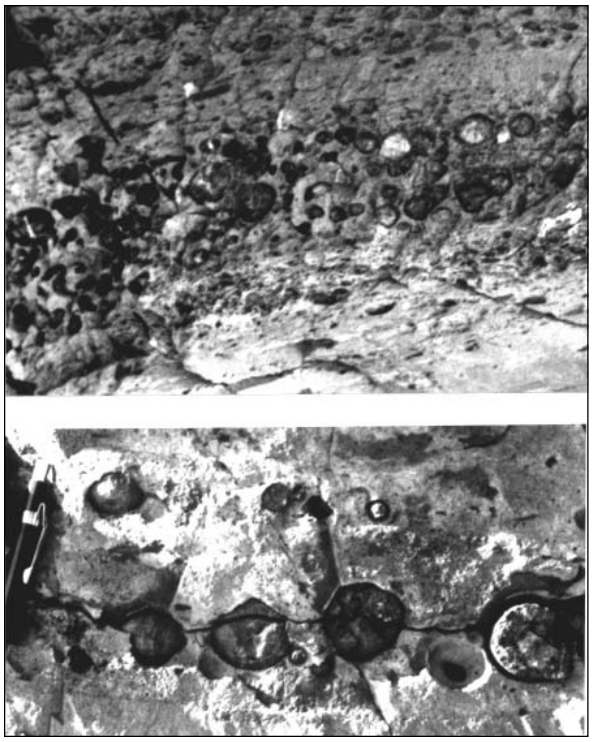

Figure 7. Heterastridium conglobatum *from near Shotgun Creek. Upper photo (x 0.25) shows stratiform deposits of these fossils. Lower photo (x 0.50) shows details. Concentrations of these spherical organisms in beds indicate possible storm deposits (photo courtesy of Karen Clautice).*

CONCLUSIONS

Although the fossiliferous biostromal limestone interval exposed at Long Creek (Chulitna terrane) is small compared to the voluminous limestone deposits in terranes such as Stikinia (Reid and Tempelman-Kluit, 1987), Quesnellia (Stanley and Senowbari-Daryan, 1999), and Wallowa (Stanley and Senowbari-Daryan, 1986), valuable data can be gleaned from the rock. A rich fossil assemblage of scleractinian corals, spongiomorph hydrozoans, chaetetid sponges, brachiopods, bivalves, and echinoderms is now known from the tiny Chulitna terrane. This terrane can be viewed as an 'orphan' in search of larger parents. One of the parent terranes being considered is Wrangellia, but how do the faunas compare?

Recently, six corals common to other North American terranes, as well as the former Tethys region in Europe, have been described from Long Creek in the Chulitna terrane (Yarnell, 2000; Yarnell and Stanley, 2000; Yarnell and Stanley, in prep.). Other important fossils, including a wallowaconchid bivalve, brachiopods, a sponge, and a spongiomorph, also have been discovered at Long Creek and are currently under study. Statistical analyses of the coral from Long Creek show distinct paleogeographic relationships between the Chulitna terrane and other Cordilleran terranes. Although questions of its precise paleogeography remain unanswered, relationships with Wrangellia remain weak. This places in question whether Wrangellia is the parent of the Chulitna terrane. Tentative analyses with coral faunas show the Chulitna terrane allied with the inboard terranes of Stikine, Quesnel, Eastern Klamath, Antimonio and Luning Allochthon rather than with Wrangellia (Yarnell and Stanley, 2000).

ACKNOWLEDGMENTS

We thank Karen Clautice and the Alaska Division of Geological & Geophysical Surveys for generous field support during the field session 1998 and for sharing her geologic knowledge of the Upper Chulitna district. Robert B. Blodgett and Sarah Schlichtholz kindly shared field notes and specimens. We are grateful to Dr. Michael Sandy and Dr. Robert Blodgett for their thoughtful reviews of this paper. This research was supported by the National Science Foundation (EAR 9615401).

REFERENCES

Blodgett, R.B., and Clautice, K.H., 2000, Fossil locality map for the Healy A-6 Quadrangle, south-central Alaska: Alaska Division of Geological & Geophysical Surveys Report of Investigations 2000-5, 42 p., 1 pl.

Flügel, E., 1994, Pangean shelf carbonates: controls and paleoclimatic significance of Permian and Triassic reefs, *in* Klein, G.D., ed., Pangea: paleoclimate, tectonics, and sedimentation during accretion, zenith, and breakup of a supercontinent: Geological Society of America Special Paper 288, p. 247–266.

Frech, F. 1890, Die Korallen der Trias.—I. Die Korallen der juvavischen Triasprovinz, Paleontographica, v. 37, p. 1–116.

Hawley, C.C., and Clark, A.L., 1974, Geology and mineral deposits of the Upper Chulitna district, Alaska: U.S. Geological Survey Professional Paper 758-B, 47 p.

Jones, D.L., Silberling, N.J., Csejtey, Bela, Jr., Nelson, W.H., and Blome, C.D., 1980, Age and structural significance of ophiolite and adjoining rocks in the Upper Chulitna district, south-central Alaska: U.S. Geological Survey Professional Paper 1121-A, 21 p.

Nichols, K.M., and Silberling, N.J., 1979, Early Triassic (Smithian) ammonites of paleoequatorial affinity from the Chulitna terrane, south-central Alaska: U.S. Geological Survey Professional Paper 1121-B, 5 p.

Reid, R.P., 1985, The facies and evolution of an Upper Triassic reef complex in northern Canada: Miama, Florida, University of Miami, Ph.D. dissertation, 343 p.

Reid, R.P., and Tempelman-Kluit, D.J., 1987, Upper Triassic Tethyan-type reefs in the Yukon: Bulletin of Canadian Petroleum Geology, v. 35, p. 316–332.

Reuss, A.E., 1854, Beiträge zur Charakteristik der Kreideschichten in den Ostalpen, besonders im Gosauthale und am Wolfgangsee: Denkschriften der Akademie der Wissenschaften, v. Mathemathisch-naturwissenschaftliche Klasse, 157 p.

Roniewicz, Ewa, 1989, Triassic scleractinian corals of the Zlambach beds, Northern Calcareous Alps, Austria: Denkschreiber der Österreichischen Akademie der Wissenschaft, mathematisch-naturwissenschaftliche Klasse, v. 126, p. 152.

Stanley, G.D., Jr., 1996, Confessions of a displaced reefer: Palaios, v. 11, no. 1, p. 1-2.

Stanley, G.D., Jr., and Senowbari-Daryan, B., 1986, Upper Triassic, Dachstein-type, reef limestone from the Wallowa Mountains, Oregon: First reported occurrence in the United States: Palaios, v. 1, p. 172–177.

———1999, Upper Triassic reef fauna from the Quesnel terrane, central British Columbia, Canada: Journal of Paleontology, v. 73, no. 5, p.787–802.

Stefanoff, M., Sandy, M.R., and Blodgett, R.B., 1999, Late Triassic brachiopods from the Chulitna terrane, south-central Alaska, and their paleogeographic significance: Geological Society of America Abstracts with Programs, v. 31, p. A-472.

Whalen, M.T., Clough, J.G., Blodgett, R.B., Stanley, G.D., Jr., Clautice, K.H., and Newberry, R.J., 1999, Late Paleozoic and Early Mesozoic carbonate rocks and depositional history of the Chulitna terrane: 2 p., *in* Reifenstuhl, R.R., ed., The Alaska Geological Society 1999 Science and Technology Conference, April 23–24, 1999, Fairbanks, Alaska.

Yancey, T.E., and Stanley, G.D., Jr. 1999, Giant alatoform bivalves in the Upper Triassic of western North America: Palaeontology, v. 42, no. 1, p. 1–23.

Yarnell, J.M., 2000, Paleontology of two North American Triassic reef faunas: Implications for terrane paleogeography: Missoula, Montana, University of Montana, Masters thesis, 141 p.

Yarnell, J.M., and Stanley, G.D., Jr., 2000, Two Triassic reef faunas from terranes in Alaska and Yukon and their paleogeographic significance: Geological Society of America Abstracts with Programs v. 32, no. 7, p. 12.

Short Notes on Alaska Geology 2003
Previous Editions of Short Notes on Alaska Geology

Short Notes on Alaskan Geology 1976: **DGGS Geologic Report 51 (out of stock, $3.50 photocopied)**

Reconnaissance geology along the Variegated Glacier, Saint Elias Mountains
Evidence for early Cenozoic orogeny in central Alaska Range
The Shumagin-Kodiak batholith: A Paleocene magmatic arc?
Speculative tectonic evolution of the Cenozoic Shelikof Trough, south-central Alaska
Discovery of blueschists on Kodiak Island
Large kaolinite crystals in the Chignik Formation (Upper Cretaceous), Herendeen Bay
Occurrence of sodic amphibole-bearing rocks in the Valdez C-2 Quadrangle
High-quality coal near Point Hope, northwestern Alaska

Short Notes on Alaskan Geology 1977**: DGGS Geologic Report 55 (out of stock, $5.00 photocopied)**

A Givetian (Late Middle Devonian) fauna from Healy B-4 Quadrangle, central Alaska Range
Probable karst topography near Jade Mountains, southwestern Brooks Range
Tectonic significance of the Knik River schist terrane, south-central Alaska
Geochronology of southern Prince of Wales Island Katmai caldera: Glacier growth, lake rise, and geothermal activity
Geology and K-Ar age of mineralized intrusive rocks from the Chulitna mining district, central Alaska
The Richardson lineament: A structural control for gold deposits in the Richardson mining district, interior Alaska
Boulder Creek tin lode deposits
Comparison of mercury-antimony-tungsten mineralization of Alaska with strata-bound cinnabar-stibnite-scheelite deposits of the Circum-Pacific and Mediterranean regions
Earthquake recurrence and location in the western Gulf of Alaska

Short Notes on Alaskan Geology 1978**: DGGS Geologic Report 61 ($2.00)**

Holocene displacements measured by trenching the Castle Mountain fault near Houston
Bluff Point landslide, a massive ancient rock failure near Homer
Recurrent late Quaternary faulting near Healy
Glaciation of Indian Mountain, west-central Alaska
The Cantwell ash bed, a Holocene tephra in the central Alaska Range
Geochronology of metamorphic and igneous rocks in the Kantishna Hills, Mount McKinley Quadrangle
The Chilikadrotna Greenstone, an Upper Silurian metavolcanic sequence in the central Lake Clark Quadrangle
Tectonic and economic significance of Late Devonian and late Proterozoic U-Pb zircon ages from the Brooks Range

Short Notes on Alaskan Geology 1979-80**: DGGS Geologic Report 63 ($1.00)**

Lead isotope ratios from the Red Dog and Drenchwater Creek lead-zinc deposits, De Long Mountains, Brooks Range
^{40}K-^{40}Ar ages from rhyolite of Sugar Loaf Mountain, central Alaska Range: Implications for offset along the Hines Creek strand of the Denali fault system
Multiple glaciation in the Beaver Mountains, western interior Alaska
Fossil algae in Lower Devonian limestones, east-central Alaska
Tertiary tillites(?) on the northeast flank of Granite Mountain, central Alaska Range
Evidence for suprapermafrost ground-water blockage, Prudhoe Bay oil field

Short Notes on Alaskan Geology 1981: **DGGS Geologic Report 73 ($3.00)**

Alkaline igneous rocks in the eastern Alaska Range
Shear moduli and sampling ratios for the Bootlegger Cove Formation as determined by resonant-column testing
Clinoptilolite and mordenite deposits of possible economic value at Iliamna Lake, Alaska
The Keete Inlet thrust fault, Prince of Wales Island
Two Holocene maars in the central Alaska Range
Radiometric-age determinations from Kiska Island, Aleutian Islands, Alaska
Geochemical signature of the Goon Dip Greenstone on Chicagof Island, southeastern Alaska
Uranium mineralization in the Nenana Coal Field, Alaska
Reconnaissance of rare-metal occurrences associated with the Old Crow batholith, eastern Alaska - north-western Canada
A recent earthquake on the Denali fault in the southeast Alaska Range
Triassic paleomagnetic data and paleolatitudes for Wangellia, Alaska

Short Notes on Alaskan Geology 1982-83**: DGGS Professional Report 86 ($2.50)**

An unconformity with associated conglomeratic sediments in the Berners Bay area of southeast Alaska
An iron-rich lava flow from the Nenana coal field, central Alaska
Results of shallow seismic survey for ground water at McGrath
Evaluation of a shallow sand-and-gravel aquifer at Eagle River
Correlation of geophysical well logs for a water development in south Anchorage
Garnet compositional estimates as indicators of progressive regional metamorphism in polymetamorphic rocks, Kantishna Hills
Geology of the Miss Molly molybdenum prospect, Tyonek C-6 Quadrangle Glacial geology of the Mt. Prindle area, Yukon-Tanana Upland

***Short Notes on Alaskan Geology 1991*: DGGS Professional Report 111 ($8.00)**

Tin placers associated with the downcutting of fissure basalts, Ray River drainage, Alaska
Geology and geochemistry of the Gagaryah barite deposit, western Alaska Range, Alaska
Geology and geochemistry of Tatlawiksuk Hot Springs, a newly discovered geothermal area in western Alaska
Geology and geochemistry of the Sleitat Mountain tin deposit, southwestern Alaska
Native mercurian-silver, silver, and gold nuggets from Hunter Creek, Alaska
Late Pleistocene volcanic deposits near the Valley of Ten Thousand Smokes, Katmai National Park, Alaska
Deglaciation of the Allison-Sawmill Creeks area, southern shore of Port Valdez, Alaska
Dating Holocene moraines of Canwell Glacier, Delta River valley, central Alaska Range
Gilead sandstone, northeastern Brooks Range, Alaska: An Albian to Cenomanian marine clastic succession
Kikiktat Mountain klippe: A link between the Copter Peak and Nuka Ridge allochthons, northcentral Brooks Range, Alaska
Sample media useful for a systematic geochemical survey of upper Valdez Creek, Alaska

***Short Notes on Alaskan Geology 1993*: DGGS Professional Report 113 ($6.00)**

Mississippian terrigenous clastic and volcaniclastic rocks of the Ellesmerian sequence, upper Sheenjek River area, eastern Brooks Range, Alaska
The penultimate great earthquake in southcentral Alaska: evidence from a buried forest near Girdwood
Geology, alteration, and mineralization of the Vinasale Mountain gold deposit, west-central Alaska
Fumarolic gas chemistry (1982) and thermal spring water chemistry (1985), Crater Peak, Mount Spurr, Alaska
Organic-rich shale and bentonite in the Arctic Creek unit, Arctic National Wildlife Refuge: implications for stratigraphic and structural interpretations
Dating Holocene moraines of Black Rapids Glacier, Delta River valley, central Alaska Range
Paleomagnetism of the Fairbanks basalts, interior Alaska
The Hayes Glacier fault, southern Alaska Range: evidence for post-Paleocene movement
Detachment folds and a passive-roof duplex: examples from the northeastern Brooks Range, Alaska

***Short Notes on Alaskan Geology 1995*: DGGS Professional Report 117 ($15.00)**

Radiocarbon age of probable Hayes tephra, Kenai Peninsula, Alaska
Geochemistry of saline lakes of the northeastern Yukon Flats, eastcentral Alaska
Geometry and deformation of a duplex and its roof layer: Observations from the Echooka anticlinorium, northeastern Brooks Range, Alaska
Late-Wisconsin events in the Upper Cook Inlet region, southcentral Alaska
Stratigraphy and implications of a lakeside section, Glacial Lake, southwestern Kigluaik Mountains, Seward Peninsula, Alaska
Lithofacies, petrology, and petrophysics of the Kemik Sandstone (Lower Cretaceous), eastern Arctic Slope, Alaska
A new species of the conodont *amydrotaxis* From the Early Devonian of southwestern Alaska
Early Devonian and Late Triassic conodonts from Annette and Hotspur Islands, southeastern Alaska
Mineralization and zoning of polymetallic veins in the Beaver Mountains volcano-plutonic complex, Iditarod Quadrangle, westcentral Alaska
Possible thrust windows on the central Seward Peninsula, Alaska

***Short Notes on Alaskan Geology 1997*: DGGS Professional Report 118 ($9.00)**

Geochronologic investigations of magmatism and metamorphism within the Kigluaik Mountains gneiss dome, Seward Peninsula, Alaska
Composite standard correlation of the Mississippian-Pennsylvanian (Carboniferous) Lisburne Group from Prudhoe Bay to the eastern Arctic National Wildlife Refuge, North Slope, Alaska
Enigmatic source of oil from Chukchi Sea, northwestern Alaska
Emsian (late Early Devonian) fossils indicate a Siberian origin for the Farewell Terrane
Growth-position petrified trees overlying thick Nanushuk Group coal, Lili Creek, Lookout Ridge Quadrangle, North Slope, Alaska
Paleotopographic control on deposition of the lower Kayak Shale, northern Franklin Mountains, Brroks Range, Alaska
Cooling history of the Okpilak batholith, northeastern Brooks Range, as determined from potassium-feldspar thermochronometry
First occurrence of a hadrosaur (Dinosauria) from the Matanuska Formation (Turonian) in the Talkeetna Mountains of south-central Alaska
Petrography of the Tingmerkpuk Sandstone (Neocomian), northwestern Brroks Range, Alaska: A preliminary study
Lower to Middle Devonian (latest Emsian to earliest Eifelian) conodonts from teh Alexander Terrane, southeastern Alaska
Preliminary petrography and provenance of six Lower Cretaceous sandstones, northwestern Brooks Range, Alaska

***Short Notes on Alaskan Geology 1999*: DGGS Professional Report 119 ($9.00)**

The Soda Creek Limestone, a new upper Lower Devonian formation in the Medfra Quadrangle, west-central Alaska
Duplex structure and Paleocene displacement of the Toyuk thrust zone near the Dalton Highway, north-central Brooks Range
Borehole breakouts and implications for regional *in situ* stress patterns of the northeastern North Slope, Alaska
Measured section and interpretation of the Tingmerkpuk sandstone (Neocomian), northwestern DeLong Mountains, western Arctic Slope, Alaska
Stratigraphic architecture of the Upper Jurassic–Lower Cretaceous Nutzotin Mountains sequence, Nutzotin and Mentasta mountains, Alaska
Stratigraphy, depositional systems, and age of the Tertiary White Mountain basin, Denali fault system, southwestern Alaska
Late Devonian (early Frasnian) conodonts from Denali National Park, Alaska
Geology and gold mineralization at the Donlin Creek prospects, southwestern Alaska
Preliminary $^{40}Ar/^{39}Ar$ ages from two units in the Usibelli Group, Healy, Alaska: New light on some old problems
Sedimentology and provenance of the Paleocene–Eocene Arkose Ridge Formation, Cook Inlet–Matanuska Valley forearc basin, southern Alaska
Late Devonian (Late Famennian) radiolarians from the Chulitna Terrane, south-central Alaska

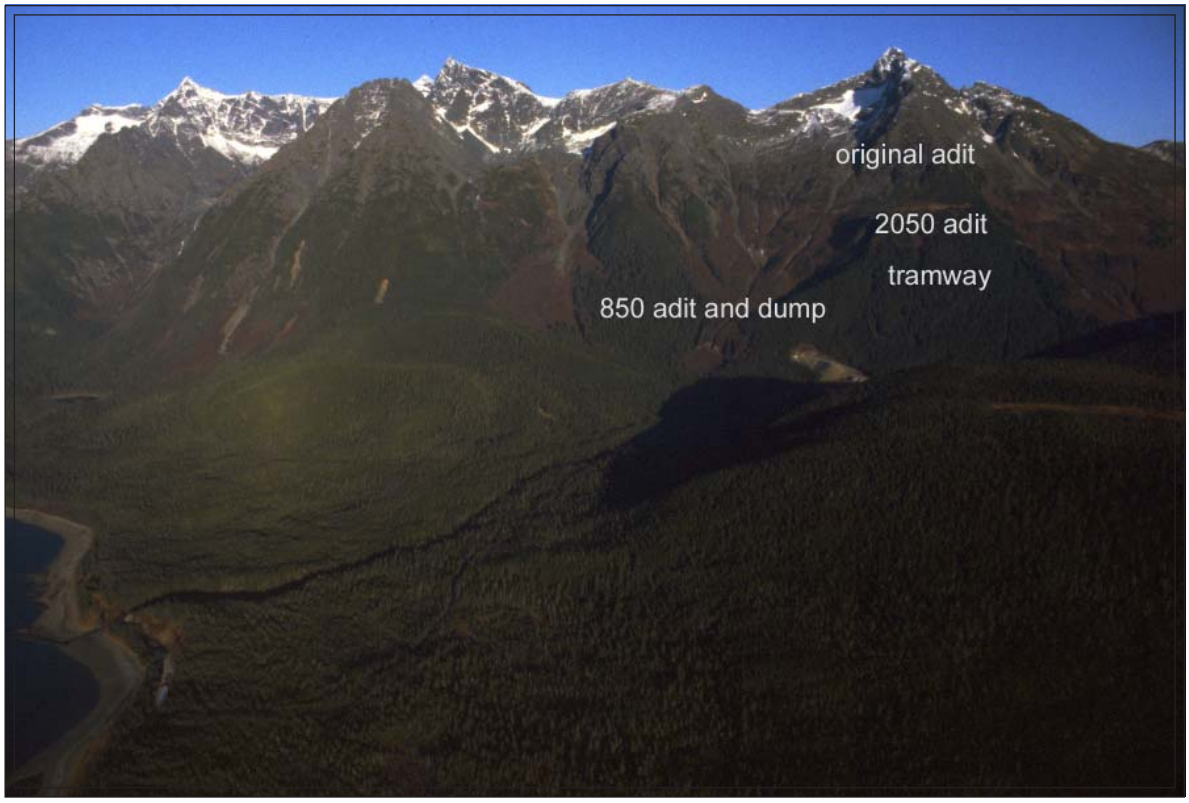

Photo of the Kensington Mine area, southeastern Alaska, showing the locations of the original glory hole (2,800 ft elevation), 2050 adit, tramline down to the original mill, and 850 adit and dump. (Photo by Earl Redman).

Quartz-filled dilation of Zone No. 41 at the Kensington Mine, southeastern Alaska. The bottom shear, delineated by orange painted arrows, is filled with massive gold-bearing pyrite that averages 0.5 ounces per ton gold. (Photo by Earl Redman)